

Summer 8-1-2021

Ensemble Data Fitting For Bathymetric Models Informed by Nominal Data

Samantha Zambo

Follow this and additional works at: <https://aquila.usm.edu/dissertations>



Part of the [Computational Engineering Commons](#), [Data Science Commons](#), [Design of Experiments and Sample Surveys Commons](#), [Geomorphology Commons](#), [Numerical Analysis and Computation Commons](#), [Numerical Analysis and Scientific Computing Commons](#), [Oceanography Commons](#), [Software Engineering Commons](#), [Statistical Models Commons](#), and the [Theory and Algorithms Commons](#)

Recommended Citation

Zambo, Samantha, "Ensemble Data Fitting For Bathymetric Models Informed by Nominal Data" (2021). *Dissertations*. 1897.
<https://aquila.usm.edu/dissertations/1897>

This Dissertation is brought to you for free and open access by The Aquila Digital Community. It has been accepted for inclusion in Dissertations by an authorized administrator of The Aquila Digital Community. For more information, please contact Joshua.Cromwell@usm.edu.

ENSEMBLE DATA FITTING FOR BATHYMETRIC MODELS INFORMED BY
NOMINAL DATA

by

Samantha J. Zambo

A Dissertation
Submitted to the Graduate School,
the College of Arts and Sciences
and the School of Computing Sciences and Computer Engineering
at The University of Southern Mississippi
in Partial Fulfillment of the Requirements
for the Degree of Doctor of Philosophy

Approved by:

Dr. Dia Ali, Committee Chair
Dr. A. Louise Perkins
Dr. Brian S. Bourgeois
Dr. Bo Li
Dr. John Harris

August 2021

COPYRIGHT BY

Samantha J. Zambo

2021

Published by the Graduate School



ABSTRACT

Due to the difficulty and expense of collecting bathymetric data, modeling is the primary tool to produce detailed maps of the ocean floor. Current modeling practices typically utilize only one interpolator; the industry standard is splines-in-tension.

In this dissertation we introduce a new nominal-informed ensemble interpolator designed to improve modeling accuracy in regions of sparse data. The method is guided by a priori domain knowledge provided by artificially intelligent classifiers. We recast such geomorphological classifications, such as ‘seamount’ or ‘ridge’, as nominal data which we utilize as foundational shapes in an expanded ordinary least squares regression-based algorithm. To our knowledge we are the first to utilize the output of classifiers as input into a numerical model. This nominal information provides meta-knowledge about seafloor creation and growth into our models implicitly.

We performed two suites of experimental studies designed to clarify when these techniques add value. In our first study, we utilized the MergeBathy software for DBM construction to extensively investigate existing interpolators for feature-favoritism on different synthetic, idealized morphologies. This study reduced the possibility that the interpolators were a significant source of error in sparse data regions. Two feature-favoring interpolators then served as our nominal-informed interpolators and ensemble members. In our second study, we utilized Friedman’s hypothesis testing to verify that our nominally informed ensemble method outperforms splines-in-tension in the presence of sparse data. To our knowledge, this is the first comparison study of interpolation over sparse bathymetric data to verify statistically significant improvement in sparse-data regions.

ACKNOWLEDGMENTS

This work was sponsored by the Office of Naval Research through the “Irregular Multiresolution Database Algorithm” Base Program Project at the Naval Research Laboratory. The authors are very grateful to Dr. Martin Jakobsson (Stockholm University in Sweden) and Dr. Brian Calder (University of New Hampshire) who provided us with the data they used for their 2002 paper on the Monte Carlo procedure and technical guidance. We also thank Dr. Elmore (Naval Research Laboratory), Dr. Bourgeois (Naval Research Laboratory), Dr. Calder and Dr. Fred Petry (Naval Research Laboratory) for their helpful discussions and feedback.

DEDICATION

I dedicate this dissertation to Christopher D. Stringer. Your love, support, and sacrifice made this possible. Without your kind heart and willingness to help, attending graduate school would have been a missed opportunity I would have regretted. It was your sacrifice and belief in me that made this dream a reality. You are a good person, a rarity. I am extremely grateful to have been gifted the opportunity and privilege, to not only know you, but to learn from you. You are an aspirational human being.

I would like to thank Dr. A. Louise Perkins for being an inspiring role model. You broke the “smart female” stereotypes and expectations placed on women and showed me it was ok to vary from the status quo. Your confidence, strength, and perseverance gave me hope. I will always remember you and aspire to be the same.

I would also like to thank Dr. Brian S. Bourgeois, for without his guidance, I would have never attended graduate school. I could not have asked a better mentor as an undergraduate beginning in research. Thank you for your encouragement and kindness. You have greatly affected the course of my life by making me aware of what I could be. You opened my eyes to dream big.

Christopher Stringer, Dr. Perkins, and Dr. Bourgeois, it is when I found you three that I finally found a place I felt I belonged, and I thank you again for your acceptance and inspiration.

To Cameryn Phoenix, who loved me unconditionally. I could not have asked for a better study partner or friend.

I thank Sandra Duvic and Derek Duvic whose kind hearts took me in, supported me through my hardships, and helped me get my GED and enroll in college. Without

you, I would not be where I am today: from a high school drop out to a Doctor of Philosophy.

Finally, I thank the strongest woman I knew, my grandmother Armida “Mamie” Seale. Through her sacrifices, determination, and love, she came to the United States of America from Nicaragua many years ago. You were always there when I needed you. You were the most important person in my life, and I will never love anyone as much as I loved you. I will always love you. I will never forget what a wonderful and incredible person you were. You are missed. In November 2020, Armida passed away from Covid-19. She was so proud and excited to see me graduate. This dissertation is in her memory.

TABLE OF CONTENTS

ABSTRACT	ii
ACKNOWLEDGMENTS	iii
DEDICATION	iv
LIST OF TABLES	xi
LIST OF ILLUSTRATIONS	xiv
LIST OF ABBREVIATIONS	xvii
CHAPTER I – INTRODUCTION	1
1.1 Machine Learning and Ensembles	2
1.2 Contribution and Motivation	5
1.3 Dissertation Prologue	9
CHAPTER II – BACKGROUND	12
2.1 Bathymetry	15
2.2 Bathymetry Modeling	21
2.3 Regression	24
2.3.1 The Bias-Variance Trade-Off	26
2.3.2 Least Squares Assumptions	28
2.3.3 Relaxing OLS Assumptions	32
2.3.3.1 LOESS	32
2.3.3.2 Stochastic Estimation	34

2.3.3.2.1 Bathymetric Data as a Gaussian Process	34
2.3.3.2.2 Ordinary-Kriging	34
2.3.3.2.3 Kalman Filter	38
2.3.3.3 Smoothing Splines	39
2.3.4 Regression in Modeling Sparse Bathymetric Data	40
2.3.5 Linear Mixed Effect Models	41
2.3.6 Checking Assumptions	43
2.4 MergeBathy (2015)	48
2.4.1 Introduction	48
2.4.2 Problems and Background	49
2.4.3 Software Functionalities	50
2.4.4 Implementation	51
2.5 MergeBathy Interpolation Schemes (First Study Evaluated Methods)	53
2.6 Uncertainty Estimation for Sparse Data Gridding Algorithms	57
2.6.1 CURVE Algorithm	60
2.6.1.2 Selecting Support Points	62
2.6.1.3 Propagated Variance	63
2.6.1.3.1 CUBE	63
2.6.1.3.2 Bottom Slope	64
2.6.1.4 Computing Attributed Uncertainty	66

2.6.2 Case Studies	68
CHAPTER III – A NEW INFORMED ENSEMBLE APPROACH TO BATHYMETRY UTILIZING MACHINE LEARNERS	
3.1 Geomorphological Seafloor Primitive Nominal Data.....	81
3.2 ELS for an Informed Differentially Weighted Ensemble of DBMs	84
3.2.1 Regression Models.....	92
3.2.1.1 Planar Model (Un-Informed)	95
3.2.1.2 Custom Model (Nominal-Informed).....	96
3.3 Additional Methods to Assess	100
CHAPTER IV – RESEARCH APPROACH.....	
4.1 Design of Experiments.....	104
4.1.1 Study 1: The Uniform Experiments (UEs)	105
4.1.2 Study 2: The Randomized Experiments (REs)	107
4.2 Analyses of Experiment.....	109
4.3 Metrics	112
CHAPTER V – FIRST STUDY: FEATURE-FAVORING INTERPOLATION	
5.1 Data.....	117
5.2 Results.....	131
5.2.1 Test 1: Censored UEs.....	133
5.2.1.2 2D Truncated Seamount	136

5.2.1.3 1D Gaussian Ridge	141
5.2.1.4 Discussion: Seamount versus Ridge Censored UEs (Test 1).....	145
5.2.2 Test 2: Noise UEs	145
5.2.3 Test 3: Combined Censored and Noise UEs.....	149
5.2.4 Identifying Feature-Favoring Interpolators.....	162
CHAPTER VI – SECOND STUDY: EVALUATING ENSEMBLES	169
6.1 Study 2 (REs) Test 3a: Random Configurations.....	173
6.1.1 Data	174
6.1.2 Results.....	180
6.2 Study 2 (RE) Test 3b: Sparse Configurations.....	182
6.2.1 Data	184
6.2.2 Results.....	190
6.3 Friedman’s Test	192
6.3.1 Study 2 Subsection 1: Importance of Nominal-Informed Modeling (NI)	196
6.3.2 Study 2 Subsection 2: Importance of Post-Regressing with a Nominal- Informed Model (PR).....	205
6.3.3 Study 2 Subsection 3: Importance of Regressing on Accurate Data with a Nominal-Informed Model when Estimating from Fit.....	211
6.3.3.1 Study 2 Subsection 3.1: Comparing Five Interpolators (ADall).....	212
6.3.3.2 Study 2 Subsection 3.2: Comparing Four Interpolators (ADsubset)	216

6.3.4 Study 2 Subsection 4: Importance of Utilizing All Influential Information (AII)	223
6.3.5 Study 2 Subsection 5: Importance of Utilizing All Influential Primitives in the ELS Regression Model, when Estimating from Fit (AIP)	232
6.3.6 Study 2 Subsection 6: Importance of \mathbf{w} -ELS over ELS (wE)	242
6.4 Discussion	247
CHAPTER VII – SUMMARY	252
APPENDIX A – MergeBathy (2015) Metadata	257
APPENDIX B – Contributions	258
REFERENCES	265

LIST OF TABLES

Table 2.1 OLS Regression Assumptions	32
Table 2.2 Individual MergeBathy Interpolation Schemes Utilized in our First Study.	55
Table 3.1 Additional Methods Assessed.....	100
Table 4.2 Studies Performed.....	105
Table 4.3 UE Test Data Sets	107
Table 4.4 RE Test Data Sets	109
Table 5.1 Study 1 (UEs) Tests	118
Table 5.2 Study 1 Test 1: Uniformly Censored Data Set Designs to Test Sparsity	119
Table 5.3 Study 1 Test 2: Gaussian Contaminated Data Set Designs to Test Noise	120
Table 5.4 Study 1 Test 1: Seamount Censored CumRAE Results (Results rounded to 2 decimals, but color coding is accurate.).....	134
Table 5.5 Study 1 Test 1: Ridge Censored CumRAE Results (Results rounded to 2 decimals, but color coding is accurate.).....	135
Table 5.6 (Annotation 1 of Table 5.4) Study 1 Test 1: Seamount Censored CumRAE Results (Results rounded to 2 decimals, but color coding is accurate.).....	137
Table 5.7 (Annotation 2 of Table 5.4) Study 1 Test 1: Seamount Censored CumRAE Results (Results rounded to 2 decimals, but color coding is accurate.).....	139
Table 5.8 Groups A, C, E, and F divided by MBZ SIT (EM32) from Table 5.4 for Study 1 Test 1: Seamount Censored CumRAE Results (Results rounded to 2 decimals, but color coding is accurate.)	140
Table 5.9 (Annotated Table 5.5) Study 1 Test 1: Ridge Censored CumRAE Results (Results rounded to 2 decimals, but color coding is accurate.)	143

Table 5.10 Groups A, C, E, and F divided by MBZ SIT (EM32) from Table 5.5 for Study 1 Test 1: Ridge Censored CumRAE Results (Results rounded to 2 decimals, but color coding is accurate.)	144
Table 5.11 Study 1 Test 2: Seamount Noise CumRAE Results (Results rounded to 2 decimals, but color coding is accurate.).....	147
Table 5.12 Study 1 Test 2: Ridge Noise CumRAE Results (Results rounded to 2 decimals, but color coding is accurate.).....	148
Table 5.13 Study 1 Test 3: Seamount Censored and Noise CumRAE Results (Results rounded to 2 decimals, but color coding is accurate.).....	150
Table 5.14 Study 1 Test 3: Ridge Censored and Noise CumRAE Results (Results rounded to 2 decimals, but color coding is accurate.).....	155
Table 5.15 (Reduced Table 5.13) Study 1 Test 3: Seamount Censored and Noise CumRAE Results (Results rounded to 2 decimals, but color coding is accurate.).....	160
Table 5.16 (Reduced Table 5.14) Study 1 Test 3: Ridge Censored and Noise CumRAE Results (Results rounded to 2 decimals, but color coding is accurate.).....	161
Table 6.1 Selected Methods (SM) Utilized in our Second Study (REs).....	172
Table 6.2 Study 2 (RE) Test 3a: Random Configuration Details	177
Table 6.3 Study 2 (RE) Test 3a: Random Configuration CumRAE Results (Results rounded to 2 decimals, but color coding is accurate.).....	180
Table 6.4 Study 2 (RE) Test3b: Sparse Configuration Details	187
Table 6.5 Study 2 (RE) Test 3b: Sparse Configuration CumRAE Results (Results rounded to 2 decimals, but color coding is accurate.).....	190

Table 6.6 Friedman’s Tests Performed to Evaluate Nominal-Informed Modeling and Ensembles in our Second Study (REs).	193
Table 6.7 Cheat Sheet: Friedman’s Tests for our Second Study (REs) Test 3a and 3b.	195
Table A.1 Software metadata.....	257
Table A.2 Code metadata.....	257

LIST OF ILLUSTRATIONS

Figure 2.1 “The World Reference for Raw Bathymetry” (International Hydrographic Organization, n.d.-b).	17
Figure 2.2 Example of multibeam bathymetric data collection.	20
Figure 2.3 Example of sparse data interpolation failures.	24
Figure 2.4 High-level MergeBathy flow for processing bathymetric data.	51
Figure 2.5 Illustration of CURVE.....	61
Figure 2.6 Bottom-slope	66
Figure 2.7 IDW versus linear interpolation.	67
Figure 2.8 East Pacific Rise data	68
Figure 2.9 Case study area ground truth data.	68
Figure 2.10 Case study area slopes.	69
Figure 2.11 Randomly selected data points using 10% of the ground truth data.	69
Figure 2.12 DBM created using GMT SIT on the 10%-thinned data.....	70
Figure 2.13 Uncertainty for the 10%-thinned data set, using (2.2).....	71
Figure 2.14 Uncertainty for the 10%-thinned data set, using (2.3).....	71
Figure 2.15 Uncertainty difference using (2.2) and (2.3).	72
Figure 2.16 Single latitude slice for the 10%-thinned data set passing through one of the volcanoes.....	73
Figure 2.17 DBM created using GMT SIT on the 20%-thinned data.....	74
Figure 2.18 Randomly selected data points using 20% of the ground truth data.	74
Figure 2.19 Single latitude slice for the 20%-thinned data set.	75

Figure 2.20 DBM created using GMT SIT with a middle 1/3 latitude data points removed.....	76
Figure 2.21 Single latitude slice through the region where 1/3 of the data points removed.....	76
Figure 3.1 Example of seafloor surface decomposed into primitives.....	83
Figure 4.1 Process flow for synthetic experiments.....	102
Figure 5.1 Original morphology truth surfaces.....	122
Figure 5.2 Study 1 Test 1: truncated seamount data sets with censoring.	124
Figure 5.3 Study 1 Test 1: Gaussian ridge data sets with censoring.....	126
Figure 5.4 Study 1 Test 2: truncated seamount data sets with noise.	128
Figure 5.5 Study 1 Test 2: Gaussian ridge data sets with noise.....	130
Figure 5.6 Study 1 Test 1: Example of feature-favoring DBMs at censored level 1.....	166
Figure 5.7 Study 1 Test 2: Example of feature-favoring DBMs at noise level 1.	167
Figure 5.8 Study 1 Test 3: Example of feature-favoring DBMs at censored level 1 and noise level 1.	168
Figure 6.1 Study 2 (RE) Test 3a: Random configurations.....	176
Figure 6.2 Study 2 (RE) Test 3b: Sparse configurations.	186
Figure 6.3 Study 2 subsection 6.3.1 (NI) results on the truncated hybrid.	199
Figure 6.4 Analysis of subsection 6.3.1 (NI).	200
Figure 6.5 Study 2 subsection 6.3.2 (PR) results on the truncated hybrid.....	208
Figure 6.6 Analysis of subsection 6.3.2 (PR).	211
Figure 6.7 Study 2 subsection 6.3.3.1 (ADall) results on the truncated hybrid.....	214
Figure 6.8 Study 2 subsection 6.3.3.2 (ADsubset) results on the truncated hybrid.....	219

Figure 6.9 Study 2 subsection 6.3.4 (AII) results on the truncated hybrid.	227
Figure 6.10 Study 2 subsection 6.3.5 (AIP) results on the truncated hybrid.	235
Figure 6.11 Study 2 subsection 6.3.6 (wE) results on the truncated hybrid.	244
Figure 6.12 Analysis of subsection 6.3.6 (wE)	247
Figure 7.1 Example of our new nominal-informed ensemble <i>w</i> -ELS compared to the industry standard GMT SIT.	255

LIST OF ABBREVIATIONS

<i>AI</i>	Artificial Intelligence
<i>ANOVA</i>	Analysis of Variance
<i>BAG</i>	Bathymetry Attributed Grid
<i>BLUE</i>	Best Linear Unbiased Estimator
<i>BLUP</i>	Best Linear Unbiased Predictor
<i>CUBE</i>	Combined Uncertainty and Bathymetry Estimator
<i>CURVE</i>	CUBE Uncertainty pPropagated Variance Estimator
<i>CumRAE</i>	Cumulative Relative Absolute Error
<i>DBM</i>	Digital Bathymetric Model
<i>DBDB-V</i>	Digital Bathymetric DataBase - Variable
<i>ELS</i>	Ensemble Least Squares
<i>GEBCO</i>	General Bathymetric Chart of the Oceans
<i>GIS</i>	Geographic Information Systems
<i>GMT</i>	Generic Mapping Tools
<i>IID</i>	Independent and Identically Distributed
<i>IDW</i>	Inverse Distance Weighting
<i>LMM</i>	Linear Mixed Model
<i>LOESS</i>	Locally Estimated Scatterplot Smoothing
<i>LOWESS</i>	Locally Weighted Estimated Scatterplot Smoothing
<i>LOESS (LOWESS)</i>	Locally Weighted Regression
<i>MB-System</i>	Multi-Beam System
<i>MBZ</i>	Multi-Beam System mb_zgrid routine

<i>ML</i>	Machine Learning
<i>MSE</i>	Mean Square Error
<i>OLS</i>	Ordinary Least Squares
<i>RMS</i>	Root Mean Square
<i>RE</i>	Randomized Experiment
<i>RSRRN</i>	Random Swath Removal Random Noise
<i>SIT</i>	Splines-in-Tension
<i>TIN</i>	Triangulated Irregular Network
<i>UE</i>	Uniform Experiment
<i>USM</i>	The University of Southern Mississippi
<i>w-ELS</i>	<i>w</i> weighted informed ensemble via ELS

CHAPTER I – INTRODUCTION

In this dissertation, we demonstrate that the addition of nominal data with ensemble averaging adds knowledge about a region for improved accuracy of digital bathymetric models (DBMs) in areas with sparse data. Benefits of this capability to add knowledge to (or in other words, be informed about) a region for an improved gridding are applicable to all environmental sciences, including terrestrial, seafloor, and planetary. In this dissertation, we investigate the efficacy of utilizing nominal data and ensembles when modeling bathymetric surfaces. This chapter introduces the various related fields and background information that provide the context for this problem.

Bathymetry is the estimation of seafloor depth, including both measurement and modeling. Unlike other fields, bathymetric estimation faces the unique situation that it needs to provide conservative estimates when their usage is navigation. Areas that are well measured are known to be quite accurate and provide few problems, but sparsely measured areas of unknown quality are still prevalent. The gravity-based methods (Hu et al., 2015; W. H. F. Smith & Sandwell, 1994) have filled these sparse areas with a smoothed approximation of the seafloor (Weatherall et al., 2015), but the resulting DBMs are not always trustworthy. Traditionally, conservative measures are coupled with these smoothed areas (B. R. Calder & Mayer, 2003).

In this research, we assume nominal data exists to impute structure in such sparse regions (Lawson et al., 2017). Such an approach has the advantage that it can be tailored to conservative assumptions.

Section 1.1 introduces machine learning (ML) and ensemble concepts and in section 1.2, we highlight our contributions. In this chapter, we describe work performed,

in part, with Paul Elmore, A. Louise Perkins, and Brian Bourgeois. Section 1.3 outlines the remainder of this dissertation.

1.1 Machine Learning and Ensembles

The artificial intelligence (AI) field of ML developed techniques that make predictions based on what it learns from data. These techniques may be discretizing identifiers called classifiers that map data to classification clusters for a nominal prediction, or regression-based for a continuous numerical prediction. When nominal predictor algorithms output a discrete value from a finite set of possible discrete output results, the application is ‘classification’. Numerical regression-based algorithms output a numerical predictor from a continuous range of values.

For over twenty years, ML classification and regression algorithms have been an active field of research with application across a wide range of problems. D. Smith et al. (2016), for example, show skill in classifying seamounts. In consumer commerce, Xbox (development by Microsoft) was sufficiently skilled at recognizing and classifying human gestures to be a commercially successful human-computer interface device (Criminisi et al., 2011). In medicine, a rule-based medical diagnosis tool for typhoid fever, developed in and focused on Africa, was effective in reducing infections (Oguntimilehin et al., 2013). There are a vast number of papers applying machine-learning technology to nearly all search problems.

Some commonly employed machine learning algorithms are ensemble algorithms constrained from a set of weak learners to form a strong learner. They include AdaBoost (boosting) (Freund & Schapire, 1997), ensemble decision trees (bagging [bootstrap aggregate]) (Breiman, 1996) such as random forest (Breiman, 2001) and extra-tree

(Geurts et al., 2006), and stacked generalization (stacking) (Wolpert, 1992). Weak learners are individual algorithms that do slightly better than random guessing while strong learners are those that are highly accurate (Schapire, 1989). Examples of learners are decision trees (Breiman et al., 1984), linear discriminate analysis (Fisher, 1936; McLachlan, 2004), support-vector machines (Cortes & Vapnik, 1995), and back-propagation neural networks (Werbos, 1982).

The wide usage of ML algorithms is due, in part, to readily available software and computational resources for their implementation. Common ML software available includes MATLAB (MathWorks, 2015c), Python Scikit-learn (Pedregosa et al., 2011), Microsoft Azure Machine Learning (Microsoft, 2016), C++ mlpack (Curtin et al., 2013) and Shogun (Shogun Toolbox Foundation, 2016), Java-ML (Abeel et al., 2009), and Spark MLlib (The Apache Software Foundation, 2016).^{1,2}

An ensemble ML algorithm combines multiple, individual machine-learned outputs, based on various methodologies, initial parameters, or both to produce one single classification or regression output. The intent is to utilize multiple outputs from different models for a more accurate result. Ensembles generally are less sensitive to outliers, overfitting, and model approximation errors when compared to single machine learners alone.³

¹ MATLAB Statistics and Machine Learning Toolbox(MathWorks, 2015e), Neural Network Toolbox(MathWorks, 2015d), Computer Vision System Toolbox(MathWorks, 2015a) and Fuzzy Logic Toolbox(MathWorks, 2015b).

² Spark is a “unified analytics engine for large-scale data processing” (The Apache Software Foundation, 2016) for big-data cluster environments.

³ Some fields of study interchange the word ‘ensemble’ with ‘combination’ and ‘aggregation’.

The ensemble approach has been a valuable research tool for half a century. In 1969, Edward Epstein noted that a single forecast could not completely describe the atmosphere due to inherent uncertainty. He proposed a Monte Carlo simulation to address this deficit (Epstein, 1969). He perturbed initial conditions to build an ensemble of inputs that produced a more accurate single result when one averaged their outputs. This idea of an ensemble of results for a single, better result rests upon the No Free Lunch Theorem (Wolpert & Macready, 1997), which supposes that each method has merit under different circumstances.

Another popular ensemble approach, boosting, uses the same algorithm successively on re-weighted training data to produce a suite of learners, each trained on predicting a subset of the data correctly (Freund & Schapire, 1997; Schapire, 1989).⁴ The most widely used boosting algorithm is AdaBoost.

Bagging takes a quasi-random approach by using bootstrap sampling to generate a suite of overlapping training data (Breiman, 1996). This approach reduces variance and increases accuracy by being robust against outliers or noisy data and avoiding overfitting (LeDell, 2016). Decision trees commonly employ bagging. The state-of-the-art bagging algorithms are ensemble decision trees such as random forest and extra-tree.

The stacking ensemble method combines predictions from different learners by training a black-box meta-learner: a combiner algorithm that trains on the original

⁴ Data is iteratively reweighted where weights increase for misclassified data and decrease for correctly classified data. The algorithm then trains on the new data set and the new classifier joins the ensemble. The process continues in this fashion (reweighting, learning, and adding) until meeting a threshold or terminating criteria. Each successive classifier focuses on predicting the subset of data misclassified previously. AdaBoost (Freund & Schapire, 1997) follows this approach.

predictions of independently trained learners to make a final prediction (Rokach, 2010; Wolpert, 1992). This work is stacking; ensemble least squares (ELS), described in Chapter III, will act as our black-box learner for obtaining ensemble weights (of which an external ensemble obtained by this ELS weighting is w -ELS, our new nominal-informed ensemble approach to bathymetric modeling). ELS was developed by the author with A. Louise Perkins to facilitate data assimilation of categorical data in DBM construction. Nominal data is output from a classifier; nominal data is the classification. Utilizing nominal data (information) to inform an approach a priori is to be nominally informed; the process was informed by the nominal data. The approach then is a nominal-informed approach producing a nominal-informed product. Therefore, not utilizing nominal information is decidedly an un-informed approach producing an un-informed product. In our research, we label the most widely applied interpolator in hydrography for generating DBMs as our un-informed interpolator.

There is a variety of ensemble combination or aggregation approaches including weighted, simple, and trimmed averages. A simple average assigns equal weights (probabilities) to the ensemble members. This approach may be sensitive to outliers, which is problematic in sparse data situations. A weighted average assigns differential weights capable of adjusting to different circumstances. A trimmed average avoids the undesirable effects of outliers by eliminating the highest and lowest predictions before averaging.

1.2 Contribution and Motivation

The goal of AI-based classifiers is to achieve good class separation for better generalization. State-of-the-art classifier techniques use ensembles of ML algorithms.

Our approach follows these popular ensemble approaches in ML and is most like stacking than other popular ML ensemble approaches. The ELS algorithm I developed (Chapter III) acts as a black-box meta-learner, and geomorphological-shaped primitive functions represent classifications predicted from independently trained classifiers. For black-box ensembles, weighted majority voting is frequently the best ensemble when given a priori knowledge.

I use a suite of interpolators available in the MergeBathy software tool (S. J. Zambo et al., 2016) supplemented with additional interpolators devised and implemented external to MergeBathy for experimentations.⁵ Following Armstrong et al. (2015), each ensemble will be the weighted average of two different interpolation methods; we assure that the different interpolations are heterogeneous.⁶

We developed the ELS algorithm based on the ordinary least squares (OLS) framework that selects the regressors from a suite of nominal forms representing the categorical geomorphological shapes typically found on a seabed. We utilize only geomorphological shapes that have already been studied in the literature (cf. Lawson et al., 2017) and assume an outside study has quantified and identified the categories.

More sophisticated least squares frameworks are available (cf. Sapp et al., 2014), but were not necessary for our proof of concept.

⁵ MergeBathy is a software tool for processing sparse bathymetric data developed by the Naval Research Laboratory for the Naval Oceanographic Office. The Naval Oceanographic Office is responsible for worldwide ocean mapping.

⁶ Classifiers uphold heterogeneity through trained data, the model, or both.

We remind the reader that the a priori domain knowledge from the classifiers determines the underlying nominal or feature primitives that make up the seafloor and suggests feature-favoring interpolators as ensemble members.

Current guidelines (J. Scott Armstrong et al., 2015) advise forging ensembles according to knowledge of the specific problem in the selection of its ensemble members and weights. In our bathymetric setting, randomly selecting ensemble members has a worst-case scenario of selecting interpolators with the largest errors and giving the largest weight to the worst. Ensembles guarantee performance no worse than the average of its ensemble members, thus, choosing better (or the best) performing interpolators as ensemble members will give an average performance better than that of the worst-case scenario and appropriately weighting the members avoids reducing ensemble performance below the mean of its ensemble members by giving too much credence to the worst of the ensemble members. By utilizing classifiers to inform the weights used in unequally weighted ensembles, we may be able to lower our error, on average.

In this dissertation, we test the effectiveness of using ensemble techniques and classifiers to reduce inaccuracies incurred from utilizing only one interpolator with sparse data. We hypothesize that 1) ensembles reduce overfitting and outlier sensitivity and 2) classifiers provide supplemental a priori information for an improved nominal-informed ensemble to reduce inaccuracies as well. More generally, we investigate the efficacy of utilizing nominal information in DBM construction (nominal-informed modeling), through interpolator selection and ensembles.

This work began with the extensive modification and utilization of the MergeBathy software suite, described in section 2.4, including providing support for bathymetric uncertainty estimation, described in section 2.6.

The technical approach of this work (outlined in Chapter IV) includes conducting two studies, each comprising of sets of numerical experiments. We construct primitives (basic, idealistic seafloor shapes) and combined seafloor surfaces (complex, weighted compositions of primitives) for synthetic experimentation, and evaluate the accuracy and precision of the DBMs produced by the interpolators.

The first study (presented in Chapter V) conducts numerical experiments of candidate ensemble techniques (MergeBathy interpolators) to investigate feature favoritism in sparse regions. From this study, we select two different interpolators to utilize in our second study.

The second study (presented in Chapter VI) conducts numerical experiments of selected interpolators from the first study, ensemble techniques, and additional methods implemented for investigative purposes to investigate ensembles (and more generally, nominal-informed modeling) in sparse regions.

We developed a nominal-informed ensemble technique (presented in Chapter III) that utilizes an ELS of DBMs (primitives) to find ensemble weights. We evaluated our ELS algorithm using idealistic, synthetic data sets by comparing to a splines-in-tension (SIT) benchmark to validate and verify the algorithm.

This work assumes conflicting (disagreeing) classifiers: classifiers which output different nominal values (classifications) that are conflicting (in disagreement) for the same data set. A feature-favoring interpolator shows an aptitude (favoritism) for a

morphology (feature) identified by the nominal data (classification). Our nominal-informed modeling utilizes the nominal information to select feature-favoring interpolators and, when conflicting, construct their ensembles.

Our motivation for constructing nominal-informed ensembles in this work is that current bathymetric modeling techniques have not evolved with forecasting methodologies as in other fields (J. Scott Armstrong et al., 2015). Likewise, over the past twenty years, machine learning has gained recognition for the ability to discover successfully dynamics that were not obvious in data across multiple disciplines, popularity beginning with the advent of stacked generalization (Wolpert, 1992). For bathymetric data, the practice is to use all supplemental information available, yet knowledge obtained by machine learners lack utilization. Recently, D. Smith et al. (2016) used machine learners to successfully identify seafloor features, providing vital topological domain knowledge for knowledge-limited areas. We take the next step, showing how such nominal-informed results may be used to weight and select ensemble members.

1.3 Dissertation Prologue

In Chapter II, we review background material beginning with an overview of bathymetry in section 2.1 and bathymetric modeling in section 2.2. In section 2.3, we present an overview of regression to familiarize the reader with the most common bathymetric modeling techniques, distinctions between them, and when preferential. In our experimentations, we utilize interpolation schemes (via the MergeBathy software suite) based on these reviewed regression techniques to construct DBMs. Additional

methods implemented by the author external to MergeBathy for DBM construction and analyses of experimentations were also OLS based, including our new w -ELS/ELS.

Before introducing regression techniques, however, we discuss the bias-variance trade-off in section 2.3.1 to aid in contrasting techniques and their application in bathymetric modeling. In section 2.3.2, we begin with a review of the seminal OLS. OLS is the foundation from which we obtain other regression techniques by relaxing its assumptions in section 2.3.3. In section 2.3.4, we discuss how these regression techniques apply to modeling sparse bathymetric data. In section 2.3.5, we introduce linear mixed models (LMMs) which were employed in analyses for our experimentations. Finally, in section 2.3.6, we close our review of regression with a discussion of the diagnostic and statistical tools that were employed to check regression assumptions (for regressions implemented external to MergeBathy either for DBM construction or analyses of our experimentations).

Section 2.4 presents the MergeBathy software suite vital in our experimentations for efficient DBM generation of various interpolation schemes. Using the same platform, avoids effects from utilizing different software tools that may affect DBM accuracy in our experiments. Section 2.5 presents the set of MergeBathy interpolation schemes we evaluate in our first study. From the results of the first study, we select two interpolation schemes to serve as our nominal-informed primitive interpolators and ensemble members in our second study. We evaluate these methods, along with the most widely used bathymetric gridding technique, Generic Mapping Tools (GMT) (Paul Wessel et al., 2013) SIT, against additional methods implemented by the author external to

MergeBathy to investigate the efficacy of our new nominal-informed ensemble approach, w -ELS, (and more generally, nominal-informed modeling) for modeling bathymetry.⁷

Section 2.6 presents the combined bathymetric and uncertainty estimator (CUBE) uncertainty propagated variance estimator (CURVE) for uncertainty estimation, developed by Paul Elmore in communications with Brian Calder. The author implemented this procedure in MergeBathy and for GMT. The procedure attributes gridded uncertainty to a DBM for methods lacking inherent uncertainty estimation, common of the preferred more efficient techniques for modeling sparse bathymetric data.

In Chapter III, we present our new nominal-informed ensemble bathymetric modeling approach. In section 3.1, we consider our seafloor as a weighted composition of geomorphological primitives which we assume are identifiable by classifiers as nominal data. In section 3.2, we present 1) ELS, an OLS framework to include full utilization of conflicting nominal information in DBM construction and 2) w -ELS, our new nominal-informed differentially weighted ensemble approach in DBM construction that utilizes ELS to compute an informed differential weighting to ensemble nominal-informed DBMs.

In Chapter IV, we present our research approach and outline our testing procedures for our experimentations, organized as two studies. Chapter V presents our first study which investigates the use of nominal information to select feature-favoring interpolators. Chapter VI presents our second study which evaluates the use of nominal information in bathymetric modeling. We conclude with a summary in Chapter VII.

⁷ GMT “are widely used across the Earth, Ocean, and Planetary sciences and beyond. A diverse community uses GMT to process data” (The GMT Developers, 2021). See <https://www.generic-mapping-tools.org/>.

CHAPTER II – BACKGROUND

In this chapter, we present relevant background materials. In section 2.1, we introduce bathymetry, including its history and the problems posed. In section 2.2, we discuss the modeling techniques employed to construct seafloor interpretations from depth measurements and their inherent problems. In section 2.3, we present an overview of regression in the context of bathymetric modeling, highlighting interpolators utilized in our research. Section 2.4 presents the MergeBathy software suite utilized to generate DBMs and where upon critical efforts were made in support of this dissertation. Section 2.5 lists the various interpolation schemes utilized in MergeBathy. In section 2.6, we discuss a bathymetric uncertainty attribution algorithm implemented in support of this dissertation.

In section 2.1 and section 2.2, we describe work performed, in part, with Paul Elmore, A. Louise Perkins, and Brian Bourgeois. In section 2.3, my specific contributions are:

- I implemented in a script various statistical and diagnostic tools to validate and inspect DBMs and regressions.
- I implement in a script frequentist and Bayesian linear mixed model, along with statistical and diagnostic tools to validate and perform inferences.

In section 2.4, we describe work performed, in part, with Todd Holland, Nathaniel Plant, Kevin Duvieih, Paul Elmore, Will Avera, Brian Bourgeois, A. Louise Perkins, and David Lalejini. My specific contributions are:

- A poster and paper from which this section on MergeBathy is adapted. Co-authors and developers include Todd Holland, Nathaniel Plant, Kevin Duvieih, Paul

Elmore, Will Avera, Brian Bourgeois, A. Louise Perkins, and David Lalejini (S. J. Zambo et al., 2016, 2017a; S. Zambo et al., 2018).

- The following text highlights my involvement in MergeBathy and applies to both C++ and MATLAB versions.
 - I modified, extended, and validated MergeBathy versions, originally developed by Todd Holland and Nathaniel Plant, and extended by Paul Elmore.
 - I extensively debugged MergeBathy for correct computations and DBM generation, and significantly improved performance and stability.
 - I rectified multi-threading and cross-platform compilation.
 - I aligned output from C++ and MATLAB versions.
 - I developed a suite of test cases to validate MergeBathy.
 - I updated MergeBathy documentation and test cases originally developed by Todd Holland and Nathaniel Plant.
 - I updated and implemented test cases developed by Paul Elmore.
 - I implemented and validated many computational procedures including Brian Bourgeois' Kalman filter algorithm, handling of uncertainty, and Paul Elmore's CURVE discussed in section 2.6.
 - I implemented and validated the CURVE algorithm into the opensource GMT software code base for their inclusion.
 - I compiled and updated third-party libraries.
 - I implemented additional user-specified input parameters for better user control and flexibility, for example, uncertainty handling.

- I implemented the bathymetric attributed grid (BAG) files output format (Brian R. Calder et al., 2005; Open Navigation Surface Working Group, 2006).^{8, 9}
- I setup Mercurial, “a free, distributed source control management tool” (Mercurial, n.d.).
- I setup MergeBathy (pre-compiled, source code, examples, data, documentation) for open-source development and freeware availability for bathymetric processing on GitHub.
- MergeBathy was a project deliverable to the Naval Oceanographic Office. The Naval Oceanographic Office is responsible for worldwide ocean mapping and MergeBathy is one of their key tools to produce hydrographic products.

In section 2.5, we discuss the MergeBathy interpolation schemes investigated in our first study. MergeBathy interpolators, originally implemented in MergeBathy by Todd Holland and Nathaniel Plant and extended by the author with Paul Elmore and Brian Bourgeois, were extensively utilized in our experimentations to construct DBMs.

In section 2.6, we describe CURVE work performed, in part, with Paul Elmore, A. Louise Perkins, and Brian Bourgeois. My specific contributions are:

⁸ BAG is a non-proprietary file format developed by the Open Navigation Surface Working Group; version 1.0.0 (Brian R. Calder et al., 2005; Open Navigation Surface Working Group, 2006).

⁹ BAG utilizes additional third-party libraries not listed.

- A poster and paper from which this section on CURVE is adapted. Co-authors include Paul Elmore, A. Louise Perkins, and Brian Bourgeois (S. J. Zambo et al., 2015a, 2015b).
- The CUBE propagated uncertainty equation was originally developed by Brian Calder. The additive bottom-slope term was suggested by Brian Calder in communication with Paul Elmore. Paul Elmore added this bottom-slope term and developed the CURVE algorithm.
- I implemented and validated the CURVE algorithm into the MergeBathy C++ and MATLAB versions.
- I implemented and validated the CURVE algorithm into the opensource GMT software code base for their inclusion.

2.1 Bathymetry

The ocean composes 71% of Earth's surface and is the driving force of many natural processes (Weatherall et al., 2015). The topography of the ocean floor is as diverse as the forces that form it. Tectonic plates (and their underlying heat element) drive common topological features of interest. Hot-spot volcanic activity forms seamounts of varying size, steepness, and shape. Mid-oceanic ridges, which are large chains of mountains, form from mantle upwelling that pushes the seafloor apart at the boundaries of tectonic plates. The plate often then subducts back into the mantle at a trench located at an opposite end from the ridges. As the plate grows at one end and subducts at the other, the seamounts and ridge mountains slowly move away from the thermal sources that created them. In time, seamounts submerge further under the ocean due to erosion and sediment fills in valleys.

Accurate maps of the seafloor add value to communities from environmental societies and organizations, commercial and governmental agencies, and university research. Accurate topography improves other related interests, including navigation safety, military operations, conservation of biological habitats and processes, shipping, transoceanic cables, fisheries, wind and current turbines, solar farms, and gas and oil operations.

Direct measurements of the ocean floor are very expensive and time-consuming to collect, however. Within the public domain, survey data account for only 18% of prepared bathymetric grids of our ocean seafloor; the other 82% are predictions from satellite altimetry data (International Hydrographic Organization - Intergovernmental Oceanographic Commission, 2019; L. Mayer et al., 2018; Weatherall et al., 2015).¹⁰ Worldwide collaborative initiatives are making large efforts towards completely mapping the ocean floor (L. Mayer et al., 2018; Wölfl et al., 2019). For example, crowdsourced bathymetry has been embraced (Brian R. Calder et al., 2018, 2020; International Hydrographic Organization, 2018). Figure 2.1 depicts total soundings for the world (International Hydrographic Organization, n.d.-b).

¹⁰ Satellite altimetry predictions are restricted in areas covered by ice (Weatherall et al., 2015).

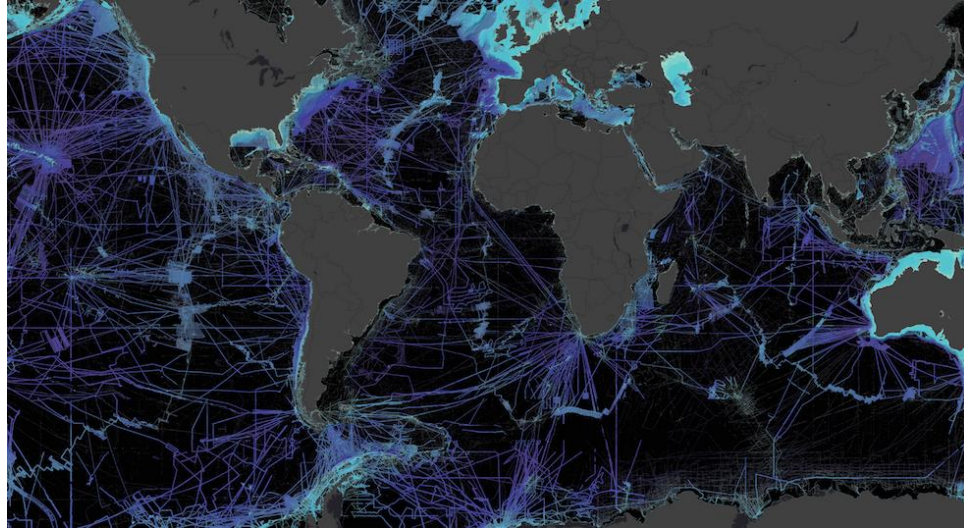


Figure 2.1 “The World Reference for Raw Bathymetry” (International Hydrographic Organization, n.d.-b).

“Less than 18% of the deep ocean floor has been mapped with direct measurement and approximately 50% of the world’s coastal waters remain unsurveyed. (Source: GEBCO 2019).” (International Hydrographic Organization, n.d.-b). Black regions indicate no data (unsurveyed).

Submarine geomorphology (Micallef et al., 2017; Ziyin et al., 2021) is a new field of research quickly gaining momentum in bathymetric modeling, and within it, the research fields of seafloor classification and marine geomorphometry (Lecours et al., 2016; V. Lucieer et al., 2019; Submarine Geomorphology Working Group, 2021).¹¹

Geomorphology is “the interdisciplinary and systematic study of landforms, their landscapes and the earth surface processes that create and change them.” (Submarine Geomorphology Working Group, 2021). Research in seafloor classification extends well beyond identifying geomorphological functional forms, as in this dissertation, to meet a wide variety of objectives (Vanessa Lucieer et al., 2018) (for example, segmenting the

¹¹ The Submarine Geomorphology Working Group of the International Association of Geomorphologists (IAG) was established in 2013 to support research in these emerging fields (Micallef et al., 2017; Submarine Geomorphology Working Group, 2021).

seafloor (Giuseppe Masetti et al., 2018) for mapping bio-diversities, habitats, or for geographic information systems [GIS]). Typically, classifying seafloor topography utilizes dense multibeam data coverage over shallow regions, however, (A. Wang et al., 2021) provided a method for classifying in deep waters using dense multibeam, and (Lawson et al., 2017) performed deep-water classification utilizing sparse data.

Geomorphometry is the derivation of various topographic metrics from models (T. Hengl & Reuter, 2008; Pike et al., 2009). Often, machine learners learn from these derived metrics. In (Franklin, 2020), they discuss the important benefits and necessity of properly utilizing geomorphometry in remote sensing.

Current maps and grids that combine both data products (predicted bathymetry from altimetry and gridded bathymetry from measurements) into a worldwide map are available from the General Bathymetric Chart of the Oceans (2020) (GEBCO) (Weatherall et al., 2015).

Combining bathymetry of variable resolutions and quality requires efficient algorithms to mitigate inaccuracies incurred from combining heterogeneous data. Typically, research focus has been through mathematical improvements. Brian R Calder (2019b) developed an efficient algorithm to determine the spatial resolution of a merged DBM by aggregating at spatial levels, where one begins with fine resolution bathymetry and increases the number of points utilized in computations until reaching an acceptable threshold number of points, and then proceeding to coarser resolutions. Brian R Calder (2019a) devised an efficient spatially parallelized technique.

However, new research has been towards aiding users who typically suffer from the difficulties of merging variable bathymetry by developing algorithms and tools based

on ML and AI techniques. In particular, the inclusion of subjective expertise and utilization of all available supplemental information towards guided systems for informed decision-making approaches. Elmore et al. (2018) utilized Bayesian and fuzzy logic to create an expert system to inject subjective experience. Similarly, Kastrisios et al. (2020) utilized an all-encompassing worldview approach to inject subjective experience for comprehensive decision-making.

Before 1940, depth measurements were slow and error-prone lead-line surveys, where surveyors lowered a plumb bob to the ocean floor and determined the depth from markings on the attaching rope or cable (Carpine-Lancre et al., 2003; L. A. Mayer, 2006a, 2006b). Their replacement was single beam echo sounders, which dominated surveys until the 1980s.

Multibeam echo sounder systems followed and are still the leading technique for deep-water surveys. Multibeam systems work by using two arrays, one positioned along the ship track and another orthogonally placed across the ship track. The along-track array lies in the direction of the ship's heading and transmits a narrow beam perpendicular to the ship's heading, while the across-track array lies perpendicular to the ship's heading and forms many narrow receive-beams that are parallel to the ship's heading, as seen in Figure 2.2.¹² This technology provides for full coverage (full ensonification of the local seafloor) by allowing the reception of many simultaneous

¹² Along-track array transmit beams are typically 120 – 150 degrees wide in the direction perpendicular and narrow in the direction parallel to the ship's heading. Across-track array forms typically 100 - 240 narrow receive beams parallel to the ship heading (L. A. Mayer, 2006b).

returned signals (the intersection of the transmit beam with the receive beam) along the wide width of the transmit swath.¹³

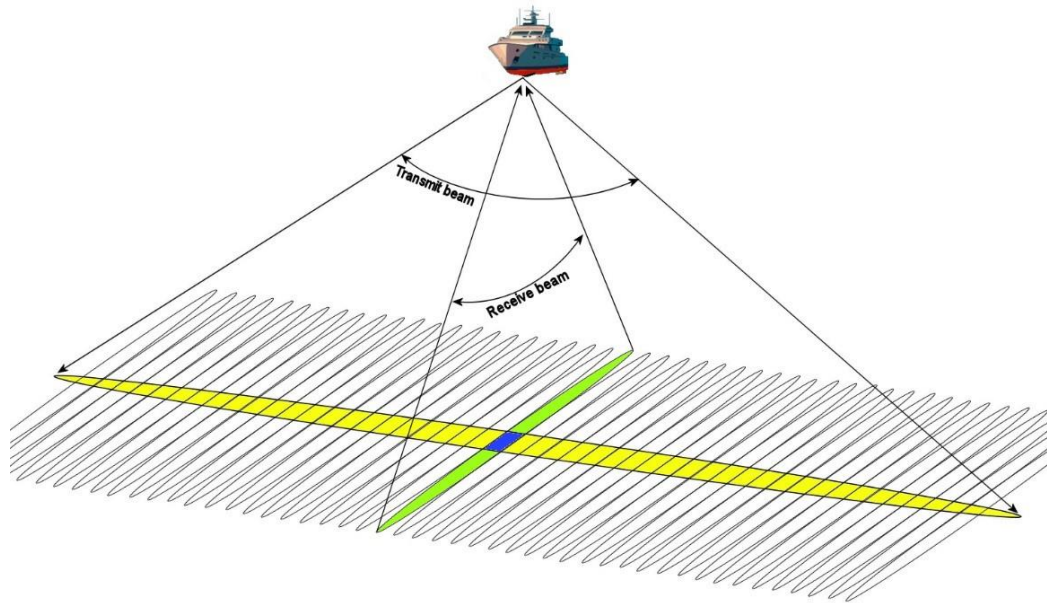


Figure 2.2 Example of multibeam bathymetric data collection.

Multibeam orthogonal arrays where the along track transmits a narrow beam perpendicular to the ship's heading (yellow) and the across track receives many narrow beams parallel to the ship's heading (green) (AML Oceanographic, 2016). The blue square is a single sounding (measurement).

Bathymetry predicted from satellite altimetry computes from an ill-posed inversion of marine geoid height measurements collected by satellite altimeters (W. H. Smith & Sandwell, 1997). Approaches for predicted bathymetry surfaces in knowledge-limited areas are documented in W. H. Smith & Sandwell (1997) and Calmant et al. (2002) who combined altimetry with echo sounding data. Bathymetry measurements constrain the ill-posed problem. The resultant map of predicted bathymetry has an average global resolution of 2 arcminutes (about 3 km) with up to 30 arcseconds (about 1

¹³ “as much as 7.5 times the water depth ... with each measurement having excellent horizontal and vertical resolution.” (L. A. Mayer, 2006b)

km) in some regions.¹⁴ Later, Sandwell & Smith (2009) improved the use of gravitational anomalies to resolve features greater than 24 km by reducing Root Mean Square (RMS) errors in their source data. Recently, Hu et al. (2015) then incorporated information from the lithosphere to compute the gravity anomalies and the vertical gravity gradient to gain greater resolution in sparse data regions.

Tozer et al. (2019) produced the newest global bathymetry and topography grid at 15 arcseconds which serves as the base global grid utilized in the newest GEBCO grid (GEBCO Compilation Group, 2020). Verron et al. (2020) anticipate valuable altimetry data resulting from a satellite drifting out of orbit to provide great insight in bathymetric modeling, including the identification of many undocumented seamounts less than 2 km.

2.2 Bathymetry Modeling

Algorithms used to generate DBMs for the ocean floor fall into two general categories, either for dense or sparse data.¹⁵

Dense data techniques, based on statistical estimation, include the Kalman filter and localized regression (LOESS/LOWESS). The Kalman filter (Kalman, 1960) is a Bayesian linear estimator, used by the combined uncertainty and bathymetry estimator (CUBE) for on-scene multibeam sonar data cleaning and gridding (B. R. Calder & Mayer, 2003). Based on the method of Cleveland (1979), Holman et al. (2013) used localized regression for coastal bathymetry, while Bourgeois et al. (2016) and B. Calder (2006) used localized regression for archived bathymetry processing.

¹⁴ We have less than 10% coverage at 1-arcminute (1,852 m) resolution explored (Becker et al., 2009).

¹⁵ See (Ladner et al., 2017) for a novel approach that spans both of these categories.

The second category is sparse data appropriate techniques. These techniques honor the data points¹⁶ – a necessity when we have sparse data, as there is not enough information to discard data as errant. These include bi-cubic interpolation, splines-in-tension (SIT), and kriging.

Bi-cubic interpolation (De Boor, 1962) is one of the many techniques used by the Naval Oceanographic Office Digital Bathymetric Data Base - Variable Resolution (DBDB-V) (U.S. Naval Oceanographic Office (NAVO), 2003) to stitch together data from different data sources to provide bathymetric data grids of varying resolutions from 2 arcminute to 30 arcseconds (Steed & Rankin, 2003).¹⁷ SIT computes a minimum curvature spline with a tension term to reduce spurious oscillations (W. Smith & Wessel, 1990). It is the de facto standard for processing bathymetric data, available as the primary interpolation technique of the de facto standard bathymetric processing software utilities, GMT (Paul Wessel et al., 2013) and Multibeam (MB) – System (Schmidt et al., 2003). Kriging (Matheron, 1963) is a spatial best linear unbiased estimators (BLUE), meaning out of all unbiased estimators, it provides the lowest variance of the estimate. Kriging builds variograms of spatial autocorrelations, but its $O(n^4)$ complexity makes it undesirable for large data sets (Srinivasan et al., 2010). Since kriging is a data-honoring interpolator, P. A. Elmore & Steed (2008), International Hydrographic Organization - Intergovernmental Oceanographic Commission (2019), and B. Calder (2006) utilized ordinary kriging to restore finer details lost from performing localized regression.¹⁸ The

¹⁶ Techniques that ‘honor the data points’ or are ‘data-honoring’ mean the DBM goes through the data points.

¹⁷ DBDB-V is no longer available and has been replaced by GEBCO.

¹⁸ Ordinary kriging assumes the mean is constant and unknown (N. A. C. Cressie, 1993).

localized regression is capable of modeling complex topographies by providing a scale-controlled smoothed surface (B. Calder, 2006; P. A. Elmore & Steed, 2008), but it does not honor the data points. By adding the kriged residuals, the smoothed surface becomes an exact fit (a necessity for sparse data) that decays smoothly (a necessity for a continuous topography) and remains scale-controlled (a necessity for modeling).

Regardless of the quality of any single interpolator, they are prone to over-fitting errors and outlier sensitivity when used alone in uninformed sparse data regions.

Interpolators may over-fit to the data and not generalize to the actual surface well, thereby fitting to noise instead for increased inaccuracies. Interpolators sensitive to outliers allow bad data points (outliers) to affect the computed model negatively for high inaccuracies. Figure 2.3 demonstrates the negative effects of utilizing an interpolator alone with sparse data. This figure shows a common bathymetric scene composed of high-resolution multibeam sonar data illustrated in color. The regularly shaded gray areas, or swaths, lack data. When interpolated with SIT, physically unrealistic contours, denoted in white, occur in the swaths with no data. These aberrations require a cartographer to correct manually based on subjective, unstructured expertise.

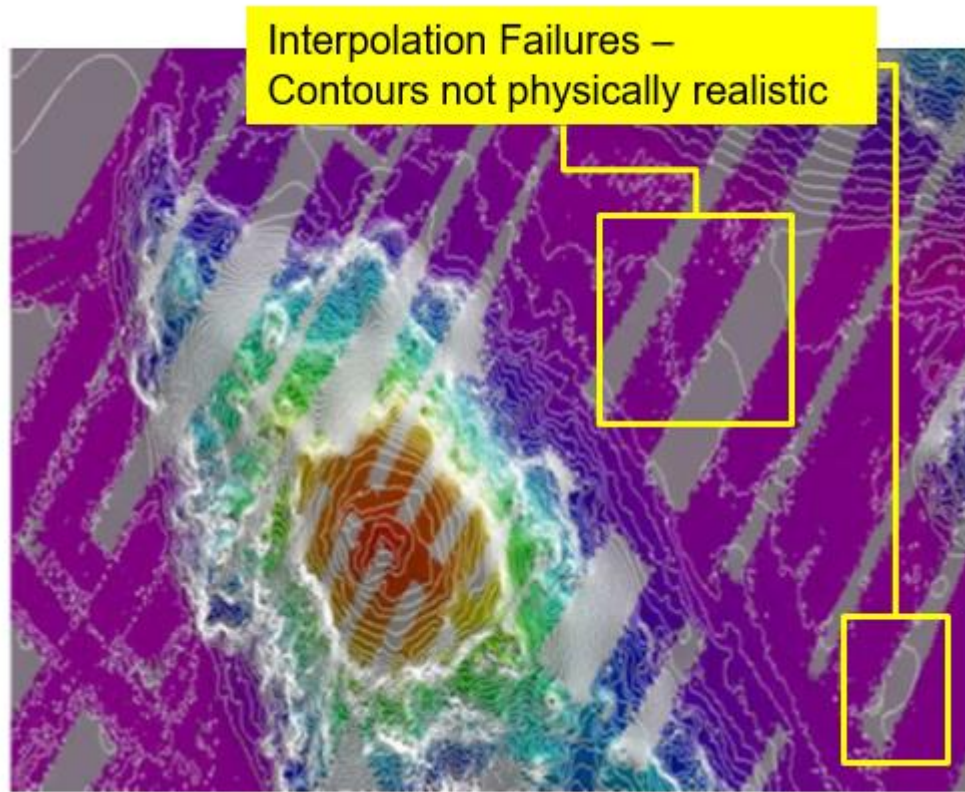


Figure 2.3 Example of sparse data interpolation failures.

Multibeam sonar survey of a seamount where color indicates measurements, gray has no data and white contour lines are one-interpolation predictions (SIT) (P. Elmore, personal communication, May 5, 2016). Depths are equal on a contour.

Next, in section 2.3, we present an overview regression as it pertains to the interpolators utilized in this work for modeling bathymetry.

2.3 Regression

In this section, we present an overview of regression in the context of our bathymetric modeling techniques, utilized in in our experimentations and in support of this research, for an understanding as to how these various interpolators relate to each other. Regression creates a model of the relationship between independent and dependent

variables. We consider regression as a tool for the construction of DBMs. In general, regression techniques may be either parametric or non-parametric.¹⁹ ELS is parametric.

Parametric techniques estimate coefficients of assumed model statistics from data which are then used to make estimations of unseen dependent variable values.²⁰ The models may be linear or nonlinear in the unknown coefficient parameters and may model linear or nonlinear relationships in the data. OLS is one example of a parametric regression technique.

Non-parametric regression techniques do not use a given global model explaining the relationship between the independent and dependent variables but discover it implicitly through the data.²¹ In these techniques, we control how and to what extent the model is fit rather than by building an explicit model function defining the relationship. These relationships may be linear or nonlinear. The main purpose of non-parametric regression is to make estimations of unknown dependent variable values as needed rather than obtaining an explicit functional form. Therefore, they do not estimate the coefficients of a global model, but instead locally smooth the data towards the local mean. Non-parametric regression techniques are preferred when the global model is unknown.

We first present the bias-variance trade-off in section 2.3.1 which will facilitate our theoretical overview of regression and differentiation between methods. Section 2.3.2 presents the general assumptions for least squares, the most rudimentary. Those

¹⁹ There are also semi-parametric techniques (Frank E. Harrell, 2001).

²⁰ This has a greater generalization probability (Vapnik, 1998)

²¹ Work in AI over the last half century demonstrated that this step is not always generalizable (Vapnik, 1998).

fundamental assumptions may be relaxed as discussed in section 2.3.3. Section 2.3.4 discusses regression when modeling sparse bathymetric data. Section 2.3.5 introduces LMMs as they were utilized in analyses, and section 2.3.6 discuss checking regression assumptions.

2.3.1 The Bias-Variance Trade-Off

Our regressions utilize squared error loss. Error can be split into reducible and irreducible components. The irreducible component is the orthogonal error that we cannot control, and the reducible component is error within our approximation space during the modeling process. Of the reducible part, we have error due to the bias and error due to the variance – for example, the mean square error (MSE) for the bias-variance decomposition of squared error (Hastie et al., 2009). MSE evaluates the overall performance of an estimator by conveying the trade-off between bias and variance (Kennedy, 2008). This is the bias-variance decomposition,

$$MSE = variance + bias^2.$$

The squared bias term represents the portion of the error due to the difference of the estimated mean from the true mean. The variance is the expected squared deviation of the regression surfaces about its mean (Hastie et al., 2009). For an unbiased estimator, MSE reduces to the variance and RMS becomes the standard deviation. OLS, LOESS, and kriging provide uncertainty as MSE.

The bias-variance trade-off is the balancing of errors incurred from assumption violations biasing the estimator and reducing prediction inconsistencies. A biased estimator uses an incorrect model (Geman et al., 1992).

Regression techniques control the bias-variance trade-off in a variety of ways. Through various diagnostic tools, one evaluates and modifies the trade-off according to what is reasonable for the problem at hand. Balancing bias-variance trade-off is subjective, but one aims to obtain the BLUE. High bias or variance for an estimator makes its estimates suspect. Suspect estimates are untrustworthy, and caution is necessary in their use. It is crucial to investigate assumption violations to understand the bias-variance trade-off for any estimator to gain reasonable confidence in its estimates.

Even with care, assumptions are rarely met. In general, we investigate for assumption violations via the residuals and make modifications accordingly to reduce violations and limit their effects for estimators that are near unbiased and consistent (Kennedy, 2008; Wooldridge, 2015). In other words, how we model the data controls the bias-variance trade-off.

An example of an effective trade-off is a model that fits the data well and generalizes well. A model that accurately and precisely represents the generating function of observed data will model well the observed data and generalize well to unseen data. Such a model is beyond the scope of this dissertation, however. We desire an accurate and precise model having the lowest bias and variance.

MSE is useful in representing the bias-variance trade-off for our theoretical overview of regression, and when discussing methods and how they relate.²² However, in our experimentations, we utilize the RMS and cumulative relative absolute error (CumRAE) to compare the performance of our models. Relative metrics give an intuitive

²² MSE, along with other standard metrics, proved useful in our preliminary analysis but their details have been omitted here for brevity.

and effortless way to compare the performance of the interpolation techniques (J Scott Armstrong & Collopy, 1992; J. Scott Armstrong, 2001).

2.3.2 Least Squares Assumptions

When we measure a phenomenon, noise obscures the generating functions, and we may utilize regression to reduce the noise. In OLS, we select a candidate model and fit it to the data. OLS estimates the parameters of the model which minimize the mean squared residuals. If it fits well, we utilize the model, but if it does not then we try another model. Only through various diagnostics on the residuals can we gain confidence that our model has a low bias and variance. Simpler, over-smoothed models tend to increase bias and reduce variance. Too complex, under-smoothed models overly fit to the noise in the data which tends to increase variance and reduce bias. A variance increase may introduce non-physical inconsistencies. In general, bias affects accuracy and variance affects precision. When we over-smooth, we lose information, and when we under-smooth, we do not remove enough noise.

When performing linear regression, we want to obtain the BLUEs of the coefficients in a linear model. These are the estimators with the lowest variance out of all the unbiased estimators. That is, they are the most efficient meaning they require fewer observations to obtain similar performance (Wooldridge, 2015). An unbiased estimator is one which estimates the true value on average (Draper & Smith, 2014).

The Gauss-Markov theorem (Wooldridge, 2015) states that, if it exists, OLS is a BLUE of model coefficients, if the errors are uncorrelated and homoscedastic with a zero-mean. Homoscedasticity is when the variance of the error remains constant across

the values of the independent variables. Uncorrelated and homoscedastic errors are spherical errors. For errors ε , the Gauss-Markov assumptions are expressed as

- 1: $E[\varepsilon_i] = 0$ (*zero mean*)
- 2: $Var(\varepsilon_i) = I\sigma^2$ (*homoscedastic constant variance*)
- 3: $Cov(\varepsilon_i, \varepsilon_j) = 0, \forall i \neq j$ (*uncorrelated*).

When these ideal assumptions are met, the Gauss-Markov theorem assures the OLS estimators have the lowest variance of all unbiased linear estimator. When performing nonlinear regression, the Gauss-Markov theorem does not apply as solving a nonlinear least square may introduce bias via linearization which approximates the nonlinear function by truncating a series expansion (Draper & Smith, 2014).

Both linear and nonlinear least squares make these three BLUE assumptions. For dependent variable y , independent variables $\{x_i\}_{i=1\dots k}$, unknown parameters $\{\beta_i\}_{i=1\dots k}$, and error ε , we express a linear fit as

$$y = \beta_0 + \beta_1 x_1 + \beta_2 x_2 + \dots + \beta_k x_k + \varepsilon.$$

Any model that utilizes non-constant $\beta_i, i = 1, \dots, k$ values is nonlinear.²³

However, intrinsically nonlinear models cannot be linearly transformed and require nonlinear regression. Typically, nonlinear regression performs linearization which transforms an intrinsically nonlinear model into a linear approximation by performing a Taylor series expansion about point and truncating to the first derivatives (Draper & Smith, 2014). Linearization introduces bias. Thus, regression is a trade-off between either

²³ We may transform any nonlinear models that is not intrinsically nonlinear into a linear model via a linear transformation. A linear transformation applies an operator on the dependent variable to transform the model such that it is linear in the parameters. If assumptions are maintained, this transformation incurs no trade-off between bias and variance, else we have a variance increase.

increasing bias by using the nonlinear model or increasing variance by using a simpler linear model.

Another assumption of least squares is there are no errors in the independent variables, and they are not correlated with the error. This assumption is weak as there are cases where violations of this assumption will incur “little to no bias” (Draper & Smith, 2014, p. 90). Thus, errors in the independent variables leads to a trade-off between either increasing bias by utilizing least squares or increasing variance by utilizing other techniques (Draper & Smith, 2014). We may write

$$E[X^T \varepsilon_i] = 0$$

for uncorrelated regressors with errors. Regression assumes linear independence and when this is violated, the residual error variance increases. If not accounted for in the model, correlated regressors may result in numerically unstable estimates due to incorrectly specifying the relationship between the dependent and independent variables and also has the potential to enhance matrix-rank deficiencies resulting in ill-conditioned results (Draper & Smith, 2014). Thus, multicollinearity may lead to a trade-off between either increasing bias by omitting correlated variables or increasing variance by including them (Wooldridge, 2015).

While least squares do not require errors be normally distributed nor IID, making these assumptions allows for the use of significance testing to check for several assumption violations. Many of these tests, as well as confidence interval computations, depend on the additional assumption of normal errors (Draper & Smith, 2014). We may write

$$\varepsilon \sim \mathcal{N}(0, \sigma^2) \text{ (normality and independence).}$$

To utilize OLS, we would like to setup the regression problem and determine if the assumptions on the errors are appropriate to make. When the problem meets the OLS assumptions on the errors, we try to find a linear model that produces residuals which reflect the errors by upholding the assumptions. This is an iterative process of applying a model, investigating the residuals for violations, and modifying the model. However, if initial assumptions on the errors are incorrect, which is typically the case, we will not be able to find a model that produces residuals that do not violate assumptions.

We check if the initial assumption on the errors were incorrect by investigating the residuals, as well. When we model the data well, the residuals will reflect the errors and we can check them to see if our initial assumptions on our errors were incorrect. However, it is difficult to determine if assumption violations are from an insufficient model or incorrect initial assumptions on the errors.

The quality of the regression, then, depends on the extent of assumption violations and trade-offs made between the bias and variance. Poorly modeled data lead to biased and inconsistent estimators.

We list the classical least squares assumptions of OLS in Table 2.1 for reference. Assumptions 1-3 are needed for the Gauss-Markov theorem to assure OLS is the BLUE, assumptions 1-6 are OLS model assumptions, and assumption 7 is a distributional assumption on the errors for statistical testing.

Table 2.1

OLS Regression Assumptions

ID	Assumption	Description
1	$E[\varepsilon_i] = 0$ (0 - mean)	0-mean
2	$Var(\varepsilon_i) = 1\sigma^2$	Homoscedastic errors (constant variance)
3	$Cov(\varepsilon_i, \varepsilon_j) = 0, \forall i \neq j$	Uncorrelated errors
4	$y = \beta_0 + \beta_1 x_1 + \beta_2 x_2 + \dots + \beta_k x_k + \varepsilon$	Linear in parameters
5	$E[X^T \varepsilon_i] = 0$	Uncorrelated regressors with errors
6	$P[rank(X) = p] = 1$	Linear independence
7	$\varepsilon \sim \mathcal{N}(0, \sigma^2)$	Normality and independence of errors

Summary of OLS assumptions presented in the text.

2.3.3 Relaxing OLS Assumptions

In this section, we relax various OLS assumptions presented previously in section 2.3.2 to obtain methods with greater flexibility. We discuss the consequence of relaxing assumptions in terms of the bias-variance trade-off, discussed in section 2.3.1. Often, real-world problems do not meet the OLS model assumptions, and we need another way to model the data without these restrictions. This is our bathymetric data scenario. Various non-parametric techniques exist which relax OLS assumptions. These include LOESS, kriging, and smoothing splines. Both LOESS and smoothing splines are smoothers, and as such may increase bias to reduce variance (Geyer, 2006). We utilize ordinary kriging on LOESS residuals to restore finer details lost by over-smoothing in LOESS. Ordinary kriging is the best linear unbiased predictor (BLUP).

2.3.3.1 LOESS

LOESS is a technique which fits functions to data by smoothing the data locally (Cleveland & Loader, 1996). LOESS performs a locally weighted least squares polynomial regression at each point. It is a non-parametric technique that assumes parametric localization. Parametric localization assumes that the function can be well approximated locally by a parametric function (Cleveland & Loader, 1996). In LOESS, a specified span value controls the number of points to use which are then weighted by a

specified weight function (originally, the tricube function) when it performs the weighted least squares regression (Cleveland, 1979).

LOESS adheres to the same assumptions as OLS regression except for linearity (Cleveland et al., 1988). Instead of assuming linearity in the global regression function, LOESS assumes smoothness. LOESS relaxes the linearity assumption such that it adheres only within the local area under consideration instead of globally. This linearity relaxation is why locally weighted regression approaches are so advantageous. They allow for simple analysis of complex relationships, both linear and non-linear, by approximating a local subset with low-degree models.

In general, the OLS assumptions adhere locally in LOESS. The number of points used in the local regression and the degree of the model fit to the data affect the bias-variance trade-off (Cleveland & Loader, 1996). Using too many points will over-smooth the data for a loss of information and an insufficient number of points will overly fit the data by not smoothing enough for an increase variance (Hastie et al., 2009). A higher-degree model may reduce bias but leads to potential overfitting and requires estimating more coefficients which increases the variance. The weighting function also affects the bias-variance trade-off, but not as much as the span and polynomial degree. Typically, we choose a smooth and continuous weighting function.

One performs the same diagnostic checks as those for OLS to validate the LOESS assumptions, restricting the linearity assumption locally in evaluating a model's fit. A well fit local model will have lower overall residuals.

2.3.3.2 Stochastic Estimation

Another approach is to model the probability density function directly, and then use the probability density function to generate real world results. This, of course, is a generalization.

2.3.3.2.1 Bathymetric Data as a Gaussian Process

Kriging and the Kalman filter consider data as a Gaussian Process. These statistical estimators estimate parameters by estimating the joint conditional (bivariate or more generally, multivariate) probability distribution of the data. In these terms, our bathymetric data are a set of observations that are continuous random variables with Gaussian distributions and are spatially continuous. In other words, our bathymetric data is a random Gaussian process with a joint Gaussian distribution of all the random variables. Techniques which model data from a random process as a Gaussian process account for the spatial continuity in its estimators.

2.3.3.2.2 Ordinary-Kriging

Kriging is a geostatistical technique that uses the spatial information within the data to form its predictors. We use the term predictors here instead of estimators because we want to model the random-effects in the data, having assumed data are from a random (stochastic) process (C. R. Henderson, 1963; C. Henderson, 1949). Kriging has similar structure as mixed-effect models, where the data is modeled as having fixed-effect and random-effect components along with the traditional independent random error component. Fixed effects are the deterministic components of the trend modeled by traditional deterministic methods, such as OLS and LOESS. Random effects are the stochastic components of the autocorrelated variations in the detrended residuals modeled

by geostatistical methods, such as kriging. We want the BLUP instead of the BLUE. BLUP is of random-effects while BLUE is of fixed-effects (Goldberger, 1962; C. R. Henderson, 1963). Kriging, interchangeably referred to as Gauss-Markov estimation and Gaussian process regression, uses variograms to map the spatial correlations between points.

There are many variations of kriging, so we narrow our discussion here to the scope of its current use within MergeBathy: ordinary kriging of LOESS residuals. MergeBathy uses ordinary kriging on LOESS residuals to restore finer details lost by over-smoothing for a reduced bias. Here, kriging is an exact interpolator which honors data. Kriging upholds the assumptions for LOESS with additional kriging assumptions on the LOESS residuals.

Ordinary kriging (N. A. C. Cressie, 1993) assumes an intrinsically stationary model where the data are from a continuously spatial, random (stochastic) process with an unknown constant mean. It also assumes that the predicted linear coefficients sum to 1 which guarantees unbiasedness. A third kriging assumption is normality and IID (OLS assumption 7), which LOESS already makes.

Under the assumptions of stationarity in the errors and the additional assumption isotropy in the errors, ordinary kriging is the BLUE (N. A. C. Cressie, 1993; N. A. Cressie, 1990; Srinivasan et al., 2010). Here, isotropy implies equal directional correlations among points (N. A. C. Cressie, 1993; Li & Heap, 2008). By manipulating the size of the neighborhood, we manipulate the nugget effect and control the bias-variance trade-off. A large kriging neighborhood reduces variance by reducing the nugget effect. Additionally, decomposition of data into non-stationary and stationary

components, the variogram fitted, and size of the neighborhood control the bias-variance trade-off (N. A. C. Cressie, 1993; N. A. Cressie, 1990; Tomislav Hengl, 2009; C. J. Paciorek, 2010; C. Paciorek, 2008; Zimmerman & Cressie, 1992).

While there are no explicit checks to validate ordinary kriging assumptions, initial exploratory data analysis ensures that any assumptions made are reasonable for the data. There are several diagnostic plots to investigate intrinsic stationarity including mean-median plot, square-root difference clouds, and pocket plots (N. A. C. Cressie, 1993). If these plots exhibit a trend, then the data must first be detrended before performing ordinary kriging. The detrending technique approximates the large variations to remove from the data, leaving the residuals as an estimate of the correlated errors.

Typically, bathymetric data are non-stationary (non-constant mean and variance), but we may decompose it into components based on spatial scales of fluctuations to utilize kriging. To meet the first assumption, we decompose non-stationary bathymetric data into a non-stationary trend and a stationary stochastic component via LOESS. Detrending with LOESS removes the larger-scale variations from the non-stationary data, leaving the correlated smaller-scale variations which include the random errors and those variations too small to predict from the resolution. For a given spatial lag and variogram, the correlated error component is intrinsically stationary (N. A. C. Cressie, 1993).

Under the LOESS assumptions, the LOESS residuals will be stationary with a zero-mean and constant variance, normal and IID. LOESS aids in the decomposition of non-stationary data into a deterministic non-stationary non-constant trend and a zero-mean stochastic intrinsically stationary, spatially correlated error component. LOESS estimates the large-scale variations, and we remove them from the data in a process

known as detrending. When detrending data for kriging, a robust method resistant to outliers is recommended (N. A. C. Cressie, 1993). While there is a robust version of LOESS, MergeBathy does not utilize it since we assume bathymetric data errors are normally distributed, making the non-robust LOESS sufficient (Cleveland, 1979). MergeBathy implements this approach following (B. Calder, 2006).

Since data decomposition is not unique and is the primary objective of utilizing LOESS, assumption checks to optimally balance the bias-variance trade-off of LOESS are not necessary. However, the adequacy of this decomposition in obtaining an intrinsically stationary component, from which to model the spatial dependences, may introduce bias in the variogram estimator since it utilizes LOESS residuals (N. A. C. Cressie, 1993). Leaving a substantial trend in the LOESS residuals, for example, may corrupt the variogram: an over-specification of the trend increases bias for a negligible effect on the variogram, while an under-specification leaves too much trend in the LOESS residuals and may corrupt the variogram by increasing its bias substantially. By electing to over-smooth the trend during LOESS, we take a conservative approach to help stabilize the empirical variogram computed (B. Calder, 2006). Moreover, kriging on the residuals introduces bias in the variogram estimation and is why we utilize a robust variogram estimator (N. A. C. Cressie, 1993).

To remove the large-scale variations, LOESS estimates the non-constant deterministic trend by performing a low-resolution mapping of the data. We utilize various diagnostic tools to check that the LOESS residuals are intrinsically stationary. From the LOESS residuals, one can estimate the variogram which characterizes the spatial dependence in the residuals and fit to it a variogram model. One can evaluate the

fit of the variogram to the estimated variogram via the diagnostic tools of OLS. From the fitted variogram, one can make spatial predictions utilizing the BLUP, ordinary kriging. Ordinary kriging of the LOESS residuals allows for a higher-resolution mapping by adding the spatial prediction to the lower-resolution mapping predictions.

The geostatistical approach implemented in MergeBathy follows (B. Calder, 2006). MergeBathy assumes data is second-order stationary, an assumption necessary for kriging in terms of the covariance function instead of the variogram. MergeBathy uses the methods of moments estimator to compute the empirical variogram and fits it to a spherical variogram model.²⁴ MergeBathy assumes anisotropy when computing the variogram.

2.3.3.2.3 Kalman Filter

The author would like to thank Brian Bourgeois for his extensive explanations on how Kalman filters work. The Kalman filter (Kalman, 1960) is a Bayesian linear estimator (Meinhold & Singpurwalla, 1983). This statistical estimator smooths data and as such, may not be suitable for sparse bathymetric data. However, it is suitable for dense bathymetric data and was used in CUBE for real-time gridding of high-resolution multibeam data (B. Calder, 2006).

The Kalman filter is a recursive process; at each iteration, it improves past estimates. It begins by computing estimates and uncertainties based on current information available and then updates these values when presented with a new

²⁴Equation 15-17 of (B. Calder, 2006)

observation by performing a weighted average, weighting estimates with a higher uncertainty more. This weighting is the Kalman gain.

Bathymetric data typically assumes Gaussian noise (International Hydrographic Organization, 2008), (see section 2.3.6). For white Gaussian noise, the Kalman filter is optimal; it minimizes the mean square error of the estimated parameters (Anderson & Moore, 1979).²⁵ The Kalman filter removes white noise from the data. If the error is not white noise, then given the mean and standard deviation of the noise, it is the best linear estimator (Anderson & Moore, 1979). We may check the optimality of the Kalman filter by checking if the residuals are Gaussian.

MergeBathy implements the Kalman filter using the same neighborhood data points as those of LOESS.

2.3.3.3 Smoothing Splines

Similar to LOESS, smoothing splines is a nonparametric regression technique which relaxes the OLS model linearity assumptions by instead assuming the regression function is smooth (Press et al., 2007). Since it does not evaluate a model's fit or assume a distribution, it does not perform any OLS assumption checks. Smoothing splines utilize a roughness penalty to control the amount of smoothness. Recall that the amount of smoothing performed controls the bias-variance trade-off. As smoothing increases, the bias increases and the variance decrease (Hastie et al., 2009). Both SIT techniques in MergeBathy are smoothing splines.

²⁵ White noise has uniform power at all frequencies in the frequency domain. Each data point has a noise value that is an independent (uncorrelated) and identically distributed random sample.

2.3.4 Regression in Modeling Sparse Bathymetric Data

When modeling sparse bathymetric data, we typically smooth locally while trying to honor the data. We smooth locally because there are not enough data points to approximate the mean by fitting a global model by least squares and we do not know the global function specifying the relationship between variables. In fact, this global function is what we are trying to learn from the data given the limited predictors we have. At the same time though, we would like to honor data points since we are limited in information for the bathymetric region since data points are distant from each other. Without multiple nearby data points (repeated measures) to average out error, we must trust in the data at hand.

Thus, we utilize nonparametric regression techniques that approximate the mean locally, such as smoothing splines and LOESS. Smoothing splines honor the data points located as the knots of the splines.²⁶ We smooth the spline function between the knots. LOESS does not honor the data but by kriging the LOESS residuals, we can force it. After performing LOESS, we have the additional option to correct for over-smoothing (a too-low bias) by kriging the LOESS residuals. Kriging the residuals produces a smooth curve of the small-scale variations. Small-scale variations are those variations not including the global trend, the random error, or variations smaller than the resolution. The smooth curve of residuals when added back to the LOESS approximation restores over-smoothed values to honor the data.

²⁶ When knots are co-located with the data points.

MergeBathy also allows local smoothing by smoothing splines before continuing to LOESS with optional kriging. Performing smoothing splines before LOESS may improve the LOESS approximation by up-sampling data. When data is too sparse for the resolution desired, smoothing splines provide a way to increase the data density along the smoothing spline approximation. When performing smoothing splines, we want to limit the amount of smoothing for a low-bias, high-variance approximation since we are up-sampling and not generalizing. The up-sampling of points will reduce the bias in LOESS. We wish to balance the bias-variance trade-off of the LOESS approximation such that it will generalize well. By compounding smoothing splines and LOESS, we incur an increase in variance for a potentially important decrease in bias, respectively. Since bias eventually dominates the bias-variance trade-off, the smoothing splines provide a way to keep the bias low when performing LOESS.

The performance of the various regression techniques depends on how the bias-variance trade-off was balanced for each technique given the data scenario. Typically, we play with balancing the bias-variance trade-off to obtain a nearly unbiased and consistent estimator by checking and correcting assumption violations and manipulating smoothing parameters. However, the intent of this study is not in optimally manipulating the bias-variance trade-offs of each regression technique but in the use of ensembles to mitigate the trade-off to produce a nearly unbiased and consistent estimator.

2.3.5 Linear Mixed Effect Models

Linear mixed effect models (or simply LMMs) (Andrew Gelman & Hill, 2006; Searle et al., 2006, 2006; West et al., 2014) extend linear models by allowing additional random effect terms, other than the error term, to be modeled. LMMs relax the normality

assumption on the error term by allowing autocorrelations and heteroscedasticities in the errors to be modeled. We use LMM when analyzing our experimentations.

Typical linear models are fixed-effect models which only include fixed effects with strong assumptions on the random errors. LMM include both fixed effects and random effects, other than the error term. LMMs allow additional random effects and the structure of the errors to be modeled (West et al., 2014). When analyzing our experimental data, we have random effects due to blocking, where we wish to account for correlated residuals within the same test case, and heterogeneous residual variances between interpolation schemes, because we expect the performance capabilities of the interpolations schemes to vary resulting in different variances.

A strict normality assumption is necessary for the analysis of variances (ANOVAs) to compute F-statistics for valid inference (Draper & Smith, 2014). An F-statistic is the ratio of two means which follows the F-distribution (chi squared distribution). An F-test computes an F-statistic and compares against an F-value derived by integrating the densities over intervals of the F-distribution. A p-value is the probability of getting data as extreme or more extreme than currently being tested under a true null hypothesis. A null hypothesis is the conjecture being tested at the unchanged, current state. The alternative hypothesis is the conjecture being tested. If the p-value computed from the F-test is too small, then we reject the null hypothesis in favor of the alternative hypothesis (Diez et al., 2013). This does not say the alternative is true, only that the probability of getting this data is too small assuming the null hypothesis is true. F-statistics are utilized when comparing means such as in ANOVAs (Draper & Smith, 2014).

The Friedman’s test is a non-parametric alternative to the one-way ANOVA for when data violates the strong normality assumptions with its restrictive equal variances. Instead of computing F-statistics, Friedman’s test computes Friedman statistics after ranking data within each ‘block’. The Friedman statistic is the deviation of the observed rank totals from those expected under the null hypothesis of equality and it approximately follows the chi-square distribution (Milton & Arnold, 2003). We use Friedman’s test for our second study (Chapter VI) due to its reduced constraints (no distribution assumptions).²⁷

2.3.6 Checking Assumptions

In this last section of our regression review, we discuss checking assumptions. Depending on the regression technique, we make certain assumptions about our data. We must check that these assumptions are reasonable by looking for indications of assumption violations. Finding such evidence solicits reconsideration of the model and cautionary use. Regression modeling is an iterative process whereby evidence of violations (poor initial conditions) necessitates modifying the defined model or employing a different technique. Typically, not all assumptions will be met, and it is up to the modeler to cautiously determine if violations are detrimental.

For example, approaches exist to handle when errors are non-normal, autocorrelated, or heteroscedastic. When errors are non-normal, a generalized linear

²⁷ We are not able to employ the Friedman’s test for our first study because it is inappropriate for factorial experimental designs (having more than one factor). While frequentist and Bayesian LMM were performed on 200 replications of the test data set combining a subset of censor and noise levels, it was ultimately computationally prohibitive. We present a single experimental run (replication) for investigation for the set of interpolators in our first study.

model allows non-normal errors to be modeled. Common approaches to handling errors exhibiting autocorrelation or heteroscedasticity include data transformations for their removal and LMMs for their modeling. When only heteroscedasticity exists, weighted least squares which is a special case of generalized least squares allows for modeling heteroscedasticity and correlation in the errors. Generalized LMMs allow non-normal errors and any autocorrelation-and heteroscedasticity to be model, making them the most flexible.

We use diagnostic statistics and plots to evaluate model fits in regression (implemented in a script).²⁸ Spatial data requires alternative tests and checks not traditionally employed for checking OLS assumptions. For regression in a spatial context, there are eight assumptions.

For spatial data, we must consider spatial autocorrelation and non-stationarity typically exhibited. These two elements complicate traditional OLS. Spatial autocorrelation “creates an overcount type of bias” and non-stationarity in the independent variables prevents the model from representing the extremes in the geography well (Esri, n.d.-b). Properly specifying the model to include the explanatory variables responsible for the spatial structure avoids the overcounting bias due to spatial autocorrelation. Properly specifying the explanatory variables that capture the regional variations avoids non-stationarity issues. Properly specifying the model is a complex and challenging task beyond the scope of this work.

²⁸ These diagnostics proved useful in our preliminary analysis, but their details have been omitted here for brevity.

Our ELS technique utilizes different models to ensemble conflicting surfaces: a planar model and nominal-informed models of primitive functional forms.

We expect the simpler generic planar model, our zeroth order approximation, to be poorly specified and perform worse than the primitive-function model. The planar model will fit a plane to data and will fail to capture the regional variations (non-stationarity). This will elicit autocorrelation in the residuals. Furthermore, when modeling the truncated seamount, there will be nonlinearity unaccounted for in the dependent variable. The primitive-function model, however, contains explanatory variables capturing the regional variations (non-stationarity) and the nonlinearity.

Least squares regression (Draper & Smith, 2014) assumes errors are independent and normally distributed with a zero-mean and constant σ^2 , $\epsilon_i \sim \mathcal{N}(0, \sigma^2)$. We check the residuals for contradictions of these assumptions to determine if the model fit is appropriate. Identifying assumption violations informs us of the trustworthiness our estimates.

A script was written to compute the various statistical tests on DBMs created to check standard regression assumptions. However, these results were affected by additional post-processing of the DBMs in MergeBathy. Assumptions checks should be performed on the un-altered residuals resulting immediately after regressing within MergeBathy. Instead, our implemented checks are external to MergeBathy on the DBM output; MergeBathy manipulates the residuals to obtain a proper DBM (e.g., adding back trends, applying additional interpolators, etc.), see (S. J. Zambo et al., 2017a, 2017c).

We check the first assumption of independent errors by investigating the residuals for autocorrelations. The residuals should be randomly distributed, indicating random

over-predictions and under-predictions spatially. Qualitative diagnostic tools include residual versus fitted and observed versus fitted plots (Draper & Smith, 2014). Moran's I is a statistical test for spatial autocorrelations (Esri, n.d.-a, n.d.-b).

Least squares regression ensures residuals have a zero mean if the model includes an intercept, thus, not requiring a check for the second assumption (Draper & Smith, 2014, p. 61). However, we check the second assumption of errors having a zero mean by investigating qualitative diagnostic tools, including the residual versus fitted plot which may indicate other assumption violations (e.g., non-stationarity and heteroscedasticity). The residuals should appear stationary and constant, indicating no bias and constant variance.

We check the third assumption of errors having a constant variance by investigating the residuals for heteroscedasticity. The residuals should appear random when compared against each explanatory variable, indicating the residuals change consistently with explanatory variables thereby exhibiting homoscedasticity. Qualitative diagnostic tools include residual versus observed and residual versus fitted plots (Draper & Smith, 2014). Quantitative diagnostic tools include the Koenker Breush-Pagan test (Esri, n.d.-a, n.d.-b).

Repercussions of heteroscedasticity include unreliable errors. Remedies include using the Eicker-Huber-White heteroscedastic-consistent errors, commonly called robust errors, when performing inferences such as determining coefficient significance and utilizing the joint Wald-statistic instead of the joint F-statistic when evaluating overall model performance (Esri, n.d.-a, n.d.-b).

We check the fourth assumption of normally distributed errors by investigating the residuals for signs of non-normality. The residuals should appear to follow the normal distribution. Qualitative diagnostic tools include probability, quantile-quantile, histograms and stem-and-leaf plots of the residuals (Draper & Smith, 2014). Quantitative diagnostic tools include the Jarque-Bera test for skewness and kurtosis, and the chi-square test (Esri, n.d.-a, n.d.-b).

Our synthetic bathymetric data assumes independent (uncorrelated) and identically Gaussian distributed (white) noise: $\epsilon_i \sim \mathcal{N}(0, \sigma^2)$ and are independent (International Hydrographic Organization, 2008). The residuals estimated for these errors, however, are not independent as they are related by explanatory variables in the model, but typically is of no consequence in checking the normality assumption via the residuals unless the number of observations are large compared to the number of coefficients estimated by the model (Draper & Smith, 2014, p. 61).

With each technique, parametric or nonparametric, we make choices in the balancing of the bias-variance trade-off. Through ensembles, we may alleviate problems of estimators having too high a bias or variance by combining them into an ensemble for an estimator with a lower bias or variance. These types of ensemble technique include boosting and bagging, respectively (Geman et al., 1992; Sammut & Webb, 2011).

Next, in section 2.4, we present MergeBathy, a central tool utilized in this research. MergeBathy houses the regression techniques we discussed and utilized in this research to construct DBMs for our experimentations, however, MergeBathy does not perform any assumption checks. These interpolators are explicitly listed in section 2.5.

2.4 MergeBathy (2015)

Originally developed in C++ by Nathaniel Plant and Todd Holland, and updated and extended by the author, MergeBathy (2015) is a cross-platform and multi-threaded software suite for constructing DBMs (S. J. Zambo et al., 2016, 2017a; S. Zambo et al., 2018). It provides the user with a set of modeling tools to construct custom bathymetric surfaces, including splines-in-tension routines for interpolation output or as an intermediate resampling step when merging multiple bathymetry data sets. Notable to MergeBathy is its user-friendly and flexible processing options made possible from its integrated bathymetric process framework.

2.4.1 Introduction

A DBM is an estimate of the shape of the seafloor created from bathymetric soundings (measurements). Utilized for safety of navigation of ships and underwater vessels, geophysics research, bounding of ocean or acoustic models, and the study of marine life ecosystems (Pitcher et al., 2008), DBMs have significant economic importance. Aracri et al. (2021) highlight the economic importance of hard to survey regions with their research to utilize soft robotics.²⁹

Measurements stem from a wide variety of sensors including space-borne gravity, airborne laser, ship and underwater vehicle sonar, and Lidar (Weatherall et al., 2015). Due to the high collection cost, high-resolution data is scarce over most of the world's ocean. The measurements used to create a DBM for a specific area of interest therefore come from a variety of different technologies with different vertical/horizontal resolution,

²⁹ Soft robotics are composed of flexible, fluid, 'organism'-like materials, as opposed to rigid typically metal robots (Trivedi et al., 2008).

accuracy, etc. Input data with multiple resolutions pose a significant challenge for the computation of an output DBM. MergeBathy (2015) is an integrated software suite for processing bathymetric data of varying resolution for the creation of a DBM (S. J. Zambo et al., 2016) that utilizes the latest academic advances in processing techniques. MergeBathy streamlines the steps of taking cleaned bathymetric sonar data and producing final DBM products.

2.4.2 Problems and Background

Bathymetric modelers need flexible tools to process potentially large amounts of bathymetry data for the creation of DBMs (International Hydrographic Organization - Intergovernmental Oceanographic Commission, 2019). Current modeling tools for DBM construction involve individual algorithms, toolkits, or GIS software. MergeBathy is the accumulation of efforts to provide an integrated approach that is between toolbox software and GIS system software in terms of architecture complexity.

This software tool incorporates SIT algorithms from GMT and MB-System for sparse data set interpolation or resampling. Dense data set algorithms include LOESS (Cleveland & Devlin, 1988; Cleveland, 1979) or the Kalman filter algorithms to generate a DBM. Since these dense data algorithms produce a smoothed surface, higher details can be restored by adding ordinary kriging of the residuals as published in B. Calder (2006) and in N. A. C. Cressie (1993) to restore the finer details lost from over-smoothing. MergeBathy also utilizes CURVE (S. J. Zambo et al., 2015a) to attribute uncertainty (presented in section 2.6). Smoothing locally allows for a user-specified, scale-controlled surface reconstruction of sparse data that is capable of modeling complex surfaces (Plant et al., 2002) and kriging the residuals (B. Calder, 2006) honors data points in the

reconstructed surface when desired by the modeler. In general, MergeBathy has a defined process flow that alleviates some of the burden from the user in constructing DBMs.

2.4.3 Software Functionalities

We present MergeBathy's high-level process flow diagram in Figure 2.4. The merging of multiple input data sets into a single input data set for further computations is part of MergeBathy preprocessing (data fusion) functionality. To merge these data sets, MergeBathy must first apply any metadata to the individual files (not shown), transform and rotate coordinates, create an output grid, remove offsets between data sets, and optionally pre-spline to account for data sets of different resolutions.

Once the software computes a single unified data set, MergeBathy begins its trend surface analysis functionalities seen in the final two sections, which generate the final surface. Here, MergeBathy regresses to compute the trend surface, smooths the de-trended surface to highlight desired features, optionally kriges the residual to restore finer details, restores the residual and trend surface, and estimates uncertainty. A Monte Carlo estimator is also available for computation uncertainties for input data.

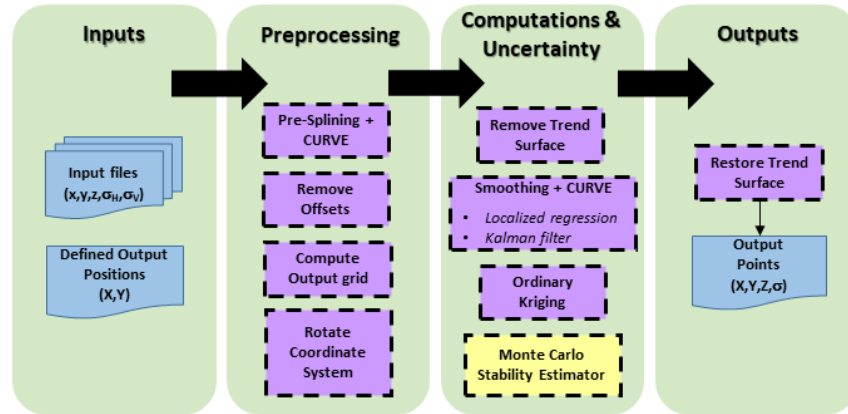


Figure 2.4 High-level MergeBathy flow for processing bathymetric data.

This diagram illustrates the process flow of MergeBathy at a high-level when processing bathymetric data. It begins by taking input files of measurement data listing positions, depths, and uncertainties. It may also take an optional input file of interpolation points on to which to grid. The inputs pass to the preprocessing phase where the data is prepared for the bathymetric modeling and uncertainty estimation algorithms in the computational and uncertainty phase before finally producing an output bathymetric surface product.

2.4.4 Implementation

Multi-threaded and cross-platform in design, MergeBathy is available for the Windows x86, x64, Linux x86, and Linux x64 C and C++ codebase.³⁰ MergeBathy utilizes several third-party libraries including GMT, MB-System, BAG files (Brian R. Calder et al., 2005; Open Navigation Surface Working Group, 2006).^{31, 32}

MergeBathy (2015) is a post-processing bathymetric software suite for constructing custom DBMs with uncertainty attribution. MergeBathy differs from its predecessors by being the first fully integrated system to stream-line the processing of (cleaned) bathymetric data of variable resolution to produce DBM products and, in contrast to existing toolkits, is flexible and user-friendly.

³⁰ We suggest a 64-bit processor for large input data sets.

³¹ BAG is a non-proprietary file format developed by the Open Navigation Surface Working Group; version 1.0.0 (Brian R. Calder et al., 2005; Open Navigation Surface Working Group, 2006).

³² BAG utilizes additional third-party libraries not listed.

MergeBathy has a defined process flow that removes some of the burden of processing bathymetric data from the user. It also is the first software package to handle sparse bathymetric data and bathymetric data of varying resolutions. While MergeBathy can process any elevation data, it targets bathymetric data, giving the extra functionality and flexibility unique to bathymetric problems, most notably, the merging of multiple variable-resolution data sets.

The flexibility of MergeBathy to create highly customizable DBM makes it suitable for most bathymetric problems. MergeBathy is open-source freeware available to the interested bathymetrists or citizen scientist that is completely adaptable and customizable to any of their needs and interests, having the base bathymetry computations necessary already in place.³³ Its foundation and framework for the inclusion of new techniques allows MergeBathy to continuously evolve with bathymetric processing solutions and needs.

MergeBathy software and source code (S. J. Zambo et al., 2017a), along with the source code (S. J. Zambo et al., 2017d) and data (S. J. Zambo et al., 2017b) for test cases presented (S. Zambo et al., 2018), ample documentation (S. J. Zambo et al., 2017c), and source code for GMT inclusion of CURVE (S. J. Zambo, 2017), are available on GitHub.³⁴

³³ With the rise of crowd-sourced bathymetry (Brian R. Calder et al., 2020), we have seen the interest in and availability of bathymetric data expand (L. Mayer et al., 2018) (International Hydrographic Organization, 2018). One crowd-sourced bathymetry portal is (International Hydrographic Organization, n.d.-a) and there is a push for more transparent bathymetric tools (G Masetti et al., 2019).

³⁴ Adapted from “MergeBathy (2015)” by S. Zambo et al. *SoftwareX*, 7, 180–183. (<https://doi.org/10.1016/j.softx.2018.05.005>). Copyright 2018 by Elsevier. Adapted with permission. Under the Creative Commons CC-BY license.

2.5 MergeBathy Interpolation Schemes (First Study Evaluated Methods)

This section presents the interpolation schemes investigated in our first study (presented in Chapter V) for feature-favoritism. All interpolations schemes in our first study utilized MergeBathy to construct DBMs which we evaluated externally from MergeBathy. Interpolators were originally developed for MergeBathy by Nathaniel Plant and Todd Holland. The author extended, validated, and utilized MergeBathy as a shared platform for convenience in executing experiments for compatible and consistent DBMs, and aversion of system influences. Fundamentals of these well-known interpolation schemes were reviewed in section 2.3. We consider these interpolation schemes and MergeBathy as black-boxes. As such, we will not have access to the underpinnings of either.

We investigated 32 interpolation schemes (combinations of interpolators available in MergeBathy). They are:

- GMT SIT,
- MBZ SIT,
- localized Kalman filtering,
- localized regression utilizing either of the window weightings (also referred to as filters):
 - boxcar (uniform weighting scheme),
 - loess (linear weighting scheme),
 - quadloess (quadratic weighting scheme), or
 - hann (hanning weighting scheme),

- either localized Kalman or localized regression (with any window) plus splining beforehand (pre-splining) with either GMT or MBZ SIT,
- either localized Kalman or localized regression (with any window) plus residual kriging (simply referred to as kriging), and
- either localized Kalman or localized regression (with any window) plus residual kriging and pre-splining with either SIT routine.

Enumerated in Table 2.2, these interpolators are evaluated methods identified by EM<Id> (e.g., EM02 for kriging with loess window) in our first study (presented in Chapter V).

Table 2.2

Individual MergeBathy Interpolation Schemes Utilized in our First Study.

EM	Abbreviation	Description
1	Krigquadloess	Localized regression with quadratic window weighting function plus residual kriging
2	Krigloess	Localized regression with linear window weighting function plus residual kriging
3	Krigboxcar	Localized regression with boxcar window weighting function plus residual kriging
4	Krighann	Localized regression with hann window weighting function plus residual kriging
5	Krigkalman	Localized Bayesian estimator plus residual kriging
6	Krig_GMTquadloess	Localized regression with quadratic window weighting function plus residual kriging and pre-splining with GMT SIT
7	Krig_GMTloess	Localized regression with linear window weighting function plus residual kriging and pre-splining with GMT SIT
8	Krig_GMTboxcar	Localized regression with boxcar window weighting function plus residual kriging and pre-splining with GMT SIT
9	Krig_GMTthann	Localized regression with hann window weighting function plus residual kriging and pre-splining with GMT SIT
10	Krig_GMTkalman	Localized Bayesian estimator plus residual kriging and pre-splining with GMT SIT
11	Krig_MBZquadloess	Localized regression with quadratic window weighting function plus residual kriging and pre-splining with MBZ SIT
12	Krig_MBZloess	Localized regression with linear window weighting function plus residual kriging and pre-splining with MBZ SIT
13	Krig_MBZboxcar	Localized regression with boxcar window weighting function plus residual kriging and pre-splining with MBZ SIT
14	Krig_MBZhann	Localized regression with hann window weighting function plus residual kriging and pre-splining with MBZ SIT
15	Krig_MBZkalman	Localized Bayesian estimator plus residual kriging and pre-splining with MBZ SIT
16	GMTquadloess	Localized regression with quadratic window weighting function plus pre-splining with GMT SIT
17	GMTloess	Localized regression with linear window weighting function plus pre-splining with GMT SIT
18	GMTboxcar	Localized regression with boxcar window weighting function plus pre-splining with GMT SIT
19	GMTthann	Localized regression with hann window weighting function plus pre-splining with GMT SIT
20	GMTkalman	Localized Bayesian estimator plus pre-splining with GMT SIT
21	MBZquadloess	Localized regression with quadratic window weighting function plus pre-splining with MBZ SIT
22	MBZloess	Localized regression with linear window weighting function plus pre-splining with MBZ SIT
23	MBZboxcar	Localized regression with boxcar window weighting function plus pre-splining with MBZ SIT
24	MBZhann	Localized regression with hann window weighting function plus pre-splining with MBZ SIT
25	MBZkalman	Localized Bayesian estimator plus pre-splining with MBZ SIT
26	Quadloess	Localized regression with quadratic window weighting function
27	Loess	Localized regression with linear window weighting function
28	Boxcar	Localized regression with boxcar window weighting function
29	Hann	Localized regression with hann window weighting function
30	Kalman	Localized Bayesian estimator
31	GMT SIT	Generic Mapping Tools (GMT) splines in tension (SIT) routine
32	MBZ SIT	MultiBeam (MB)-System splines in tension (SIT) routine

These are the individual interpolation schemes available in MergeBathy (2015) which produce a DBM. For each morphology-based

data set, we compute DBMs with each individual interpolation scheme and investigate to identify any which are feature-favoring.

As discussed in section 2.3, there exists a suite of algorithms typically used to generate DBMs and, as discussed in section 2.4, MergeBathy is one software suite that makes them available, notable for its user-friendly and streamlined approach for processing bathymetry. However, as already mentioned in section 2.2, the software products most widely used by the bathymetric community are GMT and MB – System of which both provide the most-widely used interpolator for constructing DBMs: SIT (both available in MergeBathy and utilized via MergeBathy in our experimentations). For these reasons and since MB – System installation depends on GMT, we have selected GMT SIT to serve as our benchmark to evaluate against in our experimentations.

The GMT *surface* and MB-System *mb_zgrid* commands are SIT routines to compute a minimum curvature spline.^{35,36} Smith and Wessel W. Smith & Wessel (1990) added tension to the splines to eliminate extraneous inflection points.

For comparison with my new method nominal-informed modeling approach for creating DBMs (presented in Chapter III), we briefly present SIT details. The spline interpolator solves the modified differential equation that results from balancing minimum curvature with tension. The equation

$$(1 - T)\nabla^2(\nabla^2 z) + T\nabla^2 z = \sum_i f_i \delta(x - x_i, y - y_i) = q, \quad (2.1)$$

taken with modifications from (W. Smith & Wessel, 1990), performs this balance via the choice of (internal) tension parameter T .³⁷ In (2.1), the ∇ is the coordinate-free notation for the gradient, q is the forcing term, and z is the continuous function we sample to

³⁵ GMT newest release available is 6.0 (P. Wessel et al., 2019)

³⁶ MB—System newest release available is 5.7.8 (Caress & Chayes, 2021)

³⁷ W. Smith & Wessel (1990) notate our T as T_I .

produce the DBM output sounding values, while (x_i, y_i) are the locations of the input sounding points. An internal tension value of 0.0 yields a minimum curvature solution whereas a value of 1.0 yields a second order harmonic solution.³⁸ MergeBathy uses a value of $T > 0.0$ to suppress the spurious oscillations typically associated with minimum curvature solutions. Empirically, geoscientists use $T \sim 0.25$ where the bottom is nearly constant and $T \sim 0.35$ for steep topography (International Hydrographic Organization - Intergovernmental Oceanographic Commission, 2019). The author has implemented uncertainty estimation within MergeBathy and within GMT (for their inclusion) via Paul Elmore's CURVE, discussed in section 2.6, available to attribute uncertainty to SIT bathymetric grids.

2.6 Uncertainty Estimation for Sparse Data Gridding Algorithms

While newer multibeam technologies can produce very dense measurements, it is more typical for bathymetric data to be a sparse and irregular sampling of which it is desirable (viz., convenience of processing and display) and common practice to process to obtain a regular a grid. As discussed in section 2.5, there are many bathymetric processing tools available to construct DBMs.

While the synthesis of uncertainty with gridded output surfaces for dense data is now a required practice, fast approximation algorithms that map sparse data to a regular grid typically do not include uncertainty estimates.

The SIT technique (W. Smith & Wessel, 1990) utilized by the most commonly used bathymetric processing tools, GMT and MB – System, do not inherently estimate

³⁸ $T = 1.0$ is equivalent to having equal weights at all frequencies.

uncertainty.³⁹ However, through collaboration, GMT now offers uncertainty estimation when constructing DBMs via the worked .presented in this section.

For sparse data, SIT is a historically used algorithm for determining the best fit surface that passes through available measurement data to create a DBM. Unlike dense data, where we can use averaging of the measurement data to reduce the DBM error, with sparse data our ‘best’ approximation of the true surface must be a fit through the existing data. This interpolator and many others akin to it (e.g., Press et al., 2007, Chapter 3) often lack a native uncertainty estimator.

Here, we define dense data as meaning the data count \gg grid cell size and sparse data as data count \ll grid cell size.

A modeled bathymetric surface known as a DBM is not considered complete without an estimation of uncertainty (International Hydrographic Organization - Intergovernmental Oceanographic Commission, 2019). We utilized our own CURVE algorithm to attribute uncertainty to our ensemble estimates.

MergeBathy utilizes CURVE, developed by Paul Elmore and Brian Bourgeois and coded by the author, to attribute uncertainties to a produced DBM.⁴⁰ CURVE was designed with sparse bathymetric data as one of its requirements (S. J. Zambo et al., 2015a). Our source code for CURVE has been incorporated into GMT and is available through *triangulate* in the latest GMT version 6.1.1 (The GMT Team, 2020a) and

³⁹SIT solves a fourth-order differential equation to produce a grid (W. Smith & Wessel, 1990).

⁴⁰ For patent information see (Paul A Elmore & Zambo, 2013, 2014).

preceding versions up till when first introduced in GMT version 5.4.6 (The GMT Team, 2020b).⁴¹

For this dissertation, encapsulated in CURVE, we developed a method for uncertainty attribution for sparse data that uses a circumscribed, nearest neighbor algorithm to identify local support and determine which data points should contribute to the uncertainty estimate for each gridded output location. Additionally, we included an extension of the work of B. R. Calder & Mayer (2003) by including the influence of navigational uncertainty over a sloping seafloor, which is applicable to both dense and sparse data and estimates the increased uncertainty in areas with steep slope suggested by Paul Elmore. Studies demonstrate the ability of this uncertainty formulation to adequately provide realistic uncertainty values that bound the error between ground truth and grids created with sparse data.

It might seem reasonable to treat the measurement errors associated with the measurement data as an independent surface and simply interpolate that surface directly to compute the uncertainty values at each grid point. For dense data however, this does not take advantage of our ability to effectively reduce DBM error by averaging. Also, the farther apart data points are in a geophysical system, the more distance correlations may vary significantly (Davis, 2002; Tobler, 1970). This suggests that uncertainty propagation, which allows for an increase in uncertainty proportional to the distance from known data, is a reasonable approach for our problem.

⁴¹ The code is also available on GitHub (S. J. Zambo, 2017).

CUBE does in fact apply propagated uncertainty to the measurement data, as well as averaging to reduce error. We modified the CUBE propagated variance equation for gridded output uncertainty estimation to adapt to the sparse data problem and then augmented it with a first-order term to account for additional uncertainty due to bottom slope. We term this modified CUBE equation as CURVE.

In section 2.6.1, we present the CURVE algorithm including the Delaunay triangulation used for selecting support points (section 2.6.1.2), the equations for propagated uncertainty including the new slope term (section 2.6.1.3), and the use of inverse distance weighting (IDW) function to combine the propagated uncertainties into a total uncertainty at the grid point (section 2.6.1.4). In section 2.6.2, several case studies are presented that demonstrate the effect of the propagated uncertainty for varying degrees of sparsity, showing an increase in uncertainty in high slope areas, and the efficacy of the proposed uncertainty algorithms in bounding the error between the truth and the DBM generated using sparse data, within local assumptions.

2.6.1 CURVE Algorithm

We present a three-step algorithm for obtaining a gridded uncertainty value to accompany our gridded bathymetry surface depth value from sparse input data. The first step (section 2.6.1.2) of the process selects the local support points that will be used to propagate uncertainty by creating a Delaunay triangulated irregular network (TIN) from the sparse data. The second step (section 2.6.1.3) propagates the uncertainty from each of the triangle's vertices to the grid point, increasing this value based on the range and slope between each vertex and the grid point. The third step (section 2.6.1.4) combines the uncertainty values from each of the three bounding vertices to obtain the grid point

uncertainty using an IDW average of the propagated uncertainties. This general approach should be applicable to a variety of geophysical data. Figure 2.5 shows a depiction of this process.

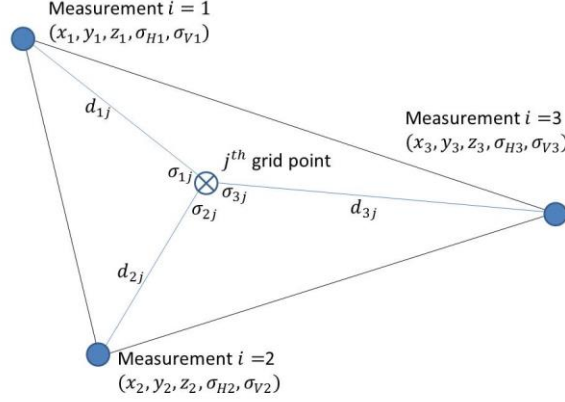


Figure 2.5 Illustration of CURVE.

Depiction of CURVE method for computing an uncertainty for a grid point from sparse data. The three measurement points $i = 1, 2, 3$ that bound the j^{th} grid point was selected using Delaunay triangulation. Each measurement has a depth z , location (x, y) , horizontal uncertainty σ_H and vertical uncertainty σ_V . The measurement horizontal and vertical uncertainties are weighted by the distance between each measurement and the grid point (d_{1j}, d_{2j}, d_{3j}) to compute the propagated uncertainties ($\sigma_{1j}, \sigma_{2j}, \sigma_{3j}$) from each measurement. These are then combined to create the attributed uncertainty at the grid point σ_j .

Our required inputs for creating a gridded uncertainty estimation from our CURVE algorithm are:

- the input depth values (\vec{z}_{iN}),
- their positions ($\vec{x}_{iN}, \vec{y}_{iN}$) with horizontal and vertical uncertainty ($\vec{\sigma}_{H_{iN}}, \vec{\sigma}_{V_{iN}}$),
- the locations for the output gridded bathymetric surface $\vec{E}(\vec{x}_{OUT}, \vec{y}_{OUT}, \vec{z}_{OUT})$,
- the output grid spacing (Δ_{grid}), and
- the output gridded slope ($\vec{\theta}_{OUT}$).

2.6.1.2 Selecting Support Points

The first step of the CURVE algorithm locates the surrounding neighbors $\{i\}$ for each output gridded surface point j by creating a Delaunay TIN from the input measurement positions, where each vertex is an input data point. Each vertex of a TIN triangle likewise provides an uncertainty value that we can propagate to each output grid point enclosed within that triangle. All $\{j\}$ grid points are contained inside the convex hull of the created TIN and each grid point j identifies with just one enclosing triangle.

For each of these points, the Euclidian distance (in meters) from j to the circumscribing vertices, d_{ij} , is computed and used to compute the propagated uncertainty. As discussed in (Davis, 2002) for Delaunay triangulation, circumscribing neighbors guarantee that each triangle's vertices are the nearest points from the expanding vertex. However, it does not guarantee that a point interior to the triangle has these same vertices as its nearest neighbor. When they are not, this approach introduces C^1 discontinuities in the resulting output values.

Enclosing geometric shapes, such as triangles, have well-known computational advantages. No searches for nearest neighbors are necessary. The method is $\mathcal{O}(1)$ per interpolation point, with a small constant. They may also have less well-known disadvantages, such as loss of derivative continuity which may have no influence on a physical map. However, when subsequently utilizing that physical quantity to force an ocean model, we would expect the output gridded surface to impart the same effect that

(Perkins, 1995) found in their data initialization/assimilation studies.⁴² Since oceanographic models utilize bathymetric gridded surfaces as forcing terms, this effect may be relevant.

2.6.1.3 Propagated Variance

To present the CURVE propagated variance equation, we begin by first presenting CUBE in section 2.6.1.3.1. In section 2.6.1.3.2, we present the new bottom-slope term developed by Paul Elmore in communication with Brian Calder to form the new CURVE propagated variance equation.

2.6.1.3.1 CUBE

For the case of dense bathymetry data, the standard method for computing the propagated uncertainty of a measurement for a grid point is given in (B. R. Calder & Mayer, 2003) and is shown below in (2.2).

$$\sigma_{ij}^2 = \sigma_{V,i}^2 \left(1 + \left[\frac{d_{ij} + S_H \sigma_{H,i}^2}{\Delta_{grid}} \right]^\alpha \right) \quad (2.2)$$

As in Figure 2.5, (2.2) has $\sigma_{H,i}^2$ and $\sigma_{V,i}^2$, the horizontal and vertical uncertainties of the measurement points, and d_{ij} which represents the radial distance of propagation between i and j . In (2.2), Δ_{grid} is the gridded surface spacing (or minimum spacing for non-square grids). The end-user sets parameters S_H , a magnification coefficient for worst-case $\sigma_{H,i}$, and α , which adjusts for relative distance between the measurement and grid

⁴² In (Perkins, 1995), they studied the influence of C^1 discontinuities in both initial conditions and data assimilation gridded fields on ocean model integration. These C^1 discontinuities introduced significant high frequency noise that was slow to dissipate. They removed these C^1 discontinuities by adapting their bi-linear interpolation (which originally had fully 1/2 of the interpolation points using non-nearest neighbor input) to a bi-linear nearest neighbor scheme, where the x -pair and y -pair interpolation points were selected by nearest distance rather than because they lay within an enclosing shape.

points. For dense measurement data, values of $S_H = 1.96$ and $\alpha = 2$ are typically used (B. R. Calder & Mayer, 2003). Within CUBE, all measurement points within a circle of radius of $\Delta grid$ of a grid point are used with (2.2) to compute the propagated uncertainty of each.

The use of (2.2) within CUBE for increasing the contribution of measurement data uncertainty to a grid point gives no regard to the density or sparsity of the measurement data and, thus, we can use it at most as our starting point for computing propagated uncertainty for sparse data. Appropriate values of the parameters S_H and α in sparse data need further consideration. Of concern are situations where the measurement data is so sparse that significant features (local minima and maxima) are not adequately sampled. We desire that the values of the user-set parameters be set appropriately depending upon data density and seafloor morphology to ensure that the resulting grid's uncertainty reliably bounds the possible extremes of the actual seafloor surface. This is left as future work.

2.6.1.3.2 Bottom Slope

As shown in (Jakobsson et al., 2002), bottom slope affects total uncertainty. To reflect this, we modify (2.2) with an additional term that approximates a sloping seafloor (as suggested in (B. R. Calder & Mayer, 2003) and implemented in S. J. Zambo et al. (2015a), S. J. Zambo et al. (2017a), and The GMT Team (2020a)) to form the CURVE propagated uncertainty equation. Trigonometrically, along the path of steepest descent (seafloor aspect) with slope at angle θ , this added uncertainty is $\Delta z = \sigma_H \tan \theta$ (Figure 2.6). For each grid point of our output gridded bathymetry, \vec{E} , relabeled with just one index j , we augment (2.2) to account for this slope by adding $\sigma_{H,i}^2 \tan^2 \theta_j$ as an extra

variance term, as in (2.3). This term serves to increase the uncertainty obtained from (2.2) to account for the additional vertical uncertainty due to the horizontal position uncertainty of the survey ship when over a sloped bottom. To some extent, this term may also help to compensate in rugged, sparsely sampled areas by amplifying the uncertainty based on the dominant slope.

$$\sigma_{ij}^2 = \sigma_{v,i}^2 \left(1 + \left[\frac{d_{ij} + S_H \sigma_{H,i}}{\Delta grid} \right]^\alpha \right) + \sigma_{H,i}^2 \tan^2 \theta_j \quad (2.3)$$

In the CURVE formulation, the slopes $\{\theta_j\}$ are computed using the gridded digital bathymetric model. However, computation of the steepest decent is expensive, so we approximate the slope using the third-order finite difference weighted by reciprocal of (Jakobsson et al., 2002) squared distance (3FDWRSD) shown in Table 1 of (Zhou & Liu, 2004). As $\theta \rightarrow 90$, this new term can result in unacceptably high uncertainty where high seafloor slopes exist, even if we have data with sufficiently high spatial resolution. Consequently, it would be appropriate to clip this result at a minimal level.

In shallow water, particularly in areas where there are seafloor outcroppings, a reasonable limit would be the depth of the water in the area. For deep water, Smith and Sandwell's gravity derived bathymetry (Sandwell et al., 2014) has a nominal standard deviation of about 100 m. This derived bathymetry often serves as a baseline in regions where no soundings exist, so $\min(\sigma_H \tan \theta, 100)$ may be an appropriate limit.

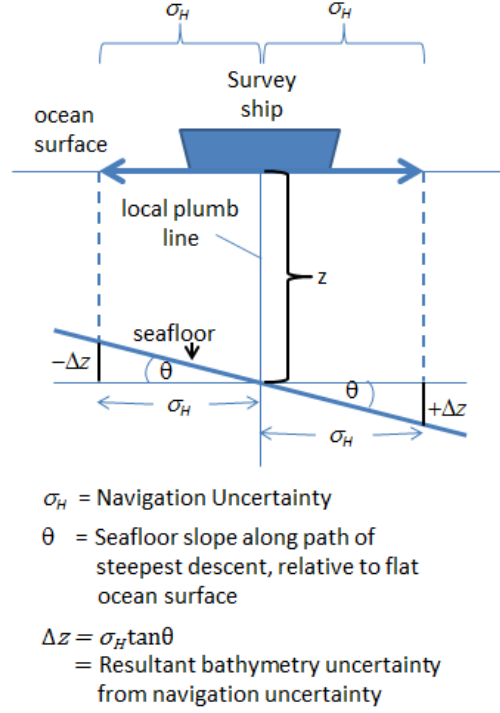


Figure 2.6 Bottom-slope

The uncertainty in the position of the survey ship for the i th sounding (measurement) is σ_H . When a slope is present this horizontal position uncertainty translates to an additional vertical uncertainty of Δz . This yields the additional uncertainty term $\sigma_{H,i}^2 \tan^2 \theta_j$, computed using the above assumptions.

2.6.1.4 Computing Attributed Uncertainty

After propagating the uncertainty for each vertex, j , we have three estimates, $\sigma_{1j}^2, \sigma_{2j}^2, \sigma_{3j}^2$. The attributed uncertainty for grid point j is computed using an IDW based variance estimate for σ_j^2 as shown in (2.4).

$$\sigma_j^2 = \frac{\sum_{i=1}^3 d_{ij}^{-1} \sigma_{ij}^2}{\sum_{i=1}^3 d_{ij}^{-1}} \quad (2.4)$$

Equation (2.4) is an implementation of Shepard's interpolation (Press et al., 2007), a special class of radial primitive functions for linear IDW. As noted in (Press et al., 2007), Shepard's interpolation is less accurate than other commonly used radial primitive functions, but it is free from the need to solve linear algebraic equations and is

computationally fast. This formulation provides an intuitive way to combine the propagated uncertainties and it retains the min/max bounds of the input points.

A possible disadvantage of IDW is that the interpolated surface is not C^0 . The plots in Figure 2.7(a-b) show the effects of potential discontinuities along cell (triangle) edges. In the first plot, Figure 2.7a, we show an IDW interpolation that fails to produce even a C^0 interpolant, whereas the second plot shows a linear interpolator that demonstrates its results are C^0 , but not C^1 (see clear chevron pattern in the lower right quadrant of Figure 2.7b). Since the uncertainty values are not used in ocean models, the loss of continuity between cells may not be a concern.

While Delaunay triangulation allows for a rapid search for three spatially equitable control input points (Press et al., 2007) and IDW fast computation of the attributed uncertainty, our ongoing research includes developing methods that extend the number and nature of the contributing vertices; in this dissertation, however, our results are all from enclosing triangles.

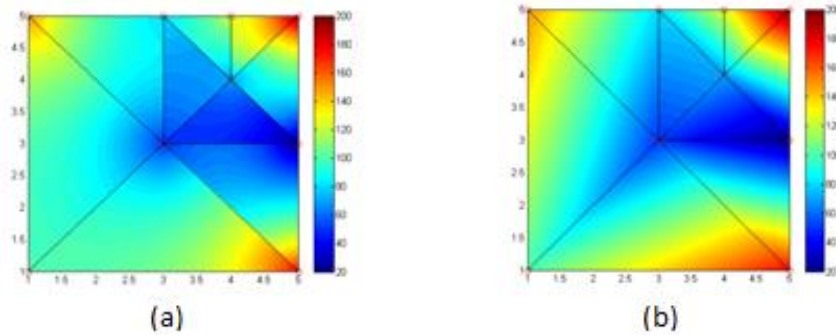


Figure 2.7 IDW versus linear interpolation.

The figures depict the discontinuities along triangle edges: (a) an IDW interpolator that fails to produce a C^0 interpolant; (b) a linear interpolator producing a C^0 , but not C^1 interpolant. The vertices values are: (1, 1, 100), (1, 5, 150), (3, 3, 50), (1, 5, 150), (3, 5, 80), (5, 3, 20), (4, 4, 70), (4, 5, 125), and (5, 5, 200).

2.6.2 Case Studies

Figure 2.8 shows a section of the East Pacific Rise which has very rugged terrain and large depth variations. Figure 2.9 shows the bathymetry for a subarea of Figure 2.8 that we use as the ground truth and Figure 2.10 shows the slopes for this subarea. As expected, the greatest slopes are along the caldera perimeters of the seamounts.

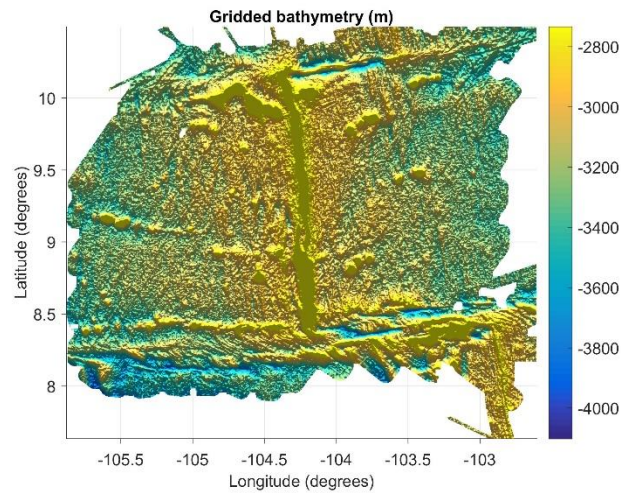


Figure 2.8 East Pacific Rise data

Multibeam data collected of a section of the East Pacific Rise southwest of Mexico.

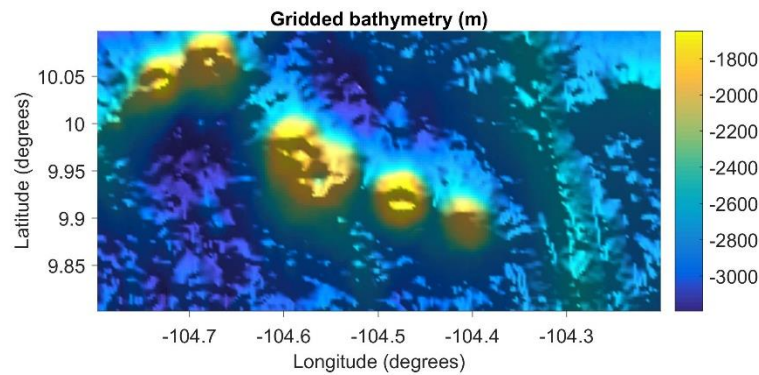


Figure 2.9 Case study area ground truth data.

The subsection of the multibeam East Pacific Rise data studied. This case study area is a 219 by 110 grid with 300 m grid resolution. The maximum depth in this area is 3,193 m and the minimum is 1,648 m. The yellow areas are volcanoes known as seamounts and to the right of the seamounts, running North to South, is a ridge.

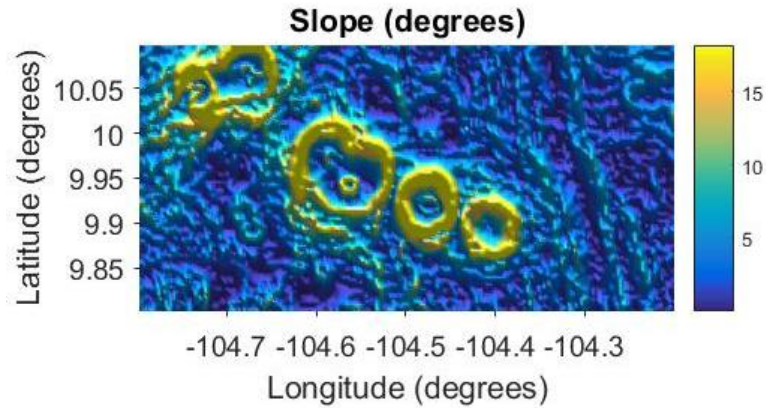


Figure 2.10 Case study area slopes.

The slope in the East Pacific Rise case study area. The areas of highest slope (18 deg) are seen around the caldera perimeter of the seamounts, with the ridge differences showing up along the right boundary.

We create a sparse data set by randomly selecting a subset of the points from the ground truth data and then use GMT SIT to fill in the missing data locations. Figure 2.11 shows a set of data points that were randomly selected using 10% of the ground truth data to create a new DBM. Figure 2.12 shows the resulting DBM created using GMT SIT on the 10%-thinned data. Comparing with Figure 2.9, we can clearly see the loss of resolution and detail.

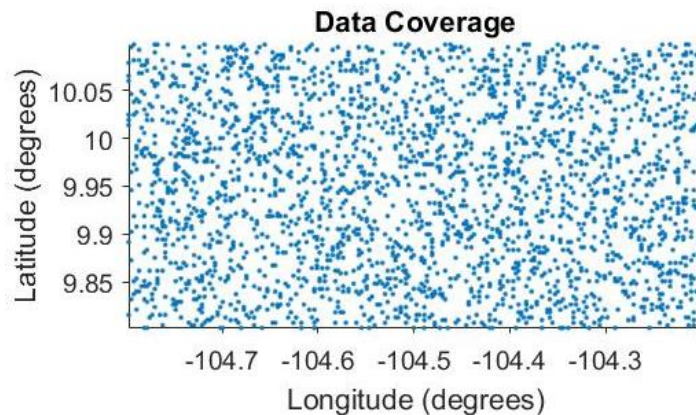


Figure 2.11 Randomly selected data points using 10% of the ground truth data.

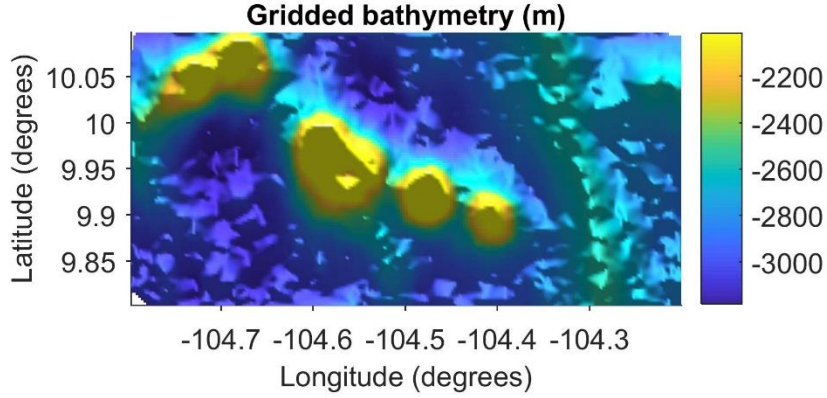


Figure 2.12 DBM created using GMT SIT on the 10%-thinned data.

To illustrate the impact of CURVE on the estimated uncertainty for the DBM created with the sparse data, we assign realistic measurement error values of $\sigma_V = 10$ m and $\sigma_H = 200$ m to our truth data. For Figure 2.13, we use (2.2) to propagate uncertainties and compute the total propagated uncertainty at each grid point by computing the IDW of these propagated uncertainties.

The optimal total uncertainty values occur at grid locations that exactly match those of the input data. When grid and input locations exactly match, the distance to propagate uncertainty $d_{ij} = 0$ and the propagated uncertainty computes for the matching point only, instead of propagating uncertainties from neighboring points. For regions where the data is sparse, $d_{ij} > 0$, the total uncertainty grows accordingly as grid points move further away from soundings.

In Figure 2.13, we show the uncertainty using (2.2), which includes the growth term for the measurement horizontal error. We can see in the figure that this results in higher values of about 50 m that correspond to the regions shown in Figure 2.11 with sparse data.

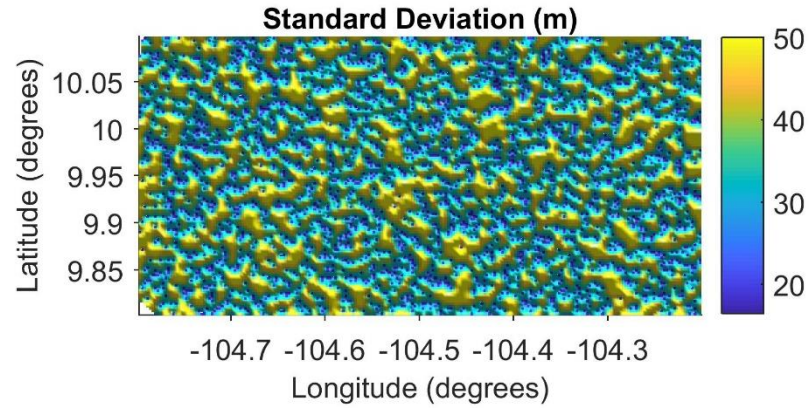


Figure 2.13 Uncertainty for the 10%-thinned data set, using (2.2).

In Figure 2.14, we show the total uncertainty using (2.3) which has increased values in the areas of high slope. The increase is relatively small for the values used but could be significantly larger with some historic data having much higher horizontal uncertainties. Though small, the difference between the figures is clearly visible, shown in Figure 2.15, and corresponds well with the high slope areas in Figure 2.10 at an intuitive level.

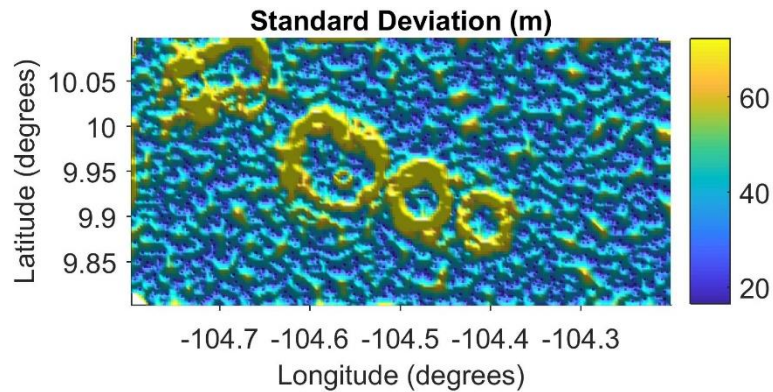


Figure 2.14 Uncertainty for the 10%-thinned data set, using (2.3).

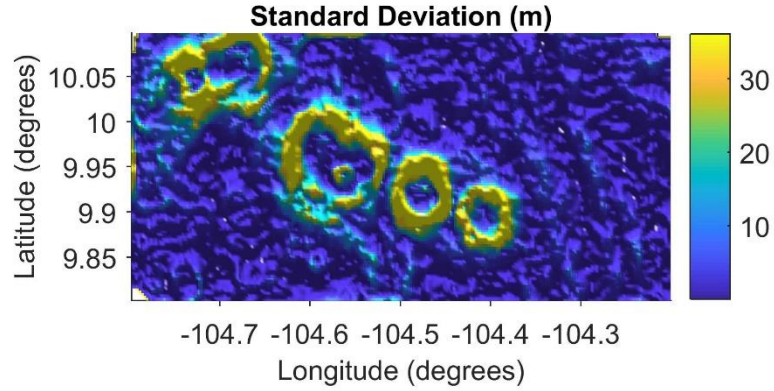


Figure 2.15 Uncertainty difference using (2.2) and (2.3).

In Figure 2.16, we show the truth data (red middle line) versus the GMT SIT estimated depth values (green middle line) for a single latitude slice. The remaining top and bottom blue lines show the 1σ bounds on the GMT SIT estimated values and we see that they completely enclose the error (difference between truth and GMT SIT) for this slice. For the entire re-gridded 10%-thinned data set, only 4% of the GMT SIT points fall outside of the 1σ bounds and these points are dispersed throughout the test area. For 3σ , only 0.04% of the GMT SIT points fall outside of the error bounds, for the selected values of S_H and α . These parameters could be tuned to modify these results in either direction.

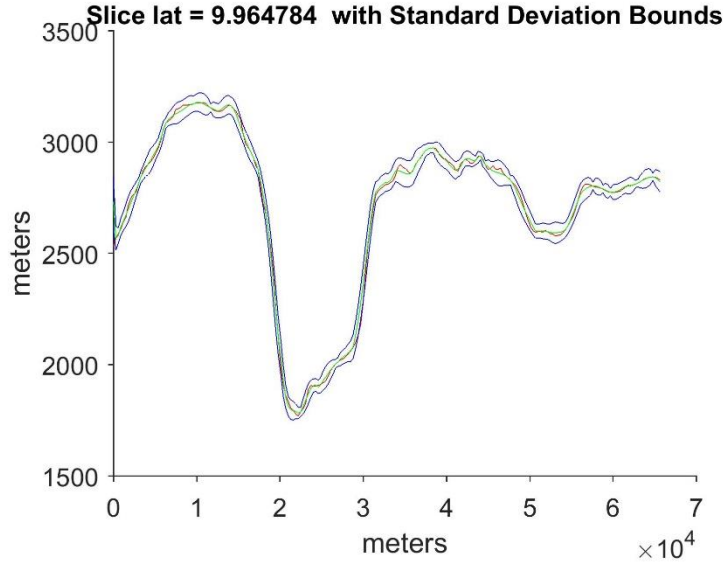


Figure 2.16 Single latitude slice for the 10%-thinned data set passing through one of the volcanoes.

The red middle line is the truth depth values and the green middle line is the GMT SIT depth values computed using the 10%-thinned data. The blue top and bottom lines show the 1σ upper and lower bounds.

Figure 2.17 shows the DBM created using GMT SIT on a 20%-thinned data set and Figure 2.18 shows the selected ground truth data points. Compared to Figure 2.9, there is significant loss of detail. In Figure 2.19, we see considerably larger standard deviation due to the greater sparsity of data; the error between the truth and the GMT SIT estimated depth values is still well bounded by the 1σ bounds. For 3σ , 0.19% of the points fall outside of the error bounds, for the selected values of S_H and α .

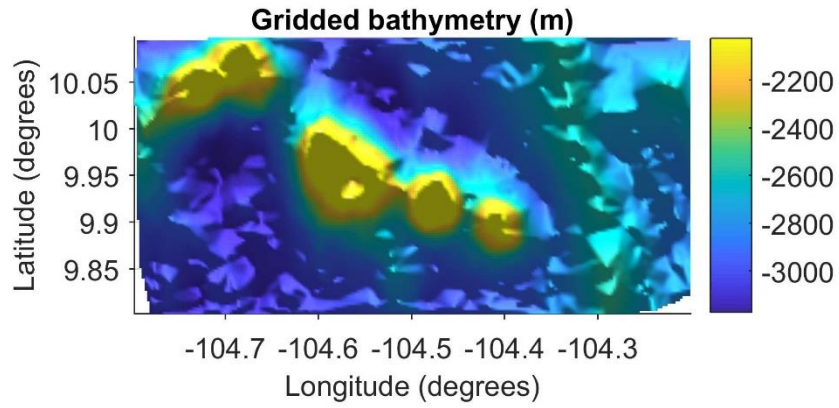


Figure 2.17 DBM created using GMT SIT on the 20%-thinned data.

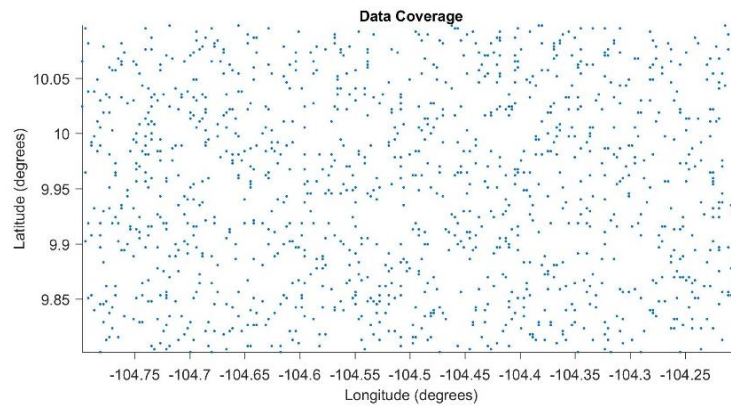


Figure 2.18 Randomly selected data points using 20% of the ground truth data.

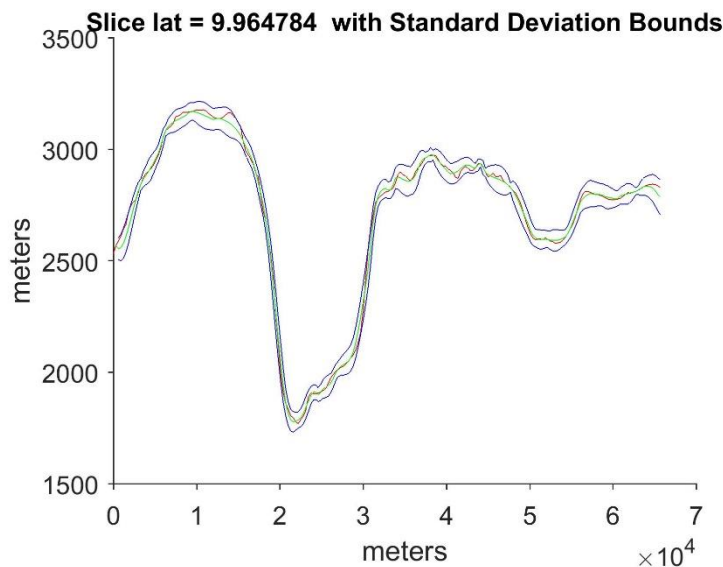


Figure 2.19 Single latitude slice for the 20%-thinned data set.

The red middle line is the truth depth values and the green middle line is the GMT SIT depth values computed using the 20%-thinned data. The blue top and bottom lines show the 1σ bounds.

The DBM for the final case is shown in Figure 2.20, where a large swath of data is removed from the truth data set. This is a typical issue encountered in the deep water where survey ships skip lines to save time or due to inclement weather. Post processing of this type of data is often dealt with by an expert by manually adding in control points in the gapped area based on visual interpretation of the seafloor morphology or other known data. Figure 2.21 shows the significantly poorer fit of the GMT SIT to the truth data in the gapped area. For this case 9.55% of the GMT SIT points fall outside of the 2σ bounds. Of the 3σ bounds, 5.04% of the GMT SIT points fall outside.

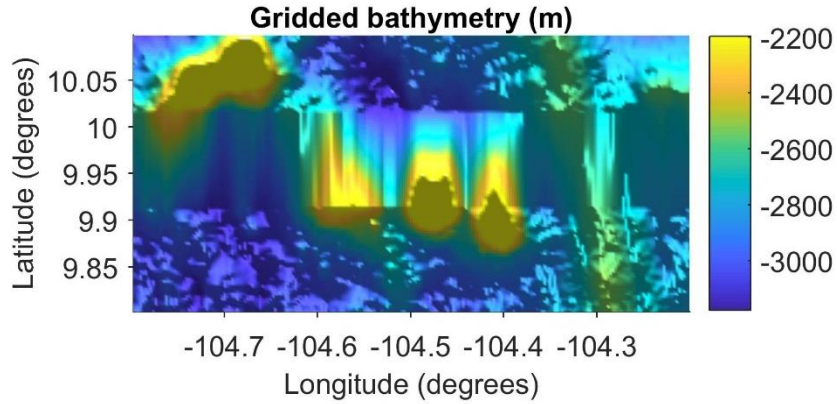


Figure 2.20 DBM created using GMT SIT with a middle 1/3 latitude data points removed.

The undesired behavior of GMT SIT with large gaps in the source data is apparent in this result.

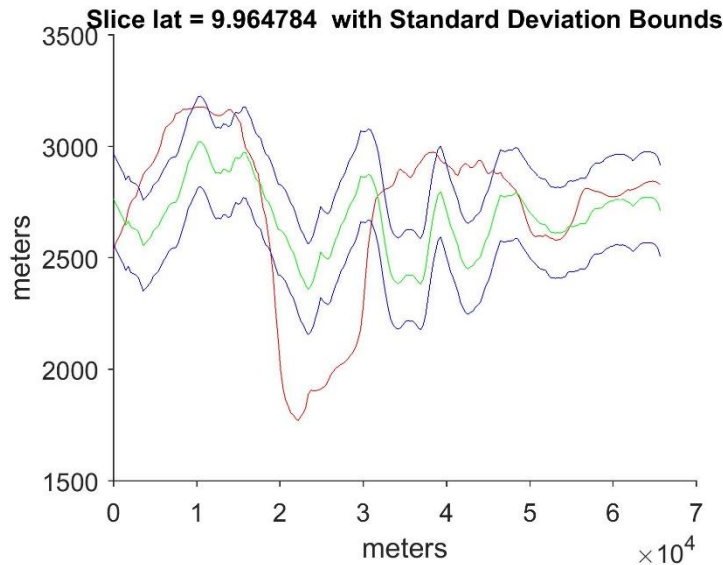


Figure 2.21 Single latitude slice through the region where 1/3 of the data points removed.

The red ‘middle’ line is the truth depth values and the green ‘middle’ line is the GMT SIT depth values computed using the 20%-thinned data. The blue top and bottom lines show the 1σ bounds.

The case studies used GMT SIT to up-sample the sparse data grid to a gridded surface and MATLAB for its Delaunay TIN, but the CURVE uncertainty estimator is independent of both the gridding interpolator and the nearest neighbor routine. Indeed, this estimator is applicable to other gridding routines that lack an inherent uncertainty

estimator. It is also implementable regardless of scripting and programming languages as TINs and nearest neighbor algorithms are textbook mature (O'Rourke, 1998; cf. Press et al., 2007).

As previously mentioned, we use a TIN to locate the control points for each gridded surface location. This nearest neighbor search is $O(n \lg n)$, which is pragmatic for general use. For situations where there are points that lie outside the hull (extrapolation), one may need to segregate those points and find the nearest neighbors with an alternative method. One could easily use alternative nearest neighbor methodologies that do not use TINs.

The slope θ_j from the gridded surface provides a smooth surface. We found that the randomly generated sparse data slopes were potentially noisy because they were, in some sense, non-physical. Based on the results with real data, however, we do not expect this problem to carry over to real situations.

Notice that in the third term of (2.3), $\sigma_{H,i}^2 \tan^2 \theta_j$ increases the uncertainty attributed to variable slope while incurring nominal computational expense. The line segment between i and j is generally at an azimuthal angle $\psi_{i,j}$, thus an end-user could modify the third term to be $\sigma_{H,i}^2 \tan^2 \theta_j \cos^2 \psi_{i,j}$ for a lower estimate if desired, but at additional computational cost. Angle $\psi_{i,j}$, however, will vary by $\pm \Delta \psi_{i,j}$ due to $\sigma_{H,i}$. The maximum $\Delta \psi_{i,j}$ occurs when this position varies perpendicular to line segment d_{ij} by $\pm \sigma_{H,i}$ so that $\Delta \psi_{i,j} = \arctan\left(\frac{\sigma_{H,i}}{d_{ij}}\right)$. Therefore, the modified third term is the product of $\sigma_{H,i}^2 \tan^2 \theta_j$ and the maximum value of $\cos^2 \psi_{i,j}$ as $\psi_{i,j}$ varies by $\psi_{i,j} \pm \Delta \psi_{i,j}$.

These case studies demonstrate that the created CURVE uncertainty bounds the error between the truth data and the DBM created using GMT SIT on sparse data for this highly dynamic ocean region, given the standard values of S_H and α . Further work is needed for determining appropriate of S_H and α values as a function of sampling density, seafloor morphology and source data measurement errors. Additionally, appropriate clipping bounds (as a function of depth) need to be determined for cases where there is very high slope or poor-quality data.

Since initially presented in (S. J. Zambo et al., 2015a), there have been many extensions in attributing uncertainty to sparse data (Bourgeois et al., 2016, 2016; B. Calder & Elmore, 2017; Paul A Elmore et al., 2017; Ladner et al., 2017; Petry et al., 2015; Tavana et al., 2016), most of which this author has assisted.

Our w -ELS ensemble technique lacks an inherent uncertainty estimator. Although we utilize ELS to estimate weight \mathbf{w} , w -ELS does not make point estimates from the fitted regression but instead use \mathbf{w} to weight the conflicting surfaces for point estimates. Thus, we do not use the uncertainties computed by ELS and use CURVE to compute the uncertainties instead for w -ELS.

The remaining ensemble techniques utilize CURVE to compute their uncertainties, as well. Applying CURVE to the various interpolation schemes is straightforward.

Hence, all the ensembles compute the same uncertainties, and these uncertainties may match those computed by an individual interpolator, if it employed CURVE to compute its uncertainties as well.

Next, in Chapter III, we present our new nominal-informed modeling approach for constructing DBMs via differentially weighted ensembles according to nominal information and our ELS technique presented therein. ⁴³

⁴³ Adapted from “Uncertainty Estimation for Sparse Data Gridding Algorithms” by S. Zambo et al. In proceedings of the U. S. Hydro Conference (and poster presentation of the Tenth Annual GEBCO Bathymetric Science Day (Symposium). 2015. No copyright. Adapted with permission. (https://www.gebco.net/about_us/gebco_symposium/documents/gebco_sd_2015_zambo.pdf)

CHAPTER III – A NEW INFORMED ENSEMBLE APPROACH TO BATHYMETRY UTILIZING MACHINE LEARNERS

In this chapter, we present my new approach to constructing DBMs that utilizes nominal information provided by machine learners identifying geomorphological seafloor primitives to model ‘smarter’. This smart (nominal-informed) modeling of bathymetry uses conflicting nominal data provided by different machine learners to 1) select informed (feature-favoring) interpolators to produce informed (feature-favoring) DBMs to ensemble according to an informed differential-weight \mathbf{w} computed via ELS, and to 2) construct an informed regression model to utilize in ELS via a differential-weighting of primitive functional forms identified by the nominal data.

Section 3.1 considers a seafloor surface as a hybrid mixture of geomorphological primitives. Particularly, we consider our hybrid as a weighted combination of a seamount and ridge primitive. These constitute primitives are our nominal data (classifications). Section 3.2 presents our ELS approach for computing ensemble weights for competing DBMs produced by conflicting nominal data. Section 3.3 presents additional methods implemented to aid in our investigations.

In section 3.1 and section 3.2, we describe work performed, in part, with Paul Elmore and A. Louise Perkins. My specific contributions to section 3.1 are:

- I developed a model composed of nominal primitives.
- I implemented a 2D Gaussian seamount and a 1D Gaussian ridge primitive, and hybrid mixtures thereof proposed by A. Louise Perkins in a script.

- I devised and implemented an additional more diverse 2D truncated cone seamount primitive and hybrid mixtures thereof with the 1D Gaussian ridge in a script.

My specific contributions to section 3.2 are:

- I implemented ELS and w -ELS computations.
- I implemented a planar regression model.
- I devised and implemented nominal-informed custom regression models.
- Evaluation and diagnostic tools for ELS and w -ELS.
- Original discussions for using classifications in an interpolator were done with A. Louise Perkins.

My specific contributions to section 3.3 are:

- I devised and implemented additional methods in a script to evaluate against w -ELS/ELS.

3.1 Geomorphological Seafloor Primitive Nominal Data

The seafloor surface may be viewed abstractly as a composite of geomorphological-shaped primitive space functions. We will refer to these geomorphological –shaped primitive space functions as primitives. These primitives may vary across the seafloor as well as amongst themselves, and the set is amendable as we discover new and more appropriate primitives. We employ classifiers to learn and predict seafloor primitives. Classifiers have already demonstrated success in identifying seafloor geomorphological features (D. Smith et al., 2016). More work has been spent on GIS classifications of terrain primitives. This expanding body of work is applicable to the

seabed as well, with some modifications (Franklin, 2020; Lecours et al., 2016; V. Lucieer et al., 2019).

Figure 3.1 illustrates this redefined problem space. Primitive 1 and 2 of Figure 3.1a are functions representing geomorphological shapes and their composition makes up the seafloor surface in Figure 3.1b, having its result determined by the weight (probability) \mathbf{w} . Classifiers identify predominate shapes, those having the most influence on the overall surface shape. Diverse classifiers suggest that the surface shape had high influences from more than one primitive. Current practices are to utilize a winner-take-all strategy for conflicting classifications. Instead, we propose utilizing all classifications, conflicting or otherwise, since they all have skill in identifying some aspect of the domain. We also may find areas where the classification is undetermined, which could enable algorithms to identify areas that require human analysis. This learned knowledge about the domain is valuable and may assist in forging ensembles with lower error than the current approach of utilizing an individual interpolator.

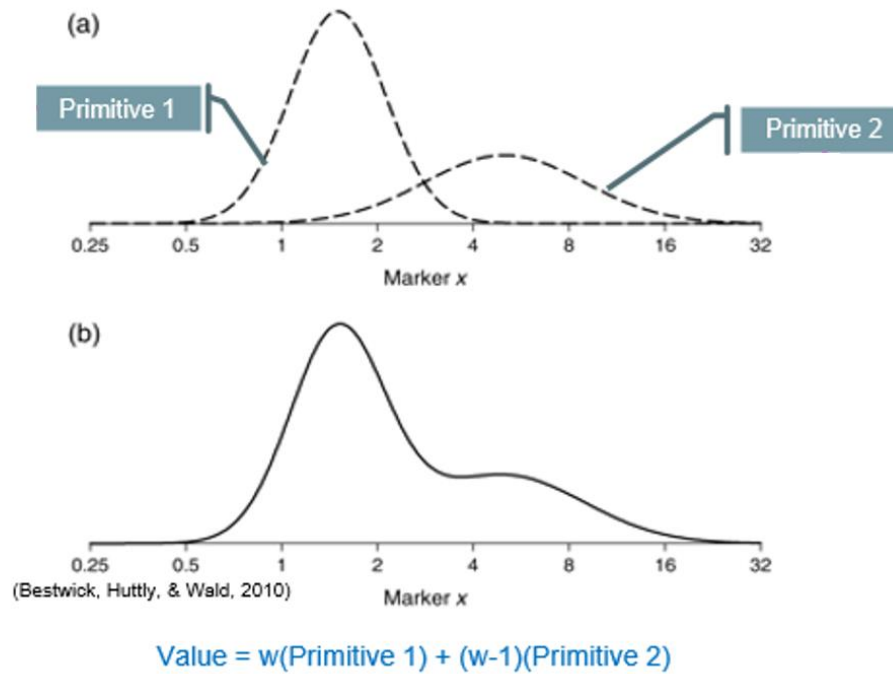


Figure 3.1 Example of seafloor surface decomposed into primitives.

A seafloor surface illustrated as a weighted composition of geomorphological-shaped primitive space functions known as primitives.

Primitive 1 and 2 are members of the a) primitive space of geomorphological-shaped functions for the b) composite seafloor (Bestwick et al., 2010) and are the classes determined by the classifiers (Polikar, 2006).

Future work will be able to identify primitives, and based on the primitives, we may select the interpolators that are most suited (feature-favoring) as the ensemble members. By considering our surface as a weighted composition of primitives, we could utilize such classifiers trained to identify these contributing primitives as a mechanism to provide a priori domain knowledge to our ensembles. This domain knowledge may suggest the ensemble members, weights, or both.

To compute the ensemble weights, we utilize an OLS-based framework, ELS, presented next in section 3.2, to calculate the weighting between different nominal-

informed DBMs.⁴⁴ ELS regresses on an unascertained-weighted ensemble of DBMs, whereby a final ensembled DBM may be estimated from the regressed model. Extracting the computed primitive weighting \mathbf{w} , w -ELS externally weights the ensemble members (DBMs) according to the ELS computed ensemble weights \mathbf{w} .

3.2 ELS for an Informed Differentially Weighted Ensemble of DBMs

I add a mathematical approach for folding all conflicting nominal domain knowledge provided by our classifiers into a least-squares computation on an ensemble of DBMs (ELS). This ensemble method will utilize an OLS framework to determine the ensemble weights of nominal-informed DBMs. Specifically, this approach solves the overdetermined set of equations,

$$Ax \approx b \quad (Ax - b = r),$$

by minimizing the residual r . Specifically, one minimizes the linear square residual equation

$$r^2 = \sum_i (y_i - (mx_i + b))^2. \quad (3.1)$$

Utilization of weights in regression is common practice. For example, weighted regression provides a means to incorporate uncertainty for heteroscedastic data into the solution process. Additionally, Cleveland (1979) constructed a (non-parametric) locally weighted regression (LOWESS/LOESS) that used a neighborhood of points only, allowing one to model a wider class of functions. The tri-cube weighting function they introduced as a robust measure is accurate through the third moment of the probability

⁴⁴ Personal communication with A. Louise Perkins.

density function. We utilize a differential weighting of DBMs in an OLS framework (ELS).

We develop an ensemble method that utilizes both traditional and nominal data (i.e., data derived from classifiers) to incorporate a priori geomorphological knowledge for constructing a more realistic synthetic seafloor (Perkins, 2016). This RMS-based method will utilize two geophysical nominal data values or primitive shapes, seamounts, and ridges as a proof of concept.

Our ELS approach is constrained-interval OLS. Starting with $Ax \approx b$, an over-constrained system, we solve for the weights \mathbf{w} , and the m and b from (3.1), subject to the constraint that our ensemble weight falls within the interval $[0, 1]$. OLS leads to a solution of the form

$$x = (A^T A)^{-1} A^T y.$$

Following the notation in Pierce & Rust (1985), ridge regression selects

$$x = [A^T A + \lambda I]^{-1} A^T y,$$

where the arbitrary parameter λ is the ridge. The interval constraint given in that same publication takes the form

$$x = \left[A^T A + \frac{\tau}{\eta} Q^{-2} \right]^{-1} \left[A^T y + \frac{\tau}{\eta} Q^{-2} d \right],$$

where Q is a function of the interval defined, η is a linear combiner for the ellipsoids that replace the interval, and τ is related to the confidence interval.

Our fundamental idea behind ELS is to relax the typical interpolation constraint that disallows competing values at the same physical location, admitting instead an ensemble weight of similarly located values that adjust dynamically to a minimum unbiased estimation.

To model seamounts, we will use a conical frustum (or hyperboloid), which we refer to as a truncated seamount,

$$f(x, y) = A_S - \sqrt{\frac{(x - \mu_x)^2}{\sigma_x^2} + \frac{(y - \mu_y)^2}{\sigma_y^2} - r^2}, \quad (3.2)$$

where A_S is the amplitude, r is a scaling factor, μ is the mean, and σ is the standard deviation. We retain only real roots. For our test cases, we used $A_S = 1,200$ m and $r = 0.5$.

To model ridges, we use a 1D Gaussian,

$$f(x, y) = A_R e^{-\left(\frac{(x - \mu_x)^2}{2\sigma_x^2}\right)}, \quad (3.3)$$

where A_R is again the amplitude, μ is the mean, and σ is the standard deviation.

We use these functions to generate synthetic data sets by forming a weighted combination,

$$f(x, y) = \mathbf{w} \left(A_S - \sqrt{\frac{(x - \mu_x)^2}{\sigma_x^2} + \frac{(y - \mu_y)^2}{\sigma_y^2} - r^2} \right) + (1 - \mathbf{w}) A_R e^{-\left(\frac{(x - \mu_x)^2}{2\sigma_x^2}\right)} + b. \quad (3.4)$$

where weight \mathbf{w} controls the amount of influence each primitive has in the combined surface. These analytic studies allow us to quantify the ensemble value-added by providing us with an absolute error analysis in sparse data situations.

We have designed the experiments to highlight not only where nominal data adds value, but also where it may mislead our results.

For our nominal regression, we assume that we have two competing solutions, $\{(x_i, y_{i_1})\}$ and $\{(x_i, y_{i_2})\}$, derived from the nominal geomorphological models. Notice that these sets agree on their independent location but differ in their dependent result. We

seek a local linear approximation, $y = mx + b$, where there are two residuals at each x_i location, $r_1 = y_{i_1} - mx_i + b$ and $r_2 = y_{i_2} - mx_i + b$, so that our total residual is a sum over the individual nominal residuals at each x_i location. (For clarity and simplicity, we omit the terms for interval constraining and ridge regression in subsequent derivations.)

Introduce the weight \mathbf{w} , such that

$$y_i = \mathbf{w}y_{i_1} + (1 - \mathbf{w})y_{i_2}.$$

We wish to minimize our overall residual sum by solving for an optimal weighting concurrently with solving for the variables m and b . To do this, using y_i as defined above, we minimize

$$r_T^2 = \sum_i (y_i - (mx_i + b))^2.$$

Writing y_i in terms of its component parts, we have

$$\begin{aligned} r_T^2 &= \sum (\mathbf{w}y_{i_1} + (1 - \mathbf{w})y_{i_2})^2 - 2m \sum (\mathbf{w}y_{i_1} + (1 - \mathbf{w})y_{i_2})x_i \\ &\quad - 2b \sum (\mathbf{w}y_{i_1} + (1 - \mathbf{w})y_{i_2}) + m^2 \sum x_i^2 + 2mb \sum x_i + nb^2 \\ &= \mathbf{w}^2 \sum (y_{i_1} - y_{i_2})^2 + 2\mathbf{w} \sum (y_{i_1} - y_{i_2})y_{i_2} + \sum y_{i_2}^2 - 2m\mathbf{w} \sum (y_{i_1} - y_{i_2})x_i \\ &\quad - 2m \sum y_{i_2}x_i - 2b\mathbf{w} \sum (y_{i_1} - y_{i_2}) - 2b \sum y_{i_2} + m^2 \sum x_i^2 \\ &\quad + 2mb \sum x_i + nb^2. \end{aligned}$$

Now instead of minimizing to find only the m and b , we have redefined our problem to include this unknown weight \mathbf{w} . To simplify, let

$$\bar{x} = \frac{1}{n} \sum x_i$$

$$\overline{x^2} = \frac{1}{n} \sum x_i^2$$

$$\Delta y_i = (y_{i_1} - y_{i_2})$$

$$\overline{\Delta y} = \frac{1}{n} \sum \Delta y_i$$

$$\overline{\Delta y^2} = \frac{1}{n} \sum \Delta y_i^2$$

$$\overline{\Delta y x} = \frac{1}{n} \sum \Delta y_i x_i$$

$$\overline{\Delta y y_{N2}} = \frac{1}{n} \sum \Delta y_i y_{i_2}$$

$$\overline{y_{N2}^2} = \frac{1}{n} \sum y_{i_2}^2$$

$$\overline{y_{N2} x} = \frac{1}{n} \sum y_{i_2}^2 x_i.$$

To minimize, we need to solve

$$\frac{\partial r_T}{\partial m} = -2\mathbf{w}n\overline{\Delta y x} - 2n\overline{y_{N2} x} + 2mn\overline{x^2} + 2bn\bar{x} = 0$$

$$\frac{\partial r_T}{\partial b} = -2\mathbf{w}n\overline{\Delta y} - 2n\overline{y_{N2}} + 2mn\bar{x} + 2nb = 0$$

$$\frac{\partial r_T}{\partial \mathbf{w}} = 2\mathbf{w}n\overline{\Delta y^2} + 2n\overline{\Delta y y_{N2}} - 2mn\overline{\Delta y x} - 2bn\overline{\Delta y} = 0.$$

The matrix form of these equations is

$$\begin{bmatrix} 2n\overline{x^2} & 2n\bar{x} & -2n\overline{\Delta y x} \\ 2n\bar{x} & 2n & -2n\overline{\Delta y} \\ -2n\overline{\Delta y x} & -2n\overline{\Delta y} & 2n\overline{\Delta y^2} \end{bmatrix} \begin{bmatrix} m \\ b \\ \mathbf{w} \end{bmatrix} = \begin{bmatrix} -2n\overline{y_{N2} x} \\ -2n\overline{y_{N2}} \\ -2n\overline{\Delta y y_{N2}} \end{bmatrix}.$$

When nonsingular, for example,

$$8n^3 \left[(\overline{x^2})(\overline{\Delta y^2}) - (\overline{x^2})(-\overline{\Delta y})^2 - (\overline{x})^2(\overline{\Delta y^2}) + (\overline{x})(-\overline{\Delta y})^2 \right. \\ \left. + (-\overline{\Delta y x})(-\overline{\Delta y})^2 - (-\overline{\Delta y x})^2 \right] \neq 0,$$

we may solve for slope, bias, and weight. We check the determinant to insure it remains above a given stability tolerance, τ .

For a two-dimensional surface, such as bathymetry, the problem becomes

$$r_{2D} = \sum_i \left(y_i - (m_1 x_{i_1} + m_2 x_{i_2} + b) \right)^2.$$

Expanding this, nets

$$\begin{aligned} r_{2D} &= \sum (\mathbf{w} y_{i_1} + (1 - \mathbf{w}) y_{i_2})^2 - 2m_1 \sum (\mathbf{w} y_{i_1} + (1 - \mathbf{w}) y_{i_2}) x_{i_1} \\ &\quad - 2m_2 \sum (\mathbf{w} y_{i_1} + (1 - \mathbf{w}) y_{i_2}) x_{i_2} - 2b \sum (\mathbf{w} y_{i_1} + (1 - \mathbf{w}) y_{i_2}) \\ &\quad + m_1^2 \sum x_{i_1}^2 + 2m_1 m_2 \sum x_{i_1} x_{i_2} + 2m_1 b \sum x_{i_1} + m_2^2 \sum x_{i_2}^2 \\ &\quad + 2m_2 b \sum x_{i_2} + nb^2 \\ &= \mathbf{w}^2 \sum (y_{i_1} - y_{i_2})^2 + 2\mathbf{w} \sum (y_{i_1} - y_{i_2}) y_{i_2} + \sum y_{i_2}^2 \\ &\quad - 2m_1 \mathbf{w} \sum (y_{i_1} - y_{i_2}) x_{i_1} - 2m_1 \sum y_{i_2} x_{i_1} \\ &\quad - 2m_2 \mathbf{w} \sum (y_{i_1} - y_{i_2}) x_{i_2} - 2m_2 \sum y_{i_2} x_{i_2} - 2b \mathbf{w} \sum (y_{i_1} - y_{i_2}) \\ &\quad - 2b \sum y_{i_2} + m_1^2 \sum x_{i_1}^2 + m_1 m_2 \sum x_{i_1} x_{i_2} + 2m_1 b \sum x_{i_1} \\ &\quad - m_2^2 \sum x_{i_2}^2 + 2m_2 b \sum x_{i_2} + nb^2. \end{aligned}$$

To locate a minimum solution, we require

$$\begin{aligned}\frac{\partial r_{2D}}{\partial m_1} = & -2\mathbf{w} \sum (y_{i_1} - y_{i_2})x_{i_1} - 2 \sum y_{i_2}x_{i_1} + 2m_1 \sum x_{i_1}^2 + 2m_2 \sum x_{i_1}x_{i_2} \\ & + 2b \sum x_{i_1} = 0\end{aligned}$$

$$\begin{aligned}\frac{\partial r_{2D}}{\partial m_2} = & -2\mathbf{w} \sum (y_{i_1} - y_{i_2})x_{i_2} - 2 \sum y_{i_1}x_{i_2} - 2m_2 \sum x_{i_2}^2 + 2m_1 \sum x_{i_1}x_{i_2} \\ & + 2b \sum x_{i_2} = 0\end{aligned}$$

$$\begin{aligned}\frac{\partial r_{2D}}{\partial w} = & 2\mathbf{w} \sum (y_{i_1} - y_{i_2})^2 + 2 \sum (y_{i_1} - y_{i_2})y_{i_2} - 2m_1 \sum (y_{i_1} - y_{i_2})x_{i_1} \\ & - 2m_2 \sum (y_{i_1} - y_{i_2})x_{i_2} - 2b \sum (y_{i_1} - y_{i_2}) = 0\end{aligned}$$

$$\frac{\partial r_{2D}}{\partial b} = -2\mathbf{w} \sum (y_{i_1} - y_{i_2}) - 2 \sum y_{i_2} + 2m_1 \sum x_{i_1} + 2m_2 \sum x_{i_2} + 2nb = 0.$$

Writing these equations without explicit sums nets

$$\frac{\partial r_{2D}}{\partial m_1} = -2\mathbf{w}n\overline{\Delta y x_{D1}} - 2n\overline{y_{N2}x_{D1}} + 2m_1\overline{nx_{D1}^2} + 2m_2n\overline{x_{D1}x_{D2}} + 2bn\overline{x_{D1}} = 0,$$

$$\frac{\partial r_{2D}}{\partial m_2} = -2\mathbf{w}n\overline{\Delta y x_{D2}} - 2n\overline{y_{N2}x_{D2}} + 2m_2\overline{nx_{D2}^2} + 2m_1n\overline{x_{D1}x_{D2}} + 2bn\overline{x_{D2}} = 0,$$

$$\frac{\partial r_{2D}}{\partial b} = -2\mathbf{w}n\overline{\Delta y} - 2n\overline{y_{N2}} + 2m_1n\overline{x_{D1}} + 2m_2n\overline{x_{D2}} + 2nb = 0,$$

$$\frac{\partial r_{2D}}{\partial w} = 2\mathbf{w}n\overline{\Delta y^2} + 2n\overline{\Delta y y_{N2}} - 2m_1n\overline{\Delta y x_{D1}} - 2m_2n\overline{\Delta y x_{D2}} - 2bn\overline{\Delta y} = 0.$$

The matrix form for two independent variables is

$$\begin{bmatrix} 2n\overline{x_{D1}^2} & 2n\overline{x_{D1}x_{D2}} & 2n\overline{x_{D1}} & -2n\overline{\Delta y x_{D1}} \\ 2n\overline{x_{D1}x_{D2}} & 2n\overline{x_{D2}^2} & 2n\overline{x_{D2}} & -2n\overline{\Delta y x_{D2}} \\ 2n\overline{x_{D1}} & 2n\overline{x_{D2}} & 2n & -2n\overline{\Delta y} \\ -2n\overline{\Delta y x_{D1}} & -2n\overline{\Delta y x_{D2}} & -2n\overline{\Delta y} & 2n\overline{\Delta y^2} \end{bmatrix} \begin{bmatrix} m_1 \\ m_2 \\ b \\ \mathbf{w} \end{bmatrix} = \begin{bmatrix} -2n\overline{y_{N2}x_{D1}} \\ -2n\overline{y_{N2}x_{D2}} \\ -2n\overline{y_{N2}} \\ 2n\overline{\Delta y y_{N2}} \end{bmatrix}.$$

When nonsingular, we may again solve for the unknown slope, bias, and weight.

The more complex 2D determinate is given by

$$\begin{aligned}
& 2n\overline{x_{D1}^2} \left((2n\overline{x_{D2}^2})(2n)(2n\overline{\Delta y^2}) - (2n\overline{x_{D2}^2})(-2n\overline{\Delta y})(-2n\overline{\Delta y}) \right. \\
& \quad - (2n\overline{x_{D2}})(2n\overline{x_{D2}})(2n\overline{\Delta y^2}) \\
& \quad + (2n\overline{x_{D2}})(-2n\overline{\Delta y})(-2n\overline{\Delta y x_{D2}}) + (-2n\overline{\Delta y x_{D2}})(2n\overline{x_{D2}})(-2n\overline{\Delta y}) \\
& \quad \left. - (-2n\overline{\Delta y x_{D2}})(2n)(-2n\overline{\Delta y x_{D2}}) \right) - \\
& 2n\overline{x_{D1} x_{D2}} \left((2n\overline{x_{D1} x_{D2}})(2n)(2n\overline{\Delta y^2}) - (2n\overline{x_{D1} x_{D2}})(-2n\overline{\Delta y})(-2n\overline{\Delta y}) \right. \\
& \quad - (2n\overline{x_{D1}})(2n\overline{x_{D2}})(2n\overline{\Delta y^2}) \\
& \quad + (2n\overline{x_{D1}})(-2n\overline{\Delta y})(-2n\overline{\Delta y x_{D2}}) + (-2n\overline{\Delta y x_{D1}})(2n\overline{x_{D2}})(-2n\overline{\Delta y}) \\
& \quad \left. - (-2n\overline{\Delta y x_{D1}})(2n)(-2n\overline{\Delta y x_{D2}}) \right) + \\
& 2n\overline{x_{D1}} \left((2n\overline{x_{D1} x_{D2}})(2n\overline{x_{D2}})(2n\overline{\Delta y^2}) - (2n\overline{x_{D1} x_{D2}})(-2n\overline{\Delta y x_{D2}})(-2n\overline{\Delta y}) \right. \\
& \quad - (2n\overline{x_{D1}})(2n\overline{x_{D2}^2})(2n\overline{\Delta y^2}) \\
& \quad + (2n\overline{x_{D1}})(-2n\overline{\Delta y x_{D2}})(-2n\overline{\Delta y x_{D2}}) + (-2n\overline{\Delta y x_{D1}})(2n\overline{x_{D2}^2})(-2n\overline{\Delta y}) \\
& \quad \left. - (-2n\overline{\Delta y x_{D1}})(2n\overline{x_{D2}})(-2n\overline{\Delta y x_{D2}}) \right) - \\
& -2n\overline{\Delta y x_{D1}} \left((2n\overline{x_{D1} x_{D2}})(2n\overline{x_{D2}})(-2n\overline{\Delta y}) - (2n\overline{x_{D1} x_{D2}})(-2n\overline{\Delta y x_{D2}})(2n) \right. \\
& \quad - (2n\overline{x_{D1}})(2n\overline{x_{D2}^2})(-2n\overline{\Delta y}) \\
& \quad + (2n\overline{x_{D1}})(-2n\overline{\Delta y x_{D2}})(2n\overline{x_{D2}}) + (-2n\overline{\Delta y x_{D1}})(2n\overline{x_{D2}^2})(2n) \\
& \quad \left. - (-2n\overline{\Delta y x_{D1}})(2n\overline{x_{D2}})(2n\overline{x_{D2}}) \right) \neq 0,
\end{aligned}$$

This matrix trivially degenerates when all inputs are identical (when $\overline{\Delta y} = 0$, for example), as with 1D, and again we may check the determinate to insure it remains above a given stability tolerance, τ .

The external weighting of DBMs according to weight \mathbf{w} computed by ELS is our w -ELS ensemble. For simplicity, we will refer to the general approach as ELS. In this section, we presented ELS by utilizing a planar model. However, from the tenets of regression, it is desirable to utilize a model that well-approximates our generating function. We further utilize nominal data to obtain an informed regression model and investigate its efficacy in our second study.

We obtain a nominal-informed regression model as a weighted combination of primitive shape functional forms identified by nominal data. We assume that in identifying the geomorphological primitives of our seafloor, our classifiers provide functional forms for the identified primitives. In our experiments, our assumed classifiers provide nominal data by identifying the true functional forms of our truncated seamount (3.2) and ridge (3.3) primitives that compose our hybrid morphology for a true-approximating nominal-informed custom regression model (3.4).

Section 3.2.1 discusses the (un-informed) planar and (nominal-informed) custom model utilized in our second study to investigate the efficacy of nominal-informed modeling.

3.2.1 Regression Models

In this section, we discuss the two models used by our w -ELS/ELS methods: a simple (un-informed) planar model and a more complex (nominal-informed) custom model.

As previously discussed, our w -ELS/ELS technique uses classification information from machine learners. This classification information is known as nominal data. The machine learners classify bathymetric data as being one of many morphological

primitive shape functions. In this dissertation, we consider machine learners which classify data as either the 2D truncated cone seamount or the 1D Gaussian ridge presented in section 3.2 as (3.2) and (3.3). When machine learners disagree, they have conflicting classifications (nominal data). Ensembles allow us to utilize all nominal-information for fully informed modeling.

In our first study, we demonstrate interpolator preference (favoritism) in generating DBMs for primitive (feature) classifications (nominal data). These interpolators and DBMs are feature-favoring for the identified primitive classification. We selected these preferences by evaluating validity (signal persisted through for a physically realistic surface) and trustworthiness (too high a bias or variance) when computationally feasible. However, limited computational resources restricted the amount of work we performed here.

When we have conflicting classifications (nominal data), the machine learners will have identified more than one primitive shape function – the nominal data will suggest more than one interpolator for surface generation. In our second study, we investigate whether:

- Our w -ELS/ELS methodology mitigates the penalties of selecting a less-optimal interpolator stemming from classifications of a complex morphology, limited (sparse) data, diverse machine learners, or combinations thereof.
- By utilizing an ensemble technique based on composite primitive forms, we compensate for non-validity and untrustworthiness that may occur when utilizing an inappropriate DBM. In a worst-case scenario, a machine

learner would make an incorrect classification and suggest an inadequate interpolator for the data.

- w -ELS/ELS (and more generally, ensemble techniques) reduce the effects of utilizing an inadequate DBM by combining it with a (hopefully) more adequate DBM.
- w -ELS/ELS mitigates between individual point estimates for a conservative surface when both interpolators produce DBM surfaces that are seemingly adequate.
 - Due to the random variability in the data, along with the bias-variance trade-off of our OLS computations discussed in section 2.3.1, interpolator results have different accuracies.

For our nominal-informed custom model, instead of only using the nominal classifications in selecting interpolators, we additionally use the identified primitive shape functional forms directly in a custom nominal-informed regression model. The nominal data implies that the data have similarities consistent with the selected primitive shape functions, enough so to garner classification as determined by a classifier's unique a priori criteria. We combine the primitive shape functions into a single model for utilization in w -ELS/ELS.

Our morphological primitive shape functions could be replaced by models which use explanatory variables that capture the physics responsible for the feature's evolution. These types of models would provide better fits to the data than simplistic, overgeneralized models, because they capture the underlying phenomenon responsible for the feature shapes. Further research is needed in developing adequate models for the

various seafloor features. These advanced models may be added to the primitive space for utilization by the classifiers and our w -ELS/ELS technique. Indeed, what is needed is a dictionary for the collection of morphological primitive shape functions that have been rigorously tested and evaluated. This would provide a comprehensive reference for oceanography modelers studying various dynamics and would facilitate cohesive modeling practices.

In section 3.2.1.1, we summarize the planar model already presented in section 3.2, and similarly present in section 3.2.1.2, the new informed custom model.

3.2.1.1 Planar Model (Un-Informed)

As discussed previously, our planar model is a simple zeroth order linear model,

$$f(x_{i_1}, x_{i_2}) = m_1 x_{i_1} + m_2 x_{i_2} + b.$$

When performing w -ELS/ELS, the planar model fits to the conflicting DBMs $\{y, (x_1, x_2)\}$ to estimate the coefficients that minimize the squared total residuals between the model and the conflicting DBMs,

$$r_{2D} = \sum_i \left(y_i - (m_1 x_{i_1} + m_2 x_{i_2} + b) \right)^2.$$

We summarize the high-level details here for the convenience of the reader and easy comparison with our next nominal-informed custom model,

$$y_i = \mathbf{w}y_{i_1} + (1 - \mathbf{w})y_{i_2}.$$

This expands to

$$r_{2D} = \sum_i \left(y_{i_2} - (\mathbf{w}(y_{i_2} - y_{i_1}) + m_1 x_{i_1} + m_2 x_{i_2} + b) \right)^2$$

with the model

$$f(x_{i_1}, x_{i_2}, y_{i_1}, y_{i_2}) = \mathbf{w}(y_{i_2} - y_{i_1}) + m_1 x_{i_1} + m_2 x_{i_2} + b$$

fitting to the conflicting DBMs to estimate the coefficients that minimize the squared residuals. For ELS, we make point predictions from the estimated regression line to obtain our ensemble DBM $\{f(x_{1_{grid}}, x_{2_{grid}}, y_1, y_2), (x_{1_{grid}}, x_{2_{grid}})\}$, and for w -ELS, we use weight w to weight our conflicting surfaces to obtain our ensemble DBM $\{y, (x_{1_{grid}}, x_{2_{grid}})\}$.

Additionally, the planar model is fit to the scattered input measurements $\{y_{in}, (x_{1_{in}}, x_{2_{in}})\}$ to estimate the coefficients that minimize the squared residuals

$$r_{2D} = \sum_i (y_i - (m_1 x_{i_1} + m_2 x_{i_2} + b))^2.$$

From the estimated regression line, we make point predictions to obtain our final DBM $\{f(x_{1_{grid}}, x_{2_{grid}}), (x_{1_{grid}}, x_{2_{grid}})\}$.

3.2.1.2 Custom Model (Nominal-Informed)

Our nominal-informed custom model goes a step beyond using the nominal data from the machine learners to only guide interpolator selections. It uses the primitive functional forms on which the machine learners made their classifications, to determine an appropriate model for the data. The insight provided by the machine learners allow for a nominal-informed custom model instead of a generic planar model to be fit. The better the model fits, the smaller its total residuals will be, and the more accurately and precisely it will estimate its coefficients and make point predictions. Our second study investigates the efficacy of utilizing the nominal-informed custom model in w -ELS/ELS against the (un-informed) planar model to determine the sensitivity of w -ELS/ELS to how well the nominal-informed model approximates the underlying morphology.

The informed custom model uses the primitive shape functional forms implied by the machine learners to classify the region. The idea is to let the machine learners select the model components. In this dissertation, we study a hybrid morphology generating a truncated seamount and ridge conffliction.

We utilized a Gaussian ridge and a conical frustum (or hyperboloid), which we have referred to as a truncated seamount.⁴⁵

Both morphologies were given a height (amplitude) of 1,200 m.⁴⁶ We constructed combined surfaces by weighting the seamount primitive-shape function by 75% in an average with our ridge primitive-shape function. We chose a seafloor depth of 11,200 m. We arbitrarily selected 15,800 to 41,800 m North and South positional boundaries for the regions to obtain a 51 by 51 grid of 520 m grid spacing.

For a combined 2D truncated cone seamount and 1D Gaussian ridge surface, our nominal-informed custom model is a more complex nonlinear model,

$$f(x_{i_1}, x_{i_2}) = w_1 \left(A_S - \sqrt{\frac{(x_{i_1} - \mu_{x_1})^2}{\sigma_{x_1}^2} + \frac{(x_{i_2} - \mu_{x_2})^2}{\sigma_{x_2}^2} - r^2} \right) + (1 - w_1) A_R e^{-\left(\frac{(x_{i_1} - \mu_{x_1})^2}{2\sigma_{x_1}^2}\right)} + b.$$

When performing w -ELS/ELS, the custom model fits to the conflicting DBMs $\{y, (x_1, x_2)\}$ to estimate the coefficients that minimize the squared total residuals between the custom model and the conflicting DBMs,

⁴⁵⁴⁵ Seamounts typically have a conical shape where length/width ratio is less than 2 (GRID-Arendal, n.d.; International Hydrographic Organization, 2008; Mitchell, 2001).

⁴⁶ Seamounts typically have elevations greater than 1,000 m above the seafloor.

$$r_{2D} = \sum_i \left(y_i - \left(w_1 \left(A_S - \sqrt{\frac{(x_{i_1} - \mu_{x_1})^2}{\sigma_{x_1}^2} + \frac{(x_{i_2} - \mu_{x_2})^2}{\sigma_{x_2}^2} - r^2} \right) + (1 - w_1) A_R e^{-\left(\frac{(x_{i_1} - \mu_{x_1})^2}{2\sigma_{x_1}^2}\right)} + b \right) \right)^2$$

where

$$y_i = \mathbf{w}y_{i_1} + (1 - \mathbf{w})y_{i_2}.$$

This expands to

$$r_{2D} = \sum_i \left(y_{i_2} - \left(\mathbf{w}(y_{i_2} - y_{i_1}) + w_1 \left(A_S - \sqrt{\frac{(x_{i_1} - \mu_{x_1})^2}{\sigma_{x_1}^2} + \frac{(x_{i_2} - \mu_{x_2})^2}{\sigma_{x_2}^2} - r^2} \right) + (1 - w_1) A_R e^{-\left(\frac{(x_{i_1} - \mu_{x_1})^2}{2\sigma_{x_1}^2}\right)} + b \right) \right)^2.$$

with the model

$$\begin{aligned} & f(x_{i_1}, x_{i_2}, y_{i_1}, y_{i_2}) \\ &= \mathbf{w}(y_{i_2} - y_{i_1}) + w_1 \left(A_S - \sqrt{\frac{(x_{i_1} - \mu_{x_1})^2}{\sigma_{x_1}^2} + \frac{(x_{i_2} - \mu_{x_2})^2}{\sigma_{x_2}^2} - r^2} \right) \\ &+ (1 - w_1) A_R e^{-\left(\frac{(x_{i_1} - \mu_{x_1})^2}{2\sigma_{x_1}^2}\right)} + b \end{aligned}$$

fitting to the conflicting DBMs to estimate the coefficients that minimize the squared residuals. For ELS, we make point predictions from the estimated regression line to obtain our ensemble DBM $\{f(x_{1_{grid}}, x_{2_{grid}}, y_1, y_2), (x_{1_{grid}}, x_{2_{grid}})\}$, and for w -ELS, we use weight \mathbf{w} to weight our conflicting DBMs to obtain our ensemble DBM $\{y, (x_{1_{grid}}, x_{2_{grid}})\}$.

The custom model is fit to the scattered input measurements $\{y_{in}, (x_{1_{in}}, x_{2_{in}})\}$ to estimate the coefficients that minimize the squared residuals.

$$r_{2D} = \sum_i \left(y_i - \left(w_1 \left(A_S - \sqrt{\frac{(x_{i_1} - \mu_{x_1})^2}{\sigma_{x_1}^2} + \frac{(x_{i_2} - \mu_{x_2})^2}{\sigma_{x_2}^2} - r^2} \right) + (1 - w_1) A_{Re}^{-\left(\frac{(x_{i_1} - \mu_{x_1})^2}{2\sigma_{x_1}^2}\right)} + b \right) \right)^2.$$

From the estimated regression line, we make point predictions to obtain our DBM

$$\{f(x_{1_{grid}}, x_{2_{grid}}), (x_{1_{grid}}, x_{2_{grid}})\}.$$

3.3 Additional Methods to Assess

To evaluate ensembles, I devised and implemented additional ensemble and non-ensemble methods to compute for investigative purposes in a second study detailed in Chapter VI. These additional methods were chosen to gather insight into the benefits of utilizing nominal data and ensembles. Table 3.1 lists the additional methods. A script was written to compute these methods and any additional tests, metrics, and diagnostics they required.

Table 3.1

Additional Methods Assessed.

EM	Abbreviation	Description
Ensembles		
33	Mean	Arithmetic mean of conflicting surfaces. For two conflicting surfaces, the mean, median, and midrange are equal.
34	w-ELS (Planar Model)	Performs ELS using a planar model to estimate weight w weight conflicting surfaces for an ensemble surface
35	w-ELS (Custom Model)	Performs ELS using a custom model informed by the machine learners to estimate weight w weight conflicting surfaces for an ensemble surface
36	ELS (Planar Model)	Performs ELS using a planar model to estimate ensemble surface
37	ELS (Custom Model)	Performs ELS using a custom model informed by the machine learners to estimate ensemble surface
Non-Ensembles		
38	OLS on soundings (Planar Model)	Performs OLS fitting planar model on input data to estimate surface
39	OLS on soundings (Custom Model)	Performs OLS fitting custom model on input data to estimate surface
40	OLS on DBM1 (Primitive1 Model)	Performs OLS fitting seamount primitive on DBM from seamount favoring interpolator (EM06) to estimate surface
41	OLS on DBM2 (Primitive2 Model)	Performs OLS fitting ridge primitive on DBM from ridge favoring interpolator (EM18) to estimate surface
42	OLS on DBM1 (Custom Model)	Performs OLS fitting seamount primitive on DBM from seamount favoring interpolator (EM06) to estimate surface
43	OLS on DBM2 (Custom Model)	Performs OLS fitting ridge primitive on DBM from ridge favoring interpolator (EM18) to estimate surface
44	ELS (Primitive1 Model)	Performs ELS using seamount primitive informed by the machine learners to estimate ensemble surface
45	ELS (Primitive2 Model)	Performs ELS using ridge primitive informed by the machine learners to estimate ensemble surface
46	OLS GMT SIT (Custom Model)	Performs OLS fitting custom model on benchmark GMT SIT DBM to estimate surface
47	3mean	Mean of EM06, EM18, EM31
48	OLS on Mean (Custom Model)	Performs OLS fitting custom model on mean of EM06 and EM18 to estimate surface
49	OLS on 3Mean (Custom Model)	Performs OLS fitting custom model on mean of EM06, EM18, and EM31 to estimate surface
50	AllIndivMean	Mean of EM < 33
51	AllMean	Mean of all EM methods

The methodologies listed here are additional interpolation schemes computed for evaluation against the individual feature-favoring interpolation schemes in Table 2.2.

These methods each utilize nominal information differently (partially, fully, or un-informed) in DBM selection and regression models via either w -ELS, ELS, OLS, or equally weighted average. In Chapter VI, we utilize different sets of methods for different investigative purposes in our second study and we postpone further discussion until then.

The informed custom model for the truncated seamount and ridge hybrid surface is a nonlinear model, as well as any model utilizing the truncated seamount functional form. We utilized linearization in the Levenberg-Marquardt (Draper & Smith, 2014; Gavin, 2011) computations in fitting nonlinear models.

CHAPTER IV – RESEARCH APPROACH

In this chapter, we discuss the experiments, metrics, and analysis tools utilized in our research. Figure 4.1 outlines our testing procedures.

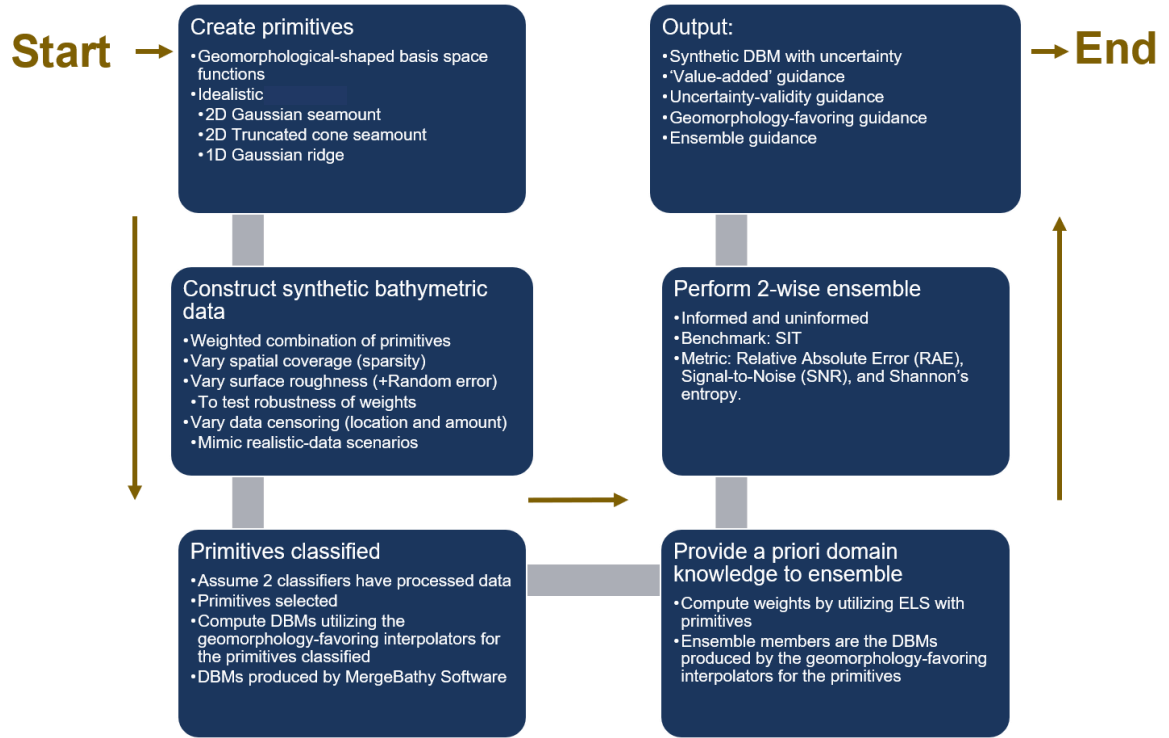


Figure 4.1 Process flow for synthetic experiments.

Outlines experimentation steps.

As a proof of concept, we performed a series of experiments, suggested by Paul Elmore, using ELS together with the DBM modeling techniques available in MergeBathy (Kalman filter, LOESS, and SIT). This allowed us to evaluate ensemble performance and viability using a priori domain-specific guidance from nominal data.

Holland (2005) originally developed the MergeBathy software suite. The software was extended by S. J. Zambo et al. (2015a). MergeBathy allows us to run the different interpolation schemes to reconstruct the seafloor as a DBM. Due to computational limits, our ensemble combinations were limited to two. This provides an opportunity to study

the functional relationship between individual and ensembled interpolation methods, albeit in a limited sense.

The SIT interpolator provided in GMT currently provides the de facto standard for sparse bathymetric data. SIT honors each data point in knowledge-limited regions, as it is a true interpolator, but its built-in bias suffers from underestimation.⁴⁷ Due to its ubiquitous usage, SIT is our benchmark modeling technique in our experiments. We choose GMT SIT (instead of MB – System SIT) to serve as our benchmark as GMT is most widely used and is a requirement of MB – System.

Utilizing the suite of MergeBathy interpolators along with additional methods, devised and implemented in an external script, we construct DBMs on synthetic sampling configuration over different morphologies. We utilize a variety of diagnostic tools and metrics to investigate, validate, and evaluate our DBMs. We evaluated performance qualitatively through various graphical techniques and quantitatively through significance testing.

Our objective is to evaluate the efficacy of nominal-informed modeling to see if utilizing nominal information when constructing DBMs is beneficial for improved accuracy. Particularly, we investigate the efficacy of utilizing nominal-information in selecting interpolators to construct DBMs and in constructing ensembles of DBMs.

The following sections present our experimentations. In section 4.1, we introduce our experimental studies. In section 4.2, we discuss the various analyses employed and in section 4.3, we discuss metrics utilized.

⁴⁷ Bathymetry prefers overestimation.

In this chapter, we describe work performed, in part, with Paul Elmore and A. Louise Perkins. My specific contributions are:

- I implemented in a script RMS, and signal-to-noise and entropy information metrics attribution for DBMs proposed by Paul Elmore for their evaluation.
- I implemented additional standard error metrics including CumRAE, and image evaluation metric attributions for DBMs in a script for DBM evaluation.
- I implemented various visualization and regression diagnostic plots, and statistical tests in a script.
- I implemented experiments proposed by Paul Elmore according to experimental designs (Montgomery, 2017).
- I devised and implemented a randomized experiment according to experimental designs (Montgomery, 2017).
- I setup and utilized cloud computing environments for additional computation resources.
- I implemented frequentist and Bayesian analyses of experiments.

4.1 Design of Experiments

We designed two studies to investigate the efficacy of nominal-informed modeling for DBM construction. Primary, we 1) investigate interpolation schemes for feature favoritism, 2) investigate efficacy off ensembles vis-à-vis feature-favoritism, and 3) evaluate ensemble performance comparative to individual interpolation schemes for both sparse and dense sampling configurations. Our first study is a set of controlled uniform experiments (UEs) and our second study is a set of randomized experiments (REs). Our studies are listed in Table 4.2.

Table 4.1

Studies Performed

Id	Name	Description
1	Uniform Experiments (UEs)	Uniform down-sampling of each feature data set. Controlled study on our seamount and ridge primitives to identify feature-favoring interpolators from the entire set of MergeBathy interpolators for nominal-informed modeling via interpolator selection.
2	Randomized Experiments (REs)	Random number of measurements randomly drawn from the sample region with random noise and random data censoring (swaths of random width, location, and direction were removed). A separate dataset, aside from the complete dataset, was composed of only those configurations which met our sparsity criterion (section 4.1.2). Randomized study on a hybrid morphology to evaluate the efficacy of nominal-informed modeling (interpolator selection and ensemble construction).

Studies performed. Each study is comprised of multiple experiments and utilizes different sets of tests (sampling configurations).

Both studies are composed of a set of experiments. The first study is a set of controlled uniform experiments (UEs) on our seamount and ridge primitives and utilizes three test data sets on each primitive, for a total of six UEs (three UEs for each primitive). The second study is a set of randomized experiments (REs) on our hybrid morphology (weighted mixture of our seamount and ridge primitive) and utilizes two test data sets where each test data set is a RE, for a total of two REs.

For each study, DBMs were constructed on for the original 51 by 51 uniform grid. We removed three (or more) rows and columns from each edge to form a 45 by 45 (or less) uniform grid during post-processing to remove any boundary effects prior to evaluation.

We discuss our first study (UEs) in section 4.1.1, followed by our second study (REs) in section 4.1.2.

4.1.1 Study 1: The Uniform Experiments (UEs)

The UEs were performed to identify whether feature-favoring interpolators exist. We utilize a synthetic, idealistic truncated seamount and ridge as separate primitives. In the UEs, we add various amounts of sparsity via uniform down-sampling combined with Gaussian white noise to create a suite of test cases. For each test case, we used the entire suite of MergeBathy interpolators, producing in turn a suite of DBMs to analyze.

The UEs are controlled experiments where the test data sets were designed to investigate the behavior of interpolation schemes with regards to certain feature characteristics.⁴⁸ We utilize the results from this controlled first study to provide guidance for the second study – the ability to be nominal-informed.

Table 4.2 lists the tests performed in our first study (UEs). Each test obtains a set of sampling configurations which are applied to both our seamount and ridge primitives to investigate the efficacy of the interpolators under different sparsity and noise conditions. From these tests, we will identify a set of interpolators that is feature-favoring for each of our primitives. Feature-favoring interpolators will indicate an aptitude (favoritism) for the given morphology (feature). From each primitive’s set of identified feature-favoring interpolators, we will select one to serve as our nominal-informed seamount interpolator and one as our nominal-informed ridge interpolator (each producing nominal-informed DBMs). These selected interpolators are utilized in our second study (REs) to evaluate the efficacy of nominal-informed modeling.

⁴⁸ (e.g., Do any interpolations schemes perform poorly when the peak of a feature is not recorded in the measurement? How do they perform in these crucial measurement gaps?)

Table 4.2

UE Test Data Sets

Id	Name	Description
Test 1	Censored UEs	Set of uniform down-sampling (censoring) levels applied to the original 51 by 51 truth grid of 520 m grid spacing for a set of sampling configurations evaluated over both our seamount and ridge primitives. These data sets investigate the efficacy of the interpolators under sparsity for different morphologies.
Test 2	Noise UEs	Set of uniform Gaussian white noise levels applied to the original 51 by 51 truth grid of 520 m grid spacing for a set of sampling configurations with additive noise over both our seamount and ridge primitives. These data sets investigate the efficacy of the interpolators under noise for different morphologies.
Test 3	Combined censored and noise UEs	Crosses the set of uniform down-sampling levels with the set of uniform noise levels for a set of configurations that are applied to both our seamount and ridge primitives. These data sets investigate the efficacy of the interpolators under both sparsity and noise (interaction).

Tests performed for our first study (UEs). Each test obtains a set of sampling configurations which are applied to both our seamount and ridge primitives to investigate the efficacy of the interpolators under different sparsity and noise conditions. From these tests, we will identify a set of interpolators that is feature-favoring for each of our primitives. Feature-favoring interpolators will indicate an aptitude (favoritism) for the given morphology (feature). From each primitive's set of identified feature-favoring interpolators, we will select one to serve as our nominal-informed seamount interpolator and one as our nominal-informed ridge interpolator. These selected interpolators are utilized in our second study (REs).

4.1.2 Study 2: The Randomized Experiments (REs)

The REs utilized a synthetic, idealistic hybrid that is a geometrically weighted superposition of our seamount and ridge primitives. In the REs, we randomly apply swath removal and Gaussian white noise (random swath removal random noise [RSRRN]) to randomly sampled dense and sparse configurations, creating a suite of test cases which mimic real-data collection scenarios. For each test case, we compute DBMs with GMT's SIT, our selected seamount and ridge interpolators from our first study (UEs), and additional methods we developed and implemented for investigation into the efficacy of nominal-informed modeling. The selected seamount and ridge interpolators serve as ensemble members and in our ensembles.

The second study (REs) involved randomly simulated test data sets of 100 independent configurations with a random number of measurements randomly drawn from the sample with random noise and random data censoring. Data swaths of random

width, location, and direction were removed. These test cases were designed to mimic real data collections under sparse conditions. These data sets were designed to investigate the ensembles compared to individual interpolators.

We perform a right-tail sign hypothesis test to separate out sparse data sets, as defined here. For our synthetic features, we will consider a data set sparse if the median data gap is statistically greater than 1 arcminute or 1,852 m, about 3.5 times our final grid resolution, at the 5% significance level.

- Our null hypothesis is that the median data gap in a configuration (determined by a Delaunay triangulation) is 1,852 m or less, on average, and
- our alternative hypothesis is that it is larger.

Typically, a set of seafloor samplings are categorized as either dense or sparse depending on the resolution and its ability to capture features in a surveyed region at a desired detail. As discussed earlier, less than 10% of the ocean has been surveyed at 1 arcminute (1,852 m). Since we grid our morphologies from 15,000 to 41,520 m in the x and y direction at a resolution (grid spacing) of 520 m, data sets with data gaps greater than 1,040 m, on average, will be considered sparse. With that being said, we will utilize 1 arcminute (1,852 m) to define sparsity for our sparse configuration set Test3b in the second study (REs) (further discussed in Chapter VI).

Over our hybrid morphology (of weighted seamount and ridge primitives), various samples were obtained at various densities and locations and then corrupted with random noise and censored with random swaths. From a set of selected methods, DBMs were constructed.

Table 4.3 lists the tests performed in our second study (REs). Each test data set is a RE composed of 100 independent randomly generated sampling configurations with random swath removal and additive noise on our hybrid morphology (of our weighted primitives). All swath removal, noise, and densities are independent within each set of configurations. These test data sets investigate the efficacy of nominal-informed modeling (interpolator selection and ensemble).

Table 4.3

RE Test Data Sets

Id	Name	Description
Test 3a	Random configurations RE	Random swath removal and additive Gaussian white noise applied to a set of random sampling configurations of random density.
Test 3b	Sparse configurations RE	Random swath removal and additive Gaussian white noise applied to a set of random sampling configurations of sparse only random density as determined by our sparsity criteria.

Tests performed for our second study (REs). Each test data set is a RE composed of 100 independent randomly generated sampling configurations with random swath removal and additive noise on our hybrid morphology (of our weighted primitives). All swath removal, noise, and densities are independent within each set of configurations. These test data sets investigate the efficacy of nominal-informed modeling (interpolator selection and ensemble).

4.2 Analyses of Experiment

The experiments were designed to provide insight into the cause-and-effect relationship of various bathymetric input configurations on the final output grids computed from various interpolation schemes (i.e., feature-favoring). In the first study UEs, we purposefully changed the amount of uniform sparsity (down-sampling) and corruption (noise). In the second study (REs), we randomly changed the sampling density (size), corruption (noise), and missing data swaths (location and width). We did not look for the best results, but rather, for intuition on why one would outperform the others. Our objective is to determine which interpolation schemes work better on which types of geomorphological features.

To analyze feature-capture ability, we constructed Bayesian and frequentist LMMs, and utilized Friedman's test. Bayesian modeling reallocates credibility to parameter values to produce probable models given the data by estimating posterior distributions for parameters. This may be contrasted with frequentist LMM where we estimate point parameter values and perform null hypothesis tests to evaluate the probability of getting data as extreme or more under the null hypothesis (A. Gelman et al., 2014; Kruschke, 2015; McElreath, 2020).

Bayesian modeling was utilized to analyze the experimental runs via LMM. Traditional frequentist methods, including ANOVA, were unsuitable in modeling the experiments due to their high computational requirements. The frequentist methods typically require a large amount of replicated experimental runs to estimate small effects with high power, especially when discerning many factor levels. Bayesian modeling curbs these high computational demands by allowing the injection of additional information via informed prior probability distributions (A. Gelman et al., 2014; Kruschke, 2015; McElreath, 2020). In the absence of informed prior probability distributions, Bayesian modeling is consistent with the frequentist maximum likelihood estimate. The LMM were constructed with random group-effect variations for the intercept population-effect to capture correlated observations (blocking) between experimental run replications. LMM additionally allowed for the modeling of heterogenous residual variance structures.

Bayesian modeling was performed in R programming language utilizing the *brms* (Bürkner, 2017, 2018) package, which interfaces to the STAN Bayesian computational engine (Stan Development Team, 2021). Additional Bayesian packages utilized include

RStan (Stan Development Team, 2020), cmdstanR (Stan Development Team, 2021), and bayesplot (Gabry & Mahr, 2021; Gabry et al., 2019). For additional computational resources, we utilized Amazon Web Service (AWS) Elastic Cloud Compute services (Amazon EC2) (Amazon Web Services, n.d.) to run RStudio Server Amazon Machine Image (AMI) (Aslett, 2020). Additionally, brms newly released multi-threading within multi-parallel chain computing capabilities for Hamilton No-U Turn Sampler (NUTS) Monte Carlo Markov Chain (MCMC) (Hoffman & Gelman, 2011; Shalizi, 2019; Stan Development Team, 2021) were utilized.

Microsoft R Open 3.5.3 using “the Intel [Math Kernel Library] MKL for parallel mathematical computing” was utilized for computational gains through intrinsic parallelism and reproducibility via their snapshot repositories for R packages (Microsoft & R Core Team, 2019). Additional software investigations include: MATLAB (MathWorks, 2019), nlme (Pinheiro & Bates, 2006; West et al., 2014), lme4 (West et al., 2014), and DHARMA (Hartig & Lohse, 2020) R packages, and Julia (Bezanson et al., 2017) used to model frequentist LMM.⁴⁹

Alternatively, Friedman’s test is a non-parametric one-way ANOVA for repeated measures. The Friedman’s test has less-restrictions than LMMs as it does not assume normal errors or require model specification (Milton & Arnold, 2003). For Bayesian analysis, multiple experimental runs were performed for the UEs in the First Study and REs in the second study. Our first study UEs had 200 replications while the second study

⁴⁹ Julia “is a flexible dynamic language, appropriate for scientific and numerical computing, with performance comparable to traditional statically-typed languages.” (The Julia Project, 2021)

REs had 100 replications.⁵⁰ The complexity of the experimental design for the UEs requires LMMs, while the simpler experimental design of the REs allows the Friedman’s Test.

4.3 Metrics

We compute two error metrics, RMS and CumRAE. Of the two, the latter will be the definitive marker in our evaluations.

RMS is the square root of the mean of squared deviations,

$$RMS_{interp} = \sqrt{\frac{\sum_{i=1}^n (\widehat{y_{iinterp}} - y_{itruth})^2}{n}}.$$

CumRAE is the total sum of the relative absolute errors,

$$CumRAE_{interp} = \frac{\sum_{i=1}^n |\widehat{y_{iinterp}} - y_{itruth}|}{\sum_{i=1}^n |\widehat{y_{ibench}} - y_{itruth}|}.$$

We chose to use CumRAE as our definitive metric in our evaluations because it is scaled comparative to a known benchmark (J Scott Armstrong & Collopy, 1992; Jon Scott Armstrong, 2001). Our benchmark is GMT SIT (EM31).

In our first study (UEs), we analyzed the DBMs produced by the various interpolation schemes to determine which were feature-favoring interpolators. Recall that those are the interpolators we then couple with *w*-ELS/ELS in the second study.

In our second study (REs), we evaluated the ensembles by performing significance tests to compare CumRAEs. Each CumRAE ‘observation’ corresponds to a sampling configuration test case ‘subject’ and interpolation scheme ‘treatment’. We use

⁵⁰ A replication for the First Study is an additional independent run of all UEs while for the second study, each random sampling configuration generated is a replication.

Friedman's test to determine if there are any statistically significant differences in our interpolation schemes.

When we found statistical significances, we performed a post-hoc analysis of multiple pairwise comparison hypothesis testing to investigate which treatments are significant. A significant p-value indicates a significant difference in median CumRAE values between interpolation schemes.

Before selecting the above two metrics, we considered six standard error metrics:

- RMS,
- mean absolute deviation,
- mean absolute percentage error,
- mean relative absolute error,
- CumRAE, and
- median relative absolute error.

We also considered two image quality metrics (Z. Wang & Bovik, 2009; Z. Wang & Li, 2007; Z. Wang et al., 2004):

- structural similarity and
- structural dissimilarity,

and four information metrics:

- signal-to-noise ratio,
- peak signal-to-noise ratio,
- peak signal-to-noise ratio with human visual system properties and visual masking, and
- entropy.

RMS is not always reliable when comparing methods (J Scott Armstrong & Collopy, 1992; J. Scott Armstrong, 2001), but is a well understood metric and we kept it. Primarily, we utilized the CumRAE to compare our interpolation schemes. CumRAE is a relative error metric based on the absolute error loss function⁵¹ – as opposed to the squared-error loss function employed by RMS. Both CumRAE and median relative absolute error are recommended error metrics for selecting the method with the most accuracy. Relative metrics give an intuitive and effortless way to compare the performance of the interpolation techniques, while median metrics are less sensitive to outliers. We used RMS and MSE, along with the other aforementioned metrics, for several analyses that are not included in this dissertation due to length.

⁵¹ An \mathcal{L}_1 measure more related to generalizability.

CHAPTER V – FIRST STUDY: FEATURE-FAVORING INTERPOLATION

In this chapter, we describe the selection of feature-favoring interpolation schemes for our geomorphological primitives, the truncated seamount and Gaussian ridge, through our UEs in this first study. We utilize the set of interpolation schemes discussed in section 2.5 (listed in Table 2.2) to construct a set of DBMs and evaluated these interpolation schemes using the post-processing metrics discussed in section 4.3 to determine their fitness for the primitives. We did not discard test cases that resulted in physically unrealistic DBMs for certain interpolators because we wished to see how the ensemble methods would handle these DBMs. Due to both computational and space limitations, the results presented herein come from hand-selected feature-favoring interpolation schemes. However, one should always investigate surfaces regardless of whether they were generated by a feature-favoring interpolation scheme before using for best results.⁵²

The suite of tests used to select feature-favoring interpolators are referred to in Table 4.1 as the first study UEs. For the first study, which was suggested by Paul Elmore, we used synthetic data generated by adding a random sample of noise to the truth sampling locations and then down-sampling, or censoring, from the interpolation points.⁵³ We then reconstructed the surface using a suite of MergeBathy interpolation schemes and computed the RMS and CumRAE for each surface. We performed 200 replicated controlled experiments to analyze the performance of the interpolation

⁵² Traditionally this investigation is accomplished with a combination of manual and analytic metrics (e.g., section 2.3.6). What is missing for bathymetry is image processing analysis. Blurry, non-physical images are easy to detect programmatically and could help speed this process.

⁵³ In general, we censor data sets to simulate data sparsity.

schemes as uniform sparsity increases, random Gaussian noise increases, and seafloor morphology changes. In this dissertation, we present one of these replicated controlled experiments for investigation.

From these first study (UEs) results, identifying the set of feature-favoring interpolators for each primitive, we selected two different interpolation schemes to utilize as ensemble members across all second study (REs) sampling configurations (Chapter VI). These selected interpolation schemes serve as our nominal-informed feature-favoring primitive interpolators.

We investigated DBM depths and errors along with CumRAE to determine validity before identifying the set of interpolators that are feature-favoring for each primitive. For the noisy data sets (first study Test 2: Noise UEs), we expect test cases where the global trend was lost to the noise to produce DBMs that are unable to reconstruct the underlying morphology and are simply noise, thus an invalid DBM. For the highly censored data sets (first study Test 1: Censored UEs), we expect test cases where the sampling configuration was too sparse to produce DBMs that are also unable to reconstruct the underlying morphology because of the lack of information (data), and are thus, an invalid DBM. We could at this point, identify invalid DBMs and remove them from the set of contending DBMs. However, to exemplify the benefits of ensembles and test our proposed nominal-informed ensemble technique (w -ELS/ELS) (and more generally, nominal-informed modeling), we identified invalid DBMs but left them in the set of contending DBMs.

Section 5.1 presents the data in our first study (UEs). Section 5.2 presents the results from our first study (UEs) and selects our two feature-favoring interpolation schemes to utilize in our second study (REs).

In this chapter, we describe work performed, in part, with Paul Elmore. My specific contributions are:

- I implemented un-replicated controlled experiments proposed by Paul Elmore.
- I added replication and performed frequentist and Bayesian analyses.

5.1 Data

To generate the synthetic data, we began with the original data set of truth-values for each morphology, computed from the morphology-based shape primitive functions using the full grid of sampling locations of the truth data. The sampling locations of the truth data is a regularly spaced grid of 51 by 51 at 520 m spacing from an arbitrarily selected coordinate position range starting at 15,800 m and ending at 41,800 m in both directions.

Table 5.1 lists the tests performed in the first study (UEs). After obtaining the truth data for each primitive, we generated the suite of synthetic data by increasing sparsity (Test 1: Censored UEs), noise (Test 2: Noise UEs), or both (Test 3: Combined censored and noise UEs) uniformly. Test 3 combines Test 1 and Test 2 by crossing the censored levels with the noise levels; it increases both sparsity and noise uniformly. Each test was performed on both the truncated seamount and Gaussian ridge primitives.

Table 5.1

Study 1 (UEs) Tests

Test	Description
1	Censored levels 1-11. Tests sparsity by uniformly down-sampling.
2	Noise levels 1-11. Tests noise by uniformly increasing noise.
3	Censored levels 1-11 crossed with noise levels 1-11. Tests the interaction of sparsity with noise.

Tests in the first study (UEs). Each test was performed on both the truncated seamount and Gaussian ridge primitives.

For the first study Test 1 sparser data sets, we uniformly down-sampled the original grid of truth values by a factor of 520 m in both directions. Table 5.2 lists the censored data set sampling designs created by each level of down-sampling to test sparsity. Dimension x and y are the number of grid locations sampled in each direction with x-step and y-step denoting the grid spacing between grid points. The last column gives the ratio of the true grid spacing to that of the level. For example, level 1 down-samples the original 51 by 51 grid of truth values with 520 m between grid points in both directions to a 26 by 26 grid with a grid spacing of 1,040 m between points which is two times the grid spacing of the true grid for a 1:2 ratio. For a further example, level 5 down-samples to a 6 by 6 grid with a 5,200 m grid spacing between points which is ten times the grid spacing of the true grid for a 1:10 ratio. We note that although the dimensions of the data set designs are the same for levels 7 and 8 and for levels 9, 10, and 11, the locations of the points differ. This was done to see how the interpolators would perform when specific information about the morphologies in question, such as the peak of a seamount, is not sampled.

Table 5.2

Study 1 Test 1: Uniformly Censored Data Set Designs to Test Sparsity

Censored Level (Id)	Dimensions		Grid Spacing (m)		Ratio (Truth: Down-Sample)	
	X	Y	X-step	Y-step	X	Y
1	26	26	1040	1040	1:2	1:2
2	13	13	2080	2080	1:4	1:4
3	9	9	3120	3120	1:6	1:6
4	7	7	4160	4160	1:8	1:8
5	6	6	5200	5200	1:10	1:10
6	5	5	6240	6240	1:12	1:12
7	4	4	7280	7280	1:14	1:14
8	4	4	8320	8320	1:16	1:16
9	3	3	9360	9360	1:18	1:18
10	3	3	10,400	10,400	1:20	1:20
11	3	3	11,440	11,440	1:22	1:22

Each censored level uniformly down-samples the truth sampling locations. Dimension x and y are the number of grid locations sampled in each direction with x-step and y-step denoting the grid spacing between grid points. The last column gives the ratio of the true grid spacing to that of the level. For example, level 1 down-samples the original 51 by 51 grid of truth values with 520 m between grid points in both directions to a 26 by 26 grid with a grid spacing of 1,040 m between points which is two times the grid spacing of the true grid for a 1:2 ratio. For a further example, level 5 down-samples to a 6 by 6 grid with a 5,200 m grid spacing between points which is ten times the grid spacing of the true grid for a 1:10 ratio.

For the first study Test 2 noisy data sets, we added random Gaussian white noise to the truth values for each morphology. The first noise level adds noise randomly sampled from a Gaussian distribution with a mean of 0 and standard deviation of 257.60 m to the original data set of truth-values. To uniformly increase noise, each subsequent level multiplicatively increases the standard deviation by simply multiplicatively increasing the random noise sample. We selected 257.60 m to use for the default standard deviation because, according to the error limits expected for a max depth of 11,200 m following the standards for hydrographic surveys (International Hydrographic Organization, 2008),

$$\sqrt{1^2 + (0.023 * 11200)^2} = 257.60 \text{ m.}$$

Table 5.3 lists the Gaussian contamination created by each level of increasing noise threshold to test noise. We categorically selected 11 noise levels based on multiplicative increases of the IHO acceptable amount of 257.60 m. Level 1 is the acceptable IHO noise, while levels 2-11 are selected multipliers relative to the amplitude of our shapes (1,200 m) with the last level 11 indicating standard deviation larger than our specified max ocean depth.

For example, noise generated for noise level 1 comes from a Gaussian distribution with mean 0 and standard deviation 1σ , which is the acceptable allowance limit, while noise generated for level 5 is 19 times the allowance coming from a Gaussian distribution with mean 0 and standard deviation 19σ , and is 4 times our amplitude of 1,200 m.

Table 5.3

Study 1 Test 2: Gaussian Contaminated Data Set Designs to Test Noise

Noise Threshold Level	Categorical Description (Amplitude = 1,200 m)	Standard Deviation ($\sigma = 257.6$)	Additive Noise Range
1	Acceptable	1σ	[-955.28 – 849.34]
2	Exceeds 1 x Amplitude	5σ	[-4,776.37 – 4246.69]
3	Exceeds 2 x Amplitude	10σ	[-9,552.75 – 8,493.39]
4	Exceeds 3 x Amplitude	14σ	[-113,373.8 – 11,890.7]
5	Exceeds 4 x Amplitude	19σ	[-18,150.2 – 16,137.4]
6	Exceeds 5 x Amplitude	24σ	[-22,926.6 – 20,384.1]
7	Exceeds 6 x Amplitude	28σ	[-26,747.7 – 23,781.5]
8	Exceeds 7 x Amplitude	33σ	[-31,521.1 – 28,028.2]
9	Exceeds 8 x Amplitude	38σ	[-36,300.4 – 32,274.9]
10	Exceeds 9 x Amplitude	41σ	[-39,166.3 – 34,822.9]
11	Exceeds max depth	44σ	[-42,032.1 – 37,370.9]

Multiples of a random sample from a Gaussian distribution with mean 0 and standard deviation 257.6 m was added to the truth values to create the noisy data sets. Each noise level uniformly increases the noise sample multiplicatively; standard deviations for the noise levels are multiples of $\sigma = 257.6$ m, the error limit expected for a max depth of 11,200 m following the standards for hydrographic surveys (International Hydrographic Organization, 2008). Level 1 is acceptable noise determined by IHO. The remaining levels were categorically chosen based on how the standard deviations related to our morphology amplitude of 1,200 m. The Additive Noise Range column denotes the min and max noise values generated for the noise level.

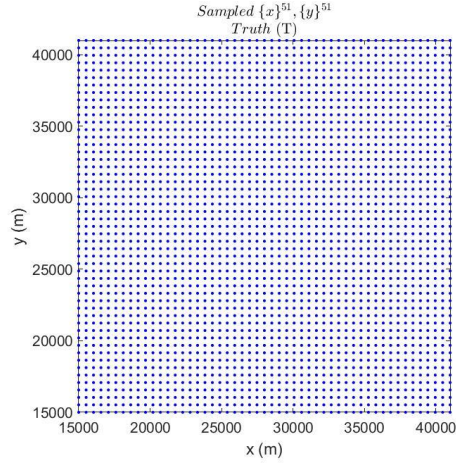
In contrast, the second study REs generated a new random sample of Gaussian noise from a distribution with a mean of 0 and a standard deviation of 300 m for each

random test case (sampling configuration). We selected 300 m to use for the default standard deviation as an approximation to 257.60 m, the error limits expected for at a max depth of 11,200 m following the standards for hydrographic surveys (International Hydrographic Organization, 2008).

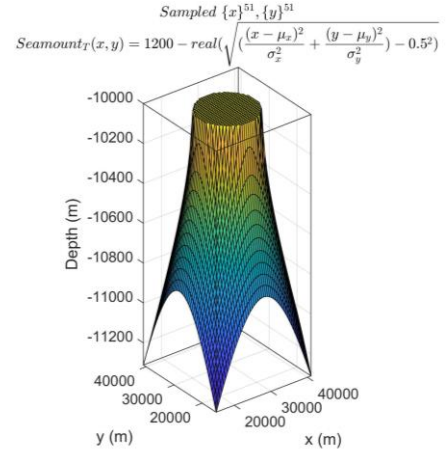
Figure 5.1 depicts the original morphological truth surfaces generated for the 2D truncated seamount and 1D Gaussian ridge (as well as the combined hybrid surfaces, we will discuss later). In the first study Test 1, Figure 5.2 and Figure 5.3 depict the down-sampled test designs for the truncated seamount and Gaussian ridge morphologies, respectively.

In the first study Test 2, Figure 5.4 and Figure 5.5 depict the noise-contaminated samplings for the truncated seamount and Gaussian ridge morphologies, respectively. As we increase the noise threshold, we quickly lose the shape of our morphology to the noise. In other words, the global trend becomes lost in the variability. It is easy to see how a few errors can significantly alter a geomorphological shape.

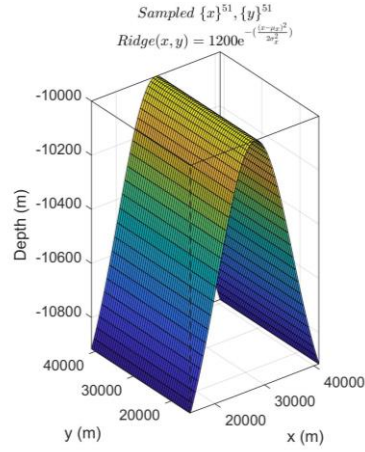
Our feature-favoring interpolator schemes were selected to minimize the average error given data sparsity and noise.



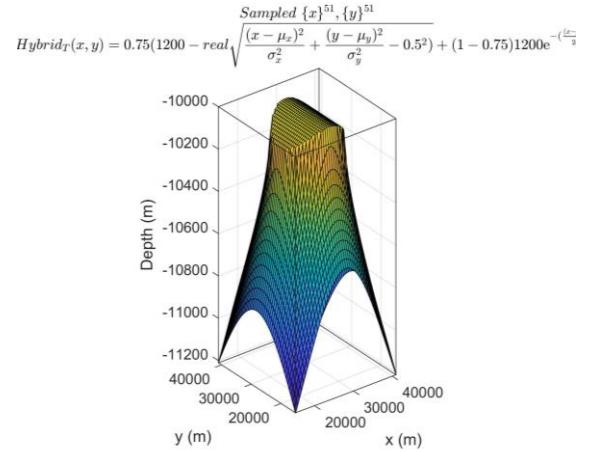
(a)



(b)



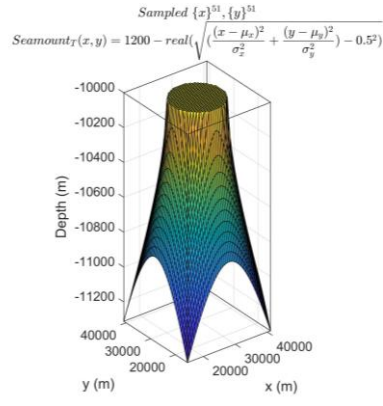
(c)



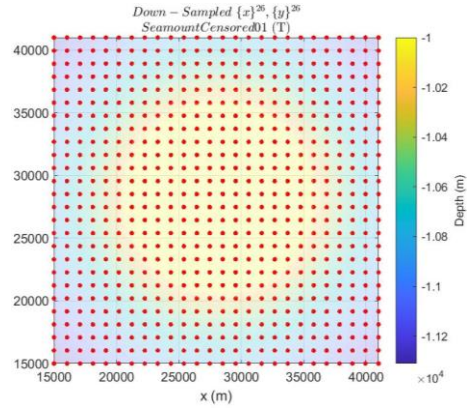
(d)

Figure 5.1 Original morphology truth surfaces.

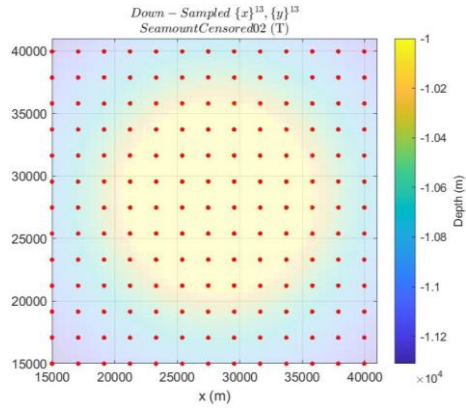
Surfaces (b)-(d) constructed at (a) (x,y) locations of original truth data values; a 51x51 regular grid at 520 m spacing in both directions. (b) 2D truncated seamount original surface of truth data values. (c) 1D Gaussian ridge original surface of truth data values. (d) Hybrid original surface of truth data values, a composite surface of (b) with weight 0.75 and (c) with weight 0.25.



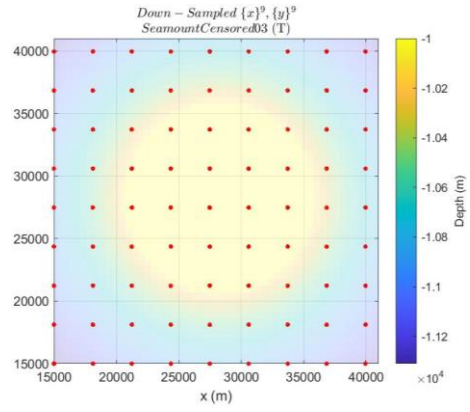
(0)



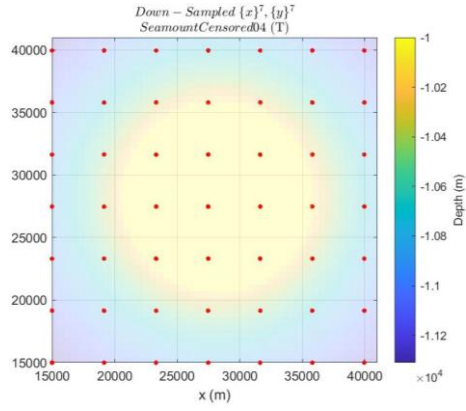
(1)



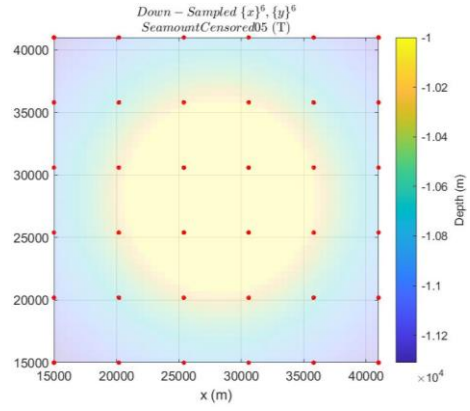
(2)



(3)



(4)



(5)

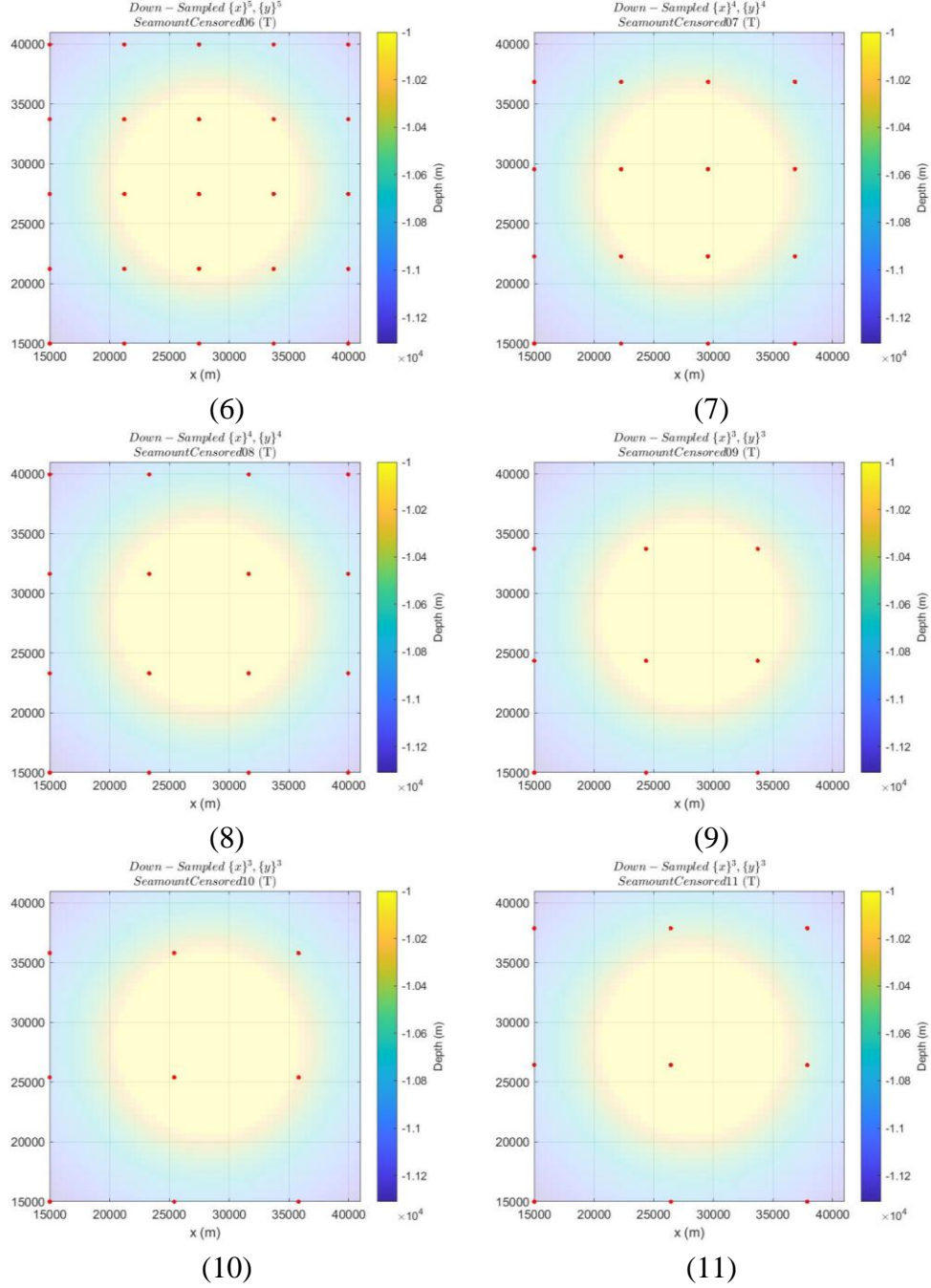
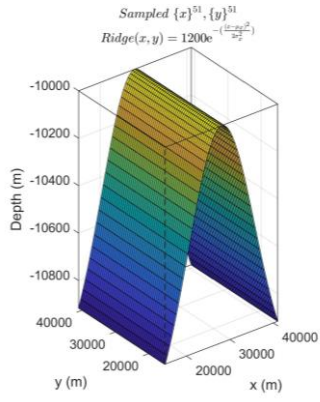
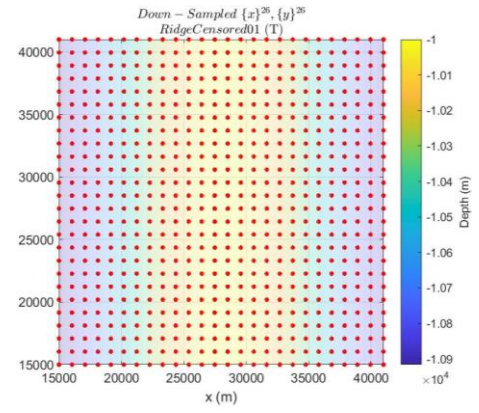


Figure 5.2 Study 1 Test 1: truncated seamount data sets with censoring.

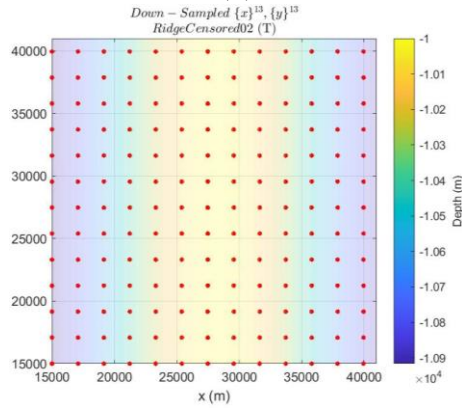
Uniformly down-sampled (0) the original 51 by 51 grid of truth values over truncated seamount. (x,y) sampled locations denoted by red markers overlaid on (0) the original truth data set for 0-11 uniform down-sampled level test cases. (0) 51x51 with 520 m grid spacing, (1) 26x26 with 1,040 m grid spacing, (2) 13x13 with 2,080 m grid spacing, (3) 9x9 with 3,120 m grid spacing, (4) 7x7 with 4,160 m grid spacing, (5) 6x6 with 5,200 m grid spacing, (6) 5x5 with 6,240 m grid spacing, (7) 4x4 with 7,280 m grid spacing, (8) 4x4 with 8,320 m grid spacing, (9) 3x3 with 9,360 m grid spacing, (10) 3x3 with 10,400 m grid spacing, (11) 3x3 with 14,440 m grid spacing.



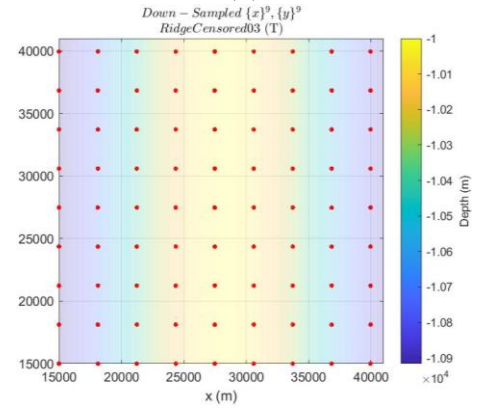
(0)



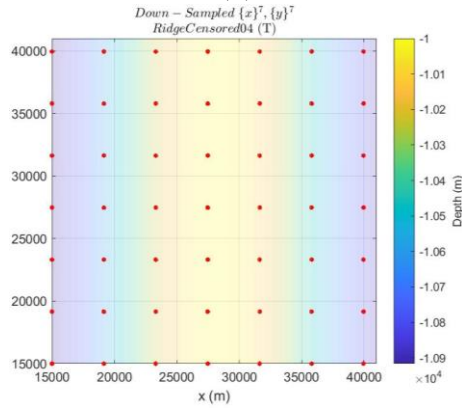
(1)



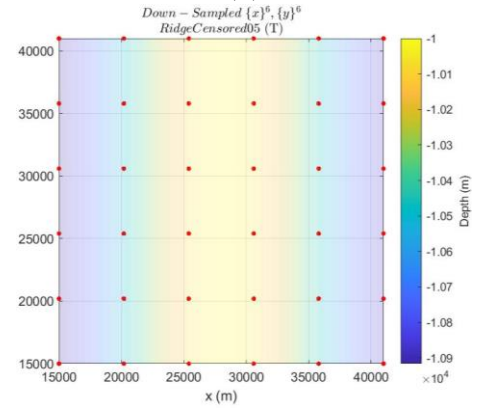
(2)



(3)



(4)



(5)

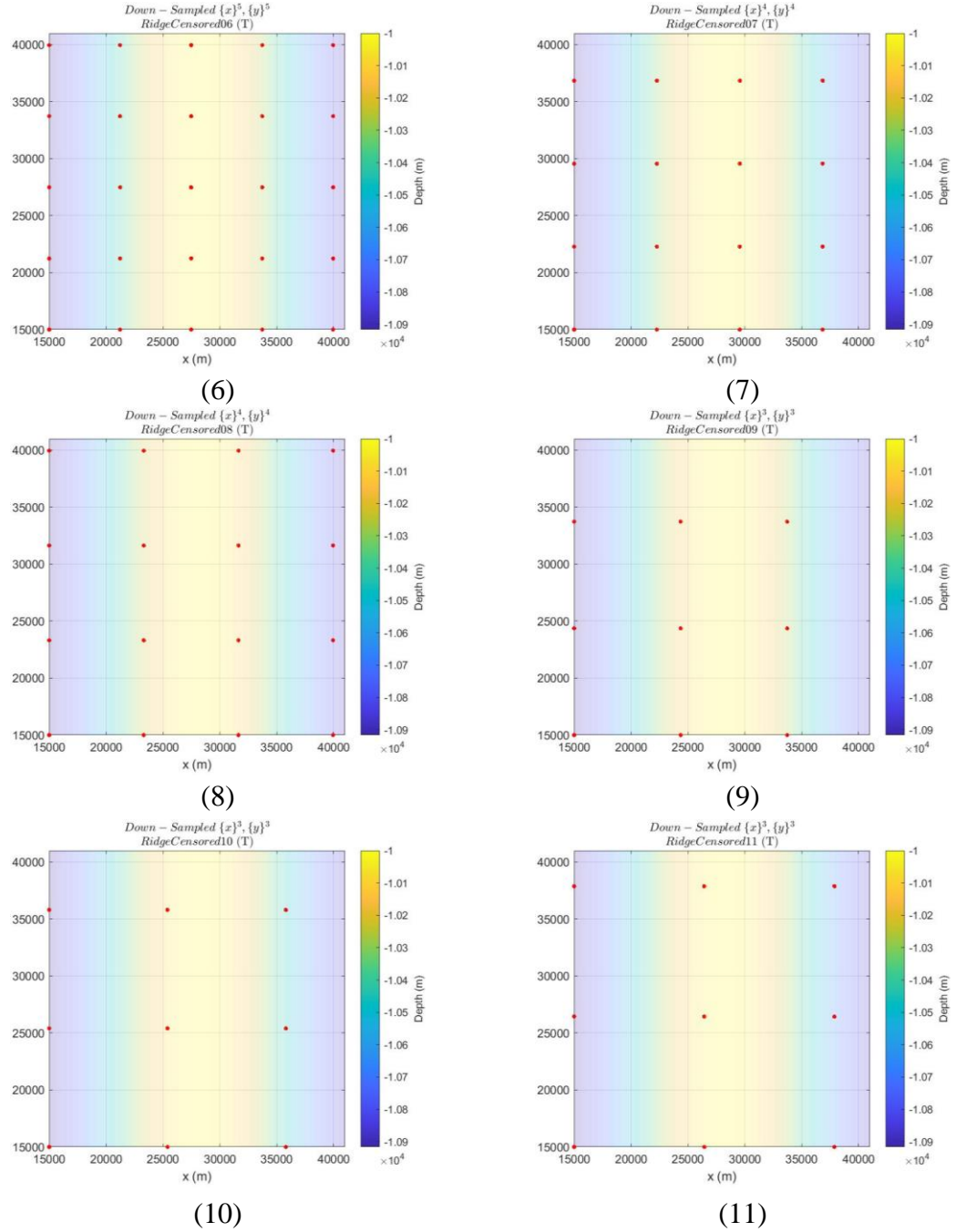
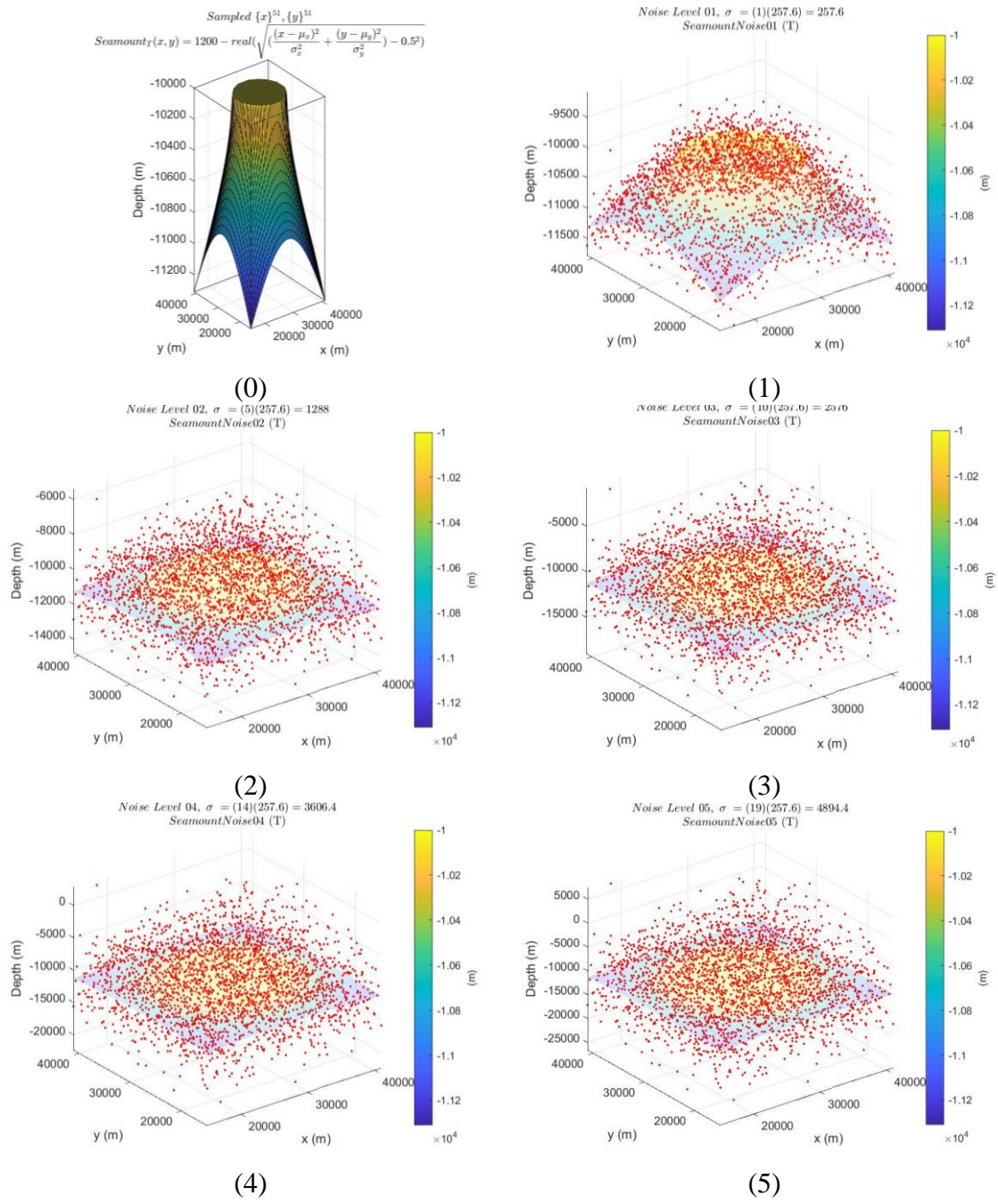


Figure 5.3 Study 1 Test 1: Gaussian ridge data sets with censoring.

Uniformly down-sampled (0) the original 51 by 51 grid of truth values over 1D Gaussian ridge. (x,y) sampled locations denoted by red markers overlaid on (0) the original truth data set for 0-11 uniform down-sampled level test cases. (0) 51x51 with 520 m grid spacing, (1) 26x26 with 1,040 m grid spacing, (2) 13x13 with 2,080 m grid spacing, (3) 9x9 with 3,120 m grid spacing, (4) 7x7 with 4,160 m grid spacing, (5) 6x6 with 5,200 m grid spacing, (6) 5x5 with 6,240 m grid spacing, (7) 4x4 with 7,280 m grid spacing, (8) 4x4 with 8,320 m grid spacing, (9) 3x3 with 9,360 m grid spacing, (10) 3x3 with 10,400 m grid spacing, (11) 3x3 with 14,440 m grid spacing.



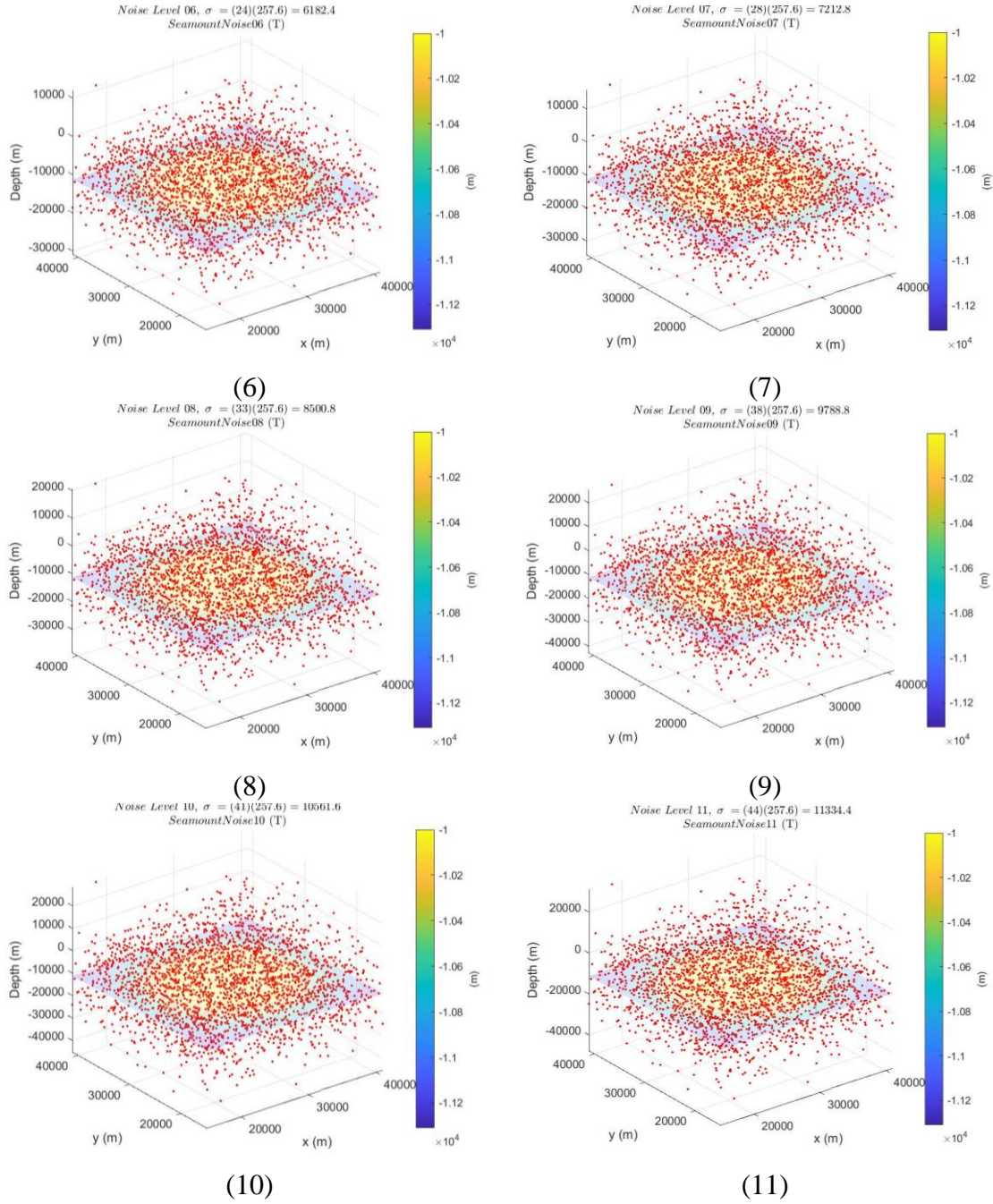
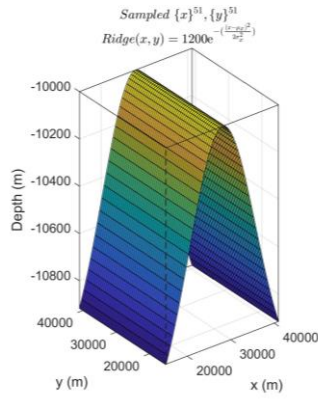
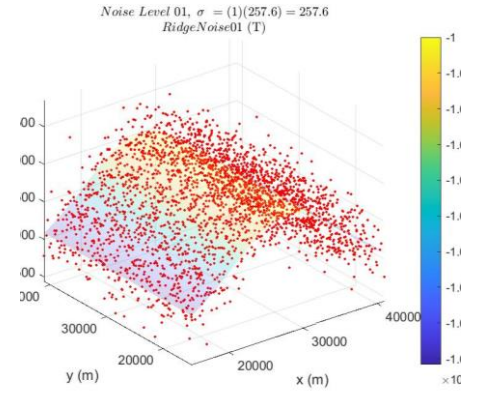


Figure 5.4 Study 1 Test 2: truncated seamount data sets with noise.

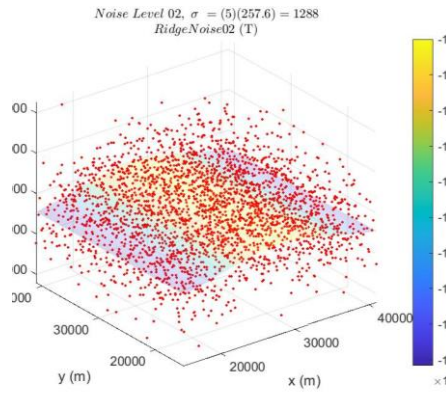
Contaminated depth measurements at the (x,y) sampled locations denoted by red markers overlaid on (a) the original truth data set for 0-11 noise level test cases. $\sigma = 257.60$ m (0) no noise, (1) 1σ , (2) 5σ , (3) 10σ , (4) 14σ , (5) 19σ , (6) 24σ , (7) 28σ , (8) 33σ , (9) 38σ , (10) 41σ , (11) 44σ .



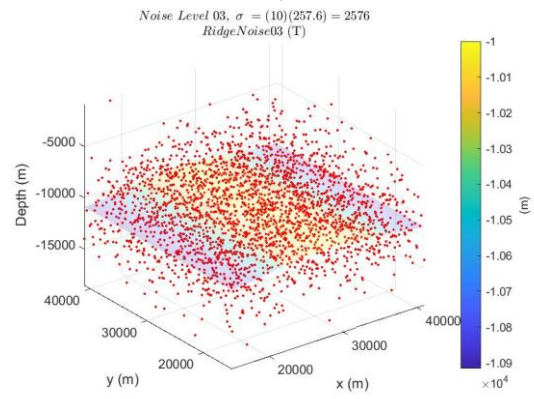
(0)



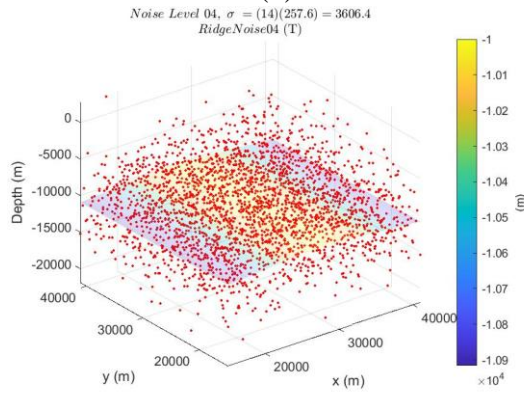
(1)



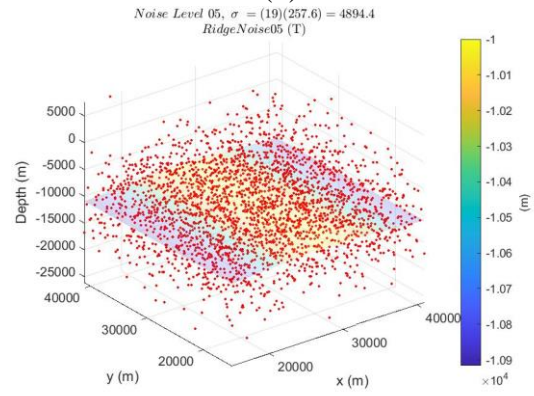
(2)



(3)



(4)



(5)

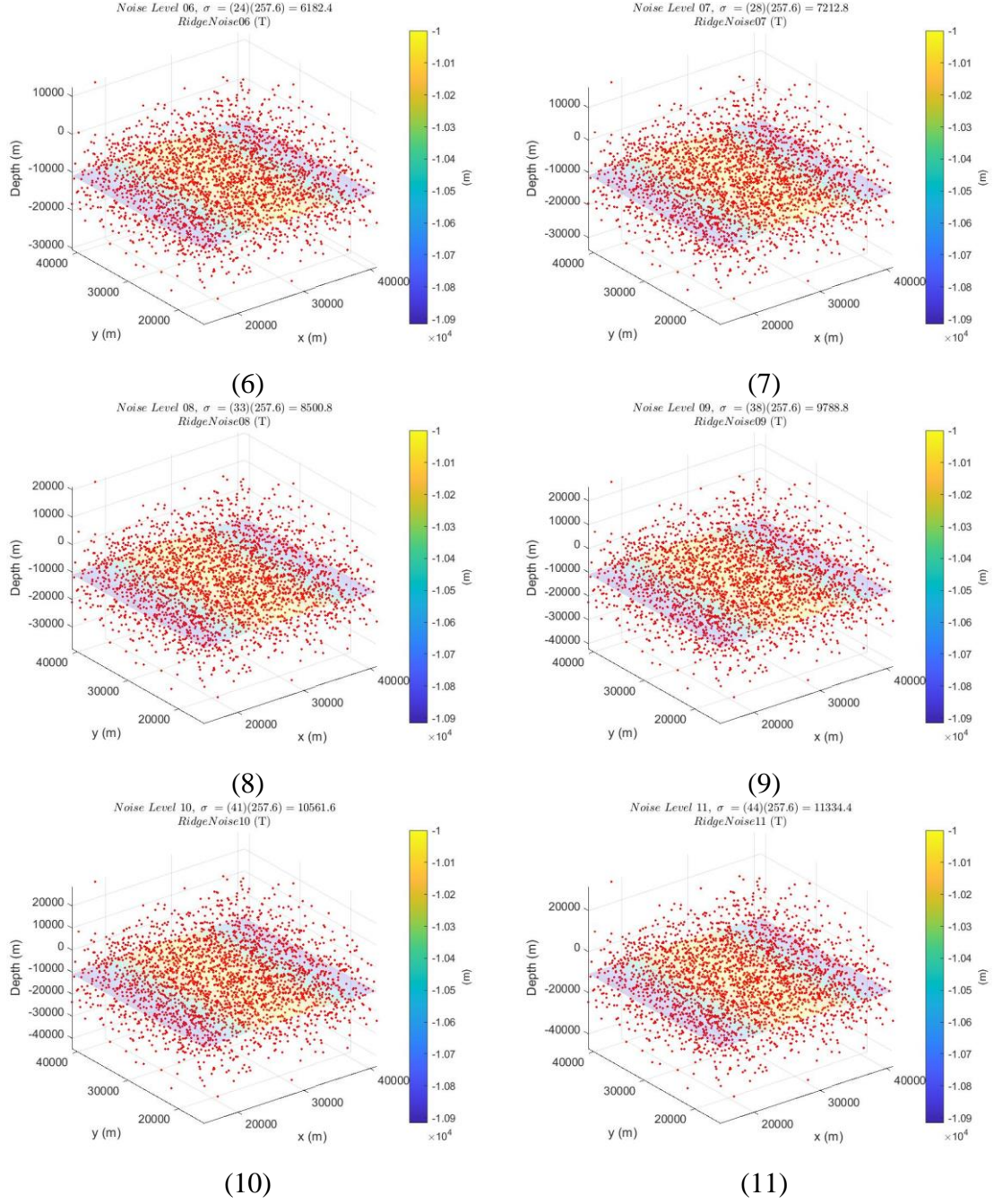


Figure 5.5 Study 1 Test 2: Gaussian ridge data sets with noise.

Contaminated depth measurements at the (x,y) sampled locations denoted by red markers overlaid on (a) the original truth data set for 0-11 noise level test cases. $\sigma = 257.60$ m (0) no noise, (1) 1σ , (2) 5σ , (3) 10σ , (4) 14σ , (5) 19σ , (6) 24σ , (7) 28σ , (8) 33σ , (9) 38σ , (10) 41σ , (11) 44σ .

5.2 Results

Results for our first study (UEs) are shown, beginning on page 134, in:

- Test 1: Censored UEs
 - Table 5.4 for our seamount (annotated in Table 5.6 and Table 5.7),
 - Table 5.5 for our ridge (annotated in Table 5.9),
- Test 2: Noise UEs
 - Table 5.11 for our seamount,
 - Table 5.12 for our ridge,
- Test 3: Combined censored and noise UEs
 - Table 5.13 for our seamount, and
 - Table 5.14 for our ridge.

The columns of all tables are our evaluated methods identified by EM<Id> in Table 2.2 on page 55. GMT SIT (EM31) is our benchmark. Rows in Table 5.4 and Table 5.5 identify censored level in Table 5.2. Rows in Table 5.11 and Table 5.12 identify noise level in Table 5.3. Rows in Table 5.13 and Table 5.14 identify censored and noise combination level by C<censored level>N<noise level> with corresponding to censored level in Table 5.2 and noise level in Table 5.3. Red stars in the tables indicate the interpolators we eventually select as our feature-favoring primitive interpolators in section 5.2.4 to use in our second study (REs) in Chapter VI.

Color coding illustrates an interpolators performance (accuracy) against our benchmark GMT SIT (EM31) according to CumRAE. A value of 1.00 (middle green) indicates equal performance to the benchmark, values greater than 1.00 (dark green) performed worse than the benchmark, and values less than 1.00 (light green), performed

better than the benchmark. For each level, the minimum CumRAE is annotated in red. CumRAE allows for direct comparison between methods. We rounded CumRAE to two decimal places, but color coding is correct. Red stars in the tables indicate the interpolators we eventually select as our feature-favoring primitive interpolators in section 5.2.4 to use in our second study (REs) in Chapter VI.

Interpolation schemes (columns) are grouped in all tables in this first study: grey letters are denoted above the groupings, separated by bold lines. These groups are:

- A: Localized regression with kriged residuals
- B: Localized regression with kriged residuals and GMT SIT pre-splining
- C: Localized regression with kriged residuals and MBZ SIT pre-splining
- D: Localized regression with GMT SIT pre-splining
- E: Localized regression with MBZ SIT pre-splining
- F: Localized regression
- G: SIT

Each group except for group G applies localized regression with all filters in the same order beginning from the left (quadloess, loess, boxcar, hann, and kalman), making grouping size five. Group G is of size two. Additionally, we note the following sets of groups we will reference in the text.

- Groups B and D are GMT SIT methods (along with GMT SIT [EM31]),
- Groups C and E are MBZ SIT methods (along with group MBZ SIT [EM32]),
- Groups A and F are non-pre-splining methods.

5.2.1 Test 1: Censored UEs

First, we discuss the censored UEs (first study Test 1) for the seamount and ridge primitives. Table 5.4 and Table 5.5 show the effects of down-sampling on the individual seamount and ridge primitive shapes. These tables are annotated in the following sections to highlight findings discussed in the text. Our findings for our Test 1: Censored UEs are presented for our truncated seamount in Section 5.2.1.2 and our ridge in section 5.2.1.3.

Table 5.4

Study 1 Test 1: Seamount Censored CumRAE Results (Results rounded to 2 decimals, but color coding is accurate.)

Level	A					B					C					D					E					F					G	
	Krigquadloess (EM01)	Krigloess (EM02)	Krigboxcar (EM03)	Krighann (EM04)	Krigkalman (EM05)	Krig_GMTquadloess (EM06)★	Krig_GMTloess (EM07)	Krig_GMTboxcar (EM08)	Krig_GMTThann (EM09)	Krig_GMTkalman (EM10)	Krig_MBZquadloess (EM11)	Krig_MBZloess (EM12)	Krig_MBZboxcar (EM13)	Krig_MBZThann (EM14)	Krig_MBZkalman (EM15)	GMTquadloess (EM16)	GMTloess (EM17)	GMTboxcar (EM18)★	GMTThann (EM19)	GMTkalman (EM20)	MBZquadloess (EM21)	MBZloess (EM22)	MBZboxcar (EM23)	MBZThann (EM24)	MBZkalman (EM25)	quadloess (EM26)	loess (EM27)	boxcar (EM28)	hann (EM29)	kalman (EM30)	GMT SIT (EM31)	MBZ SIT (EM32)
1	2.43	2.65	2.85	2.37	2.55	1.53	1.65	3.06	1.52	2.41	1.72	2.12	3.42	1.99	2.79	1.52	1.46	2.80	1.37	2.21	1.71	1.95	3.22	1.86	2.64	2.12	2.12	2.81	1.94	2.52	1.00	1.33
2	2.73	2.72	3.10	2.33	2.25	1.04	1.10	1.46	1.08	1.31	1.67	1.81	1.98	1.78	1.88	1.04	1.05	1.37	1.04	1.24	1.67	1.77	1.93	1.76	1.83	2.66	2.47	2.75	2.13	2.03	1.00	1.67
3	1.81	1.81	2.71	1.74	2.02	1.01	1.03	1.19	1.02	1.12	1.91	1.95	2.00	1.94	1.96	1.01	1.01	1.15	1.00	1.09	1.91	1.97	2.02	1.96	1.99	1.70	1.67	2.46	1.05	1.88	1.00	1.91
4	3.86	2.53	2.83	2.30	2.21	1.00	1.02	1.08	1.01	1.05	2.29	2.32	2.32	2.32	2.31	1.00	1.01	1.07	1.01	1.04	2.29	2.33	2.33	2.32	2.32	2.39	2.60	2.81	2.36	2.05	1.00	2.30
5	2.07	1.78	3.18	1.69	3.26	1.00	1.00	1.01	1.00	1.01	2.32	2.33	2.33	2.33	2.33	1.00	1.00	1.01	1.00	1.01	2.32	2.34	2.35	2.34	2.34	2.07	2.07	2.54	1.71	2.10	1.00	2.32
6	4.31	1.97	3.30	1.42	2.68	1.00	1.00	1.01	1.00	1.00	3.16	3.17	3.17	3.17	3.16	1.00	1.00	1.01	1.00	1.01	3.16	3.18	3.18	3.17	3.17	2.47	1.99	3.48	1.38	2.55	1.00	3.16
7	3.17	5.66	3.90	4.54	3.77	1.00	1.00	1.00	1.00	1.00	2.58	2.58	2.58	2.58	2.58	1.00	1.00	1.01	1.00	1.00	2.58	2.58	2.58	2.58	2.58	2.47	2.50	3.05	2.60	2.45	1.00	2.58
8	11.50	8.18	11.10	6.64	11.71	1.00	1.00	1.04	1.00	1.02	3.48	3.48	3.47	3.48	3.47	1.00	1.00	1.03	1.00	1.01	3.48	3.49	3.47	3.49	3.47	2.55	3.87	2.87	3.33	1.93	1.00	3.48
9	2.02	1.87	1.94	1.75	1.77	1.00	1.00	1.00	1.00	1.00	1.34	1.35	1.34	1.35	1.34	1.00	1.00	1.00	1.00	1.00	1.34	1.35	1.35	1.35	1.35	2.02	1.87	1.94	1.75	1.77	1.00	1.34
10	2.34	1.94	2.53	1.82	2.15	1.00	1.00	1.01	1.00	1.01	1.71	1.72	1.72	1.72	1.72	1.00	1.00	1.01	1.00	1.00	1.71	1.72	1.72	1.72	1.72	2.34	1.94	2.53	1.82	2.15	1.00	1.71
11	1.80	1.43	2.04	1.37	1.68	1.00	1.00	1.01	1.00	1.00	1.50	1.50	1.50	1.50	1.50	1.00	1.00	1.01	1.00	1.00	1.50	1.50	1.50	1.50	1.50	1.80	1.43	2.04	1.37	1.68	1.00	1.50

CumRAE for all interpolators at each censored level for the 2D truncated seamount. The columns are our evaluated methods identified by EM<Id> in Table 2.2 on page 55. GMT SIT (EM31) is our benchmark. A value of 1.00 (middle green) indicates equal performance to the benchmark, values greater than 1.00 (dark green) performed worse than the benchmark, and values less than 1.00 (light green), performed better than the benchmark. For each level, the minimum CumRAE is annotated in red. CumRAE allows for direct comparison between methods. Letters identify interpolator groupings: (A) localized regression + kriging, (B) localized regression + kriging + pre-splining with GMT SIT (EM31), (C) localized regression + kriging + pre-splining with MBZ SIT (EM32), (D) localized regression + pre-splining with GMT SIT (EM31), (E) localized regression + pre-splining with GMT SIT (EM31), (F) localized regression + pre-splining with MBZ SIT (EM32), and (G) SIT. In all groups except G, filters are from left to right: quadloess, loess, boxcar, hann, and kalman. Red stars indicate eventually selected feature-favoring interpolators: seamount interpolator EM06 and ridge interpolator EM18.

Table 5.5

Study 1 Test 1: Ridge Censored CumRAE Results (Results rounded to 2 decimals, but color coding is accurate.)

135

	Level	A					Krig_ GMTquadloess (EM06)★	B					C					GMTquadloess (EM16)	D					MBZquadloess (EM21)	E					quadloess (EM26)	F					kalman (EM30)	G	
		Krigquadloess (EM01)	Krigloess (EM02)	Krigboxcar (EM03)	Krighann (EM04)	Krigkalman (EM05)		Krig_ GMTloess (EM07)	Krig_ GMTboxcar (EM08)	Krig_ GMTThann (EM09)	Krig_ GMTkalman (EM10)	Krig_ MBZquadloess (EM11)	Krig_ MBZloess (EM12)	Krig_ MBZboxcar (EM13)	Krig_ MBZThann (EM14)	Krig_ MBZkalman (EM15)	GMTloess (EM17)		GMTboxcar (EM18)★	GMTThann (EM19)	GMTkalman (EM20)	MBZloess (EM22)	MBZboxcar (EM23)		MBZThann (EM24)	MBZkalman (EM25)	loess (EM27)	boxcar (EM28)	hann (EM29)		kalman (EM30)	GMT SIT (EM31)	MBZ SIT (EM32)					
	1	21.26	75.14	88.32	61.17	68.43	0.82	25.21	125.84	20.84	83.69	24.42	46.56	139.28	42.30	99.70	0.51	17.31	111.37	14.71	75.76	24.31	42.16	129.03	39.64	93.15	17.12	37.70	68.99	33.40	54.00	1.00	26.35					
	2	32.63	35.12	37.18	29.14	23.79	0.87	3.37	13.20	2.92	9.07	21.07	23.14	27.41	22.80	24.82	0.84	2.74	11.91	2.46	8.31	21.05	22.68	26.30	22.47	24.01	32.71	31.64	35.92	26.62	22.34	1.00	21.37					
	3	8.78	10.33	12.75	8.18	10.42	0.97	1.21	2.83	1.18	2.12	11.55	11.71	12.03	11.75	11.81	0.97	1.34	2.98	1.29	2.30	11.55	11.95	12.40	11.90	12.09	8.74	10.62	13.41	7.30	10.88	1.00	11.63					
	4	9.40	14.75	17.93	11.89	18.24	0.99	1.06	1.54	1.05	1.32	8.58	8.64	8.58	8.64	8.56	0.99	1.14	1.70	1.12	1.43	8.58	8.72	8.70	8.70	8.66	7.88	8.96	9.93	8.08	6.52	1.00	8.61					
	5	1.61	3.32	6.84	2.69	7.14	1.00	1.02	1.04	1.01	1.02	3.34	3.35	3.32	3.35	3.33	1.00	1.03	1.06	1.03	1.04	3.34	3.36	3.34	3.36	3.35	2.09	2.41	3.12	1.93	2.71	1.00	3.34					
	6	1.00	1.80	2.79	1.26	2.89	1.00	1.01	1.01	1.01	1.01	2.36	2.37	2.36	2.37	2.36	1.00	1.01	1.02	1.01	1.01	2.36	2.37	2.37	2.37	2.37	1.25	1.37	2.06	1.10	1.67	1.00	2.37					
	7	2.03	3.65	2.31	2.97	2.26	1.00	1.01	1.02	1.00	1.01	1.67	1.68	1.68	1.68	1.68	1.00	1.01	1.02	1.01	1.01	1.67	1.68	1.68	1.68	1.68	1.45	1.69	1.75	1.77	1.37	1.00	1.67					
	8	2.16	1.47	2.10	1.19	2.17	1.00	1.00	1.00	1.00	1.00	1.02	1.02	1.02	1.02	1.02	1.00	1.00	1.00	1.00	1.00	1.02	1.03	1.02	1.03	1.02	0.53	1.13	0.86	0.99	0.65	1.00	1.02					
	9	0.98	0.90	0.86	0.82	0.78	1.00	1.00	1.00	1.00	1.00	0.73	0.73	0.73	0.73	0.73	1.00	1.00	1.00	1.00	1.00	0.73	0.73	0.73	0.73	0.73	0.98	0.90	0.86	0.82	0.78	1.00	0.73					
	10	0.80	0.66	0.71	0.57	0.61	1.00	1.00	1.00	1.00	1.00	0.60	0.60	0.60	0.60	0.60	1.00	1.00	1.00	1.00	1.00	0.60	0.60	0.60	0.60	0.60	0.80	0.66	0.71	0.57	0.61	1.00	0.60					
	11	0.65	0.46	0.60	0.37	0.49	1.00	1.00	1.00	1.00	1.00	0.49	0.49	0.49	0.49	0.49	1.00	1.00	1.00	1.00	1.00	0.49	0.49	0.49	0.49	0.49	0.65	0.46	0.60	0.37	0.49	1.00	0.49					

CumRAE for all interpolators at each censored level for the 1D Gaussian ridge. The columns are our evaluated methods identified by EM<Id> in Table 2.2 on page 55. GMT SIT (EM31) is our benchmark. A value of 1.00 (middle green) indicates equal performance to the benchmark, values greater than 1.00 (dark green) performed worse than the benchmark, and values less than 1.00 (light green), performed better than the benchmark. For each level, the minimum CumRAE is annotated in red. CumRAE allows for direct comparison between methods. Letters identify interpolator groupings: (A) localized regression + kriging, (B) localized regression + kriging + pre-splining with GMT SIT (EM31), (C) localized regression + kriging + pre-splining with MBZ SIT (EM32), (D) localized regression + pre-splining with GMT SIT (EM31), (E) localized regression + pre-splining with GMT SIT (EM31), (F) localized regression + pre-splining with MBZ SIT (EM32), and (G) SIT. In all groups except G, filters are from left to right: quadloess, loess, boxcar, hann, and kalman. Red stars indicate eventually selected feature-favoring interpolators: seamount interpolator EM06 and ridge interpolator EM18.

5.2.1.2 2D Truncated Seamount

When censoring the truncated seamount, we find (illustrated in Table 5.6 by annotating Table 5.4):

- All but seven interpolators (shaded) were less accurate (dark green) than our benchmark GMT SIT (EM31) at all levels.
- The seven interpolators were negligibly more accurate (light green) than our benchmark GMT SIT (EM31) at least once at higher sparsity levels (censored levels 5-11), and less accurate everywhere else.
 - The seven interpolators pre-spline with GMT SIT (EM31).
- GMT SIT methods (groups B and D along with GMT SIT [EM31]) were the most accurate for all censored levels.
 - Our benchmark GMT SIT (EM31) was the most accurate (red) for levels 1-5 (above horizontal line).
 - The seven GMT SIT pre-splining methods were most accurate (red) for levels 6-11 (below horizontal line).

Table 5.6

(Annotation 1 of Table 5.4) Study 1 Test 1: Seamount Censored CumRAE Results (Results rounded to 2 decimals, but color coding is accurate.)

Level	A					B					C					D					E					F					G	
	Krigquadloess (EM01)	Krigloess (EM02)	Krigboxcar (EM03)	Krighann (EM04)	Krigkalman (EM05)	Krig_GMTquadloess (EM06)★	Krig_GMTloess (EM07)	Krig_GMTboxcar (EM08)	Krig_GMTThann (EM09)	Krig_GMTkalman (EM10)	Krig_MBZquadloess (EM11)	Krig_MBZloess (EM12)	Krig_MBZboxcar (EM13)	Krig_MBZThann (EM14)	Krig_MBZkalman (EM15)	GMTquadloess (EM16)	GMTloess (EM17)	GMTboxcar (EM18)★	GMTThann (EM19)	GMTkalman (EM20)	MBZquadloess (EM21)	MBZloess (EM22)	MBZboxcar (EM23)	MBZThann (EM24)	MBZkalman (EM25)	quadloess (EM26)	loess (EM27)	boxcar (EM28)	hann (EM29)	kalman (EM30)	GMT SIT (EM31)	MBZ SIT (EM32)
1	2.43	2.65	2.85	2.37	2.55	1.53	1.65	3.06	1.52	2.41	1.72	2.12	3.42	1.99	2.79	1.52	1.46	2.80	1.37	2.21	1.71	1.95	3.22	1.86	2.64	2.12	2.12	2.81	1.94	2.52	1.00	1.33
2	2.73	2.72	3.10	2.33	2.25	1.04	1.10	1.46	1.08	1.31	1.67	1.81	1.98	1.78	1.88	1.04	1.05	1.37	1.04	1.24	1.67	1.77	1.93	1.76	1.83	2.66	2.47	2.75	2.13	2.03	1.00	1.67
3	1.81	1.81	2.71	1.74	2.02	1.01	1.03	1.19	1.02	1.12	1.91	1.95	2.00	1.94	1.96	1.01	1.01	1.15	1.00	1.09	1.91	1.97	2.02	1.96	1.99	1.70	1.67	2.46	1.05	1.88	1.00	1.91
4	3.86	2.53	2.83	2.30	2.21	1.00	1.02	1.08	1.01	1.05	2.29	2.32	2.32	2.32	2.31	1.00	1.01	1.07	1.01	1.04	2.29	2.33	2.33	2.32	2.32	2.39	2.60	2.81	2.36	2.05	1.00	2.30
5	2.07	1.78	3.18	1.69	3.26	1.00	1.00	1.01	1.00	1.01	2.32	2.33	2.33	2.33	2.33	1.00	1.00	1.01	1.00	1.01	2.32	2.34	2.35	2.34	2.34	2.07	2.07	2.54	1.71	2.10	1.00	2.32
6	4.31	1.97	3.30	1.42	2.68	1.00	1.00	1.01	1.00	1.00	3.16	3.17	3.17	3.17	3.16	1.00	1.00	1.01	1.00	1.01	3.16	3.18	3.18	3.17	3.17	2.47	1.99	3.48	1.38	2.55	1.00	3.16
7	3.17	5.66	3.90	4.54	3.77	1.00	1.00	1.00	1.00	1.00	2.58	2.58	2.58	2.58	2.58	1.00	1.00	1.01	1.00	1.00	2.58	2.58	2.58	2.58	2.58	2.47	2.50	3.05	2.60	2.45	1.00	2.58
8	11.50	8.18	11.10	6.64	11.71	1.00	1.00	1.04	1.00	1.02	3.48	3.48	3.47	3.48	3.47	1.00	1.00	1.03	1.00	1.01	3.48	3.49	3.47	3.49	3.47	2.55	3.87	2.87	3.33	1.93	1.00	3.48
9	2.02	1.87	1.94	1.75	1.77	1.00	1.00	1.00	1.00	1.00	1.34	1.35	1.34	1.35	1.34	1.00	1.00	1.00	1.00	1.00	1.34	1.35	1.35	1.35	1.35	2.02	1.87	1.94	1.75	1.77	1.00	1.34
10	2.34	1.94	2.53	1.82	2.15	1.00	1.00	1.01	1.00	1.01	1.71	1.72	1.72	1.72	1.72	1.00	1.00	1.01	1.00	1.00	1.71	1.72	1.72	1.72	1.72	2.34	1.94	2.53	1.82	2.15	1.00	1.71
11	1.80	1.43	2.04	1.37	1.68	1.00	1.00	1.01	1.00	1.00	1.50	1.50	1.50	1.50	1.50	1.00	1.00	1.01	1.00	1.00	1.50	1.50	1.50	1.50	1.50	1.80	1.43	2.04	1.37	1.68	1.00	1.50

Annotations were added to Table 5.4 to highlight points of interest discussed in the text. Columns shaded are interpolators that had better accuracy than our benchmark GMT SIT (EM31) at least once, albeit negligible. All seven methods shaded are GMT SIT methods. CumRAE for all interpolators at each censored level for the 2D truncated seamount. The columns are our evaluated methods identified by EM<Id> in Table 2.2 on page 55. GMT SIT (EM31) is our benchmark. A value of 1.00 (middle green) indicates equal performance to the benchmark, values greater than 1.00 (dark green) performed worse than the benchmark, and values less than 1.00 (light green), performed better than the benchmark. For each level, the minimum CumRAE is annotated in red. CumRAE allows for direct comparison between methods. Letters identify interpolator groupings: (A) localized regression + kriging, (B) localized regression + kriging + pre-splining with GMT SIT (EM31), (C) localized regression + kriging + pre-splining with MBZ SIT (EM32), (D) localized regression + pre-splining with GMT SIT (EM31), (E) localized regression + pre-splining with GMT SIT (EM31), (F) localized regression + pre-splining with MBZ SIT (EM32), and (G) SIT. In all groups except G, filters are from left to right: quadloess, loess, boxcar, hann, and kalman. Red stars indicate eventually selected feature-favoring interpolators: seamount interpolator EM06 and ridge interpolator EM18.

In fact, as illustrated in Table 5.7, our next annotated version of Table 5.4, we find:

- All GMT SIT methods (groups B and D along with GMT SIT [EM31]) had similar accuracy.
 - Pre-splining with GMT SIT (groups B and C) was the next most accurate after our benchmark GMT SIT (EM31).
 - The GMT SIT methods in groups B and C were stable and appeared to converge to their pre-spliner GMT SIT (EM31).
- All MBZ SIT methods in groups C and E appeared converge to their pre-spliner MBZ SIT (EM32).
 - In Table 5.8, we divide the CumRAEs of groups A, C, E, and F by the CumRAEs of MBZ SIT (EM32) to see how they compared in their performances relative to GMT SIT (EM31). Color coding is as before but with blues to distinguish values are fractions of CumRAEs. Clearly, interpolators in groups C and F converged to their pre-spliner MBZ SIT (EM32).
- The convergence of pre-splining methods to their pre-spliner suggests pre-splining is highly influential as sparsity increases.

Table 5.7

(Annotation 2 of Table 5.4) Study 1 Test 1: Seamount Censored CumRAE Results (Results rounded to 2 decimals, but color coding is accurate.)

139

	Level	A					B					C					D					E					F					G	
		Krigquadloess (EM01)	Krigloess (EM02)	Krigboxcar (EM03)	Krighann (EM04)	Krigkalman (EM05)	Krig_GMTquadloess (EM06)★	Krig_GMTloess (EM07)	Krig_GMTboxcar (EM08)	Krig_GMTThann (EM09)	Krig_GMTkalman (EM10)	Krig_MBZquadloess (EM11)	Krig_MBZloess (EM12)	Krig_MBZboxcar (EM13)	Krig_MBZThann (EM14)	Krig_MBZkalman (EM15)	GMTquadloess (EM16)	GMTloess (EM17)	GMTboxcar (EM18)★	GMTThann (EM19)	GMTkalman (EM20)	MBZquadloess (EM21)	MBZloess (EM22)	MBZboxcar (EM23)	MBZThann (EM24)	MBZkalman (EM25)	quadloess (EM26)	loess (EM27)	boxcar (EM28)	hann (EM29)	kalman (EM30)	GMT SIT (EM31)	MBZ SIT (EM32)
1	2.43	2.65	2.85	2.37	2.55	1.53	1.65	3.06	1.52	2.41	1.72	2.12	3.42	1.99	2.79	1.52	1.46	2.80	1.37	2.21	1.71	1.95	3.22	1.86	2.64	2.12	2.12	2.81	1.94	2.52	1.00	1.33	
2	2.73	2.72	3.10	2.33	2.25	1.04	1.10	1.46	1.08	1.31	1.67	1.81	1.98	1.78	1.88	1.04	1.05	1.37	1.04	1.24	1.67	1.77	1.93	1.76	1.83	2.66	2.47	2.75	2.13	2.03	1.00	1.67	
3	1.81	1.81	2.71	1.74	2.02	1.01	1.03	1.19	1.02	1.12	1.91	1.95	2.00	1.94	1.96	1.01	1.01	1.15	1.00	1.09	1.91	1.97	2.02	1.96	1.99	1.70	1.67	2.46	1.05	1.88	1.00	1.91	
4	3.86	2.53	2.83	2.30	2.21	1.00	1.02	1.08	1.01	1.05	2.29	2.32	2.32	2.32	2.31	1.00	1.01	1.07	1.01	1.04	2.29	2.33	2.33	2.32	2.32	2.39	2.60	2.81	2.36	2.05	1.00	2.30	
5	2.07	1.78	3.18	1.69	3.26	1.00	1.00	1.01	1.00	1.01	2.32	2.33	2.33	2.33	2.33	1.00	1.00	1.01	1.00	1.01	2.32	2.34	2.35	2.34	2.34	2.07	2.07	2.54	1.71	2.10	1.00	2.32	
6	4.31	1.97	3.30	1.42	2.68	1.00	1.00	1.01	1.00	1.00	3.16	3.17	3.17	3.17	3.16	1.00	1.00	1.01	1.00	1.01	3.16	3.18	3.18	3.17	3.17	2.47	1.99	3.48	1.38	2.55	1.00	3.16	
7	3.17	5.66	3.90	4.54	3.77	1.00	1.00	1.00	1.00	1.00	2.58	2.58	2.58	2.58	2.58	1.00	1.00	1.01	1.00	1.00	2.58	2.58	2.58	2.58	2.58	2.47	2.50	3.05	2.60	2.45	1.00	2.58	
8	11.50	8.18	11.10	6.64	11.71	1.00	1.00	1.04	1.00	1.02	3.48	3.48	3.47	3.48	3.47	1.00	1.00	1.03	1.00	1.01	3.48	3.49	3.47	3.49	3.47	2.55	3.87	2.87	3.33	1.93	1.00	3.48	
9	2.02	1.87	1.94	1.75	1.77	1.00	1.00	1.00	1.00	1.00	1.34	1.35	1.34	1.35	1.34	1.00	1.00	1.00	1.00	1.00	1.34	1.35	1.35	1.35	1.35	2.02	1.87	1.94	1.75	1.77	1.00	1.34	
10	2.34	1.94	2.53	1.82	2.15	1.00	1.00	1.01	1.00	1.01	1.71	1.72	1.72	1.72	1.72	1.00	1.00	1.01	1.00	1.00	1.71	1.72	1.72	1.72	1.72	2.34	1.94	2.53	1.82	2.15	1.00	1.71	
11	1.80	1.43	2.04	1.37	1.68	1.00	1.00	1.01	1.00	1.00	1.50	1.50	1.50	1.50	1.50	1.00	1.00	1.01	1.00	1.00	1.50	1.50	1.50	1.50	1.50	1.80	1.43	2.04	1.37	1.68	1.00	1.50	

Annotations are points of interest discussed in the text. Columns shaded are interpolators that converge to near or better accuracy than our benchmark GMT SIT (EM31) at censoring level increases.

The GMT SIT methods in groups B and D are shaded. This suggests GMT SIT methods are feature-favoring for our truncated seamount when censoring. CumRAE for all interpolators at each censored level for the 2D truncated seamount. The columns are our evaluated methods identified by EM<Id> in Table 2.2 on page 55. GMT SIT (EM31) is our benchmark. A value of 1.00 (middle green) indicates equal performance to the benchmark, values greater than 1.00 (dark green) performed worse than the benchmark, and values less than 1.00 (light green), performed better than the benchmark. For each level, the minimum CumRAE is annotated in red. CumRAE allows for direct comparison between methods. Letters identify interpolator groupings: (A) localized regression + kriging, (B) localized regression + kriging + pre-splining with GMT SIT (EM31), (C) localized regression + kriging + pre-splining with MBZ SIT (EM32), (D) localized regression + pre-splining with GMT SIT (EM31), (E) localized regression + pre-splining with GMT SIT (EM31), (F) localized regression + pre-splining with MBZ SIT (EM32), and (G) SIT. In all groups except G, filters are from left to right: quadloess, loess, boxcar, hann, and kalman. Red stars indicate eventually selected feature-favoring interpolators: seamount interpolator EM06 and ridge interpolator EM18.

Table 5.8

Groups A, C, E, and F divided by MBZ SIT (EM32) from Table 5.4 for Study 1 Test 1: Seamount Censored CumRAE Results

(Results rounded to 2 decimals, but color coding is accurate.)

Level	A					B					C					D					E					F					G	
	Krigquadloess (EM01)	Krigloess (EM02)	Krigboxcar (EM03)	Krighann (EM04)	Krigkalman (EM05)	Krig_GMTquadloess (EM06)★	Krig_GMTloess (EM07)	Krig_GMTboxcar (EM08)	Krig_GMTThann (EM09)	Krig_GMTkalman (EM10)	Krig_MBZquadloess (EM11)	Krig_MBZloess (EM12)	Krig_MBZboxcar (EM13)	Krig_MBZThann (EM14)	Krig_MBZkalman (EM15)	GMTquadloess (EM16)	GMTloess (EM17)	GMTboxcar (EM18)★	GMTThann (EM19)	GMTkalman (EM20)	MBZquadloess (EM21)	MBZloess (EM22)	MBZboxcar (EM23)	MBZThann (EM24)	MBZkalman (EM25)	quadloess (EM26)	loess (EM27)	boxcar (EM28)	hann (EM29)	kalman (EM30)	GMT SIT (EM31)	MBZ SIT (EM32)
1	1.82	1.99	2.14	1.79	1.92						1.29	1.60	2.57	1.50	2.10						1.29	1.47	2.42	1.40	1.98	1.60	1.59	2.11	1.46	1.89		
2	1.64	1.63	1.86	1.40	1.35						1.00	1.08	1.19	1.07	1.12						1.00	1.06	1.16	1.05	1.10	1.59	1.48	1.65	1.28	1.22		
3	0.95	0.95	1.42	0.91	1.06						1.00	1.02	1.04	1.02	1.03						1.00	1.03	1.06	1.02	1.04	0.89	0.87	1.29	0.55	0.98		
4	1.68	1.10	1.23	1.00	0.96						1.00	1.01	1.01	1.01	1.00						1.00	1.01	1.01	1.01	1.01	1.04	1.13	1.22	1.02	0.89		
5	0.89	0.77	1.37	0.73	1.40						1.00	1.00	1.00	1.00	1.00						1.00	1.01	1.01	1.01	1.01	0.89	0.89	1.09	0.74	0.90		
6	1.36	0.62	1.04	0.45	0.85						1.00	1.00	1.00	1.00	1.00						1.00	1.01	1.01	1.00	1.00	0.78	0.63	1.10	0.44	0.81		
7	1.23	2.20	1.51	1.76	1.46						1.00	1.00	1.00	1.00	1.00						1.00	1.00	1.00	1.00	1.00	0.96	0.97	1.18	1.01	0.95		
8	3.31	2.35	3.19	1.91	3.37						1.00	1.00	1.00	1.00	1.00						1.00	1.00	1.00	1.00	1.00	0.73	1.11	0.83	0.96	0.56		
9	1.50	1.39	1.45	1.30	1.31						1.00	1.00	1.00	1.00	1.00						1.00	1.00	1.00	1.00	1.00	1.50	1.39	1.45	1.30	1.31		
10	1.36	1.13	1.47	1.06	1.25						1.00	1.00	1.00	1.00	1.00						1.00	1.00	1.00	1.00	1.00	1.36	1.13	1.47	1.06	1.25		
11	1.20	0.95	1.36	0.91	1.12						1.00	1.00	1.00	1.00	1.00						1.00	1.00	1.00	1.00	1.00	1.20	0.95	1.36	0.91	1.12		

Values are fractions of CumRAEs. CumRAE values indicate accuracy comparative to our benchmark. A fraction of CumRAEs indicates whether methods compared similarly to our benchmark. The columns are our evaluated methods identified by EM<Id> in Table 2.2 on page 55. GMT SIT (EM31) is our benchmark. A value of 1.00 (middle blue) indicates the method in the numerator and denominator performed equally to each other in their performance to the benchmark, values greater than 1.00 (dark blue) the numerator performed worse than the denominator in their performance to the benchmark, and values less than 1.00 (light blue), the numerator performed better than the denominator in their performance to the benchmark. CumRAE allows for direct comparison between methods. Letters identify interpolator groupings: (A) localized regression + kriging, (B) localized regression + kriging + pre-splining with GMT SIT (EM31), (C) localized regression + kriging + pre-splining with MBZ SIT (EM32), (D) localized regression + pre-splining with GMT SIT (EM31), (E) localized regression + pre-splining with GMT SIT (EM31), (F) localized regression + pre-splining with MBZ SIT (EM32), and (G) SIT. In all groups except G, filters are from left to right: quadloess, loess, boxcar, hann, and kalman. Red stars indicate eventually selected feature-favoring interpolators: seamount interpolator EM06 and ridge interpolator EM18.

5.2.1.3 1D Gaussian Ridge

When censoring the ridge, we find (illustrated in Table 5.9 by annotating Table 5.5):

- All interpolators appear to converge (red arrow) to accuracy near or better than our benchmark GMT SIT (EM31) as sparsity increased.
- At censored levels 9-11 (below horizontal line), all our non-GMT SIT methods (groups A, C, E and F along with MBZ SIT [EM32]) have accuracy better (light green) than our benchmark GMT SIT (EM31).
- Again, as in the seamount censored UE, we see the same apparent convergence of pre-splining methods to their pre-spliner.
 - MBZ SIT methods in groups C and E appear to converge to their pre-spliner MBZ SIT (EM32).
 - GMT SIT methods in groups B and D (shaded) appear to converge and stabilize to their pre-spliner GMT SIT (EM31)
 - The first method in B and D (EM06 and EM16) utilizes quadloess and are the only methods to show better accuracy (light green) at low censored levels.
- At censored levels 1-7 (above dashed horizontal line), the most accurate interpolators (in red) were GMT SIT methods (groups B and D, along with our benchmark GMT SIT [EM31]) and
 - At censored levels 8-11 (higher sparsity), they were not (below dashed horizontal line).

These findings suggest that under sparsity, the pre-splining methods (and more generally, pre-splining) are highly influential with

- GMT SIT (EM31) having better accuracy than MBZ SIT (EM32) at low sparsity (censored levels 1-8) (above horizontal line), and
- MBZ SIT (EM32) having better accuracy at higher sparsity (censored levels 9-11) (below horizontal line).
 - While non-pre-splining methods (groups A and F) appear not that different from MBZ SIT (EM32).
- In fact, if we compare groups C and D against MBZ SIT (EM32), we see that they converge similarly as our GMT SIT methods in groups B and D did to their pre-spliner GMT SIT (EM31).
 - In Table 5.10, we divide the CumRAE values of groups A, C, E, and F by the CumRAE values of MBZ SIT (EM32) to see how they compared in their performances relative to GMT SIT (EM31). Color coding is as before but with blues to distinguish values are fractions of CumRAEs. Clearly, interpolators in groups C and F converged to their pre-spliner MBZ SIT (EM32), while non-pre-splining methods (groups A and F) do not converge to MBZ SIT (EM32).

Table 5.9

(Annotated Table 5.5) Study 1 Test 1: Ridge Censored CumRAE Results (Results rounded to 2 decimals, but color coding is accurate.)

Level	A					B					C					D					E					F					G	
	Krigquadloess (EM01)	Krigloess (EM02)	Krigboxcar (EM03)	Krighann (EM04)	Krigkalman (EM05)	Krig_GMTquadloess (EM06)★	Krig_GMTloess (EM07)	Krig_GMTboxcar (EM08)	Krig_GMTThann (EM09)	Krig_GMTkalman (EM10)	Krig_MBZquadloess (EM11)	Krig_MBZloess (EM12)	Krig_MBZboxcar (EM13)	Krig_MBZThann (EM14)	Krig_MBZkalman (EM15)	GMTquadloess (EM16)	GMTloess (EM17)	GMTboxcar (EM18)★	GMTThann (EM19)	GMTkalman (EM20)	MBZquadloess (EM21)	MBZloess (EM22)	MBZboxcar (EM23)	MBZThann (EM24)	MBZkalman (EM25)	quadloess (EM26)	loess (EM27)	boxcar (EM28)	hann (EM29)	kalman (EM30)	GMT SIT (EM31)	MBZ SIT (EM32)
1	21.26	75.14	88.32	61.17	68.43	0.82	25.21	125.84	20.84	83.69	24.42	46.56	139.28	42.30	99.70	0.51	17.31	111.37	14.71	75.76	24.31	42.16	129.03	39.64	93.15	17.12	37.70	68.99	33.40	54.00	1.00	26.35
2	32.63	35.12	37.18	29.14	23.79	0.87	3.37	13.20	2.92	9.07	21.07	23.14	27.41	22.80	24.82	0.84	2.74	11.91	2.46	8.31	21.05	22.68	26.30	22.47	24.01	32.71	31.64	35.92	26.62	22.34	1.00	21.37
3	8.78	10.33	12.75	8.18	10.42	0.97	1.21	2.83	1.18	2.12	11.55	11.71	12.03	11.75	11.81	0.97	1.34	2.98	1.29	2.30	11.55	11.95	12.40	11.90	12.09	8.74	10.62	13.41	7.30	10.88	1.00	11.63
4	9.40	14.75	17.93	11.89	18.24	0.99	1.06	1.54	1.05	1.32	8.58	8.64	8.58	8.64	8.56	0.99	1.14	1.70	1.12	1.43	8.58	8.72	8.70	8.70	8.66	7.88	8.96	9.93	8.08	6.52	1.00	8.61
5	1.61	3.32	6.84	2.69	7.14	1.00	1.02	1.04	1.01	1.02	3.34	3.35	3.32	3.35	3.33	1.00	1.03	1.06	1.03	1.04	3.34	3.36	3.34	3.36	3.35	2.09	2.41	3.12	1.93	2.71	1.00	3.34
6	1.00	1.80	2.79	1.26	2.89	1.00	1.01	1.01	1.01	1.01	2.36	2.37	2.36	2.37	2.36	1.00	1.01	1.02	1.01	1.01	2.36	2.37	2.37	2.37	2.37	1.25	1.37	2.06	1.10	1.67	1.00	2.37
7	2.03	3.65	2.31	2.97	2.26	1.00	1.01	1.02	1.00	1.01	1.67	1.68	1.68	1.68	1.68	1.00	1.01	1.02	1.01	1.01	1.67	1.68	1.68	1.68	1.68	1.45	1.69	1.75	1.77	1.37	1.00	1.67
8	2.16	1.47	2.10	1.19	2.17	1.00	1.00	1.00	1.00	1.00	1.02	1.02	1.02	1.02	1.02	1.00	1.00	1.00	1.00	1.00	1.02	1.03	1.02	1.03	1.02	0.53	1.13	0.86	0.99	0.65	1.00	1.02
9	0.98	0.90	0.86	0.82	0.78	1.00	1.00	1.00	1.00	1.00	0.73	0.73	0.73	0.73	0.73	1.00	1.00	1.00	1.00	1.00	0.73	0.73	0.73	0.73	0.73	0.98	0.90	0.86	0.82	0.78	1.00	0.73
10	0.80	0.66	0.71	0.57	0.61	1.00	1.00	1.00	1.00	1.00	0.60	0.60	0.60	0.60	0.60	1.00	1.00	1.00	1.00	1.00	0.60	0.60	0.60	0.60	0.60	0.80	0.66	0.71	0.57	0.61	1.00	0.60
11	0.65	0.46	0.60	0.37	0.49	1.00	1.00	1.00	1.00	1.00	0.49	0.49	0.49	0.49	0.49	1.00	1.00	1.00	1.00	1.00	0.49	0.49	0.49	0.49	0.49	0.65	0.46	0.60	0.37	0.49	1.00	0.49

Annotations are points of interest discussed in the text. The red arrow notes accuracy converging near or better than our benchmark GMT SIT (EM31). The horizontal line indicates accuracy better than GMT SIT methods (groups B and D along with GMT SIT {EM31}) for censored levels 8-11. The dashed line indicates GMT SIT methods (groups B and D along with GMT SIT [EM31]) were the most accurate for censored levels 1-7 only. GMT SIT methods in groups B and D are shaded to indicate their stability with GMT SIT (EM31). CumRAE for all interpolators at each censored level for the 1D Gaussian ridge. The columns are our evaluated methods identified by EM<Id> in Table 2.2 on page 55. GMT SIT (EM31) is our benchmark. A value of 1.00 (middle green) indicates equal performance to the benchmark, values greater than 1.00 (dark green) performed worse than the benchmark, and values less than 1.00 (light green), performed better than the benchmark. For each level, the minimum CumRAE is annotated in red. CumRAE allows for direct comparison between methods. Letters identify interpolator groupings: (A) localized regression + kriging, (B) localized regression + kriging + pre-splining with GMT SIT (EM31), (C) localized regression + kriging + pre-splining with MBZ SIT (EM32), (D) localized regression + pre-splining with GMT SIT (EM31), (E) localized regression + pre-splining with GMT SIT (EM31), (F) localized regression + pre-splining with MBZ SIT (EM32), and (G) SIT. In all groups except G, filters are from left to right: quadloess, loess, boxcar, hann, and kalman. Red stars indicate eventually selected feature-favoring interpolators: seamount interpolator EM06 and ridge interpolator EM18.

Table 5.10

Groups A, C, E, and F divided by MBZ SIT (EM32) from Table 5.5 for Study 1 Test 1: Ridge Censored CumRAE Results (Results rounded to 2 decimals, but color coding is accurate.)

144

A						B					C					D				E					F				G			
Level	Krigquadloess (EM01)	Krigloess (EM02)	Krigboxcar (EM03)	Krighann (EM04)	Krigkalman (EM05)	Krig_GMTquadloess (EM06)★	Krig_GMTloess (EM07)	Krig_GMTboxcar (EM08)	Krig_GMTthann (EM09)	Krig_GMTkalman (EM10)	Krig_MBZquadloess (EM11)	Krig_MBZloess (EM12)	Krig_MBZboxcar (EM13)	Krig_MBZhann (EM14)	Krig_MBZkalman (EM15)	GMTquadloess (EM16)	GMTloess (EM17)	GMTboxcar (EM18)★	GMTthann (EM19)	GMTkalman (EM20)	MBZquadloess (EM21)	MBZloess (EM22)	MBZboxcar (EM23)	MBZhann (EM24)	MBZkalman (EM25)	quadloess (EM26)	loess (EM27)	boxcar (EM28)	hann (EM29)	kalman (EM30)	GMT SIT (EM31)	MBZ SIT (EM32)
1	0.81	2.85	3.35	2.32	2.60	0.93	1.77	5.29	1.61	3.78	0.92	1.60	4.90	1.50	3.53	0.65	1.43	2.62	1.27	2.05		
2	1.53	1.64	1.74	1.36	1.11						0.99	1.08	1.28	1.07	1.16						0.99	1.06	1.23	1.05	1.12	1.53	1.48	1.68	1.25	1.05		
3	0.76	0.89	1.10	0.70	0.90						0.99	1.01	1.04	1.01	1.02						0.99	1.03	1.07	1.02	1.04	0.75	0.91	1.15	0.63	0.94		
4	1.09	1.71	2.08	1.38	2.12						1.00	1.00	1.00	1.00	0.99						1.00	1.01	1.01	1.01	1.01	0.92	1.04	1.15	0.94	0.76		
5	0.48	0.99	2.05	0.80	2.14						1.00	1.00	0.99	1.00	1.00						1.00	1.01	1.00	1.01	1.00	0.62	0.72	0.93	0.58	0.81		
6	0.42	0.76	1.18	0.53	1.22						1.00	1.00	1.00	1.00	1.00						1.00	1.00	1.00	1.00	1.00	0.53	0.58	0.87	0.47	0.71		
7	1.21	2.18	1.38	1.77	1.35						1.00	1.00	1.00	1.00	1.00						1.00	1.00	1.00	1.00	1.00	0.87	1.01	1.05	1.06	0.82		
8	2.11	1.43	2.05	1.16	2.12						1.00	1.00	1.00	1.00	1.00						1.00	1.00	1.00	1.00	1.00	0.52	1.11	0.84	0.97	0.63		
9	1.34	1.23	1.18	1.13	1.07						1.00	1.00	1.00	1.00	1.00						1.00	1.00	1.00	1.00	1.00	1.34	1.23	1.18	1.13	1.07		
10	1.33	1.10	1.18	0.95	1.01						1.00	1.00	1.00	1.00	1.00						1.00	1.00	1.00	1.00	1.00	1.33	1.10	1.18	0.95	1.01		
11	1.33	0.93	1.23	0.75	0.99						1.00	1.00	1.00	1.00	1.00						1.00	1.00	1.00	1.00	1.00	1.33	0.93	1.23	0.75	0.99		

Values are fractions of CumRAEs. CumRAE values indicate accuracy comparative to our benchmark. A fraction of CumRAEs indicates whether methods compared similarly to our benchmark. The columns are our evaluated methods identified by EM<Id> in Table 2.2 on page 55. GMT SIT (EM31) is our benchmark. A value of 1.00 (middle blue) indicates the method in the numerator and denominator performed equally to each other in their performance to the benchmark, values greater than 1.00 (dark blue) the numerator performed worse than the denominator in their performance to the benchmark, and values less than 1.00 (light blue), the numerator performed better than the denominator in their performance to the benchmark. CumRAE allows for direct comparison between methods. Letters identify interpolator groupings: (A) localized regression + kriging, (B) localized regression + kriging + pre-splining with GMT SIT (EM31), (C) localized regression + kriging + pre-splining with MBZ SIT (EM32), (D) localized regression + pre-splining with GMT SIT (EM31), (E) localized regression + pre-splining with GMT SIT (EM31), (F) localized regression + pre-splining with MBZ SIT (EM32), and (G) SIT. In all groups except G, filters are from left to right: quadloess, loess, boxcar, hann, and kalman. Red stars indicate eventually selected feature-favoring interpolators: seamount interpolator EM06 and ridge interpolator EM18.

5.2.1.4 Discussion: Seamount versus Ridge Censored UEs (Test 1)

Overall, GMT SIT methods (groups B and D along with GMT SIT [EM31]) had better accuracy for most censored levels for both our seamount and ridge. However, at higher censor levels, GMT SIT methods (groups B and D along with GMT SIT [EM31]) were able to maintain accuracy better for our seamount but not for our ridge.

This suggests that the GMT SIT methods (groups B and D along with GMT SIT [EM31]) may be able to handle the nonlinearity of the seamount truncation better than the other methods, indicating feature-favoritism for the truncated seamount.⁵⁴

Observations so far are based on a relative error; from the CumRAEs alone, we cannot determine the validity of our surfaces (magnitude of surface errors). For that we inspect depths and errors of the individual DBMs which indicated GMT SIT (EM31) completely lost the trend at high sparsity (censored levels 9-11) for our ridge while MBZ SIT (EM32) did not, as was exhibited in Table 5.5 and Table 5.9 where CumRAE values indicated better accuracy than GMT SIT (EM31).

5.2.2 Test 2: Noise UEs

Next, we discuss the noise UEs (first study Test 2) for the seamount and ridge primitives. In both Table 5.11 and Table 5.12, the CumRAE for both the seamount and ridge UEs with added noise (first study Test 2) show that

- all interpolators were more accurate (light green) than GMT SIT (EM31) and MBZ SIT (EM32) for all noise levels 1-11

⁵⁴ Recall that our benchmark GMT SIT (EM31) is not the truth, just the de facto standard in DBMs.

- except for the Kalman methods (EM05, EM10, EM15, EM20, EM25, and EM30), which were less accurate (dark green) than GMT SIT (EM31) for noise levels 5-9.

Table 5.11

Study 1 Test 2: Seamount Noise CumRAE Results (Results rounded to 2 decimals, but color coding is accurate.)

Level	A					B					C					D					E					F					G	
	Krigquadloess (EM01)	Krigloess (EM02)	Krigboxcar (EM03)	Krighann (EM04)	Krigkalman (EM05)	Krig_GMTquadloess (EM06)★	Krig_GMTloess (EM07)	Krig_GMTboxcar (EM08)	Krig_GMTthann (EM09)	Krig_GMTkalman (EM10)	Krig_MBZquadloess (EM11)	Krig_MBZloess (EM12)	Krig_MBZboxcar (EM13)	Krig_MBZthann (EM14)	Krig_MBZkalman (EM15)	GMTquadloess (EM16)	GMTloess (EM17)	GMTboxcar (EM18)★	GMTthann (EM19)	GMTkalman (EM20)	MBZquadloess (EM21)	MBZloess (EM22)	MBZboxcar (EM23)	MBZthann (EM24)	MBZkalman (EM25)	quadloess (EM26)	loess (EM27)	boxcar (EM28)	hann (EM29)	kalman (EM30)	GMT SIT (EM31)	MBZ SIT (EM32)
1	0.35	0.36	0.38	0.39	0.39	0.35	0.35	0.38	0.39	0.40	0.35	0.36	0.37	0.39	0.39	0.35	0.35	0.37	0.39	0.39	0.35	0.35	0.37	0.39	0.39	0.35	0.35	0.37	0.39	0.39	1.00	1.00
2	0.35	0.35	0.37	0.39	0.46	0.35	0.35	0.37	0.38	0.46	0.35	0.35	0.37	0.39	0.46	0.35	0.35	0.36	0.38	0.46	0.35	0.35	0.36	0.38	0.46	0.35	0.35	0.36	0.38	0.46	1.00	1.00
3	0.35	0.35	0.37	0.39	0.69	0.35	0.35	0.36	0.38	0.68	0.35	0.35	0.37	0.39	0.69	0.35	0.35	0.36	0.38	0.69	0.35	0.35	0.36	0.38	0.71	0.35	0.35	0.36	0.38	0.71	1.00	1.00
4	0.35	0.35	0.37	0.39	0.96	0.35	0.35	0.37	0.39	0.96	0.35	0.35	0.37	0.39	0.96	0.35	0.35	0.36	0.38	0.98	0.35	0.35	0.36	0.38	0.98	0.35	0.35	0.36	0.38	0.98	1.00	1.00
5	0.35	0.35	0.37	0.39	1.22	0.35	0.35	0.37	0.39	1.22	0.35	0.35	0.37	0.39	1.22	0.35	0.35	0.36	0.38	1.26	0.35	0.35	0.36	0.38	1.26	0.35	0.35	0.36	0.38	1.26	1.00	1.00
6	0.35	0.35	0.37	0.39	1.30	0.35	0.35	0.37	0.39	1.30	0.35	0.35	0.37	0.39	1.30	0.35	0.35	0.36	0.38	1.36	0.35	0.35	0.36	0.38	1.36	0.35	0.35	0.36	0.38	1.36	1.00	1.00
7	0.35	0.35	0.37	0.39	1.26	0.35	0.35	0.37	0.39	1.26	0.35	0.35	0.37	0.39	1.26	0.35	0.35	0.36	0.38	1.32	0.35	0.35	0.36	0.38	1.32	0.35	0.35	0.36	0.38	1.32	1.00	1.00
8	0.35	0.35	0.37	0.39	1.14	0.35	0.35	0.37	0.39	1.14	0.35	0.35	0.37	0.39	1.14	0.35	0.35	0.36	0.38	1.21	0.35	0.35	0.36	0.38	1.21	0.35	0.35	0.36	0.38	1.21	1.00	1.00
9	0.35	0.35	0.37	0.39	1.02	0.35	0.35	0.37	0.39	1.03	0.35	0.35	0.37	0.39	1.02	0.35	0.35	0.36	0.38	1.09	0.35	0.35	0.36	0.38	1.09	0.35	0.35	0.36	0.38	1.09	1.00	1.00
10	0.35	0.35	0.37	0.39	0.96	0.35	0.35	0.37	0.39	0.97	0.35	0.35	0.37	0.39	0.96	0.35	0.35	0.36	0.38	1.03	0.35	0.35	0.36	0.38	1.03	0.35	0.35	0.36	0.38	1.03	1.00	1.00
11	0.35	0.35	0.37	0.39	0.91	0.35	0.35	0.37	0.39	0.91	0.35	0.35	0.37	0.39	0.91	0.35	0.35	0.36	0.38	0.97	0.35	0.35	0.36	0.38	0.97	0.35	0.35	0.36	0.38	0.97	1.00	1.00

CumRAE for all interpolators at each noise level for the 2D truncated seamount. The columns are our evaluated methods identified by EM<Id> in Table 2.2 on page 55. GMT SIT (EM31) is our benchmark. A value of 1.00 (middle green) indicates equal performance to the benchmark, values greater than 1.00 (dark green) performed worse than the benchmark, and values less than 1.00 (light green), performed better than the benchmark. For each level, the minimum CumRAE is annotated in red. CumRAE allows for direct comparison between methods. Letters identify interpolator groupings: (A) localized regression + kriging, (B) localized regression + kriging + pre-splining with GMT SIT (EM31), (C) localized regression + kriging + pre-splining with MBZ SIT (EM32), (D) localized regression + pre-splining with GMT SIT (EM31), (E) localized regression + pre-splining with GMT SIT (EM31), (F) localized regression + pre-splining with MBZ SIT (EM32), and (G) SIT. In all groups except G, filters are from left to right: quadloess, loess, boxcar, hann, and kalman. Red stars indicate eventually selected feature-favoring interpolators: seamount interpolator EM06 and ridge interpolator EM18.

Table 5.12

Study 1 Test 2: Ridge Noise CumRAE Results (Results rounded to 2 decimals, but color coding is accurate.)

Level	A					B					C					D					E					F					G	
	Krigquadloess (EM01)	Krigloess (EM02)	Krigboxcar (EM03)	Krighann (EM04)	Krigkalman (EM05)	Krig_GMTquadloess (EM06)★	Krig_GMTloess (EM07)	Krig_GMTboxcar (EM08)	Krig_GMTthann (EM09)	Krig_GMTkalman (EM10)	Krig_MBZquadloess (EM11)	Krig_MBZloess (EM12)	Krig_MBZboxcar (EM13)	Krig_MBZthann (EM14)	Krig_MBZkalman (EM15)	GMTquadloess (EM16)	GMTloess (EM17)	GMTboxcar (EM18)★	GMTthann (EM19)	GMTkalman (EM20)	MBZquadloess (EM21)	MBZloess (EM22)	MBZboxcar (EM23)	MBZthann (EM24)	MBZkalman (EM25)	quadloess (EM26)	loess (EM27)	boxcar (EM28)	hann (EM29)	kalman (EM30)	GMT SIT (EM31)	MBZ SIT (EM32)
1	0.35	0.35	0.38	0.39	0.39	0.35	0.35	0.37	0.39	0.39	0.35	0.35	0.37	0.39	0.39	0.35	0.35	0.37	0.38	0.39	0.35	0.35	0.37	0.38	0.39	0.35	0.35	0.37	0.38	0.39	1.00	1.00
2	0.35	0.35	0.37	0.39	0.46	0.35	0.35	0.37	0.38	0.45	0.35	0.35	0.37	0.39	0.46	0.35	0.35	0.36	0.38	0.46	0.35	0.35	0.37	0.38	0.46	0.35	0.35	0.36	0.38	0.46	1.00	1.00
3	0.35	0.35	0.37	0.39	0.69	0.35	0.35	0.37	0.38	0.68	0.35	0.35	0.37	0.39	0.69	0.35	0.35	0.36	0.38	0.70	0.35	0.35	0.36	0.38	0.71	0.35	0.35	0.36	0.38	0.71	1.00	1.00
4	0.35	0.35	0.37	0.39	0.96	0.35	0.35	0.37	0.38	0.95	0.35	0.35	0.37	0.39	0.96	0.35	0.35	0.36	0.38	0.98	0.35	0.35	0.36	0.38	0.99	0.35	0.35	0.36	0.38	0.99	1.00	1.00
5	0.35	0.35	0.37	0.39	1.23	0.35	0.35	0.37	0.39	1.23	0.35	0.35	0.37	0.39	1.23	0.35	0.35	0.36	0.38	1.27	0.35	0.35	0.36	0.38	1.27	0.35	0.35	0.36	0.38	1.27	1.00	1.00
6	0.35	0.35	0.37	0.39	1.30	0.35	0.35	0.37	0.39	1.30	0.35	0.35	0.37	0.39	1.30	0.35	0.35	0.36	0.38	1.36	0.35	0.35	0.36	0.38	1.36	0.35	0.35	0.36	0.38	1.36	1.00	1.00
7	0.35	0.35	0.37	0.39	1.26	0.35	0.35	0.37	0.39	1.26	0.35	0.35	0.37	0.39	1.25	0.35	0.35	0.36	0.38	1.32	0.35	0.35	0.36	0.38	1.32	0.35	0.35	0.36	0.38	1.32	1.00	1.00
8	0.35	0.35	0.37	0.39	1.14	0.35	0.35	0.37	0.39	1.14	0.35	0.35	0.37	0.39	1.14	0.35	0.35	0.36	0.38	1.21	0.35	0.35	0.36	0.38	1.21	0.35	0.35	0.36	0.38	1.21	1.00	1.00
9	0.35	0.35	0.37	0.39	1.02	0.35	0.35	0.37	0.39	1.02	0.35	0.35	0.37	0.39	1.02	0.35	0.35	0.36	0.38	1.09	0.35	0.35	0.36	0.38	1.09	0.35	0.35	0.36	0.38	1.09	1.00	1.00
10	0.35	0.35	0.37	0.39	0.96	0.35	0.35	0.37	0.39	0.96	0.35	0.35	0.37	0.39	0.96	0.35	0.35	0.36	0.38	1.03	0.35	0.35	0.36	0.38	1.03	0.35	0.35	0.36	0.38	1.03	1.00	1.00
11	0.35	0.35	0.37	0.39	0.90	0.35	0.35	0.37	0.39	0.90	0.35	0.35	0.37	0.39	0.90	0.35	0.35	0.36	0.38	0.97	0.35	0.35	0.36	0.38	0.97	0.35	0.35	0.36	0.38	0.97	1.00	1.00

CumRAE for all interpolators at each noise level for the 1D Gaussian ridge. The columns are our evaluated methods identified by EM<Id> in Table 2.2 on page 55. GMT SIT (EM31) is our benchmark. A value of 1.00 (middle green) indicates equal performance to the benchmark, values greater than 1.00 (dark green) performed worse than the benchmark, and values less than 1.00 (light green), performed better than the benchmark. For each level, the minimum CumRAE is annotated in red. CumRAE allows for direct comparison between methods. Letters identify interpolator groupings: (A) localized regression + kriging, (B) localized regression + kriging + pre-splining with GMT SIT (EM31), (C) localized regression + kriging + pre-splining with MBZ SIT (EM32), (D) localized regression + pre-splining with GMT SIT (EM31), (E) localized regression + pre-splining with GMT SIT (EM31), (F) localized regression + pre-splining with MBZ SIT (EM32), and (G) SIT. In all groups except G, filters are from left to right: quadloess, loess, boxcar, hann, and kalman. Red stars indicate eventually selected feature-favoring interpolators: seamount interpolator EM06 and ridge interpolator EM18.

5.2.3 Test 3: Combined Censored and Noise UEs

Table 5.13 and Table 5.14 (first study Test 3) show the CumRAE results of combining the different noise levels along with the different censored levels to see how their interaction affects accuracy for the interpolators on the different primitives. For both our seamount (Table 5.13) and ridge (Table 5.14), we see that most methods had better accuracy than our benchmark GMT SIT (EM31), with pre-splining methods appearing to converge to their pre-spliners.

GMT SIT methods (groups B and D) most consistently remained close to the same accuracy as our benchmark GMT SIT (EM31). The remaining non-GMT SIT methods (groups A, C, E, and F, along with MBZ SIT [EM32]) indicated much better accuracy even at the highest censored and noise combination levels.

Table 5.15 and Table 5.16 are reduced versions of these tables, displaying combination levels with acceptable noise (level 1) only. These tables appear similar to those for Test 2: Noise UEs (Table 5.11 and Table 5.12) and exhibit the importance of selecting feature-favoring interpolators under noise.

Table 5.13

Study 1 Test 3: Seamount Censored and Noise CumRAE Results (Results rounded to 2 decimals, but color coding is accurate.)

	Censored (C) and Noise (N) Combination Level	A					Krig_GMTquadloess (EM06)★	B					Krig_MBZquadloess (EM11)	C					GMTquadloess (EM16)	D					MBZquadloess (EM21)	E					quadloess (EM26)	loess (EM27)	F					G	
		Krigquadloess (EM01)	Krigloess (EM02)	Krigboxcar (EM03)	Krighann (EM04)	Krigkalman (EM05)		Krig_GMTloess (EM07)	Krig_GMTboxcar (EM08)	Krig_GMTthann (EM09)	Krig_GMTkalman (EM10)	Krig_MBZloess (EM12)		Krig_MBZboxcar (EM13)	Krig_MBZhann (EM14)	Krig_MBZkalman (EM15)	GMTloess (EM17)	GMTboxcar (EM18)★		GMTthann (EM19)	GMTkalman (EM20)	MBZloess (EM22)	MBZboxcar (EM23)	MBZhann (EM24)		MBZkalman (EM25)	boxcar (EM28)	hann (EM29)	kalman (EM30)	GMT SIT (EM31)			MBZ SIT (EM32)						
150	C1N1	0.73	0.57	0.52	0.58	0.50	0.79	0.75	0.72	0.78	0.43	0.67	0.64	0.62	0.66	0.40	0.79	0.75	0.72	0.78	0.43	0.67	0.64	0.62	0.66	0.40	0.71	0.55	0.50	0.57	0.48	1.00	0.83						
	C1N2	0.76	0.63	0.64	0.64	0.62	0.98	0.92	0.91	0.94	0.70	0.73	0.70	0.69	0.71	0.58	0.98	0.92	0.91	0.93	0.69	0.73	0.70	0.69	0.70	0.57	0.77	0.63	0.64	0.64	0.59	1.00	0.74						
	C1N3	0.70	0.79	0.74	0.84	0.92	1.00	0.98	0.97	0.98	0.90	0.78	0.77	0.77	0.77	0.75	1.00	0.98	0.97	0.98	0.90	0.78	0.77	0.78	0.78	0.75	0.74	0.81	0.76	0.83	0.97	1.00	0.79						
	C1N4	1.20	0.86	1.12	0.80	1.24	1.00	0.98	0.99	0.99	0.92	0.77	0.77	0.78	0.77	0.75	1.00	0.98	0.99	0.99	0.92	0.77	0.77	0.78	0.77	0.75	1.05	0.85	0.97	0.78	1.09	1.00	0.78						
	C1N5	0.88	0.77	0.88	0.81	1.32	1.00	0.99	0.98	0.99	0.95	0.81	0.81	0.81	0.81	0.81	1.00	0.99	0.99	0.99	0.95	0.81	0.81	0.81	0.81	0.81	0.84	0.76	0.90	0.75	1.33	1.00	0.82						
	C1N6	0.95	1.23	1.43	1.08	1.83	1.00	0.99	0.99	0.99	0.98	1.19	1.19	1.19	1.19	1.20	1.00	1.00	0.99	1.00	0.98	1.19	1.20	1.19	1.20	1.20	0.90	0.99	1.19	0.95	1.84	1.00	1.20						
	C1N7	1.12	1.28	1.23	1.21	1.48	1.00	1.00	1.00	1.00	1.00	1.10	1.11	1.10	1.11	1.11	1.00	1.00	1.00	1.00	1.00	1.10	1.11	1.11	1.11	1.11	1.13	1.17	1.27	1.19	1.51	1.00	1.11						
	C1N8	5.83	3.64	5.48	3.05	5.56	1.00	1.00	1.01	1.00	1.00	1.43	1.43	1.43	1.43	1.44	1.00	1.00	1.01	1.00	0.99	1.43	1.43	1.43	1.43	1.44	1.48	1.82	1.68	1.57	1.97	1.00	1.43						
	C1N9	1.46	1.38	1.46	1.36	1.44	1.00	1.00	1.00	1.00	1.01	1.10	1.10	1.10	1.10	1.10	1.00	1.00	1.00	1.00	1.00	1.10	1.10	1.10	1.10	1.10	1.46	1.38	1.46	1.36	1.44	1.00	1.10						
	C1N10	1.66	1.42	1.76	1.38	1.62	1.00	1.00	1.01	1.00	1.01	1.30	1.31	1.31	1.31	1.31	1.00	1.00	1.00	1.00	1.01	1.30	1.31	1.31	1.31	1.31	1.66	1.42	1.76	1.38	1.62	1.00	1.31						
	C1N11	1.10	0.77	1.30	0.68	1.06	1.00	1.00	1.00	1.00	1.00	0.80	0.80	0.80	0.80	0.80	1.00	1.00	1.00	1.00	1.00	0.80	0.80	0.80	0.80	0.80	1.10	0.77	1.30	0.68	1.06	1.00	0.80						
151	C2N1	0.72	0.55	0.50	0.58	0.56	0.79	0.74	0.72	0.78	0.45	0.67	0.63	0.61	0.66	0.41	0.79	0.75	0.72	0.78	0.45	0.67	0.63	0.61	0.66	0.41	0.71	0.54	0.48	0.56	0.57	1.00	0.83						
	C2N2	0.72	0.57	0.56	0.58	0.46	0.98	0.92	0.90	0.93	0.67	0.70	0.66	0.65	0.67	0.51	0.98	0.92	0.90	0.93	0.67	0.70	0.66	0.65	0.67	0.50	0.73	0.57	0.55	0.59	0.45	1.00	0.71						
	C2N3	0.66	0.75	0.64	0.79	0.38	1.00	0.97	0.97	0.98	0.87	0.69	0.68	0.68	0.68	0.63	1.00	0.97	0.97	0.98	0.87	0.69	0.68	0.68	0.68	0.63	0.70	0.76	0.64	0.80	0.47	1.00	0.70						
	C2N4	0.97	0.75	0.69	0.73	0.72	1.00	0.98	0.98	0.99	0.92	0.74	0.74	0.74	0.74	0.70	1.00	0.98	0.98	0.99	0.92	0.74	0.73	0.73	0.74	0.70	0.91	0.70	0.73	0.68	0.62	1.00	0.74						
	C2N5	0.77	0.69	0.59	0.74	0.67	1.00	0.99	0.99	0.99	0.96	0.65	0.64	0.64	0.64	0.63	1.00	0.99	0.99	0.99	0.96	0.65	0.64	0.64	0.64	0.63	0.69	0.66	0.55	0.71	0.55	1.00	0.65						
	C2N6	1.78	1.29	1.76	1.16	2.29	1.00	0.99	0.99	0.99	0.96	0.75	0.75	0.75	0.75	0.73	1.00	0.99	0.99	0.99	0.96	0.75	0.75	0.75	0.75	0.73	0.73	0.86	0.64	0.94	0.56	1.00	0.75						
	C2N7	0.98	1.19	1.06	1.11	0.84	1.00	1.00	1.00	1.00	0.99	0.65	0.65	0.65	0.65	0.64	1.00	1.00	1.00	1.00	0.98	0.65	0.65	0.65	0.65	0.64	0.74	0.82	0.72	0.76	0.52	1.00	0.65						
	C2N8	1.29	1.05	1.21	1.23	1.40	1.00	1.00	1.00	1.00	0.99	0.57	0.57	0.57	0.57	0.57	1.00	1.00	1.00	1.00	0.99	0.57	0.57	0.57	0.57	0.57	0.94	0.73	0.79	0.71	0.62	1.00	0.57						
	C2N9	0.72	0.77	0.69	0.79	0.61	1.00	1.00	1.00	1.00	0.99	0.72	0.72	0.72	0.72	0.72	1.00	1.00	1.00	1.00	0.99	0.72	0.72	0.72	0.72	0.72	0.72	0.77	0.69	0.79	0.61	1.00	0.72						
	C2N10	1.11	1.15	1.11	1.19	1.02	1.00	1.00	1.00	1.00	1.00	1.13	1.13	1.13	1.13	1.12	1.00	1.00	1.00	1.00	1.00	1.13	1.13	1.13	1.13	1.12	1.11	1.15	1.11	1.19	1.02	1.00	1.13						
	C2N11	0.84	0.78	0.87	0.80	0.85	1.00	1.00	0.99	1.00	0.99	0.64	0.64	0.64	0.64	0.64	1.00	1.00	0.99	1.00	0.99	0.64	0.64	0.64	0.64	0.64	0.84	0.78	0.87	0.80	0.85	1.00	0.64						

Table 5.13 (continued)

151	C3N1	0.72	0.55	0.50	0.58	0.85	0.79	0.74	0.71	0.78	0.58	0.67	0.63	0.61	0.66	0.53	0.79	0.75	0.72	0.78	0.58	0.67	0.63	0.61	0.66	0.53	0.71	0.54	0.48	0.56	0.94	1.00	0.83
	C3N2	0.72	0.57	0.55	0.58	0.79	0.98	0.92	0.90	0.93	0.70	0.70	0.66	0.65	0.67	0.53	0.98	0.92	0.90	0.93	0.69	0.70	0.66	0.64	0.67	0.53	0.72	0.56	0.54	0.58	0.85	1.00	0.71
	C3N3	0.68	0.77	0.65	0.81	0.57	1.00	0.97	0.96	0.97	0.85	0.71	0.69	0.69	0.70	0.64	1.00	0.97	0.96	0.97	0.85	0.71	0.69	0.69	0.70	0.64	0.72	0.78	0.65	0.82	0.77	1.00	0.71
	C3C4	0.88	0.68	0.68	0.67	1.11	1.00	0.98	0.98	0.99	0.93	0.69	0.68	0.69	0.69	0.66	1.00	0.98	0.98	0.99	0.93	0.69	0.68	0.68	0.68	0.66	0.83	0.65	0.67	0.63	0.85	1.00	0.69
	C3N5	0.89	0.82	0.69	0.88	1.28	1.00	0.99	0.99	0.99	0.96	0.77	0.77	0.76	0.77	0.76	1.00	0.99	0.99	0.99	0.96	0.77	0.77	0.77	0.77	0.76	0.82	0.78	0.64	0.84	1.48	1.00	0.77
	C3N6	1.83	1.20	1.76	1.07	2.58	1.00	0.99	0.99	0.99	0.97	0.66	0.65	0.65	0.65	0.64	1.00	0.99	0.99	0.99	0.97	0.66	0.65	0.65	0.65	0.64	0.66	0.78	0.55	0.86	0.65	1.00	0.66
	C3N7	1.09	1.52	1.21	1.36	0.65	1.00	0.99	1.00	1.00	0.97	0.66	0.66	0.66	0.66	0.65	1.00	0.99	0.99	1.00	0.97	0.66	0.66	0.66	0.66	0.65	0.79	0.88	0.75	0.79	0.44	1.00	0.66
	C3N8	1.21	1.01	1.13	0.95	1.54	1.00	1.00	1.00	1.00	0.99	0.58	0.58	0.58	0.58	0.58	1.00	1.00	1.00	1.00	0.99	0.58	0.58	0.58	0.58	0.58	0.92	0.69	0.76	0.71	0.75	1.00	0.58
	C3N9	0.74	0.76	0.72	0.79	0.47	1.00	1.00	1.00	1.00	0.99	0.70	0.70	0.70	0.70	0.70	1.00	1.00	1.00	1.00	0.99	0.70	0.70	0.70	0.70	0.70	0.74	0.76	0.72	0.79	0.47	1.00	0.70
	C3N10	0.62	0.70	0.60	0.73	0.46	1.00	1.00	1.00	1.00	0.99	0.68	0.68	0.68	0.68	0.68	1.00	1.00	1.00	1.00	0.99	0.68	0.68	0.68	0.68	0.68	0.62	0.70	0.60	0.73	0.46	1.00	0.68
	C3N11	1.24	1.29	1.15	1.34	1.76	1.00	1.00	1.00	1.00	1.00	1.18	1.17	1.17	1.17	1.17	1.00	1.00	1.00	1.00	1.00	1.18	1.17	1.17	1.17	1.18	1.24	1.29	1.15	1.34	1.76	1.00	1.18
	C4N1	0.72	0.56	0.50	0.58	1.32	0.79	0.75	0.72	0.78	0.83	0.67	0.64	0.62	0.66	0.87	0.79	0.75	0.72	0.78	0.83	0.67	0.64	0.62	0.66	0.88	0.71	0.54	0.48	0.57	1.49	1.00	0.84
	C4N2	0.73	0.58	0.56	0.59	1.41	0.98	0.92	0.90	0.93	0.72	0.71	0.67	0.66	0.68	0.65	0.98	0.92	0.90	0.93	0.71	0.71	0.67	0.66	0.68	0.65	0.74	0.58	0.55	0.59	1.56	1.00	0.72
	C4N3	0.68	0.77	0.65	0.81	0.95	1.00	0.97	0.96	0.97	0.86	0.70	0.69	0.69	0.69	0.65	1.00	0.97	0.96	0.97	0.86	0.70	0.69	0.69	0.69	0.65	0.72	0.78	0.64	0.82	1.32	1.00	0.71
	C4N4	0.95	0.75	0.73	0.74	1.53	1.00	0.98	0.98	0.99	0.93	0.76	0.75	0.75	0.75	0.73	1.00	0.98	0.98	0.99	0.93	0.76	0.75	0.75	0.75	0.73	0.91	0.71	0.73	0.69	1.30	1.00	0.76
	C4N5	0.88	0.82	0.69	0.88	2.31	1.00	0.99	0.99	0.99	0.97	0.77	0.77	0.76	0.77	0.78	1.00	0.99	0.99	0.99	0.97	0.77	0.77	0.77	0.77	0.79	0.82	0.78	0.64	0.84	2.72	1.00	0.77
	C4N6	1.66	1.06	1.56	0.91	2.63	1.00	0.99	0.99	0.99	0.96	0.57	0.57	0.57	0.57	0.55	1.00	0.99	0.99	0.99	0.96	0.57	0.57	0.57	0.57	0.55	0.58	0.69	0.48	0.76	0.88	1.00	0.57
	C4N7	1.14	1.54	1.20	1.37	0.48	1.00	1.00	1.00	1.00	0.98	0.64	0.64	0.63	0.64	0.62	1.00	1.00	1.00	1.00	0.98	0.64	0.63	0.63	0.64	0.62	0.77	0.85	0.72	0.76	0.53	1.00	0.64
	C4N8	1.19	0.99	1.12	0.94	1.75	1.00	1.00	1.00	1.00	1.00	0.59	0.59	0.59	0.59	0.59	1.00	1.00	1.00	1.00	0.99	0.59	0.59	0.59	0.59	0.59	0.92	0.69	0.75	0.71	0.99	1.00	0.59
	C4N9	0.85	0.88	0.83	0.91	0.45	1.00	1.00	1.00	1.00	0.99	0.80	0.80	0.80	0.80	0.79	1.00	1.00	1.00	1.00	0.99	0.80	0.80	0.80	0.80	0.79	0.85	0.88	0.83	0.91	0.45	1.00	0.80
	C4N10	0.93	1.07	0.89	1.11	0.57	1.00	1.00	1.00	1.00	1.00	1.03	1.03	1.03	1.03	1.02	1.00	1.00	1.00	1.00	1.00	1.03	1.03	1.03	1.03	1.02	0.93	1.07	0.89	1.11	0.57	1.00	1.03
	C4N11	1.00	1.05	0.93	1.08	1.65	1.00	1.00	1.00	1.00	1.00	0.97	0.97	0.96	0.97	0.97	1.00	1.00	1.00	1.00	1.00	0.97	0.97	0.97	0.97	0.97	1.00	1.05	0.93	1.08	1.65	1.00	0.97
152	C5N1	0.72	0.56	0.50	0.58	1.71	0.79	0.74	0.71	0.78	1.39	0.68	0.64	0.62	0.67	1.34	0.79	0.74	0.71	0.78	1.45	0.68	0.64	0.62	0.67	1.40	0.71	0.55	0.48	0.57	1.98	1.00	0.84
	C5N2	0.74	0.58	0.57	0.60	1.52	0.98	0.92	0.90	0.93	0.84	0.71	0.68	0.66	0.69	0.69	0.98	0.92	0.89	0.93	0.84	0.72	0.68	0.66	0.69	0.69	0.75	0.58	0.56	0.60	1.79	1.00	0.73
	C5N3	0.73	0.84	0.70	0.87	1.82	1.00	0.97	0.96	0.97	0.97	0.76	0.74	0.75	0.75	0.80	1.00	0.97	0.96	0.97	0.97	0.76	0.74	0.74	0.75	0.81	0.78	0.84	0.69	0.89	2.56	1.00	0.76
	C5N4	0.95	0.75	0.73	0.74	1.93	1.00	0.98	0.98	0.99	0.94	0.76	0.75	0.75	0.75	0.77	1.00	0.98	0.98	0.99	0.93	0.76	0.75	0.75	0.75	0.77	0.91	0.71	0.73	0.69	2.11	1.00	0.76
	C5N5	0.75	0.70	0.59	0.75	2.56	1.00	0.99	0.99	0.99	1.01	0.67	0.66	0.66	0.66	0.71	1.00	0.99	0.99	0.99	1.01	0.67	0.66	0.66	0.66	0.72	0.70	0.67	0.55	0.73	3.04	1.00	0.67
	C5N6	1.75	1.10	1.62	0.94	3.20	1.00	0.99	0.99	0.99	0.96	0.59	0.58	0.58	0.58	0.57	1.00	0.99	0.99	0.99	0.96	0.59	0.58	0.58	0.58	0.57	0.60	0.71	0.49	0.79	1.35	1.00	0.59
	C5N7	1.07	1.47	1.19	1.29	0.37	1.00	1.00	1.00	1.00	0.98	0.58	0.58	0.58	0.58	0.57	1.00	1.00	1.00	1.00	0.98	0.58	0.58	0.58	0.58	0.57	0.70	0.78	0.65	0.69	0.72	1.00	0.58
	C5N8	1.18	0.98	1.10	0.94	2.14	1.00	1.00	1.00	1.00	1.00	0.59	0.59	0.60	0.59	0.59	1.00	1.00	1.00	1.00	1.00	0.59	0.59	0.59	0.59	0.59	0.92	0.69	0.75	0.71	1.41	1.00	0.59
	C5N9	0.76	0.78	0.74	0.80	0.34	1.00	1.00	1.00	1.00	0.99	0.70	0.69	0.69	0.69	0.69	1.00	1.00	1.00	1.00	0.99	0.70	0.70	0.69	0.70	0.69	0.76	0.78	0.74	0.80	0.34	1.00	0.70
	C5N10	0.89	1.03	0.86	1.08	0.46	1.00	1.00	1.00	1.00	1.00	1.00	1.00	1.00	1.00	0.99	1.00	1.00	1.00	1.00	1.00	1.00	1.00	1.00	1.00	0.89	1.03	0.86	1.08	0.46	1.00	1.00	
	C5N11	0.81	0.84	0.75	0.86	1.58	1.00	1.00	1.00	1.00	1.00	0.78	0.78	0.78	0.78	0.78	1.00	1.00	1.00	1.00	1.00	0.78	0.78	0.78	0.78	0.79	0.81	0.84	0.75	0.86	1.58	1.00	0.78

Table 5.13 (continued)

C6N1	0.73	0.56	0.50	0.59	1.62	0.79	0.74	0.72	0.78	1.38	0.68	0.64	0.62	0.67	1.34	0.79	0.75	0.72	0.78	1.46	0.68	0.64	0.62	0.67	1.41	0.72	0.55	0.49	0.57	1.92	1.00	0.85
C6N2	0.75	0.60	0.58	0.61	1.72	0.98	0.92	0.90	0.93	0.91	0.73	0.69	0.68	0.70	0.77	0.98	0.92	0.90	0.93	0.92	0.73	0.69	0.68	0.70	0.78	0.76	0.59	0.57	0.61	2.06	1.00	0.75
C6N3	0.73	0.84	0.70	0.87	1.58	1.00	0.97	0.96	0.97	0.98	0.76	0.74	0.74	0.75	0.81	1.00	0.97	0.96	0.97	0.98	0.76	0.74	0.74	0.75	0.83	0.78	0.84	0.69	0.89	2.39	1.00	0.76
C6N4	0.87	0.68	0.67	0.68	1.82	1.00	0.98	0.98	0.99	0.96	0.70	0.69	0.69	0.69	0.69	1.00	0.98	0.98	0.99	0.97	0.70	0.69	0.69	0.69	0.70	0.83	0.66	0.67	0.64	1.86	1.00	0.70
C6N5	0.86	0.81	0.80	0.86	2.40	1.00	0.99	0.99	0.99	0.98	0.76	0.76	0.75	0.76	0.77	1.00	0.99	0.99	0.99	0.98	0.76	0.76	0.76	0.76	0.77	0.81	0.77	0.63	0.83	2.37	1.00	0.76
C6N6	1.90	1.18	1.74	1.01	4.02	1.00	0.99	0.99	0.99	0.97	0.63	0.62	0.62	0.62	0.61	1.00	0.99	0.99	0.99	0.97	0.63	0.62	0.62	0.62	0.62	0.64	0.76	0.52	0.85	2.01	1.00	0.63
C6N7	1.18	1.64	1.31	1.42	0.45	1.00	0.99	1.00	1.00	0.97	0.63	0.63	0.63	0.63	0.62	1.00	0.99	0.99	1.00	0.97	0.63	0.63	0.63	0.63	0.62	0.77	0.85	0.71	0.75	1.08	1.00	0.63
C6N8	1.33	1.10	1.24	1.06	3.01	1.00	1.00	1.00	1.00	1.00	0.67	0.67	0.68	0.67	0.68	1.00	1.00	1.00	1.00	1.00	0.67	0.67	0.68	0.67	0.68	1.04	0.78	0.84	0.80	2.19	1.00	0.67
C6N9	0.88	0.90	0.86	0.93	0.44	1.00	1.00	1.00	1.00	0.99	0.80	0.80	0.80	0.80	0.80	1.00	1.00	1.00	1.00	0.99	0.80	0.80	0.80	0.80	0.80	0.88	0.90	0.86	0.93	0.44	1.00	0.80
C6N10	0.55	0.63	0.53	0.66	0.26	1.00	1.00	1.00	1.00	0.99	0.61	0.61	0.61	0.61	0.60	1.00	1.00	1.00	1.00	0.99	0.61	0.61	0.61	0.61	0.60	0.55	0.63	0.53	0.66	0.26	1.00	0.61
C6N11	1.24	1.29	1.16	1.33	2.88	1.00	1.00	1.00	1.00	1.00	1.21	1.21	1.21	1.21	1.22	1.00	1.00	1.00	1.00	1.00	1.21	1.21	1.21	1.21	1.22	1.24	1.29	1.16	1.33	2.88	1.00	1.21
C7N1	0.72	0.56	0.50	0.58	1.54	0.79	0.75	0.72	0.78	1.42	0.67	0.64	0.61	0.66	1.38	0.79	0.75	0.72	0.78	1.50	0.67	0.64	0.62	0.66	1.46	0.71	0.54	0.48	0.57	1.82	1.00	0.84
C7N2	0.75	0.60	0.58	0.61	1.70	0.98	0.92	0.90	0.93	1.02	0.73	0.69	0.68	0.70	0.88	0.98	0.92	0.90	0.93	1.03	0.73	0.69	0.68	0.70	0.89	0.76	0.59	0.57	0.61	2.05	1.00	0.75
C7N3	0.67	0.76	0.63	0.79	1.27	1.00	0.97	0.96	0.97	0.92	0.69	0.68	0.68	0.68	0.70	1.00	0.97	0.96	0.97	0.93	0.69	0.68	0.68	0.68	0.70	0.70	0.76	0.63	0.81	1.94	1.00	0.69
C7N4	0.95	0.75	0.73	0.74	2.26	1.00	0.98	0.98	0.99	0.97	0.76	0.75	0.76	0.76	0.77	1.00	0.98	0.98	0.99	0.97	0.76	0.75	0.75	0.75	0.77	0.91	0.72	0.73	0.70	2.09	1.00	0.76
C7N5	0.82	0.71	0.70	0.75	1.67	1.00	0.99	0.99	0.99	0.98	0.67	0.66	0.66	0.66	0.67	1.00	0.99	0.99	0.99	0.98	0.67	0.66	0.66	0.66	0.67	0.70	0.68	0.55	0.73	2.10	1.00	0.67
C7N6	1.78	1.10	1.62	0.94	4.24	1.00	0.99	0.99	0.99	0.97	0.58	0.58	0.58	0.58	0.58	1.00	0.99	0.99	0.99	0.97	0.58	0.58	0.58	0.58	0.59	0.60	0.71	0.48	0.79	2.37	1.00	0.58
C7N7	1.18	1.65	1.32	1.43	0.57	1.00	1.00	1.00	1.00	0.98	0.63	0.63	0.63	0.63	0.62	1.00	1.00	1.00	1.00	0.98	0.63	0.63	0.63	0.63	0.62	0.76	0.85	0.70	0.74	1.31	1.00	0.63
C7N8	1.17	0.97	1.09	0.94	2.48	1.00	1.00	1.00	1.00	1.00	0.60	0.60	0.60	0.60	0.61	1.00	1.00	1.00	1.00	1.00	0.60	0.60	0.60	0.60	0.61	0.92	0.69	0.75	0.71	1.72	1.00	0.60
C7N9	0.93	0.95	0.91	0.99	0.61	1.00	1.00	1.00	1.00	0.99	0.85	0.85	0.85	0.85	0.84	1.00	1.00	1.00	1.00	0.99	0.85	0.85	0.85	0.85	0.84	0.93	0.95	0.91	0.99	0.61	1.00	0.85
C7N10	0.49	0.57	0.48	0.60	0.24	1.00	1.00	1.00	1.00	0.99	0.55	0.55	0.55	0.55	0.54	1.00	1.00	1.00	1.00	0.99	0.55	0.55	0.55	0.55	0.54	0.49	0.57	0.48	0.60	0.24	1.00	0.55
C7N11	0.97	1.01	0.91	1.04	2.57	1.00	1.00	1.00	1.00	1.00	0.95	0.95	0.94	0.95	0.96	1.00	1.00	1.00	1.00	1.00	0.95	0.95	0.94	0.95	0.96	0.97	1.01	0.91	1.04	2.57	1.00	0.95
C8N1	0.72	0.56	0.50	0.58	1.43	0.79	0.74	0.71	0.78	1.40	0.68	0.64	0.62	0.67	1.37	0.79	0.74	0.71	0.78	1.49	0.68	0.64	0.62	0.67	1.45	0.71	0.54	0.48	0.57	1.69	1.00	0.84
C8N2	0.72	0.57	0.56	0.58	1.52	0.98	0.92	0.90	0.93	0.99	0.69	0.66	0.65	0.67	0.84	0.98	0.92	0.90	0.93	1.00	0.69	0.66	0.64	0.67	0.85	0.72	0.56	0.55	0.58	1.88	1.00	0.71
C8N3	0.75	0.85	0.71	0.89	1.43	1.00	0.97	0.96	0.97	0.98	0.77	0.75	0.76	0.76	0.81	1.00	0.97	0.96	0.97	0.98	0.77	0.75	0.75	0.76	0.81	0.79	0.85	0.70	0.90	2.12	1.00	0.77
C8N4	0.88	0.68	0.67	0.68	2.08	1.00	0.99	0.99	0.99	0.98	0.70	0.69	0.69	0.69	0.73	1.00	0.98	0.98	0.99	0.98	0.70	0.69	0.69	0.69	0.73	0.83	0.66	0.67	0.64	2.01	1.00	0.70
C8N5	0.81	0.70	0.69	0.74	1.77	1.00	0.99	0.99	0.99	0.97	0.66	0.65	0.65	0.65	0.66	1.00	0.99	0.99	0.99	0.97	0.66	0.65	0.65	0.66	0.67	0.69	0.67	0.54	0.72	1.77	1.00	0.66
C8N6	1.72	1.06	1.55	0.90	4.13	1.00	0.99	0.99	0.99	0.97	0.56	0.55	0.55	0.55	0.58	1.00	0.99	0.99	0.99	0.97	0.56	0.55	0.55	0.55	0.58	0.57	0.68	0.46	0.76	2.33	1.00	0.56
C8N7	1.19	1.67	1.32	1.44	0.80	1.00	0.99	1.00	1.00	0.98	0.63	0.63	0.63	0.63	0.62	1.00	0.99	1.00	1.00	0.98	0.63	0.63	0.62	0.63	0.62	0.76	0.85	0.70	0.74	1.59	1.00	0.63
C8N8	1.27	1.06	1.19	1.00	2.81	1.00	1.00	1.00	1.00	1.00	0.66	0.66	0.66	0.66	0.68	1.00	1.00	1.00	1.00	0.99	0.66	0.65	0.66	0.65	0.68	1.00	0.76	0.81	0.78	1.94	1.00	0.66
C8N9	0.81	0.82	0.79	0.85	0.73	1.00	1.00	1.00	1.00	0.99	0.73	0.73	0.73	0.73	0.72	1.00	1.00	1.00	1.00	0.99	0.73	0.73	0.73	0.73	0.72	0.81	0.82	0.79	0.85	0.73	1.00	0.73
C8N10	0.54	0.62	0.52	0.65	0.28	1.00	1.00	1.00	1.00	0.99	0.60	0.60	0.60	0.60	0.59	1.00	1.00	1.00	1.00	0.99	0.60	0.60	0.60	0.60	0.59	0.54	0.62	0.52	0.65	0.28	1.00	0.60
C8N11	0.97	1.01	0.91	1.03	2.81	1.00	1.00	1.00	1.00	1.00	0.94	0.94	0.94	0.94	0.97	1.00	1.00	1.00	1.00	1.00	0.94	0.94	0.94	0.94	0.97	0.97	1.01	0.91	1.03	2.81	1.00	0.94

Table 5.13 (continued)

153	C9N1	0.72	0.55	0.50	0.58	1.28	0.79	0.74	0.71	0.78	1.24	0.67	0.63	0.61	0.66	1.22	0.79	0.75	0.72	0.78	1.35	0.67	0.63	0.61	0.66	1.30	0.71	0.54	0.48	0.56	1.53	1.00	0.83
	C9N2	0.72	0.57	0.55	0.58	1.29	0.98	0.92	0.90	0.93	0.92	0.69	0.66	0.65	0.67	0.75	0.98	0.92	0.90	0.93	0.93	0.69	0.66	0.64	0.67	0.76	0.72	0.56	0.54	0.58	1.62	1.00	0.71
	C9N3	0.68	0.77	0.64	0.81	1.16	1.00	0.97	0.96	0.97	0.91	0.70	0.69	0.69	0.69	0.69	1.00	0.97	0.96	0.97	0.90	0.70	0.69	0.69	0.69	0.69	0.72	0.77	0.64	0.82	1.76	1.00	0.70
	C9N4	0.95	0.74	0.73	0.74	1.71	1.00	0.99	0.98	0.99	0.98	0.76	0.75	0.76	0.76	0.79	1.00	0.98	0.98	0.99	0.98	0.76	0.75	0.75	0.75	0.78	0.91	0.72	0.73	0.70	1.87	1.00	0.76
	C9N5	0.81	0.70	0.69	0.74	1.39	1.00	0.99	0.99	0.99	0.96	0.66	0.65	0.65	0.66	0.65	1.00	0.99	0.99	0.99	0.96	0.66	0.66	0.65	0.66	0.66	0.69	0.67	0.54	0.72	1.41	1.00	0.66
	C9N6	1.92	1.18	1.73	0.99	4.37	1.00	0.99	0.99	0.99	0.98	0.62	0.62	0.61	0.62	0.62	1.00	0.99	0.99	0.99	0.98	0.62	0.62	0.61	0.62	0.62	0.64	0.75	0.52	0.84	2.36	1.00	0.62
	C9N7	1.09	1.54	1.22	1.32	0.94	1.00	1.00	1.00	1.00	0.98	0.57	0.57	0.57	0.57	0.58	1.00	1.00	1.00	1.00	0.98	0.57	0.57	0.57	0.57	0.58	0.70	0.77	0.64	0.68	1.68	1.00	0.57
	C9N8	1.27	1.05	1.19	1.00	2.47	1.00	1.00	1.00	1.00	0.99	0.66	0.66	0.66	0.66	0.67	1.00	1.00	1.00	1.00	0.98	0.66	0.66	0.66	0.66	0.66	1.00	0.76	0.81	0.78	1.60	1.00	0.66
	C9N9	0.77	0.78	0.75	0.81	0.76	1.00	1.00	1.00	1.00	0.99	0.69	0.69	0.69	0.69	0.69	1.00	1.00	1.00	1.00	0.99	0.69	0.69	0.69	0.69	0.69	0.77	0.78	0.75	0.81	0.76	1.00	0.69
	C9N10	0.54	0.62	0.52	0.65	0.32	1.00	1.00	1.00	1.00	0.99	0.60	0.59	0.59	0.59	0.59	1.00	1.00	1.00	1.00	0.98	0.60	0.59	0.59	0.59	0.59	0.54	0.62	0.52	0.65	0.32	1.00	0.60
	C9N11	0.69	0.71	0.65	0.73	1.32	1.00	1.00	1.00	1.00	1.01	0.67	0.67	0.67	0.67	0.69	1.00	1.00	1.00	1.00	1.01	0.67	0.67	0.67	0.67	0.69	0.69	0.71	0.65	0.73	1.32	1.00	0.67
153	C10N1	0.72	0.56	0.50	0.58	1.21	0.79	0.74	0.71	0.78	1.20	0.68	0.64	0.62	0.67	1.16	0.79	0.74	0.71	0.78	1.29	0.68	0.64	0.62	0.67	1.25	0.71	0.55	0.49	0.57	1.44	1.00	0.84
	C10N2	0.72	0.57	0.55	0.58	1.16	0.98	0.92	0.90	0.93	0.91	0.69	0.66	0.65	0.67	0.76	0.98	0.92	0.90	0.93	0.92	0.69	0.66	0.64	0.67	0.77	0.72	0.56	0.54	0.58	1.49	1.00	0.71
	C10N3	0.75	0.85	0.71	0.89	1.11	1.00	0.97	0.96	0.97	0.92	0.77	0.75	0.75	0.76	0.74	1.00	0.97	0.96	0.97	0.92	0.77	0.75	0.75	0.76	0.74	0.79	0.85	0.70	0.90	1.68	1.00	0.77
	C10N4	0.95	0.74	0.73	0.74	1.49	1.00	0.99	0.98	0.99	0.99	0.76	0.75	0.76	0.76	0.79	1.00	0.98	0.98	0.99	0.98	0.76	0.75	0.75	0.75	0.79	0.91	0.72	0.73	0.70	1.77	1.00	0.76
	C10N5	0.95	0.82	0.81	0.88	1.56	1.00	0.99	0.99	0.99	0.97	0.78	0.77	0.77	0.77	0.77	1.00	0.99	0.99	0.99	0.97	0.78	0.77	0.77	0.77	0.78	0.82	0.79	0.64	0.85	1.66	1.00	0.78
	C10N6	1.80	1.10	1.62	0.93	3.76	1.00	0.99	0.99	0.99	0.97	0.58	0.57	0.57	0.57	0.57	1.00	0.99	0.99	0.99	0.97	0.58	0.57	0.57	0.57	0.57	0.60	0.70	0.48	0.79	1.88	1.00	0.58
	C10N7	1.09	1.55	1.22	1.33	1.01	1.00	1.00	1.00	1.00	0.99	0.57	0.57	0.57	0.57	0.60	1.00	1.00	1.00	1.00	0.99	0.57	0.57	0.57	0.57	0.60	0.70	0.77	0.64	0.68	1.74	1.00	0.57
	C10N8	1.27	1.05	1.19	0.99	2.24	1.00	1.00	1.00	1.00	0.99	0.66	0.66	0.66	0.66	0.66	1.00	1.00	1.00	1.00	0.98	0.66	0.66	0.66	0.66	0.66	1.00	0.76	0.81	0.78	1.37	1.00	0.66
	C10N9	0.95	0.96	0.93	1.00	0.92	1.00	1.00	1.00	1.00	0.99	0.85	0.85	0.85	0.85	0.85	1.00	1.00	1.00	1.00	0.99	0.85	0.85	0.85	0.85	0.85	0.95	0.96	0.93	1.00	0.92	1.00	0.85
	C10N10	0.53	0.62	0.52	0.65	0.35	1.00	1.00	1.00	1.00	0.99	0.59	0.59	0.59	0.59	0.59	1.00	1.00	1.00	1.00	0.98	0.59	0.59	0.59	0.59	0.58	0.53	0.62	0.52	0.65	0.35	1.00	0.59
	C10N11	0.96	1.00	0.91	1.02	1.86	1.00	1.00	1.00	1.00	1.01	0.94	0.94	0.94	0.94	0.95	1.00	1.00	1.00	1.00	1.01	0.94	0.94	0.94	0.94	0.95	0.96	1.00	0.91	1.02	1.86	1.00	0.94

Table 5.13 (continued)

C11N1	0.72	0.56	0.50	0.58	1.16	0.79	0.74	0.71	0.78	1.16	0.68	0.64	0.62	0.67	1.13	0.79	0.74	0.72	0.78	1.24	0.68	0.64	0.62	0.67	1.24	0.71	0.54	0.48	0.57	1.38	1.00	0.84
C11N2	0.74	0.58	0.57	0.60	1.13	0.98	0.92	0.90	0.93	0.92	0.71	0.68	0.66	0.69	0.78	0.98	0.92	0.89	0.93	0.93	0.72	0.68	0.66	0.69	0.79	0.75	0.58	0.56	0.60	1.45	1.00	0.73
C11N3	0.75	0.85	0.71	0.89	1.01	1.00	0.97	0.96	0.97	0.92	0.77	0.75	0.75	0.76	0.73	1.00	0.97	0.96	0.97	0.91	0.77	0.75	0.75	0.76	0.73	0.79	0.85	0.70	0.90	1.52	1.00	0.77
C11N4	0.87	0.68	0.67	0.68	1.11	1.00	0.98	0.98	0.99	0.98	0.70	0.69	0.69	0.69	0.73	1.00	0.98	0.98	0.99	0.97	0.70	0.69	0.69	0.69	0.72	0.83	0.66	0.67	0.64	1.50	1.00	0.70
C11N5	0.94	0.81	0.80	0.86	1.45	1.00	0.99	0.99	0.99	0.96	0.76	0.76	0.76	0.76	0.76	1.00	0.99	0.99	0.99	0.96	0.77	0.76	0.76	0.76	0.76	0.81	0.77	0.63	0.83	1.76	1.00	0.77
C11N6	1.80	1.10	1.62	0.93	3.47	1.00	0.99	0.99	0.99	0.96	0.58	0.57	0.57	0.57	0.57	1.00	0.99	0.99	0.99	0.97	0.58	0.57	0.57	0.57	0.57	0.60	0.70	0.48	0.79	1.59	1.00	0.58
C11N7	1.20	1.69	1.33	1.45	1.25	1.00	1.00	1.00	1.00	0.98	0.63	0.62	0.62	0.62	0.66	1.00	1.00	1.00	1.00	0.98	0.63	0.62	0.62	0.62	0.66	0.76	0.84	0.70	0.74	2.05	1.00	0.63
C11N8	1.32	1.09	1.23	1.03	2.20	1.00	1.00	1.00	1.00	1.00	0.68	0.68	0.69	0.68	0.69	1.00	1.00	1.00	1.00	1.00	0.68	0.68	0.68	0.68	0.69	1.04	0.79	0.84	0.81	1.28	1.00	0.68
C11N9	0.95	0.97	0.93	1.00	0.91	1.00	1.00	1.00	1.00	0.99	0.85	0.85	0.85	0.85	0.85	1.00	1.00	1.00	1.00	0.99	0.85	0.85	0.85	0.85	0.85	0.95	0.97	0.93	1.00	0.91	1.00	0.85
C11N10	0.85	0.98	0.83	1.03	0.61	1.00	1.00	1.00	1.00	1.00	0.94	0.94	0.94	0.94	0.93	1.00	1.00	1.00	1.00	1.00	0.94	0.94	0.94	0.94	0.93	0.85	0.98	0.83	1.03	0.61	1.00	0.94
C11N11	0.69	0.72	0.65	0.73	1.25	1.00	1.00	1.00	1.00	1.00	0.67	0.67	0.67	0.67	0.68	1.00	1.00	1.00	1.00	1.00	0.67	0.67	0.67	0.67	0.68	0.69	0.72	0.65	0.73	1.25	1.00	0.67

CumRAE for all interpolators at each censored and noise combination level for the 2D truncated seamount. The rows are identified by C<censored level>N<noise level>. The columns are our evaluated methods identified by EM<Id> in Table 2.2 on page 55. GMT SIT (EM31) is our benchmark. A value of 1.00 (middle green) indicates equal performance to the benchmark, values greater than 1.00 (dark green) performed worse than the benchmark, and values less than 1.00 (light green), performed better than the benchmark. For each level, the minimum CumRAE is annotated in red. CumRAE allows for direct comparison between methods. Letters identify interpolator groupings: (A) localized regression + kriging, (B) localized regression + kriging + pre-splining with GMT SIT (EM31), (C) localized regression + kriging + pre-splining with MBZ SIT (EM32), (D) localized regression + pre-splining with GMT SIT (EM31), (E) localized regression + pre-splining with GMT SIT (EM31), (F) localized regression + pre-splining with MBZ SIT (EM32), and (G) SIT. In all groups except G, filters are from left to right: quadloess, loess, boxcar, hann, and kalman. Red stars indicate eventually selected feature-favoring interpolators: seamount interpolator EM06 and ridge interpolator EM18.

Table 5.14

Study 1 Test 3: Ridge Censored and Noise CumRAE Results (Results rounded to 2 decimals, but color coding is accurate.)

	Censored (C) and Noise (N) Combination Level	A					B					C					D					E					F					G	
		Krigquadloess (EM01)	Krigloess (EM02)	Krigboxcar (EM03)	Krighann (EM04)	Krigkalman (EM05)	Krig_GMTquadloess (EM06)★	Krig_GMTloess (EM07)	Krig_GMTboxcar (EM08)	Krig_GMTThann (EM09)	Krig_GMTkalman (EM10)	Krig_MBZquadloess (EM11)	Krig_MBZloess (EM12)	Krig_MBZboxcar (EM13)	Krig_MBZhann (EM14)	Krig_MBZkalman (EM15)	GMTquadloess (EM16)	GMTloess (EM17)	GMTboxcar (EM18)★	GMTThann (EM19)	GMTkalman (EM20)	MBZquadloess (EM21)	MBZloess (EM22)	MBZboxcar (EM23)	MBZhann (EM24)	MBZkalman (EM25)	quadloess (EM26)	loess (EM27)	boxcar (EM28)	hann (EM29)	kalman (EM30)	GMT SIT (EM31)	MBZ SIT (EM32)
SC1	C1N1	0.72	0.57	0.50	0.59	0.47	0.79	0.74	0.72	0.78	0.41	0.67	0.64	0.62	0.66	0.38	0.79	0.74	0.72	0.78	0.41	0.67	0.64	0.62	0.66	0.38	0.71	0.54	0.49	0.57	0.45	1.00	0.83
	C1N2	0.73	0.59	0.59	0.59	0.51	0.98	0.92	0.90	0.93	0.67	0.70	0.67	0.66	0.68	0.52	0.98	0.92	0.90	0.93	0.66	0.70	0.67	0.66	0.68	0.52	0.73	0.59	0.58	0.60	0.48	1.00	0.72
	C1N3	0.66	0.78	0.69	0.80	0.74	1.00	0.97	0.97	0.97	0.87	0.76	0.75	0.75	0.76	0.72	1.00	0.97	0.97	0.97	0.86	0.76	0.75	0.75	0.76	0.72	0.70	0.79	0.71	0.83	0.83	1.00	0.77
	C1N4	1.16	1.76	1.55	1.36	1.06	1.00	0.98	0.99	0.99	0.91	0.67	0.66	0.67	0.66	0.63	1.00	0.98	0.98	0.98	0.91	0.67	0.66	0.66	0.66	0.63	0.89	0.70	0.79	0.65	0.76	1.00	0.67
	C1N5	0.96	0.88	0.90	0.88	1.30	1.00	0.99	0.99	0.99	0.96	0.84	0.83	0.83	0.83	0.81	1.00	0.99	0.99	0.99	0.96	0.84	0.84	0.83	0.84	0.82	0.83	0.81	0.82	0.85	1.26	1.00	0.84
	C1N6	1.80	1.43	2.13	1.00	1.82	1.00	0.99	0.99	0.99	0.97	0.90	0.90	0.90	0.90	0.90	1.00	1.00	0.99	1.00	0.98	0.90	0.90	0.90	0.90	0.90	0.68	0.80	0.85	0.80	1.35	1.00	0.90
	C1N7	0.96	1.11	1.12	1.05	1.37	1.00	0.99	0.99	1.00	0.99	1.03	1.03	1.02	1.03	1.03	1.00	1.00	1.00	1.00	0.99	1.03	1.03	1.03	1.03	1.03	0.96	1.12	1.15	1.09	1.40	1.00	1.03
	C1N8	3.71	2.71	3.45	2.26	3.15	1.00	1.00	1.00	1.00	1.00	1.26	1.26	1.26	1.26	1.26	1.00	1.00	1.00	1.00	0.99	1.26	1.26	1.26	1.26	1.26	1.28	1.47	1.35	1.28	1.72	1.00	1.26
	C1N9	1.31	1.24	1.34	1.22	1.32	1.00	1.00	1.00	1.00	1.00	1.05	1.05	1.05	1.05	1.05	1.00	1.00	1.00	1.00	1.00	1.05	1.05	1.05	1.05	1.05	1.31	1.24	1.34	1.22	1.32	1.00	1.05
	C1N10	1.84	1.45	2.05	1.27	1.79	1.00	1.00	0.99	1.00	0.99	1.36	1.36	1.36	1.36	1.36	1.00	1.00	1.00	1.00	1.00	1.36	1.36	1.36	1.36	1.37	1.84	1.45	2.05	1.27	1.79	1.00	1.36
	C1N11	1.95	1.24	2.31	0.90	1.84	1.00	0.99	0.98	0.99	0.97	1.19	1.19	1.18	1.19	1.19	1.00	1.00	0.99	1.00	0.98	1.19	1.19	1.19	1.19	1.19	1.95	1.24	2.31	0.90	1.84	1.00	1.19
SC2	C2N1	0.73	0.56	0.50	0.59	0.58	0.79	0.74	0.71	0.78	0.44	0.68	0.64	0.62	0.67	0.42	0.79	0.74	0.71	0.78	0.44	0.68	0.64	0.62	0.67	0.42	0.72	0.55	0.49	0.57	0.58	1.00	0.84
	C2N2	0.72	0.57	0.56	0.58	0.47	0.98	0.92	0.90	0.93	0.67	0.69	0.66	0.65	0.67	0.51	0.98	0.92	0.90	0.93	0.66	0.70	0.66	0.65	0.67	0.50	0.72	0.57	0.55	0.59	0.46	1.00	0.71
	C2N3	0.73	0.84	0.70	0.87	0.42	1.00	0.97	0.96	0.97	0.85	0.77	0.75	0.75	0.76	0.70	1.00	0.97	0.96	0.97	0.85	0.77	0.75	0.75	0.76	0.69	0.77	0.84	0.70	0.89	0.50	1.00	0.77
	C2N4	0.99	0.79	0.74	0.77	0.95	1.00	0.98	0.98	0.99	0.92	0.75	0.74	0.74	0.74	0.71	1.00	0.98	0.98	0.99	0.91	0.75	0.74	0.74	0.74	0.71	0.90	0.71	0.73	0.69	0.61	1.00	0.75
	C2N5	0.87	0.80	0.68	0.86	0.50	1.00	0.99	0.99	0.99	0.95	0.75	0.75	0.74	0.75	0.73	1.00	0.99	0.99	0.99	0.95	0.75	0.75	0.74	0.75	0.73	0.80	0.76	0.63	0.82	0.67	1.00	0.75
	C2N6	1.85	1.18	1.71	1.02	2.29	1.00	0.99	0.99	0.99	0.95	0.63	0.62	0.62	0.62	0.61	1.00	0.99	0.99	0.99	0.96	0.63	0.62	0.62	0.62	0.61	0.62	0.73	0.53	0.80	0.41	1.00	0.63
	C2N7	1.09	1.43	1.15	1.32	0.84	1.00	1.00	1.00	1.00	0.97	0.68	0.68	0.68	0.68	0.67	1.00	1.00	1.00	1.00	0.97	0.68	0.68	0.68	0.68	0.67	0.76	0.85	0.72	0.76	0.47	1.00	0.68
	C2N8	1.18	1.00	1.11	0.94	1.15	1.00	1.00	1.00	1.00	0.99	0.60	0.60	0.60	0.60	0.60	1.00	1.00	1.00	1.00	0.99	0.60	0.60	0.60	0.60	0.60	0.92	0.70	0.75	0.70	0.61	1.00	0.60
	C2N9	0.78	0.81	0.77	0.83	0.65	1.00	1.00	1.00	1.00	0.99	0.71	0.71	0.71	0.71	0.71	1.00	1.00	1.00	1.00	0.99	0.71	0.71	0.71	0.71	0.71	0.78	0.81	0.77	0.83	0.65	1.00	0.71
	C2N10	1.05	0.98	1.10	1.02	0.88	1.00	1.00	1.00	1.00	1.00	1.01	1.01	1.01	1.01	1.00	1.00	1.00	1.00	1.00	1.00	1.01	1.01	1.01	1.01	1.00	1.05	0.98	1.10	1.02	0.88	1.00	1.01
	C2N11	1.01	1.05	0.95	1.10	1.06	1.00	1.00	1.00	1.00	1.00	0.97	0.97	0.96	0.97	0.96	1.00	1.00	1.00	1.00	1.00	0.97	0.97	0.97	0.97	0.97	1.01	1.05	0.95	1.10	1.06	1.00	0.97

Table 5.14 (continued)

156	C3N1	0.72	0.55	0.49	0.58	0.86	0.79	0.74	0.71	0.78	0.58	0.67	0.63	0.61	0.66	0.53	0.79	0.75	0.72	0.78	0.58	0.67	0.63	0.61	0.66	0.53	0.71	0.54	0.48	0.56	0.94	1.00	0.83
	C3N2	0.72	0.57	0.55	0.58	0.80	0.98	0.92	0.90	0.93	0.70	0.69	0.66	0.65	0.67	0.53	0.98	0.92	0.90	0.93	0.69	0.70	0.66	0.64	0.67	0.53	0.72	0.56	0.54	0.58	0.86	1.00	0.71
	C3N3	0.67	0.76	0.64	0.79	0.58	1.00	0.97	0.96	0.97	0.86	0.69	0.68	0.68	0.68	0.63	1.00	0.97	0.96	0.97	0.86	0.69	0.68	0.68	0.68	0.63	0.70	0.76	0.63	0.81	0.77	1.00	0.70
	C3C4	0.89	0.70	0.69	0.69	1.08	1.00	0.98	0.98	0.99	0.93	0.70	0.69	0.69	0.69	0.66	1.00	0.98	0.98	0.99	0.93	0.69	0.69	0.69	0.69	0.66	0.83	0.65	0.67	0.64	0.83	1.00	0.69
	C3N5	0.88	0.82	0.69	0.87	1.13	1.00	0.99	0.99	0.99	0.96	0.77	0.76	0.76	0.76	0.76	1.00	0.99	0.99	0.99	0.96	0.77	0.77	0.76	0.77	0.76	0.81	0.78	0.64	0.84	1.43	1.00	0.77
	C3N6	1.74	1.07	1.60	0.89	2.50	1.00	0.99	0.99	0.99	0.96	0.56	0.56	0.56	0.56	0.54	1.00	0.99	0.99	0.99	0.96	0.56	0.56	0.56	0.56	0.54	0.57	0.67	0.47	0.75	0.68	1.00	0.56
	C3N7	1.15	1.56	1.28	1.38	0.57	1.00	0.99	1.00	1.00	0.97	0.64	0.64	0.64	0.64	0.63	1.00	0.99	1.00	1.00	0.97	0.64	0.64	0.64	0.64	0.63	0.75	0.83	0.69	0.73	0.41	1.00	0.64
	C3N8	1.16	0.99	1.09	0.92	1.36	1.00	1.00	1.00	1.00	0.99	0.60	0.60	0.60	0.60	0.60	1.00	1.00	1.00	1.00	0.99	0.60	0.60	0.60	0.60	0.60	0.91	0.69	0.74	0.71	0.74	1.00	0.60
	C3N9	0.81	0.83	0.79	0.86	0.53	1.00	1.00	1.00	1.00	0.99	0.73	0.73	0.73	0.73	0.73	1.00	1.00	1.00	1.00	0.99	0.73	0.73	0.73	0.73	0.73	0.81	0.83	0.79	0.86	0.53	1.00	0.73
	C3N10	0.57	0.61	0.57	0.64	0.35	1.00	1.00	1.00	1.00	0.99	0.60	0.60	0.60	0.60	0.59	1.00	1.00	1.00	1.00	0.99	0.60	0.60	0.60	0.60	0.59	0.57	0.61	0.57	0.64	0.35	1.00	0.60
	C3N11	0.69	0.72	0.64	0.74	0.89	1.00	1.00	0.99	1.00	1.00	0.67	0.67	0.67	0.67	0.67	1.00	1.00	1.00	1.00	1.00	0.67	0.67	0.67	0.67	0.67	0.69	0.72	0.64	0.74	0.89	1.00	0.67
	C4N1	0.72	0.56	0.50	0.58	1.32	0.79	0.75	0.72	0.78	0.83	0.67	0.64	0.61	0.66	0.86	0.79	0.75	0.72	0.78	0.85	0.67	0.64	0.62	0.66	0.88	0.71	0.54	0.48	0.57	1.48	1.00	0.84
	C4N2	0.73	0.58	0.57	0.59	1.40	0.98	0.92	0.90	0.93	0.72	0.71	0.67	0.66	0.68	0.65	0.98	0.92	0.90	0.93	0.71	0.71	0.67	0.66	0.68	0.64	0.74	0.58	0.55	0.60	1.55	1.00	0.72
	C4N3	0.68	0.77	0.65	0.81	0.96	1.00	0.97	0.96	0.97	0.86	0.70	0.69	0.69	0.69	0.65	1.00	0.97	0.96	0.97	0.86	0.70	0.69	0.69	0.69	0.65	0.71	0.77	0.64	0.82	1.32	1.00	0.70
	C4N4	0.96	0.76	0.74	0.75	1.51	1.00	0.98	0.98	0.99	0.93	0.76	0.75	0.75	0.75	0.73	1.00	0.98	0.98	0.99	0.93	0.76	0.75	0.75	0.75	0.73	0.91	0.72	0.73	0.70	1.29	1.00	0.76
	C4N5	0.86	0.81	0.68	0.86	2.01	1.00	0.99	0.99	0.99	0.97	0.76	0.75	0.75	0.75	0.76	1.00	0.99	0.99	0.99	0.97	0.76	0.76	0.75	0.76	0.77	0.80	0.77	0.63	0.83	2.52	1.00	0.76
	C4N6	2.25	1.38	2.04	1.15	3.62	1.00	0.99	0.99	0.99	0.96	0.72	0.71	0.71	0.72	0.69	1.00	0.99	0.99	0.99	0.96	0.72	0.71	0.71	0.72	0.69	0.73	0.87	0.60	0.97	1.27	1.00	0.72
	C4N7	1.08	1.48	1.20	1.31	0.39	1.00	1.00	1.00	1.00	0.97	0.59	0.58	0.58	0.58	0.57	1.00	1.00	1.00	1.00	0.97	0.59	0.58	0.58	0.58	0.57	0.70	0.77	0.64	0.68	0.51	1.00	0.59
	C4N8	1.16	0.98	1.08	0.92	1.60	1.00	1.00	1.00	1.00	0.99	0.60	0.60	0.60	0.60	0.60	1.00	1.00	1.00	1.00	0.99	0.60	0.60	0.60	0.60	0.60	0.91	0.69	0.74	0.71	0.96	1.00	0.60
	C4N9	0.94	0.96	0.92	1.00	0.52	1.00	1.00	1.00	1.00	0.99	0.84	0.84	0.84	0.84	0.84	1.00	1.00	1.00	1.00	0.99	0.84	0.84	0.84	0.84	0.84	0.94	0.96	0.92	1.00	0.52	1.00	0.84
	C4N10	0.55	0.60	0.54	0.63	0.27	1.00	1.00	1.00	1.00	0.99	0.59	0.59	0.59	0.59	0.58	1.00	1.00	1.00	1.00	0.99	0.59	0.59	0.59	0.59	0.58	0.55	0.60	0.54	0.63	0.27	1.00	0.59
	C4N11	1.25	1.30	1.17	1.33	1.87	1.00	1.00	1.00	1.00	1.00	1.22	1.22	1.21	1.22	1.22	1.00	1.00	1.00	1.00	1.00	1.22	1.22	1.21	1.22	1.22	1.25	1.30	1.17	1.33	1.87	1.00	1.22
	C5N1	0.72	0.56	0.50	0.58	1.74	0.79	0.74	0.71	0.78	1.40	0.68	0.64	0.62	0.67	1.36	0.79	0.74	0.71	0.78	1.46	0.68	0.64	0.62	0.67	1.41	0.71	0.54	0.48	0.57	2.00	1.00	0.84
	C5N2	0.72	0.57	0.55	0.58	1.47	0.98	0.92	0.90	0.93	0.82	0.69	0.66	0.65	0.67	0.66	0.98	0.92	0.90	0.93	0.82	0.69	0.66	0.64	0.67	0.66	0.72	0.56	0.54	0.58	1.73	1.00	0.71
	C5N3	0.74	0.85	0.71	0.89	1.91	1.00	0.97	0.96	0.97	0.95	0.77	0.76	0.76	0.76	0.81	1.00	0.97	0.96	0.97	0.95	0.77	0.76	0.76	0.76	0.82	0.79	0.85	0.70	0.90	2.61	1.00	0.77
	C5N4	0.88	0.70	0.68	0.69	1.70	1.00	0.98	0.98	0.99	0.96	0.70	0.69	0.69	0.69	0.70	1.00	0.98	0.98	0.99	0.96	0.70	0.69	0.69	0.69	0.71	0.83	0.66	0.67	0.64	1.90	1.00	0.70
	C5N5	0.87	0.82	0.80	0.87	3.05	1.00	0.99	0.99	0.99	1.00	0.77	0.77	0.77	0.77	0.83	1.00	0.99	0.99	0.99	1.00	0.77	0.77	0.77	0.77	0.84	0.82	0.78	0.64	0.84	3.59	1.00	0.77
	C5N6	2.24	1.36	2.02	1.14	4.15	1.00	0.99	0.99	0.99	0.96	0.71	0.71	0.71	0.71	0.69	1.00	0.99	0.99	0.99	0.96	0.71	0.71	0.71	0.71	0.69	0.73	0.86	0.59	0.96	1.80	1.00	0.71
	C5N7	1.17	1.61	1.30	1.42	0.35	1.00	1.00	1.00	1.00	0.97	0.62	0.62	0.62	0.62	0.61	1.00	0.99	1.00	1.00	0.97	0.62	0.62	0.62	0.62	0.61	0.75	0.82	0.68	0.72	0.81	1.00	0.62
	C5N8	1.31	1.09	1.22	1.03	2.26	1.00	1.00	1.00	1.00	0.99	0.68	0.68	0.69	0.68	0.68	1.00	1.00	1.00	1.00	0.99	0.68	0.68	0.68	0.68	0.68	1.03	0.78	0.83	0.80	1.55	1.00	0.68
	C5N9	0.81	0.83	0.80	0.86	0.42	1.00	1.00	1.00	1.00	0.99	0.73	0.73	0.73	0.73	0.73	1.00	1.00	1.00	1.00	0.99	0.73	0.73	0.73	0.73	0.73	0.81	0.83	0.80	0.86	0.42	1.00	0.73
	C5N10	0.48	0.54	0.47	0.56	0.21	1.00	1.00	1.00	1.00	0.99	0.52	0.52	0.52	0.52	0.51	1.00	1.00	1.00	1.00	0.99	0.52	0.52	0.52	0.52	0.51	0.48	0.54	0.47	0.56	0.21	1.00	0.52
	C5N11	1.24	1.29	1.17	1.32	2.23	1.00	1.00	1.00	1.00	1.00	1.21	1.21	1.21	1.21	1.21	1.00	1.00	1.00	1.00	1.00	1.21	1.21	1.21	1.21	1.21	1.24	1.29	1.17	1.32	2.23	1.00	1.21

Table 5.14 (continued)

157	C6N1	0.73	0.56	0.50	0.59	1.64	0.79	0.74	0.71	0.78	1.41	0.68	0.64	0.62	0.67	1.37	0.79	0.74	0.72	0.78	1.48	0.68	0.64	0.62	0.67	1.44	0.72	0.55	0.49	0.57	1.94	1.00	0.85
	C6N2	0.75	0.60	0.58	0.61	1.72	0.98	0.92	0.90	0.93	0.91	0.73	0.69	0.68	0.70	0.77	0.98	0.92	0.90	0.93	0.92	0.73	0.69	0.68	0.70	0.78	0.76	0.59	0.57	0.61	2.06	1.00	0.75
	C6N3	0.73	0.83	0.70	0.87	1.63	1.00	0.97	0.96	0.97	0.98	0.76	0.74	0.74	0.75	0.82	1.00	0.97	0.96	0.97	0.99	0.76	0.74	0.74	0.75	0.83	0.77	0.84	0.69	0.89	2.46	1.00	0.76
	C6N4	0.88	0.69	0.67	0.68	1.79	1.00	0.98	0.98	0.99	0.96	0.70	0.69	0.69	0.69	0.69	1.00	0.98	0.98	0.99	0.96	0.70	0.69	0.69	0.69	0.70	0.83	0.66	0.67	0.64	1.90	1.00	0.70
	C6N5	0.74	0.70	0.69	0.74	1.84	1.00	0.99	0.99	0.99	0.98	0.66	0.65	0.65	0.65	0.66	1.00	0.99	0.99	0.99	0.98	0.66	0.65	0.65	0.66	0.66	0.69	0.67	0.54	0.72	2.00	1.00	0.66
	C6N6	1.74	1.05	1.56	0.88	3.74	1.00	0.99	0.99	0.99	0.96	0.55	0.55	0.54	0.55	0.54	1.00	0.99	0.99	0.99	0.96	0.55	0.55	0.54	0.55	0.54	0.57	0.67	0.46	0.74	1.91	1.00	0.55
	C6N7	1.10	1.55	1.22	1.33	0.39	1.00	1.00	1.00	1.00	0.97	0.58	0.58	0.58	0.58	0.57	1.00	1.00	1.00	1.00	0.97	0.58	0.58	0.58	0.58	0.57	0.70	0.77	0.64	0.67	1.03	1.00	0.58
	C6N8	1.31	1.09	1.22	1.03	2.89	1.00	1.00	1.00	1.00	1.00	0.69	0.69	0.69	0.69	0.69	1.00	1.00	1.00	1.00	1.00	0.68	0.68	0.69	0.68	0.69	1.03	0.78	0.84	0.80	2.14	1.00	0.68
	C6N9	0.89	0.91	0.88	0.95	0.54	1.00	1.00	1.00	1.00	0.99	0.80	0.80	0.80	0.80	0.80	1.00	1.00	1.00	1.00	0.99	0.80	0.80	0.80	0.80	0.79	0.89	0.91	0.88	0.95	0.54	1.00	0.80
	C6N10	0.84	0.93	0.82	0.98	0.37	1.00	1.00	1.00	1.00	1.00	0.91	0.90	0.90	0.90	0.89	1.00	1.00	1.00	1.00	0.99	0.91	0.90	0.90	0.90	0.89	0.84	0.93	0.82	0.98	0.37	1.00	0.91
	C6N11	0.70	0.73	0.66	0.74	1.51	1.00	1.00	1.00	1.00	1.00	0.68	0.68	0.68	0.68	0.69	1.00	1.00	1.00	1.00	1.00	0.68	0.68	0.68	0.68	0.69	0.70	0.73	0.66	0.74	1.51	1.00	0.68
	C7N1	0.72	0.55	0.49	0.58	1.52	0.79	0.74	0.71	0.78	1.40	0.67	0.63	0.61	0.66	1.36	0.79	0.75	0.72	0.78	1.48	0.67	0.63	0.61	0.66	1.44	0.71	0.54	0.48	0.56	1.80	1.00	0.83
	C7N2	0.74	0.58	0.57	0.60	1.69	0.98	0.92	0.90	0.93	1.00	0.71	0.68	0.66	0.69	0.87	0.98	0.92	0.89	0.93	1.01	0.72	0.68	0.66	0.69	0.87	0.75	0.58	0.56	0.60	2.03	1.00	0.73
	C7N3	0.68	0.77	0.64	0.81	1.31	1.00	0.97	0.96	0.97	0.92	0.70	0.69	0.69	0.69	0.71	1.00	0.97	0.96	0.97	0.93	0.70	0.69	0.69	0.69	0.72	0.71	0.77	0.64	0.82	2.03	1.00	0.70
	C7N4	0.96	0.75	0.73	0.75	2.32	1.00	0.98	0.98	0.99	0.97	0.76	0.76	0.76	0.76	0.77	1.00	0.98	0.98	0.99	0.97	0.76	0.75	0.76	0.76	0.77	0.91	0.72	0.74	0.70	2.17	1.00	0.76
	C7N5	0.95	0.82	0.81	0.87	1.92	1.00	0.99	0.99	0.99	0.98	0.78	0.77	0.77	0.77	0.77	1.00	0.99	0.99	0.99	0.98	0.78	0.77	0.77	0.77	0.78	0.82	0.79	0.64	0.85	2.43	1.00	0.78
	C7N6	1.84	1.11	1.64	0.93	4.48	1.00	0.99	0.99	0.99	0.97	0.58	0.57	0.57	0.57	0.58	1.00	0.99	0.99	0.99	0.97	0.58	0.57	0.57	0.58	0.58	0.60	0.70	0.48	0.79	2.53	1.00	0.58
	C7N7	1.19	1.69	1.32	1.44	0.59	1.00	0.99	1.00	1.00	0.97	0.62	0.62	0.62	0.62	0.61	1.00	0.99	1.00	1.00	0.97	0.62	0.62	0.62	0.62	0.61	0.75	0.83	0.69	0.73	1.36	1.00	0.62
	C7N8	1.16	0.96	1.08	0.91	2.36	1.00	1.00	1.00	1.00	1.00	0.61	0.61	0.61	0.61	0.61	1.00	1.00	1.00	1.00	1.00	0.61	0.61	0.61	0.61	0.61	0.91	0.70	0.74	0.71	1.67	1.00	0.61
	C7N9	0.78	0.79	0.76	0.82	0.59	1.00	1.00	1.00	1.00	0.99	0.69	0.69	0.69	0.69	0.69	1.00	1.00	1.00	1.00	0.99	0.69	0.69	0.69	0.69	0.69	0.78	0.79	0.76	0.82	0.59	1.00	0.69
	C7N10	0.66	0.74	0.65	0.78	0.32	1.00	1.00	1.00	1.00	1.00	0.72	0.72	0.72	0.72	0.71	1.00	1.00	1.00	1.00	1.00	0.72	0.72	0.72	0.72	0.71	0.66	0.74	0.65	0.78	0.32	1.00	0.72
	C7N11	1.23	1.28	1.16	1.31	3.08	1.00	1.00	1.00	1.00	1.00	1.21	1.20	1.20	1.21	1.22	1.00	1.00	1.00	1.00	1.00	1.21	1.21	1.20	1.21	1.22	1.23	1.28	1.16	1.31	3.08	1.00	1.21
	C8N1	0.73	0.56	0.50	0.59	1.43	0.79	0.74	0.72	0.78	1.41	0.68	0.64	0.62	0.67	1.38	0.79	0.74	0.72	0.78	1.51	0.68	0.64	0.62	0.67	1.47	0.72	0.55	0.49	0.57	1.71	1.00	0.85
	C8N2	0.75	0.60	0.58	0.61	1.59	0.98	0.92	0.90	0.93	1.03	0.73	0.69	0.68	0.70	0.90	0.98	0.92	0.90	0.93	1.05	0.73	0.69	0.68	0.70	0.90	0.76	0.59	0.57	0.61	1.97	1.00	0.75
	C8N3	0.75	0.85	0.71	0.89	1.37	1.00	0.97	0.96	0.97	0.97	0.77	0.75	0.75	0.76	0.80	1.00	0.97	0.96	0.97	0.97	0.77	0.75	0.75	0.76	0.80	0.79	0.85	0.70	0.90	2.07	1.00	0.77
	C8N4	0.88	0.69	0.67	0.68	2.01	1.00	0.98	0.98	0.99	0.98	0.70	0.69	0.70	0.69	0.73	1.00	0.98	0.98	0.99	0.98	0.70	0.69	0.69	0.69	0.73	0.83	0.66	0.68	0.64	1.93	1.00	0.70
	C8N5	0.81	0.70	0.69	0.74	1.48	1.00	0.99	0.99	0.99	0.97	0.66	0.65	0.65	0.66	0.66	1.00	0.99	0.99	0.99	0.97	0.66	0.66	0.65	0.66	0.67	0.69	0.67	0.54	0.72	1.77	1.00	0.66
	C8N6	2.09	1.26	1.87	1.06	4.89	1.00	0.99	0.99	0.99	0.99	0.66	0.65	0.65	0.65	0.68	1.00	0.99	0.99	0.99	0.99	0.66	0.65	0.65	0.65	0.68	0.68	0.80	0.55	0.89	2.71	1.00	0.66
	C8N7	1.09	1.56	1.22	1.33	0.81	1.00	1.00	1.00	1.00	0.98	0.57	0.57	0.57	0.57	0.57	1.00	1.00	1.00	1.00	0.98	0.57	0.57	0.57	0.57	0.57	0.69	0.76	0.63	0.67	1.54	1.00	0.57
	C8N8	1.15	0.96	1.07	0.90	2.47	1.00	1.00	1.00	1.00	1.00	0.60	0.60	0.61	0.60	0.63	1.00	1.00	1.00	1.00	1.00	0.60	0.60	0.60	0.60	0.63	0.91	0.69	0.73	0.71	1.73	1.00	0.60
	C8N9	0.90	0.92	0.88	0.95	0.87	1.00	1.00	1.00	1.00	0.99	0.80	0.80	0.80	0.80	0.80	1.00	1.00	1.00	1.00	0.99	0.80	0.80	0.80	0.80	0.80	0.90	0.92	0.88	0.95	0.87	1.00	0.80
	C8N10	0.67	0.75	0.65	0.79	0.38	1.00	1.00	1.00	1.00	1.00	0.73	0.73	0.73	0.73	0.72	1.00	1.00	1.00	1.00	1.00	0.73	0.73	0.73	0.73	0.72	0.67	0.75	0.65	0.79	0.38	1.00	0.73
	C8N11	0.83	0.86	0.78	0.88	2.31	1.00	1.00	1.00	1.00	1.01	0.81	0.81	0.81	0.81	0.83	1.00	1.00	1.00	1.00	1.01	0.81	0.81	0.81	0.81	0.83	0.83	0.86	0.78	0.88	2.31	1.00	0.81

Table 5.14 (continued)

158	C9N1	0.72	0.55	0.50	0.58	1.27	0.79	0.74	0.71	0.78	1.25	0.67	0.63	0.61	0.66	1.21	0.79	0.75	0.72	0.78	1.34	0.67	0.63	0.61	0.66	1.30	0.71	0.54	0.48	0.56	1.52	1.00	0.83
	C9N2	0.74	0.58	0.57	0.60	1.34	0.98	0.92	0.90	0.93	0.94	0.71	0.68	0.66	0.69	0.79	0.98	0.92	0.89	0.93	0.96	0.71	0.68	0.66	0.68	0.80	0.75	0.58	0.56	0.60	1.68	1.00	0.73
	C9N3	0.68	0.77	0.64	0.81	1.13	1.00	0.97	0.96	0.97	0.90	0.70	0.68	0.69	0.69	0.69	1.00	0.97	0.96	0.97	0.90	0.70	0.68	0.68	0.69	0.69	0.71	0.77	0.64	0.82	1.72	1.00	0.70
	C9N4	0.96	0.75	0.73	0.74	1.76	1.00	0.99	0.98	0.99	0.98	0.76	0.76	0.76	0.76	0.79	1.00	0.98	0.98	0.99	0.98	0.76	0.75	0.75	0.75	0.79	0.91	0.72	0.74	0.70	1.92	1.00	0.76
	C9N5	0.81	0.70	0.69	0.74	1.23	1.00	0.99	0.99	0.99	0.96	0.66	0.65	0.65	0.66	0.66	1.00	0.99	0.99	0.99	0.96	0.66	0.66	0.65	0.66	0.66	0.69	0.67	0.54	0.72	1.44	1.00	0.66
	C9N6	1.74	1.05	1.55	0.88	3.85	1.00	0.99	0.99	0.99	0.97	0.55	0.54	0.54	0.54	0.55	1.00	0.99	0.99	0.99	0.97	0.55	0.54	0.54	0.54	0.55	0.56	0.67	0.46	0.74	2.04	1.00	0.55
	C9N7	1.19	1.70	1.33	1.45	1.20	1.00	0.99	1.00	1.00	0.98	0.62	0.62	0.62	0.62	0.63	1.00	0.99	1.00	1.00	0.98	0.62	0.62	0.62	0.62	0.63	0.75	0.83	0.69	0.73	1.98	1.00	0.62
	C9N8	1.26	1.05	1.18	0.99	2.45	1.00	1.00	1.00	1.00	0.99	0.66	0.66	0.67	0.66	0.67	1.00	1.00	1.00	1.00	0.98	0.66	0.66	0.67	0.66	0.67	1.00	0.76	0.81	0.78	1.62	1.00	0.66
	C9N9	0.90	0.92	0.88	0.95	0.87	1.00	1.00	1.00	1.00	0.99	0.80	0.80	0.80	0.80	0.80	1.00	1.00	1.00	1.00	0.99	0.80	0.80	0.80	0.80	0.80	0.90	0.92	0.88	0.95	0.87	1.00	0.80
	C9N10	0.83	0.94	0.81	0.99	0.57	1.00	1.00	1.00	1.00	1.00	0.90	0.90	0.90	0.90	0.89	1.00	1.00	1.00	1.00	1.00	0.90	0.90	0.90	0.90	0.89	0.83	0.94	0.81	0.99	0.57	1.00	0.90
	C9N11	0.83	0.86	0.78	0.88	1.49	1.00	1.00	1.00	1.00	1.01	0.81	0.81	0.81	0.81	0.83	1.00	1.00	1.00	1.00	1.01	0.81	0.81	0.81	0.81	0.83	0.83	0.86	0.78	0.88	1.49	1.00	0.81
159	C10N1	0.72	0.56	0.50	0.58	1.21	0.79	0.74	0.71	0.78	1.20	0.68	0.64	0.62	0.67	1.17	0.79	0.74	0.71	0.78	1.29	0.68	0.64	0.62	0.67	1.25	0.71	0.54	0.48	0.57	1.44	1.00	0.84
	C10N2	0.72	0.57	0.55	0.58	1.17	0.98	0.92	0.90	0.93	0.91	0.69	0.66	0.64	0.67	0.76	0.98	0.92	0.90	0.93	0.92	0.69	0.66	0.64	0.67	0.77	0.72	0.56	0.54	0.58	1.48	1.00	0.71
	C10N3	0.75	0.85	0.71	0.89	1.09	1.00	0.97	0.96	0.97	0.92	0.77	0.75	0.75	0.76	0.74	1.00	0.97	0.96	0.97	0.92	0.77	0.75	0.75	0.76	0.74	0.79	0.85	0.70	0.90	1.68	1.00	0.77
	C10N4	0.89	0.69	0.67	0.68	1.36	1.00	0.99	0.99	0.99	0.98	0.70	0.69	0.70	0.70	0.72	1.00	0.98	0.98	0.99	0.97	0.70	0.69	0.69	0.69	0.72	0.83	0.66	0.68	0.64	1.59	1.00	0.70
	C10N5	0.95	0.82	0.81	0.87	1.47	1.00	0.99	0.99	0.99	0.97	0.78	0.77	0.77	0.77	0.77	1.00	0.99	0.99	0.99	0.97	0.78	0.77	0.77	0.77	0.78	0.82	0.79	0.64	0.85	1.80	1.00	0.78
	C10N6	1.83	1.10	1.64	0.93	3.72	1.00	0.99	0.99	0.99	0.96	0.58	0.57	0.57	0.57	0.57	1.00	0.99	0.99	0.99	0.97	0.58	0.57	0.57	0.57	0.57	0.60	0.70	0.48	0.78	1.81	1.00	0.58
	C10N7	1.19	1.69	1.32	1.44	1.46	1.00	1.00	1.00	1.00	0.98	0.62	0.62	0.61	0.62	0.64	1.00	0.99	1.00	1.00	0.98	0.62	0.62	0.61	0.62	0.64	0.75	0.83	0.68	0.72	2.19	1.00	0.62
	C10N8	1.26	1.05	1.18	0.99	2.21	1.00	1.00	1.00	1.00	0.99	0.66	0.67	0.67	0.66	0.67	1.00	1.00	1.00	1.00	0.98	0.66	0.66	0.67	0.66	0.67	1.00	0.76	0.81	0.78	1.38	1.00	0.66
	C10N9	0.78	0.79	0.76	0.82	0.72	1.00	1.00	1.00	1.00	0.99	0.69	0.69	0.69	0.69	0.69	1.00	1.00	1.00	1.00	0.99	0.69	0.69	0.69	0.69	0.69	0.78	0.79	0.76	0.82	0.72	1.00	0.69
	C10N10	0.68	0.77	0.66	0.81	0.51	1.00	1.00	1.00	1.00	1.00	0.74	0.74	0.74	0.74	0.73	1.00	1.00	1.00	1.00	1.00	0.74	0.74	0.74	0.74	0.73	0.68	0.77	0.66	0.81	0.51	1.00	0.74
	C10N11	0.83	0.86	0.78	0.88	1.51	1.00	1.00	1.00	1.00	1.01	0.81	0.81	0.81	0.81	0.82	1.00	1.00	1.00	1.00	1.01	0.81	0.81	0.81	0.81	0.82	0.83	0.86	0.78	0.88	1.51	1.00	0.81

Table 5.14 (continued)

C11N1	0.72	0.56	0.50	0.58	1.16	0.79	0.74	0.71	0.78	1.16	0.68	0.64	0.62	0.67	1.13	0.79	0.74	0.71	0.78	1.24	0.68	0.64	0.62	0.67	1.21	0.71	0.55	0.48	0.57	1.37	1.00	0.84
C11N2	0.72	0.57	0.55	0.58	1.10	0.98	0.92	0.90	0.93	0.91	0.69	0.66	0.64	0.67	0.76	0.98	0.92	0.90	0.93	0.91	0.69	0.66	0.64	0.67	0.77	0.72	0.56	0.54	0.58	1.41	1.00	0.71
C11N3	0.73	0.83	0.70	0.87	0.99	1.00	0.97	0.96	0.97	0.91	0.76	0.74	0.74	0.74	0.72	1.00	0.97	0.96	0.97	0.91	0.76	0.74	0.74	0.74	0.72	0.77	0.84	0.69	0.89	1.49	1.00	0.76
C11N4	0.96	0.75	0.73	0.74	1.19	1.00	0.99	0.98	0.99	0.98	0.76	0.76	0.76	0.76	0.79	1.00	0.98	0.98	0.99	0.98	0.76	0.75	0.75	0.75	0.78	0.91	0.72	0.74	0.70	1.60	1.00	0.76
C11N5	0.81	0.70	0.69	0.74	1.23	1.00	0.99	0.99	0.99	0.95	0.66	0.66	0.65	0.66	0.65	1.00	0.99	0.99	0.99	0.95	0.66	0.66	0.65	0.66	0.66	0.70	0.67	0.54	0.72	1.49	1.00	0.66
C11N6	2.09	1.26	1.86	1.05	3.93	1.00	0.99	0.99	0.99	0.97	0.66	0.65	0.65	0.65	0.65	1.00	0.99	0.99	0.99	0.98	0.66	0.65	0.65	0.65	0.65	0.68	0.80	0.55	0.89	1.76	1.00	0.65
C11N7	1.19	1.70	1.33	1.45	1.01	1.00	1.00	1.00	1.00	0.98	0.62	0.62	0.61	0.62	0.65	1.00	0.99	1.00	1.00	0.98	0.62	0.61	0.61	0.62	0.65	0.75	0.83	0.68	0.72	1.81	1.00	0.62
C11N8	1.26	1.05	1.18	0.99	2.07	1.00	1.00	1.00	1.00	0.99	0.66	0.67	0.67	0.66	0.67	1.00	1.00	1.00	1.00	0.98	0.66	0.66	0.67	0.66	0.67	1.00	0.76	0.81	0.78	1.23	1.00	0.66
C11N9	0.82	0.83	0.80	0.87	0.76	1.00	1.00	1.00	1.00	0.99	0.73	0.73	0.73	0.73	0.72	1.00	1.00	1.00	1.00	0.99	0.73	0.73	0.73	0.73	0.72	0.82	0.83	0.80	0.87	0.76	1.00	0.73
C11N10	0.47	0.53	0.46	0.56	0.38	1.00	1.00	1.00	1.00	0.99	0.51	0.51	0.51	0.51	0.50	1.00	1.00	1.00	1.00	0.99	0.51	0.51	0.51	0.51	0.50	0.47	0.53	0.46	0.56	0.38	1.00	0.51
C11N11	0.97	1.01	0.91	1.03	1.68	1.00	1.00	1.00	1.00	1.00	0.95	0.95	0.95	0.95	0.96	1.00	1.00	1.00	1.00	1.01	0.95	0.95	0.95	0.95	0.96	0.97	1.01	0.91	1.03	1.68	1.00	0.95

CumRAE for all interpolators at each censored and noise combination level for the 1D Gaussian ridge. The rows are identified by C<censored level>N<noise level>. The columns are our evaluated methods identified by EM<Id> in Table 2.2 on page 55. GMT SIT (EM31) is our benchmark. A value of 1.00 (middle green) indicates equal performance to the benchmark, values greater than 1.00 (dark green) performed worse than the benchmark, and values less than 1.00 (light green), performed better than the benchmark. For each level, the minimum CumRAE is annotated in red.

159

CumRAE allows for direct comparison between methods. Letters identify interpolator groupings: (A) localized regression + kriging, (B) localized regression + kriging + pre-splining with GMT SIT (EM31), (C) localized regression + kriging + pre-splining with MBZ SIT (EM32), (D) localized regression + pre-splining with GMT SIT (EM31), (E) localized regression + pre-splining with GMT SIT (EM31), (F) localized regression + pre-splining with MBZ SIT (EM32), and (G) SIT. In all groups except G, filters are from left to right: quadloess, loess, boxcar, hann, and kalman. Red stars indicate eventually selected feature-favoring interpolators: seamount interpolator EM06 and ridge interpolator EM18.

Table 5.15

(Reduced Table 5.13) Study 1 Test 3: Seamount Censored and Noise CumRAE Results (Results rounded to 2 decimals, but color coding is accurate.)

	Censored (C) and Noise (N) Combination Level	A					B					C					D					E					F					G	
		Krigquadloess (EM01)	Krigloess (EM02)	Krigboxcar (EM03)	Krighann (EM04)	Krigkalman (EM05)	Krig_GMTquadloess (EM06)★	Krig_GMTloess (EM07)	Krig_GMTboxcar (EM08)	Krig_GMTthann (EM09)	Krig_GMTkalman (EM10)	Krig_MBZquadloess (EM11)	Krig_MBZloess (EM12)	Krig_MBZboxcar (EM13)	Krig_MBZthann (EM14)	Krig_MBZkalman (EM15)	GMTquadloess (EM16)	GMTloess (EM17)	GMTboxcar (EM18)★	GMTthann (EM19)	GMTkalman (EM20)	MBZquadloess (EM21)	MBZloess (EM22)	MBZboxcar (EM23)	MBZthann (EM24)	MBZkalman (EM25)	quadloess (EM26)	loess (EM27)	boxcar (EM28)	hann (EM29)	kalman (EM30)	GMT SIT (EM31)	MBZ SIT (EM32)
091	C1N1	0.73	0.57	0.52	0.58	0.50	0.79	0.75	0.72	0.78	0.43	0.67	0.64	0.62	0.66	0.40	0.79	0.75	0.72	0.78	0.43	0.67	0.64	0.62	0.66	0.40	0.71	0.55	0.50	0.57	0.48	1.00	0.83
	C2N1	0.72	0.55	0.50	0.58	0.56	0.79	0.74	0.72	0.78	0.45	0.67	0.63	0.61	0.66	0.41	0.79	0.75	0.72	0.78	0.45	0.67	0.63	0.61	0.66	0.41	0.71	0.54	0.48	0.56	0.57	1.00	0.83
	C3N1	0.72	0.55	0.50	0.58	0.85	0.79	0.74	0.71	0.78	0.58	0.67	0.63	0.61	0.66	0.53	0.79	0.75	0.72	0.78	0.58	0.67	0.63	0.61	0.66	0.53	0.71	0.54	0.48	0.56	0.94	1.00	0.83
	C4N1	0.72	0.56	0.50	0.58	1.32	0.79	0.75	0.72	0.78	0.83	0.67	0.64	0.62	0.66	0.87	0.79	0.75	0.72	0.78	0.83	0.67	0.64	0.62	0.66	0.88	0.71	0.54	0.48	0.57	1.49	1.00	0.84
	C5N1	0.72	0.56	0.50	0.58	1.71	0.79	0.74	0.71	0.78	1.39	0.68	0.64	0.62	0.67	1.34	0.79	0.74	0.71	0.78	1.45	0.68	0.64	0.62	0.67	1.40	0.71	0.55	0.48	0.57	1.98	1.00	0.84
	C6N1	0.73	0.56	0.50	0.59	1.62	0.79	0.74	0.72	0.78	1.38	0.68	0.64	0.62	0.67	1.34	0.79	0.75	0.72	0.78	1.46	0.68	0.64	0.62	0.67	1.41	0.72	0.55	0.49	0.57	1.92	1.00	0.85
	C7N1	0.72	0.56	0.50	0.58	1.54	0.79	0.75	0.72	0.78	1.42	0.67	0.64	0.61	0.66	1.38	0.79	0.75	0.72	0.78	1.50	0.67	0.64	0.62	0.66	1.46	0.71	0.54	0.48	0.57	1.82	1.00	0.84
	C8N1	0.72	0.56	0.50	0.58	1.43	0.79	0.74	0.71	0.78	1.40	0.68	0.64	0.62	0.67	1.37	0.79	0.74	0.71	0.78	1.49	0.68	0.64	0.62	0.67	1.45	0.71	0.54	0.48	0.57	1.69	1.00	0.84
	C9N1	0.72	0.55	0.50	0.58	1.28	0.79	0.74	0.71	0.78	1.26	0.67	0.63	0.61	0.66	1.22	0.79	0.75	0.72	0.78	1.35	0.67	0.63	0.61	0.66	1.30	0.71	0.54	0.48	0.56	1.53	1.00	0.83
	C10N1	0.72	0.56	0.50	0.58	1.21	0.79	0.74	0.71	0.78	1.20	0.68	0.64	0.62	0.67	1.16	0.79	0.74	0.71	0.78	1.29	0.68	0.64	0.62	0.67	1.25	0.71	0.55	0.49	0.57	1.44	1.00	0.84
	C11N1	0.72	0.56	0.50	0.58	1.16	0.79	0.74	0.71	0.78	1.16	0.68	0.64	0.62	0.67	1.13	0.79	0.74	0.72	0.78	1.24	0.68	0.64	0.62	0.67	1.21	0.71	0.54	0.48	0.57	1.38	1.00	0.84

CumRAE for all interpolators at each censored and noise combination level for the 1D Gaussian ridge. The rows are identified by C<censored level>N<noise level>. The columns are our evaluated methods identified by EM<Id> in Table 2.2 on page 55. GMT SIT (EM31) is our benchmark. A value of 1.00 (middle green) indicates equal performance to the benchmark, values greater than 1.00 (dark green) performed worse than the benchmark, and values less than 1.00 (light green), performed better than the benchmark. For each level, the minimum CumRAE is annotated in red.

CumRAE allows for direct comparison between methods. Letters identify interpolator groupings: (A) localized regression + kriging, (B) localized regression + kriging + pre-splining with GMT SIT (EM31), (C) localized regression + kriging + pre-splining with MBZ SIT (EM32), (D) localized regression + pre-splining with GMT SIT (EM31), (E) localized regression + pre-splining with GMT SIT (EM31), (F) localized regression + pre-splining with MBZ SIT (EM32), and (G) SIT. In all groups except G, filters are from left to right: quadloess, loess, boxcar, hann, and kalman. Red stars indicate eventually selected feature-favoring interpolators: seamount interpolator EM06 and ridge interpolator EM18.

Table 5.16

(Reduced Table 5.14) Study 1 Test 3: Ridge Censored and Noise CumRAE Results (Results rounded to 2 decimals, but color coding is accurate.)

191	A					B					C					D					E					F					G	
	Censored (C) and Noise (N) Combination Level																															
	Krigquadloess (EM01)																															
	Krigloess (EM02)																															
	Krigboxcar (EM03)																															
	Krighann (EM04)																															
	Krigkalman (EM05)																															
	Krig_GMTquadloess (EM06)★																															
	Krig_GMTloess (EM07)																															
	Krig_GMTboxcar (EM08)																															
	Krig_GMTThann (EM09)																															
	Krig_GMTkalman (EM10)																															
	Krig_MBZquadloess (EM11)																															
	Krig_MBZloess (EM12)																															
Krig_MBZboxcar (EM13)																																
Krig_MBZhann (EM14)																																
Krig_MBZkalman (EM15)																																
GMTquadloess (EM16)																																
GMTloess (EM17)																																
GMTboxcar (EM18)★																																
GMTThann (EM19)																																
GMTkalman (EM20)																																
MBZquadloess (EM21)																																
MBZloess (EM22)																																
MBZboxcar (EM23)																																
MBZhann (EM24)																																
MBZkalman (EM25)																																
quadloess (EM26)																																
loess (EM27)																																
boxcar (EM28)																																
hann (EM29)																																
kalman (EM30)																																
GMT SIT (EM31)																																
MBZ SIT (EM32)																																

CumRAE for all interpolators at each censored and noise combination level for the 1D Gaussian ridge. The rows are identified by C<censored level>N<noise level>. The columns are our evaluated methods identified by EM<Id> in Table 2.2 on page 55. GMT SIT (EM31) is our benchmark. A value of 1.00 (middle green) indicates equal performance to the benchmark, values greater than 1.00 (dark green) performed worse than the benchmark, and values less than 1.00 (light green), performed better than the benchmark. For each level, the minimum CumRAE is annotated in red.

CumRAE allows for direct comparison between methods. Letters identify interpolator groupings: (A) localized regression + kriging, (B) localized regression + kriging + pre-splining with GMT SIT (EM31), (C) localized regression + kriging + pre-splining with MBZ SIT (EM32), (D) localized regression + pre-splining with GMT SIT (EM31), (E) localized regression + pre-splining with GMT SIT (EM31), (F) localized regression + pre-splining with MBZ SIT (EM32), and (G) SIT. In all groups except G, filters are from left to right: quadloess, loess, boxcar, hann, and kalman. Red stars indicate eventually selected feature-favoring interpolators: seamount interpolator EM06 and ridge interpolator EM18.

5.2.4 Identifying Feature-Favoring Interpolators

From these results, we consider which interpolators to select as our feature-favoring seamount and ridge interpolator.⁵⁵ First, we look at identifying the feature-favoring interpolators under noise (first study Test 2), as these are straightforward.

For the seamount and ridge noise UEs (first study Test 2), all interpolators except the benchmark GMT SIT (EM31) and MBZ SIT (EM32) are feature-favoring. Both the GMT SIT (EM31) and MBZ SIT (EM32) techniques are then, decidedly not feature-favoring under noise. Although these SIT techniques had practically 0 m errors when modeling on the truth data (as previously noted in section 2.2), accuracy quickly degraded as noise increased, incurring much larger inaccuracies than the rest, making the SIT techniques the least accurate. Additionally, all the Kalman methods (EM05, EM10, EM15, EM20, EM25, and EM30), while feature-favoring, seemed to suffer under increased noise, having accuracy that was inconsistently better than the SIT methods. Thus, the same feature-favoring interpolators were identified for both the seamount and ridge primitive under noise.

Upon inspection of depths and errors, we found that all interpolators incurred unacceptably large errors near or exceeding the amplitude of the primitives (1,200 m) at noise levels 2-11 for both the seamount and ridge primitive, and at noise level 1, that both GMT SIT (EM31) and MBZ SIT (EM32) incurred unacceptably large errors greater than 50% of the amplitude. The seamount and ridge UEs of varying noise (first study Test 2)

⁵⁵ It may be fair to state that we did not so much identify feature favoring interpolators, but rather feature un-favoring.

identified all interpolators except GMT SIT (EM31) and MBZ SIT (EM32) as feature-favoring in the presence of acceptable noise (noise level 1), as defined in these experiments according to IHO hydrographic standards. Although GMT SIT (EM31) and MBZ SIT (EM32) had the lowest errors (practically 0 m) when modeling on the truth grid (no perturbations), the remaining interpolators had errors that were not much larger, practically. The advantages of selecting a feature-favoring interpolator to avoid large errors in the presence of acceptable noise (level 1) outweighs the smaller and manageable increase of errors in the unlikely scenario of no noise.

The high accuracy of the SIT techniques was maintained under censoring for both seamount and ridge UEs (first study Test 1), as there was no additive noise. While some interpolators showed improved accuracy over the SIT techniques at high censored levels, upon inspection of the depth and error surfaces, we found that at these high censored levels, the data were too sparse to model accurately. We also found that at the low censored levels, all interpolators had errors that were not much larger than GMT SIT (EM31), practically, with those utilizing GMT SIT (group B and D) the closest, and as sparsity increased, all the GMT SIT methods (groups B and D along with GMT SIT [EM31]) had nearby accuracy that degraded slower than the remaining interpolators for both the seamount and ridge. Thus, the seamount and ridge UEs of varying sparsity (first study Test 1) identified all interpolators including the benchmark GMT SIT (EM31) as feature-favoring for both the seamount and ridge primitive.

To select the feature-favoring seamount and ridge interpolator, we summarize our findings:

- Seamount and ridge censored UEs found all interpolators feature-favoring.

- Seamount and ridge noise UEs found all interpolators except GMT SIT (EM31) and MBZ SIT (EM32) feature-favoring and found it advantageous to be feature-favoring under noise. Localized regression was beneficial.

Thus, neither GMT SIT (EM31) or MBZ SIT (EM32) are selected as the favoring seamount or ridge interpolator.

The feature-favoring interpolators identified for the seamount and ridge primitives are the same, but their interpretations (DBMs) will provide different information. Since the UEs found the GMT SIT methods (groups B and D along with GMT SIT [EM31]) to be particularly favoring for both seamount and ridge, we will select two different feature-favoring GMT SIT methods, excluding our benchmark GMT SIT (EM31), striving to uphold heterogeneity recommendations for ensemble members.

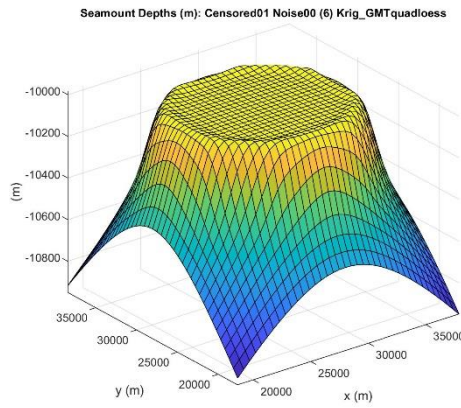
From inspecting the depths and errors, the GMT SIT methods (groups B and D along with GMT SIT [EM31]) appear to allow the truncated seamount to maintain its form and accuracy much better than any of the other feature-favoring methods and to a higher censored level, than for the ridge. Those utilizing the quadloess window were of the more accurate and smoother windows, while boxcar was of the less accurate and smooth. Due to the extra favoritism of the GMT SIT methods on the truncated seamount, we selected one of the more accurate and complex interpolators of the GMT methods to be our feature-favoring seamount interpolator, Krig_GMTquadloess (EM06).

To exemplify the power of ensembles and obtain heterogenous ensemble members, we select GMTboxcar (EM18) as our feature-favoring ridge interpolator. Unlike our seamount interpolator, our ridge interpolator does not employ kriging and utilizes the simplest weighting window available, the boxcar, instead of the most complex

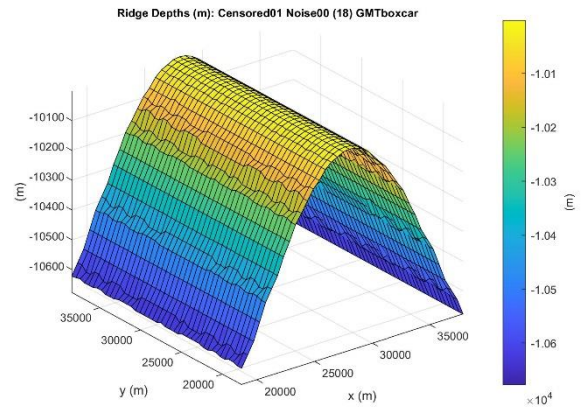
quadloess window. The ridge interpolator selected is less feature-favoring and accurate than the seamount interpolator selected but will allow us to investigate the efficacy and robustness of constructing DBMs from nominal data.

We selected Krig_GMTquadloess (EM06) as our feature-favoring seamount interpolator and GMTboxcar (EM18) as our feature-favoring ridge interpolator. These interpolators will be used in the REs in our second study to investigate the efficacy of utilizing nominal data to create DBMs. Each feature-favoring interpolator creates a feature-favoring DBM; both selected interpolator and DBM are informed by nominal data. The nominal data provided by classifiers guide the selection of interpolators towards those which tend to favor identified feature forms. Feature-favoring interpolators are not mutually exclusive as the sets of interpolators favoring different feature forms may overlap or coincide. This non-exclusivity was demonstrated in the UEs of the first study where the feature-favoring interpolators for the seamount and ridge primitive were the same; these interpolators did well on both.

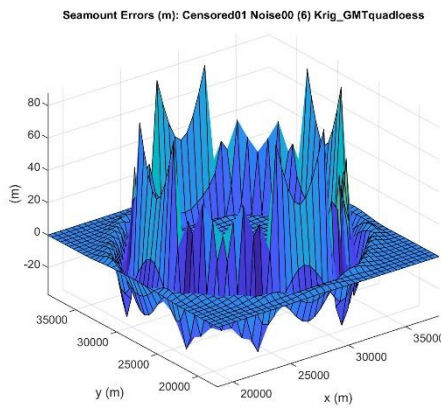
Figure 5.6, Figure 5.7, and Figure 5.8 are examples of feature-favoring DBMs produced by the selected feature-favoring seamount (Krig_GMTquadloess [EM06]) and ridge (GMTboxcar [EM18]) interpolator on their respective primitive. Figure 5.6 applies the interpolators at censored level 1 (from first study Test 1) and Figure 5.7 applies the interpolators at noise level 1 (from first study Test 2). Figure 5.8 applies the interpolators at censored level 1 and noise level 1 (from first study Test 3). Each figure shows the (a) depths and (c) errors from the seamount DBM produced by the seamount interpolator and the (b) depths and (d) errors from the ridge DBM produced by the ridge interpolator. The interpolators, in general, were more robust for sparse data than for noisy data.



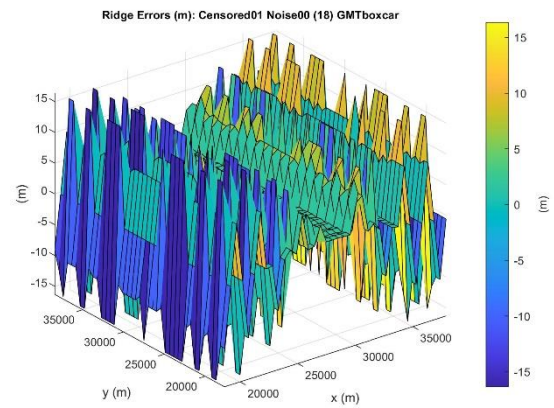
(a)



(b)



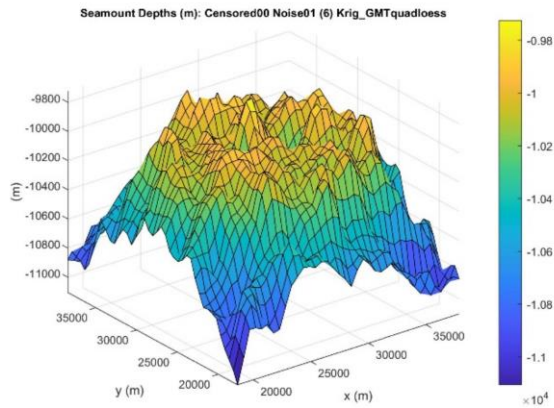
(c)



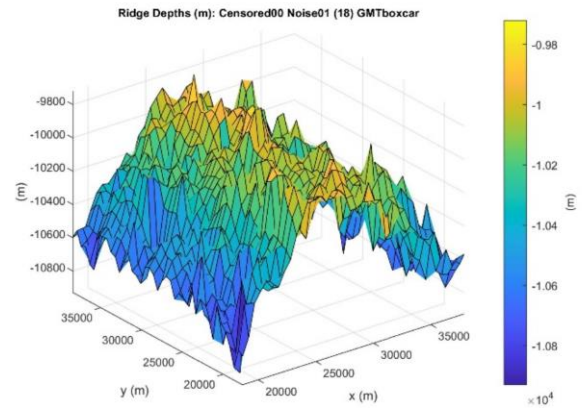
(d)

Figure 5.6 Study 1 Test 1: Example of feature-favoring DBMs at censored level 1.

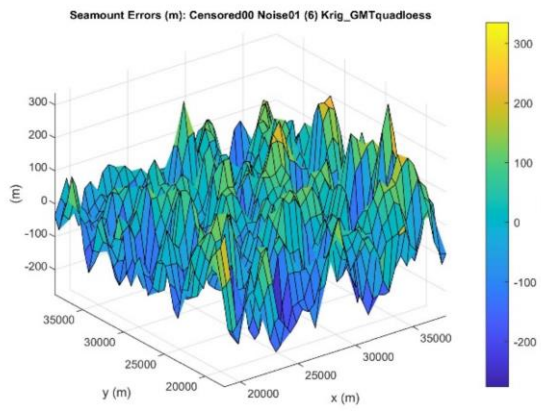
At censored level 1, the selected feature-favoring seamount interpolator Krig_GMTquadloess (EM06) on the seamount primitive produced a seamount DBM showed by (a) depths (m) and (c) errors (m), and the feature-favoring ridge interpolator GMTboxcar (EM18) on the ridge primitive produced a ridge DBM showed by (b) depths (m) and (d) errors (m).



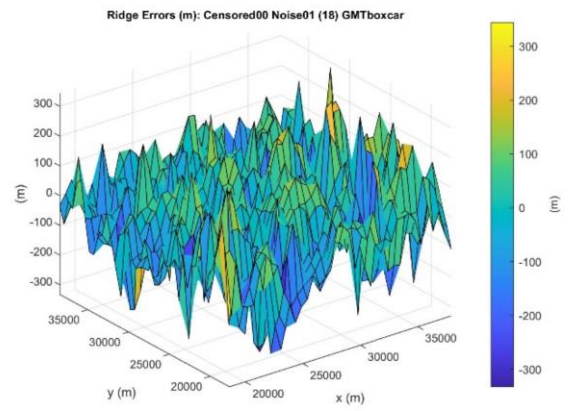
(a)



(b)



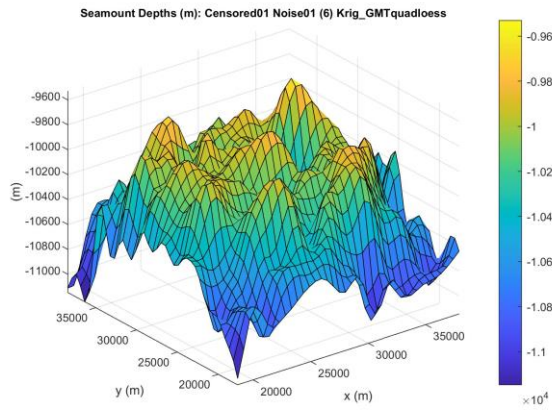
(c)



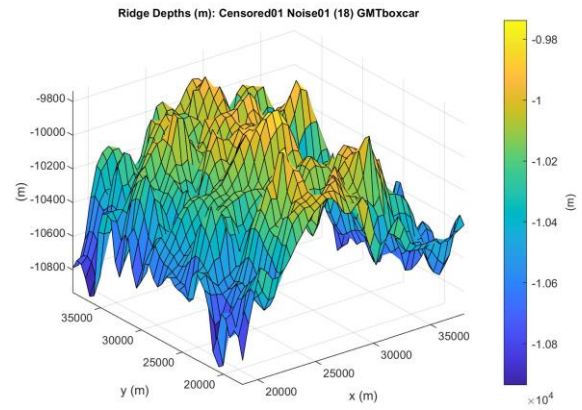
(d)

Figure 5.7 Study 1 Test 2: Example of feature-favoring DBMs at noise level 1.

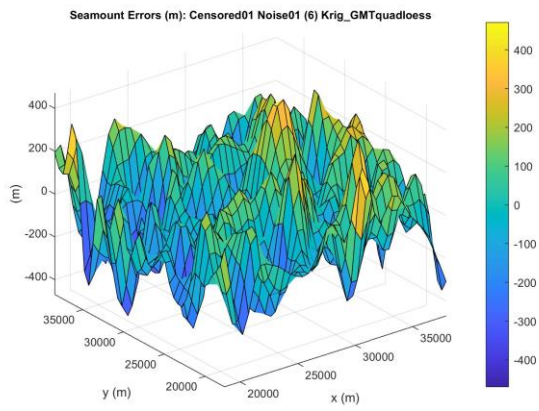
At noise level 1 (acceptable noise according to IHO standards), the selected feature-favoring seamount interpolator Krig_GMTquadloess (EM06) on the seamount primitive produced a seamount DBM showed by (a) depths (m) and (c) errors (m), and the feature-favoring ridge interpolator EM18 GMTboxcar (EM18) on the ridge primitive produced a ridge DBM showed by (b) depths (m) and (d) errors (m).



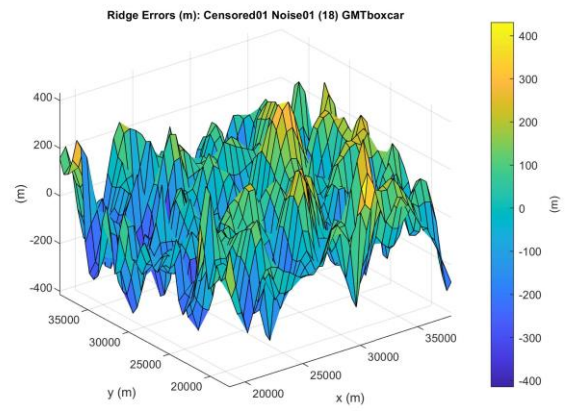
(a)



(b)



(c)



(d)

Figure 5.8 Study 1 Test 3: Example of feature-favoring DBMs at censored level 1 and noise level 1.

At censored level 1 and noise level 1, the selected feature-favoring seamount interpolator Krig_GMTquadloess (EM06) on the seamount primitive produced a seamount DBM showed by (a) depths (m) and (c) errors (m), and the feature-favoring ridge interpolator GMTboxcar (EM18) on the ridge primitive produced a ridge DBM showed by (b) depths (m) and (d) errors (m).

CHAPTER VI – SECOND STUDY: EVALUATING ENSEMBLES

In this chapter, we evaluate ensembles as DBM construction contenders.

Ensemble forecasting is appropriate where there exists either data and/or modeling errors.

In our case, each interpolant serves as a separate model. Assuming well-behaved probability density functions, we can expect ensembles to provide more accurate results on average. The prevalence of interpolation models used by the bathymetric modeling community places a thorough investigation of their interactions beyond the reach of one dissertation. Nonetheless, we have tested a complete two-model ensemble combination using the feature-favoring interpolators selected in the previous chapter (Chapter V).

The randomized swath removal experiment used for our second study is my progression of the controlled deterministic sparse data studies proposed by Paul Elmore towards more general randomized studies (Montgomery, 2017). To setup the second study (REs), we adapted our censoring technique to model real world errors by including random swath removal data gaps (with random widths), random density across our grid, and random noise. We generated two separate test sets with 100 independent instantiations each. In our first test set (Test 3a), we retained all generated instances. In our second test set (Test 3b), which is labeled sparse, we retained an instance only if a right-tail sign test determines the set of Euclidean distances between nearest neighbors has a median distance (data gap) that is statistically larger than 1,852 m at the 5% significance level (see section 6.2). This adaptation allows our censoring to be different enough from that of the first study to allow us to test if the first study results generalize.

Each ensemble constructed has two ensemble members, which are different interpretations of the sea floor obtained by reconstructing the surfaces with a given interpolation scheme.

To test the ensembles, we constructed data sets that mimic realistic data collection scenarios. These data sets were of random size up to 2601 scattered sampling points, ranging from 15,000 - 41,000 m in both the x and y directions. At these locations, we computed values from our hybrid model. The hybrid utilized a 2D truncated seamount with a weight of 0.75 and a 1D Gaussian ridge with a weight of 0.25. We modified the resulting data set through a combination of additive random Gaussian noise with 0 mean and standard deviation of 300 m, and random swath location and width removal. This noise represents signal corruption and measurement errors commonly in bathymetric data.

Table 6.1 is a list of selected methods identified by SM<Id> utilized in the REs to evaluate efficacy of *w*-ELS/ELS. DBMs were created for the interpolators listed in Table 6.1.

In this chapter, we describe work performed, in part, with Paul Elmore and A. Louise Perkins. My specific contributions are:

- I devised and implemented a replicated randomized study with randomized swath removal, density, and noise. Originally, Paul Elmore suggested an un-replicated controlled experiment with determined swath removal, density, and noise levels.
- I developed and implemented a right-tail sign test with Delaunay triangulation to obtain a set of sparse configurations.

- I utilized Friedman's test and performed multiple comparisons with Tukey's HSD test, correcting experiment-wise error with $\alpha = 0.05$, to make inferences on the general population of experimental configurations with 95% confidence.

Table 6.1

Selected Methods (SM) Utilized in our Second Study (REs).

SM	Abbreviation	Description
1	Krig_GMTquadloess (EM06)	Selected as feature-favoring seamount interpolator produces $DBM_{(S)}$.
2	GMTboxcar (EM18)	Selected as feature-favoring ridge interpolator produces $DBM_{(R)}$.
3	GMT SIT (EM31)	Selected as benchmark interpolator produces $DBM_{(B)}$.
Additional Methods		
Ensembles		
4	Mean (EM33)	Un-informed ensemble: equally weights $(0.5)DBM_{(S)} + (0.5)DBM_{(R)}$ to produce $DBM_{(E)}$. $DBM_{(E)} \sim (0.5)DBM_{(S)} + (0.5)DBM_{(R)}$
5	w-ELS (Planar Model) (EM34)	Informed ensemble: differentially weights $(w)DBM_{(S)} + (1-w)DBM_{(R)}$ to produce $DBM_{(E)}$. Uses planar model to obtain w . $DBM_{(E)} \sim \text{Planar Model}$; extracts w
6	w-ELS (Custom Model) (EM35)	Informed ensemble: differentially weights $(w)DBM_{(S)} + (1-w)DBM_{(R)}$ to produce $DBM_{(E)}$. Uses custom model to obtain w . $DBM_{(E)} \sim \text{Custom Model}$; extracts w
7	ELS (Planar Model) (EM36)	Informed ensemble: uses regression fit from EM33 to obtain $DBM_{(E)}$. $DBM_{(E)} \sim \text{Planar Model}$; uses fit
8	ELS (Custom Model) (EM37)	Informed ensemble: uses regression fit from EM34 to obtain $DBM_{(E)}$. $DBM_{(E)} \sim \text{Custom Model}$; uses fit
Non-Ensembles		
9	OLS (Planar Model) (EM38)	Performs OLS fitting planar model on input data to estimate surface. Input \sim Planar Model
10	OLS (Custom Model) (EM39)	Performs OLS fitting custom model on input data to estimate surface. Input \sim Custom Model
11	OLS on $DBM_{(S)}$ (Seamount Model) (EM40)	Performs OLS fitting seamount primitive on $DBM_{(S)}$ from seamount favoring interpolator (EM06) to estimate surface. $DBM_{(S)} \sim \text{Seamount Model}$
12	OLS on $DBM_{(R)}$ (Ridge Model) (EM41)	Performs OLS fitting ridge primitive on $DBM_{(R)}$ from ridge favoring interpolator (EM18) to estimate surface. $DBM_{(R)} \sim \text{Ridge Model}$
13	OLS on $DBM_{(S)}$ (Custom Model) (EM42)	Performs OLS fitting seamount primitive on $DBM_{(S)}$ from seamount favoring interpolator (EM06) to estimate surface. $DBM_{(S)} \sim \text{Custom Model}$
14	OLS on $DBM_{(R)}$ (Custom Model) (EM43)	Performs OLS fitting ridge primitive on $DBM_{(R)}$ from ridge favoring interpolator (EM18) to estimate surface. $DBM_{(R)} \sim \text{Custom Model}$
15	ELS (Seamount Model) (EM44)	Performs ELS using seamount primitive informed by the machine learners to estimate ensemble surface. $DBM_{(E)} \sim \text{Seamount Model}$; uses fit
16	ELS (Ridge Model) (EM45)	Performs ELS using ridge primitive informed by the machine learners to estimate ensemble surface. $DBM_{(E)} \sim \text{Ridge Model}$; uses fit
17	OLS on $DBM_{(B)}$ (Custom Model) (EM46)	Performs OLS fitting custom model on benchmark GMT SIT DBM to estimate surface. $DBM_{(B)} \sim \text{Custom Model}$

Interpolators from Table 2.2 and Table 3.1 utilizing the selected feature-favoring interpolators from the first study (UEs). Selected methods are identified by SM<Id>.

In section 6.1, we present the data (section 6.1.1) and results (section 6.1.2) for our second study (REs) with Test 3a random configurations. In section 6.2, we present the data (section 6.2.1) and results (section 6.2.2) for our second study (REs) with Test 3b sparse configurations.

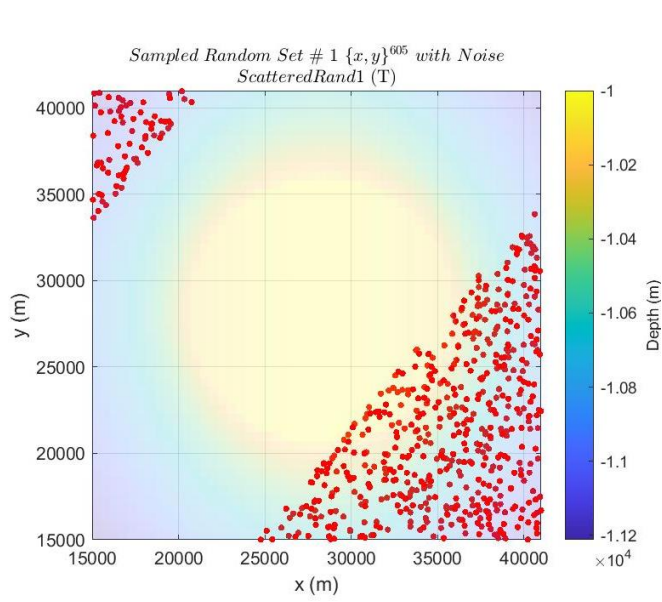
Both results tables show CumRAE for all interpolators at their 100 generated configurations on the hybrid morphology. The columns are our selected methods identified by SM<Id> in Table 3.1 on page 100. From our first study (UEs), we selected Krig_GMTquadloess (SM01) as our seamount interpolator and GMTboxcar (SM02) as our ridge interpolator. GMT SIT (EM31) is our benchmark. (see, section 5.2 or table captions for color coding details).

In section 6.3, we present the Friedman's investigations in our second study (REs) performed on both Test 3a and 3b configurations for side-by-side comparison.

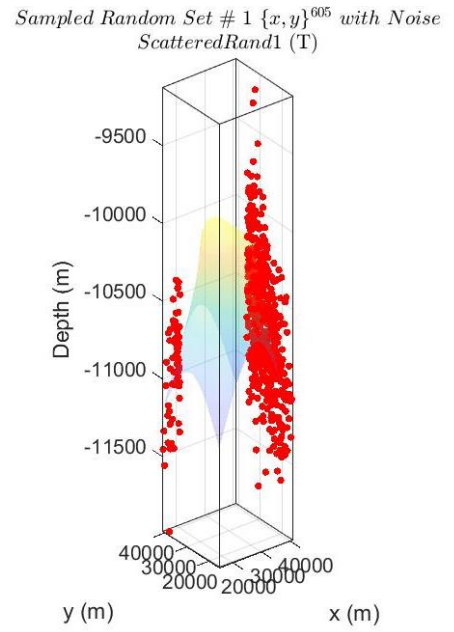
6.1 Study 2 (REs) Test 3a: Random Configurations

The data sets in the second study (RE) Test 3a configurations are randomly censored and have random noise added. Figure 6.1 shows the first five dense and sparse configurations generated and sparsity details are shown in Table 6.2. CumRAE results are shown in Table 6.3 (see table captions or Chapter VI introductory section for table description).

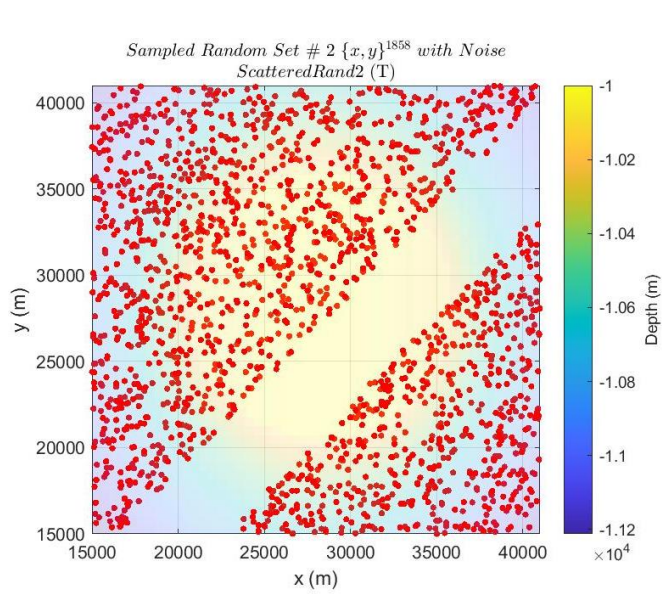
6.1.1 Data



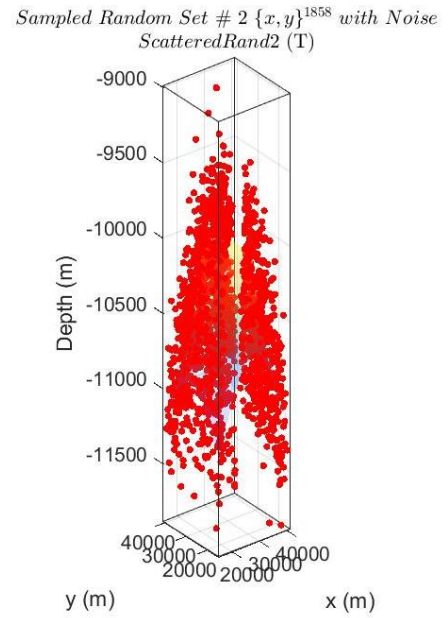
(a)



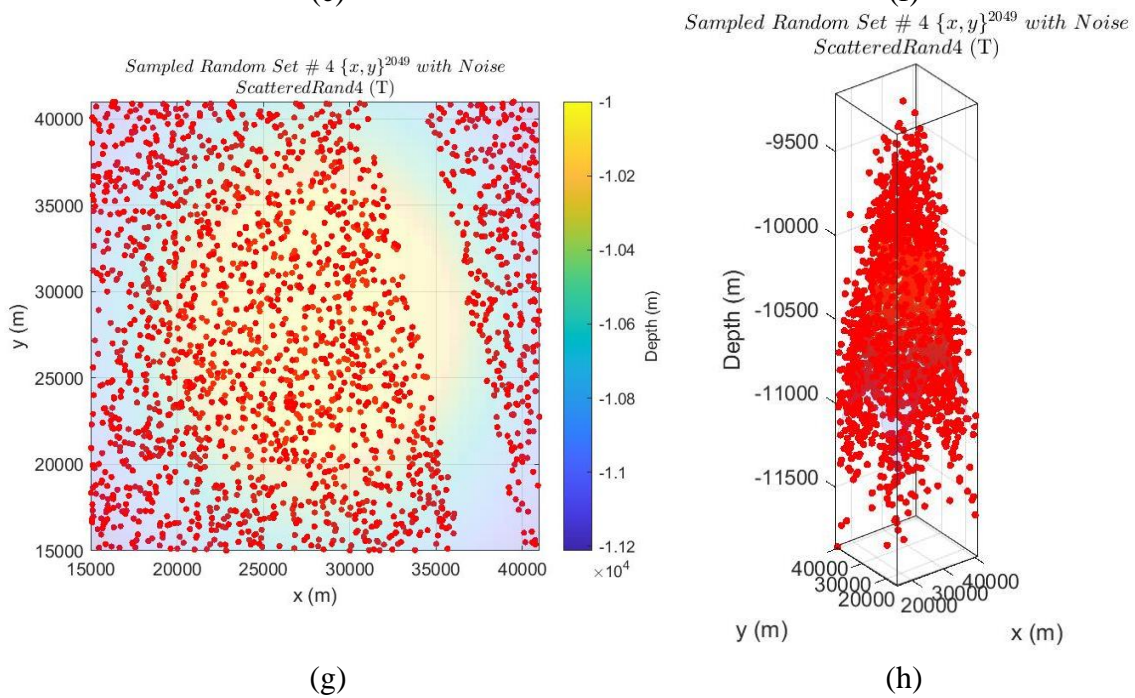
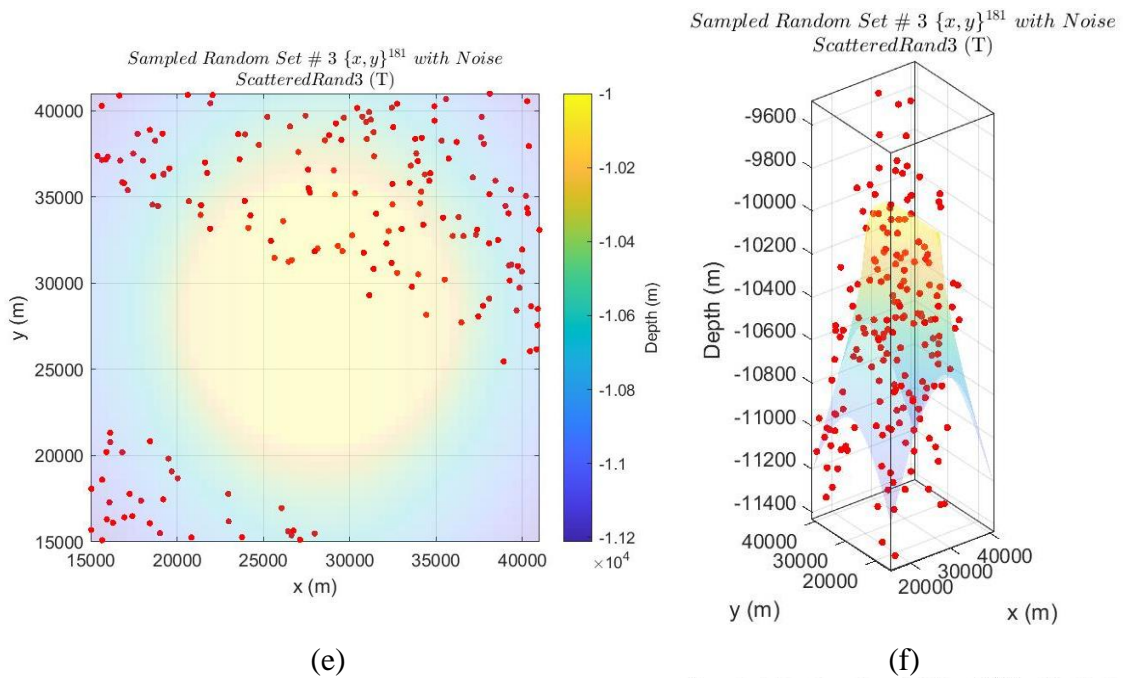
(b)



(c)



(d)



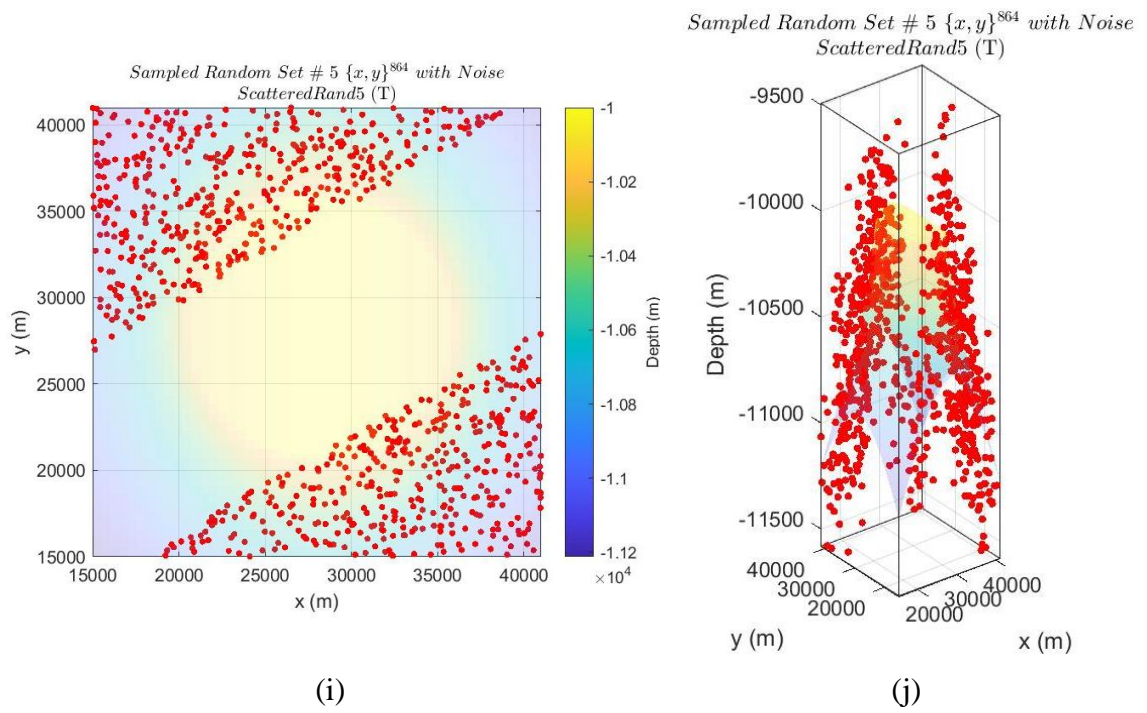


Figure 6.1 Study 2 (RE) Test 3a: Random configurations.

The first 5 sampling configurations generated in the second study (RE) Test 3a with random censoring and random noise.

Table 6.2

Study 2 (RE) Test 3a: Random Configuration Details

Id	Swath Width (m)	Num Pts Before	Num Pts After	Mean Sparsity (m)	Median Sparsity (m)	Max Sparsity (m)	Min Sparsity (m)	Noise Standard Deviation (m)	Noise Range (m)
1	19,337.70	2,119.00	605.00	691.84	614.72	19,354.55	4.66	7,506.65	[-999.175 - 938.672]
2	4,398.68	2,356.00	1,858.00	650.26	582.17	20,526.82	4.58	7,583.28	[-1074.15 - 1066.74]
3	16,316.21	330.00	181.00	1,862.60	1,563.38	22,836.26	67.51	7,642.72	[-806.09 - 731.653]
4	7,684.07	2,376.00	2,049.00	652.30	583.37	23,206.88	2.46	7,555.40	[-1154.46 - 1033.22]
5	13,298.28	1,645.00	864.00	778.88	705.01	18,587.81	6.02	7,528.96	[-1085.36 - 952.778]
6	7,312.13	253.00	186.00	2,066.12	1,808.56	18,352.77	92.76	7,911.03	[-1084.92 - 819.494]
7	2,100.48	724.00	676.00	1,209.10	1,054.37	20,809.88	22.56	7,472.19	[-837.973 - 854.708]
8	8,579.56	1,422.00	1,126.00	848.73	762.68	16,075.39	21.50	7,582.66	[-831.843 - 844.429]
9	546.62	2,491.00	2,467.00	631.92	559.02	20,294.63	8.89	7,354.65	[-1044.81 - 1274.59]
10	12,905.11	2,510.00	1,068.00	632.95	567.86	18,799.69	5.43	7,470.11	[-1168.26 - 1042.72]
11	14,351.39	410.00	166.00	1,612.62	1,445.35	21,172.11	122.40	7,582.47	[-995.09 - 844.363]
12	309.92	2,525.00	2,493.00	632.26	563.05	20,949.92	6.45	7,539.92	[-956.795 - 1190.6]
13	6,073.87	2,490.00	1,950.00	634.01	568.53	19,386.69	10.80	7,452.95	[-1071.1 - 1013.02]
14	855.95	1,262.00	1,229.00	909.64	793.07	21,309.63	7.84	7,457.62	[-1246.75 - 975.627]
15	4,750.21	2,082.00	1,735.00	697.30	622.70	19,335.63	6.14	7,546.26	[-1233.17 - 928.151]
16	274.91	369.00	366.00	1,685.85	1,509.85	16,820.77	66.52	7,331.99	[-1074.47 - 713.722]
17	9,716.43	1,097.00	717.00	951.88	847.07	13,407.85	11.86	7,330.00	[-938.537 - 957.586]
18	4,892.36	2,382.00	2,117.00	650.47	582.71	19,058.17	7.67	7,543.37	[-933.862 - 934.149]
19	616.15	2,061.00	2,025.00	701.06	628.22	21,345.65	3.63	7,497.71	[-927.243 - 918.895]
20	7,987.06	2,496.00	2,252.00	631.59	569.29	15,870.90	7.75	7,539.46	[-1068.22 - 1047.98]
21	11,721.21	1,706.00	1,152.00	777.17	693.84	22,204.04	16.57	7,459.85	[-1075.04 - 1090.58]
22	2,338.66	92.00	86.00	3,529.61	2,995.06	22,392.03	95.68	7,294.21	[-931.584 - 820.697]
23	2,513.85	2,209.00	2,169.00	680.44	602.98	22,692.63	3.19	7,488.59	[-980.306 - 1021.74]
24	11,568.71	2,430.00	1,897.00	642.75	580.79	21,112.68	11.37	7,550.99	[-924.413 - 1162.37]
25	260,667.29	1,766.00	1,124.00	754.54	678.56	21,502.59	10.85	7,398.03	[-913.297 - 967.084]
26	2,514.93	1,971.00	1,802.00	722.03	632.86	21,211.15	6.68	7,515.03	[-1030.5 - 1149.69]
27	18,811.11	1,933.00	1,402.00	725.01	643.56	21,049.61	15.40	7,351.79	[-1163.92 - 1035.19]
28	1,276.20	1,020.00	972.00	1,026.87	912.17	18,926.81	24.49	7,349.29	[-992.696 - 812.924]
29	3,947.79	1,705.00	1,410.00	767.41	692.89	19,144.28	16.49	7,470.29	[-1127.76 - 996.782]
30	31,033.92	445.00	207.00	1,554.08	1,329.83	21,952.81	15.96	7,368.63	[-999.671 - 805.309]
31	22,789.48	1,837.00	735.00	738.66	654.90	19,927.66	11.15	7,449.01	[-965.712 - 1012.48]
32	23,995.81	82.00	69.00	3,811.59	3,050.82	24,945.86	168.68	7,744.08	[-765.348 - 701.272]
33	27,349.26	720.00	127.00	1,201.20	1,093.16	15,507.59	5.21	7,779.93	[-903.717 - 1074.35]
34	21,102.62	120.00	44.00	3,105.14	2,671.97	21,555.80	125.01	8,396.68	[-585.984 - 897.459]
35	18,539.53	252.00	55.00	1,987.51	1,825.97	14,535.70	35.71	7,153.85	[-834.643 - 841.913]

Table 6.2 (continued)

37	19,980.90	1,807.00	1,247.00	745.82	660.95	17,830.89	1.77	7,446.46	[-1096.74 - 1013.15]
38	28,850.40	825.00	585.00	1,136.88	1,006.22	21,071.61	3.23	7,514.94	[-958.972 - 958.926]
39	8,747.73	2,472.00	1,583.00	630.47	571.07	20,090.35	6.15	7,490.42	[-964.779 - 963.675]
40	6,549.42	89.00	82.00	3,452.41	2,969.20	23,011.28	210.84	7,144.24	[-790.772 - 657.362]
41	14,203.03	1,141.00	850.00	956.65	853.46	19,516.59	12.54	7,524.31	[-1017.82 - 1145.44]
42	5,844.50	992.00	818.00	1,005.58	907.02	19,266.09	24.91	7,508.81	[-886.836 - 962.612]
43	48,748.00	1,991.00	1,398.00	717.84	642.85	24,377.47	2.63	7,534.53	[-929.841 - 914.593]
44	10,158.36	2,069.00	1,126.00	703.23	623.81	15,577.41	12.97	7,615.03	[-953.574 - 893.851]
45	21,051.98	486.00	274.00	1,438.33	1,247.53	18,068.33	11.30	7,316.11	[-836.475 - 988.026]
46	8,482.70	1,274.00	910.00	881.75	793.13	16,638.80	18.73	7,588.03	[-957.194 - 848.052]
47	94,034.98	1,159.00	904.00	954.55	839.67	24,310.91	11.66	7,516.69	[-838.599 - 1206.11]
48	5,434.21	1,681.00	1,236.00	771.76	685.72	16,875.60	11.68	7,451.55	[-976.053 - 1023.3]
49	46.94	1,845.00	1,843.00	741.88	662.26	23,283.59	15.88	7,527.15	[-970.325 - 911.605]
50	15,822.68	1,963.00	1,341.00	725.27	633.82	22,314.13	11.97	7,514.83	[-1130.36 - 970.773]
51	5,614.67	718.00	583.00	1,214.19	1,061.71	21,862.37	12.10	7,393.10	[-901.691 - 877.505]
52	32,531.60	1,768.00	925.00	764.91	674.32	23,235.94	5.21	7,572.95	[-1007.15 - 1088.73]
53	11,636.75	1,704.00	1,215.00	765.86	684.66	14,694.53	15.61	7,629.16	[-898.158 - 1020.55]
54	177,356.69	423.00	164.00	1,606.42	1,396.91	22,917.92	52.46	7,323.80	[-814.783 - 793.699]
55	7,251.31	309.00	242.00	1,850.41	1,653.58	19,293.10	37.69	7,368.05	[-808.553 - 939.163]
56	15,566.40	1,296.00	642.00	879.33	785.23	15,277.68	18.88	7,478.30	[-886.661 - 1082.17]
57	9,007.31	2,497.00	1,826.00	628.86	572.84	11,909.27	7.35	7,478.53	[-936.528 - 969.445]
58	279,614.10	885.00	385.00	1,101.39	956.29	19,817.15	22.57	7,624.66	[-1077.56 - 981.525]
59	19,892.46	1,522.00	567.00	834.58	736.27	24,621.18	20.59	7,496.43	[-1302.09 - 1005.23]
60	147,659.29	582.00	469.00	1,366.66	1,190.82	21,138.07	27.16	7,347.45	[-1058.3 - 1330.08]
61	33,766.96	1,954.00	1,059.00	723.94	641.59	21,828.84	11.93	7,487.45	[-905.722 - 1158.62]
62	34,739.52	663.00	124.00	1,265.00	1,119.53	18,710.39	31.02	7,508.98	[-916.56 - 1057.29]
63	19,596.08	1,316.00	470.00	882.66	777.18	16,681.65	15.75	7,531.04	[-1020.2 - 1028.67]
64	162,769.48	1,818.00	712.00	747.26	670.22	21,358.32	4.87	7,477.71	[-1205.23 - 1119.57]
65	13,430.97	2,318.00	1,889.00	658.89	589.18	18,494.00	20.33	7,499.35	[-1049.43 - 1030.05]
66	17,838.35	2,496.00	1,659.00	625.05	572.34	16,372.75	6.60	7,393.00	[-943.905 - 1030.39]
67	25,256.90	1,423.00	664.00	856.10	745.02	19,074.16	24.18	7,536.28	[-1055.31 - 1125.67]
68	2,856.45	360.00	318.00	1,728.60	1,510.72	19,128.10	108.21	7,230.41	[-804.583 - 897.56]
69	3,140.44	388.00	333.00	1,630.55	1,460.33	13,987.45	57.06	7,318.46	[-989.775 - 1134.85]
70	4,580.25	670.00	599.00	1,258.31	1,104.58	17,379.22	16.84	7,472.52	[-901.019 - 1047.17]
71	10,521.78	2,187.00	1,285.00	679.45	609.70	16,855.12	3.68	7,405.03	[-1019.45 - 968.963]
72	6,437.91	661.00	580.00	1,260.18	1,098.07	18,367.77	6.57	7,342.14	[-863.655 - 927.529]
73	4,529.21	2,118.00	1,677.00	687.53	618.72	18,011.30	7.08	7,450.94	[-1050.11 - 1297.04]
74	9,787.50	633.00	474.00	1,275.65	1,141.55	19,635.41	10.76	7,412.26	[-1068.88 - 900.593]
75	7,458.32	2,417.00	1,624.00	643.67	572.21	17,491.89	15.66	7,480.45	[-939.15 - 1006.4]
76	8,191.32	910.00	639.00	1,070.75	940.20	14,908.79	11.56	7,508.96	[-934.036 - 1008.07]
77	2,247.83	511.00	472.00	1,442.06	1,250.31	20,873.26	75.84	7,605.03	[-815.402 - 692.213]
78	5,659.09	653.00	547.00	1,272.47	1,118.08	21,639.03	24.27	7,333.74	[-888.569 - 940.715]
79	2,009.58	1,602.00	1,462.00	798.32	720.89	22,449.89	22.66	7,539.86	[-1037.55 - 974.965]
80	506.36	1,231.00	1,194.00	907.19	819.02	12,617.62	9.41	7,531.87	[-1040.88 - 1029.97]
81	1,235.09	915.00	888.00	1,070.14	932.55	19,475.90	6.91	7,519.53	[-825.86 - 1269.76]
82	196.28	2,161.00	2,155.00	679.02	611.62	16,022.32	3.13	7,514.46	[-987.624 - 1051.58]
83	1,324.80	1,522.00	1,453.00	817.97	729.22	19,613.46	7.51	7,618.39	[-1014.8 - 914.384]

Table 6.2 (continued)

84	18,221.29	1,430.00	474.00	853.10	761.79	19,549.14	10.53	7,549.68	[-1084.88 - 975.961]
85	17,097.88	2,386.00	683.00	652.46	586.54	20,039.59	5.65	7,420.22	[-1042.5 - 963.208]
86	15,629.19	743.00	598.00	1,213.59	1,036.43	24,998.36	18.79	7,669.49	[-825.167 - 894.343]
87	1,297.19	1,970.00	1,882.00	720.91	642.29	19,796.52	9.82	7,634.22	[-987.959 - 1040.6]
88	28,495.79	1,961.00	387.00	702.61	640.67	11,911.19	6.68	7,554.26	[-955.508 - 971.751]
89	6,210.16	989.00	969.00	1,019.36	913.93	19,951.42	18.75	7,359.00	[-901.818 - 842.772]
90	4,444.80	1,477.00	1,240.00	832.88	732.23	20,320.20	10.37	7,348.89	[-1078.72 - 888.413]
91	5,112.20	197.00	150.00	2,295.35	1,993.19	20,613.15	197.39	7,340.25	[-563.258 - 804.029]
92	3,824.19	140.00	130.00	2,897.66	2,534.73	21,484.65	79.99	7,349.11	[-792.265 - 616.659]
93	5,091.06	1,381.00	1,149.00	841.50	743.04	13,363.58	4.31	7,508.00	[-1129.7 - 931.729]
94	344.98	2,027.00	2,002.00	709.51	635.07	22,411.57	4.50	7,501.56	[-1151.19 - 1011.39]
95	7,738.49	2,430.00	1,786.00	641.53	572.19	19,264.41	3.70	7,599.55	[-1241.4 - 984.871]
96	6,546.80	338.00	292.00	1,742.10	1,536.55	17,507.06	93.82	7,450.69	[-936.63 - 697.922]
97	14,634.66	1,480.00	613.00	829.89	741.12	18,245.15	17.14	7,489.57	[-1005.91 - 997.704]
98	8,693.41	1,221.00	890.00	931.33	816.04	21,769.37	13.87	7,441.05	[-1024.11 - 910.463]
99	6,703.17	30.00	22.00	5,764.03	5,745.81	18,685.84	893.92	7,360.95	[-757.323 - 559.214]
100	16,504.91	877.00	320.00	1,079.82	950.83	16,012.87	8.08	7,491.75	[-946.757 - 1023.61]

Details for the 100 randomly generated \dense and sparse configurations of random censoring and noise for the second study (RE)

Test 3a. For each configuration, we list the random width of the swath removed in meters; the number of points randomly sampled before and after swath removal; the mean, median, minimum, and maximum gap between points in meters; and the standard deviation and range of the random white noise sampled from a Gaussian Distribution with mean 0 and standard deviation 300 m.

6.1.2 Results

Table 6.3

Study 2 (RE) Test 3a: Random Configuration CumRAE Results (Results rounded to 2 decimals, but color coding is accurate.)

Id	Krig_GMTquadloss (SM01)	GMTboxcar (SM02)	GMT SIT (SM03)	Mean (SM04)	w-ELS (Planar) (SM05)	w-ELS (Custom) (SM06)	ELS (Planar) (SM07)	ELS (Custom) (SM08)	OLS (Planar) (SM09)	OLS (Custom) (SM10)	OLS (DBM(S) ~ Seamount) (SM11)	OLS (DBM(R) ~ Ridge) (SM12)	OLS (DBM(S) ~ Custom) (SM13)	OLS (DBM(R) ~ Custom) (SM14)	ELS (DBM(S) + DBM(R) ~ Seamount) (SM15)	ELS (DBM(S) + DBM(R) ~ Ridge) (SM16)	OLS (GMT SIT ~ Custom) (SM17)	mean3 (SM18)	OLS (mean ~ Custom) (SM19)	OLS (mean3 ~ Custom) (SM20)	AllIndivMean (SM21)	AllMean (SM22)
1	0.95	0.95	1.00	0.95	0.95	0.95	0.96	0.63	0.88	0.88	0.64	0.70	0.65	0.64	0.62	0.70	0.65	0.96	0.63	0.63	0.96	0.72
2	0.65	0.61	1.00	0.62	0.61	0.61	1.50	0.29	1.58	0.73	0.36	0.89	0.29	0.29	0.35	0.89	0.29	0.71	0.29	0.29	0.71	0.37
3	0.97	0.94	1.00	0.95	0.91	0.91	1.07	0.66	1.12	0.86	0.66	0.81	0.65	0.65	0.67	0.81	0.65	0.97	0.65	0.65	0.97	0.73
4	0.63	0.58	1.00	0.60	0.58	0.58	1.44	0.29	1.48	0.59	0.34	0.86	0.29	0.28	0.35	0.86	0.29	0.69	0.29	0.29	0.69	0.36
5	0.83	0.80	1.00	0.81	0.79	0.80	1.44	0.31	1.62	0.86	0.36	0.87	0.30	0.30	0.36	0.87	0.29	0.86	0.30	0.30	0.86	0.46
6	0.96	0.91	1.00	0.93	0.84	0.84	1.16	0.44	1.17	0.70	0.51	0.72	0.44	0.44	0.51	0.73	0.45	0.95	0.45	0.43	0.95	0.52
7	0.81	0.74	1.00	0.77	0.72	0.72	1.54	0.32	1.58	0.64	0.36	0.92	0.32	0.32	0.36	0.93	0.32	0.83	0.32	0.32	0.83	0.42
8	0.70	0.65	1.00	0.67	0.65	0.65	1.59	0.35	1.71	0.81	0.41	0.96	0.36	0.35	0.41	0.96	0.36	0.75	0.35	0.36	0.75	0.40
9	0.59	0.57	1.00	0.57	0.57	0.57	1.44	0.28	1.46	0.51	0.34	0.86	0.28	0.28	0.33	0.86	0.28	0.67	0.28	0.28	0.67	0.36
10	0.90	0.89	1.00	0.89	0.89	0.89	1.05	0.63	1.03	0.73	0.62	0.73	0.63	0.63	0.62	0.73	0.63	0.92	0.63	0.63	0.92	0.70
11	0.97	0.95	1.00	0.96	0.94	0.94	1.36	0.56	1.59	0.94	0.69	0.90	0.54	0.55	0.67	0.90	0.54	0.97	0.54	0.55	0.97	0.73
12	0.62	0.57	1.00	0.59	0.57	0.57	1.45	0.29	1.49	0.60	0.35	0.85	0.29	0.29	0.35	0.85	0.30	0.68	0.29	0.29	0.68	0.33
13	0.70	0.67	1.00	0.68	0.67	0.67	1.43	0.28	1.55	0.84	0.38	0.86	0.28	0.28	0.38	0.86	0.29	0.75	0.28	0.28	0.75	0.41
14	0.69	0.65	1.00	0.66	0.64	0.64	1.40	0.28	1.42	0.52	0.33	0.82	0.28	0.28	0.33	0.82	0.28	0.74	0.28	0.28	0.74	0.37
15	0.68	0.64	1.00	0.66	0.64	0.64	1.45	0.35	1.49	0.70	0.39	0.88	0.36	0.35	0.38	0.88	0.35	0.73	0.35	0.35	0.73	0.40
16	0.91	0.84	1.00	0.87	0.78	0.77	1.49	0.35	1.50	0.42	0.41	0.93	0.37	0.36	0.40	0.92	0.36	0.91	0.36	0.36	0.91	0.53
17	0.85	0.82	1.00	0.83	0.81	0.81	1.23	0.48	1.29	0.64	0.52	0.82	0.45	0.45	0.52	0.82	0.46	0.87	0.45	0.45	0.87	0.62
18	0.62	0.60	1.00	0.60	0.60	0.60	1.46	0.31	1.47	0.55	0.35	0.86	0.32	0.31	0.34	0.86	0.33	0.70	0.31	0.32	0.70	0.35
19	0.62	0.60	1.00	0.60	0.60	0.60	1.47	0.29	1.51	0.59	0.35	0.89	0.29	0.29	0.35	0.89	0.30	0.70	0.29	0.29	0.70	0.39
20	0.61	0.58	1.00	0.59	0.59	0.59	1.41	0.28	1.45	0.57	0.33	0.84	0.28	0.28	0.33	0.84	0.29	0.68	0.29	0.29	0.68	0.38
21	0.82	0.78	1.00	0.80	0.78	0.79	1.36	0.52	1.46	0.79	0.58	0.82	0.53	0.52	0.57	0.82	0.53	0.84	0.53	0.53	0.84	0.47
22	0.99	0.96	1.00	0.97	0.90	0.90	1.38	0.50	1.36	0.44	0.58	0.92	0.54	0.53	0.54	0.90	0.54	0.98	0.54	0.54	0.98	0.63
23	0.59	0.57	1.00	0.57	0.57	0.57	1.37	0.29	1.39	0.48	0.34	0.83	0.29	0.29	0.33	0.83	0.29	0.67	0.29	0.29	0.67	0.35
24	0.67	0.65	1.00	0.65	0.65	0.65	1.45	0.33	1.60	0.85	0.44	0.82	0.34	0.33	0.44	0.82	0.42	0.73	0.34	0.34	0.73	0.38
25	0.73	0.69	1.00	0.70	0.69	0.69	1.54	0.40	1.57	0.76	0.44	0.95	0.41	0.40	0.45	0.95	0.41	0.77	0.41	0.41	0.77	0.45
26	0.67	0.61	1.00	0.64	0.60	0.60	1.37	0.27	1.42	0.63	0.33	0.83	0.27	0.27	0.33	0.83	0.27	0.72	0.27	0.27	0.72	0.38
27	0.72	0.68	1.00	0.70	0.68	0.68	1.45	0.35	1.50	0.93	0.41	0.81	0.36	0.36	0.40	0.81	0.36	0.77	0.36	0.36	0.77	0.41
28	0.73	0.68	1.00	0.70	0.68	0.68	1.39	0.28	1.41	0.55	0.32	0.84	0.28	0.28	0.32	0.84	0.29	0.78	0.28	0.28	0.78	0.38
29	0.70	0.67	1.00	0.68	0.68	0.68	1.40	0.33	1.45	0.63	0.38	0.83	0.34	0.33	0.37	0.83	0.33	0.75	0.33	0.34	0.75	0.36
30	0.95	0.92	1.00	0.94	0.91	0.90	1.37	0.45	1.57	1.19	0.44	0.80	0.41	0.43	0.46	0.81	0.42	0.95	0.42	0.42	0.95	0.54
31	0.89	0.86	1.00	0.87	0.86	0.86	1.52	0.44	2.01	1.27	0.40	0.94	0.45	0.47	0.41	0.95	0.48	0.90	0.46	0.45	0.90	0.57
32	0.99	0.95	1.00	0.97	0.90	0.90	1.75	0.50	1.85	0.87	0.48	1.07	0.48	0.49	0.47	1.09	0.48	0.98	0.48	0.48	0.98	0.54
33	0.99	0.99	1.00	0.99	0.99	0.99	0.96	0.87	0.84	0.73	0.87	0.87	0.87	0.87	0.87	0.87	0.87	0.99	0.87	0.87	0.99	0.89
34	1.00	0.99	1.00	0.99	0.98	0.98	1.30	0.62	1.46	1.23	0.59	0.90	0.63	0.63	0.58	0.90	0.63	0.99	0.62	0.62	0.99	0.76
35	0.99	0.99	1.00	0.99	0.98	0.98	1.00	0.71	1.51	1.12	0.74	0.80	0.69	0.70	0.75	0.80	0.70	0.99	0.70	0.69	0.99	0.78
36	0.83	0.80	1.00	0.81	0.80	0.80	1.16	0.67	1.25	0.70	0.61	0.65	0.67	0.69	0.56	0.65	0.69	0.86	0.66	0.69	0.86	0.51
37	0.73	0.70	1.00	0.71	0.70	0.70	1.52	0.39	1.72	0.50	0.43	0.91	0.41	0.41	0.43	0.91	0.39	0.78	0.39	0.40	0.78	0.49
38	0.85	0.81	1.00	0.83	0.79	0.79	1.38	0.52	1.45	0.93	0.43	0.88	0.49	0.51	0.44	0.89	0.51	0.87	0.49	0.50	0.87	0.58
39	0.80	0.78	1.00	0.79	0.78	0.78	1.26	0.53	1.34	0.72	0.51	0.88	0.52	0.53	0.52	0.88	0.52	0.83	0.53	0.52	0.83	0.57
40	0.99	0.95	1.00	0.97	0.88	0.88	1.32	0.71	1.30	0.75	0.61	0.86	0.59	0.74	0.50	0.85	0.61	0.98	0.74	0.74	0.98	0.72
41	0.80	0.76	1.00	0.78	0.76	0.76	1.41	0.39	1.57	0.89	0.44	0.82	0.40	0.39	0.44	0.82	0.40	0.83	0.39	0.39	0.83	0.43
42	0.77	0.71	1.00	0.73	0.69	0.69	1.49	0.30	1.51	0.67	0.37	0.87	0.31	0.30	0.35	0.88	0.30	0.80	0.30	0.30	0.80	0.42
43	0.80	0.77	1.00	0.78	0.77	0.77	1.36	0.44	1.48	0.83	0.55	0.80	0.45	0.44	0.54	0.80	0.46	0.83	0.45	0.45	0.83	0.46
44	0.84	0.81	1.00	0.83	0.81	0.81	1.27	0.52	1.34	0.64	0.53	0.85	0.53	0.53	0.53	0.85	0.53	0.87	0.53	0.53	0.87	0.61
45	0.93	0.89	1.00	0.91	0.86	0.86	1.45	0.50	1.61	0.99	0.62	0.91	0.51	0.50	0.61	0.91	0.50	0.93	0.50	0.50	0.93	0.59

Table 6.3 (continued)

46	0.80	0.77	1.00	0.78	0.76	0.76	1.48	0.38	1.55	0.77	0.40	0.84	0.40	0.38	0.39	0.84	0.39	0.83	0.38	0.39	0.83	0.41
47	0.79	0.75	1.00	0.76	0.74	0.74	1.38	0.39	1.45	0.70	0.46	0.78	0.40	0.40	0.46	0.78	0.41	0.82	0.40	0.40	0.82	0.39
48	0.74	0.71	1.00	0.72	0.71	0.71	1.36	0.30	1.42	0.65	0.35	0.85	0.29	0.30	0.36	0.85	0.29	0.79	0.30	0.29	0.79	0.45
49	0.62	0.59	1.00	0.60	0.59	0.59	1.49	0.30	1.52	0.60	0.35	0.91	0.30	0.30	0.35	0.91	0.31	0.69	0.30	0.30	0.69	0.40
50	0.73	0.70	1.00	0.71	0.70	0.70	1.50	0.36	1.70	0.93	0.43	0.93	0.38	0.36	0.42	0.93	0.37	0.77	0.37	0.37	0.77	0.53
51	0.84	0.78	1.00	0.81	0.75	0.75	1.43	0.39	1.47	0.72	0.49	0.85	0.40	0.39	0.40	0.85	0.45	0.86	0.40	0.45	0.86	0.47
52	0.89	0.88	1.00	0.88	0.88	0.88	1.19	0.81	1.30	0.99	0.78	0.85	0.81	0.81	0.78	0.85	0.81	0.91	0.81	0.81	0.91	0.77
53	0.74	0.71	1.00	0.72	0.70	0.70	1.48	0.33	1.54	0.86	0.37	0.92	0.33	0.33	0.38	0.92	0.33	0.79	0.33	0.33	0.79	0.46
54	0.96	0.93	1.00	0.94	0.91	0.91	1.64	0.44	2.09	1.73	0.52	1.01	0.43	0.45	0.52	1.01	0.56	0.96	0.45	0.44	0.96	0.60
55	0.94	0.89	1.00	0.91	0.84	0.85	1.35	0.34	1.40	0.75	0.38	0.82	0.31	0.33	0.39	0.83	0.33	0.94	0.33	0.31	0.94	0.50
56	0.91	0.89	1.00	0.90	0.89	0.89	1.15	0.66	1.15	0.85	0.70	0.75	0.67	0.66	0.70	0.76	0.68	0.92	0.67	0.67	0.92	0.60
57	0.73	0.69	1.00	0.70	0.69	0.69	1.36	0.40	1.39	0.76	0.48	0.87	0.40	0.40	0.48	0.87	0.40	0.77	0.40	0.40	0.77	0.50
58	0.91	0.87	1.00	0.89	0.85	0.85	1.42	0.39	1.73	1.78	0.46	0.87	0.43	0.40	0.45	0.87	0.43	0.92	0.43	0.43	0.92	0.61
59	0.91	0.89	1.00	0.89	0.89	0.89	1.21	0.67	1.27	0.93	0.65	0.85	0.67	0.67	0.64	0.85	0.66	0.92	0.67	0.67	0.92	0.73
60	0.88	0.82	1.00	0.85	0.78	0.79	1.42	0.39	1.43	0.78	0.40	0.88	0.37	0.38	0.41	0.88	0.36	0.89	0.38	0.37	0.89	0.48
61	0.87	0.85	1.00	0.86	0.85	0.85	1.12	0.68	1.01	0.82	0.68	0.80	0.68	0.68	0.69	0.80	0.68	0.89	0.68	0.68	0.89	0.71
62	0.99	0.99	1.00	0.99	0.97	0.97	0.96	0.53	0.84	0.58	0.52	0.59	0.53	0.53	0.51	0.58	0.53	0.99	0.53	0.53	0.99	0.63
63	0.94	0.92	1.00	0.93	0.92	0.92	1.29	0.68	1.41	1.23	0.73	0.85	0.69	0.68	0.73	0.85	0.68	0.95	0.68	0.68	0.95	0.71
64	0.91	0.88	1.00	0.89	0.88	0.88	1.27	0.54	1.87	1.66	0.55	0.88	0.55	0.54	0.54	0.88	0.54	0.92	0.54	0.54	0.92	0.74
65	0.67	0.64	1.00	0.65	0.64	0.64	1.55	0.30	1.66	0.84	0.38	0.94	0.30	0.30	0.37	0.94	0.31	0.73	0.30	0.30	0.73	0.41
66	0.76	0.73	1.00	0.74	0.72	0.72	1.38	0.47	1.52	1.02	0.54	0.89	0.46	0.47	0.55	0.89	0.70	0.80	0.46	0.46	0.80	0.60
67	0.89	0.88	1.00	0.88	0.88	0.88	1.26	0.78	1.60	1.17	0.79	0.99	0.77	0.78	0.79	0.99	0.77	0.91	0.77	0.77	0.91	0.83
68	0.92	0.85	1.00	0.88	0.80	0.79	1.42	0.33	1.44	0.70	0.42	0.87	0.35	0.34	0.38	0.86	0.35	0.92	0.34	0.36	0.92	0.50
69	0.92	0.86	1.00	0.89	0.81	0.81	1.32	0.38	1.36	0.55	0.40	0.84	0.34	0.35	0.42	0.85	0.33	0.92	0.35	0.34	0.92	0.52
70	0.85	0.79	1.00	0.82	0.76	0.77	1.39	0.33	1.42	0.67	0.36	0.85	0.34	0.34	0.36	0.85	0.34	0.87	0.35	0.34	0.87	0.49
71	0.81	0.78	1.00	0.79	0.78	0.78	1.35	0.62	1.47	0.78	0.64	0.76	0.63	0.63	0.63	0.76	0.64	0.84	0.63	0.58	0.84	0.52
72	0.83	0.77	1.00	0.80	0.72	0.72	1.50	0.30	1.51	0.61	0.35	0.91	0.31	0.30	0.36	0.91	0.30	0.85	0.30	0.31	0.85	0.45
73	0.70	0.66	1.00	0.68	0.66	0.66	1.50	0.32	1.56	0.74	0.40	0.89	0.35	0.34	0.39	0.89	0.33	0.75	0.34	0.32	0.75	0.36
74	0.86	0.81	1.00	0.84	0.79	0.79	1.44	0.41	1.47	0.90	0.41	0.89	0.39	0.40	0.43	0.90	0.40	0.88	0.40	0.40	0.88	0.55
75	0.75	0.72	1.00	0.73	0.72	0.72	1.28	0.39	1.33	0.63	0.43	0.81	0.37	0.38	0.44	0.81	0.37	0.79	0.38	0.38	0.79	0.50
76	0.87	0.82	1.00	0.84	0.80	0.80	1.27	0.46	1.32	0.73	0.52	0.72	0.45	0.46	0.51	0.72	0.44	0.88	0.46	0.46	0.88	0.54
77	0.87	0.81	1.00	0.84	0.77	0.77	1.44	0.29	1.50	0.65	0.34	0.85	0.29	0.29	0.34	0.85	0.28	0.88	0.29	0.29	0.88	0.41
78	0.87	0.80	1.00	0.83	0.76	0.76	1.42	0.36	1.48	0.66	0.37	0.82	0.35	0.34	0.38	0.82	0.35	0.88	0.35	0.35	0.88	0.41
79	0.69	0.65	1.00	0.66	0.64	0.64	1.45	0.28	1.50	0.65	0.43	0.88	0.28	0.28	0.39	0.88	0.28	0.74	0.28	0.28	0.74	0.37
80	0.69	0.63	1.00	0.65	0.64	0.63	1.48	0.31	1.53	0.66	0.36	0.90	0.33	0.31	0.36	0.90	0.36	0.74	0.33	0.34	0.74	0.43
81	0.76	0.70	1.00	0.73	0.68	0.69	1.42	0.29	1.45	0.57	0.34	0.85	0.31	0.31	0.34	0.85	0.30	0.80	0.31	0.31	0.80	0.38
82	0.57	0.54	1.00	0.55	0.54	0.54	1.45	0.29	1.48	0.59	0.35	0.86	0.29	0.29	0.36	0.86	0.29	0.65	0.29	0.29	0.65	0.32
83	0.69	0.64	1.00	0.66	0.65	0.64	1.50	0.32	1.53	0.60	0.36	0.89	0.32	0.32	0.37	0.89	0.32	0.74	0.32	0.32	0.74	0.38
84	0.93	0.92	1.00	0.92	0.91	0.91	1.28	0.63	1.59	0.89	0.66	0.93	0.69	0.66	0.65	0.93	0.69	0.94	0.67	0.67	0.94	0.73
85	0.95	0.94	1.00	0.94	0.94	0.94	1.09	0.66	1.12	0.89	0.60	0.73	0.66	0.66	0.61	0.74	0.67	0.96	0.66	0.66	0.96	0.75
86	0.85	0.80	1.00	0.82	0.77	0.78	1.45	0.34	1.54	0.94	0.41	0.87	0.36	0.35	0.40	0.87	0.35	0.87	0.35	0.35	0.87	0.47
87	0.63	0.59	1.00	0.60	0.59	0.59	1.42	0.29	1.48	0.67	0.34	0.83	0.29	0.30	0.34	0.83	0.30	0.70	0.30	0.30	0.70	0.38
88	0.97	0.96	1.00	0.96	0.96	0.96	1.02	0.90	1.33	1.21	0.92	0.93	0.88	0.88	0.93	0.89	0.97	0.88	0.89	0.97	0.94	
89	0.75	0.70	1.00	0.72	0.69	0.69	1.44	0.29	1.47	0.51	0.35	0.88	0.29	0.29	0.35	0.88	0.30	0.79	0.29	0.29	0.79	0.42
90	0.75	0.71	1.00	0.73	0.70	0.70	1.32	0.31	1.34	0.58	0.38	0.82	0.30	0.31	0.39	0.82	0.30	0.79	0.31	0.31	0.79	0.44
91	0.97	0.93	1.00	0.95	0.90	0.90	1.45	0.62	1.53	0.91	0.73	0.83	0.64	0.64	0.65	0.84	0.63	0.96	0.64	0.64	0.96	0.61
92	0.98	0.95	1.00	0.97	0.90	0.91	1.54	0.39	1.52	0.51	0.50	0.84	0.41	0.41	0.43	0.84	0.41	0.98	0.41	0.41	0.98	0.47
93	0.77	0.72	1.00	0.74	0.71	0.71	1.31	0.29	1.38	0.71	0.34	0.75	0.30	0.29	0.34	0.75	0.30	0.80	0.30	0.30	0.80	0.43
94	0.63	0.60	1.00	0.61	0.61	0.60	1.46	0.29	1.49	0.58	0.34	0.88	0.29	0.30	0.34	0.88	0.29	0.70	0.29	0.29	0.70	0.35
95	0.72	0.69	1.00	0.70	0.69	0.69	1.38	0.36	1.51	0.84	0.38	0.88	0.35	0.36	0.39	0.88	0.35	0.77	0.35	0.35	0.77	0.45
96	0.93	0.87	1.00	0.90	0.78	0.78	1.48	0.32	1.48	0.66	0.39	0.85	0.33	0.33	0.38	0.85	0.33	0.93	0.33	0.33	0.93	0.50
97	0.94	0.93	1.00	0.93	0.93	0.92	0.98	0.82	0.88	0.53	0.87	0.83	0.81	0.82	0.86	0.84	0.82	0.95	0.82	0.82	0.95	0.80
98	0.83	0.79	1.00	0.81	0.78	0.78	1.24	0.36	1.24	0.66	0.43	0.79	0.35	0.36	0.46	0.79	0.35	0.85	0.35	0.35	0.85	0.52
99	1.00	0.99	1.00	0.99	0.98	0.97	1.16	0.48	1.21	0.81	0.51	0.70	0.56	0.57	0.51	0.71	0.56	0.99	0.56	0.56	0.99	0.62
100	0.95	0.93	1.00	0.94	0.92	0.92	1.02	0.75	1.08	0.85	0.74	0.80	0.74	0.74	0.76	0.81	0.74	0.95	0.74	0.74	0.95	0.80

CumRAE for all interpolators at 100 randomly generated configuration of random censoring and noise for the second study (RE) Test 3a on the hybrid morphology. The columns are our selected methods identified by SM<Id> in Table 3.1 on page 100. Selected from our first study (UEs), Krig_GMTquadloess (SM01) is our seamount interpolator and GMTboxcar (SM02) is our ridge interpolator. GMT SIT (EM31) is our benchmark. A value of 1.00 (middle green) indicates equal performance to the benchmark, values greater than 1.00 (dark green) performed worse than the benchmark, and values less than 1.00 (light green), performed better than the benchmark. For each level, the minimum CumRAE is annotated in red. CumRAE allows for direct comparison between methods.

6.2 Study 2 (RE) Test 3b: Sparse Configurations

The sparse RE (Test 3b) consist of 100 random sparse configurations that were obtained by randomly sampling at varied densities, adding random Gaussian noise with a zero mean and a standard deviation of 300 m ($\mathcal{N}(0, 300)$), and randomly censoring data over a swath of random width at a random location.⁵⁶

To determine if a configuration is sparse, we first construct a Delaunay triangulation of the (x, y) coordinates of the soundings. A Delaunay triangulation requires the minimum angle of the triangulation to be maximized (Press et al., 2007). The Delaunay condition, also known as the empty circle property, utilizes circumscribed circles to uphold this requirement. A circumscribed circle is a circle where the vertices of a triangle lie on the circumference. Perpendicular bisectors on the edges of a triangle converge to form the circumcenter of the circumscribed circle. The Delaunay condition requires the circumscribed circles to be empty, having no other points enclosed within the circumscribed circles.

In a Delaunay triangulation, we first construct a TIN and then impose the Delaunay condition (Sinclair, 2010). For each triangle in the TIN, we construct the circumscribed circle and if the vertex of another triangle is enclosed within the circumscribed circle, we flip the shared edge between the two triangles to join the other two vertices in an edge instead for two new triangles that do not violate the Delaunay

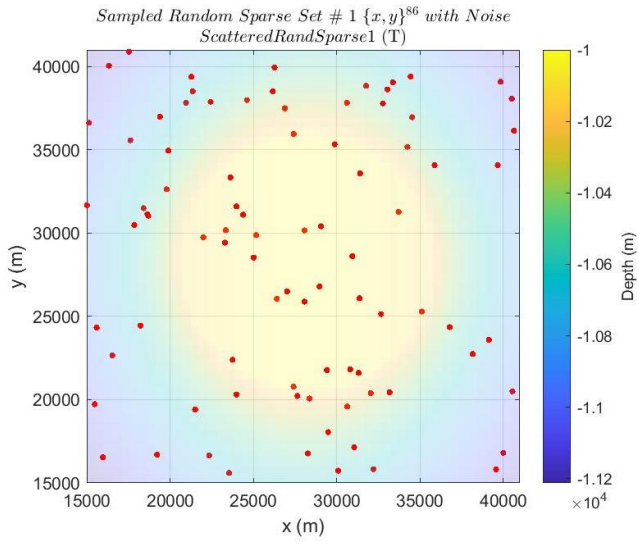
⁵⁶ A width of zero is possible.

condition. We continue iterating through the TIN, flipping edges, until the Delaunay condition is met everywhere.

A property of these circumscribed circles that Delaunay triangulations exploit is nearest neighbors. A Delaunay triangulation is the dual of a Voronoi diagram. A Voronoi diagram divides space into region of influence where the extent of a point abuts the extents of its nearest neighbors. Triangle edges of a Delaunay triangulation bisect Voronoi boundaries and connect points to their nearest. We use a Delaunay triangulation to compute the spatial data gaps as the distances between nearby points, given as the length of triangle edges.

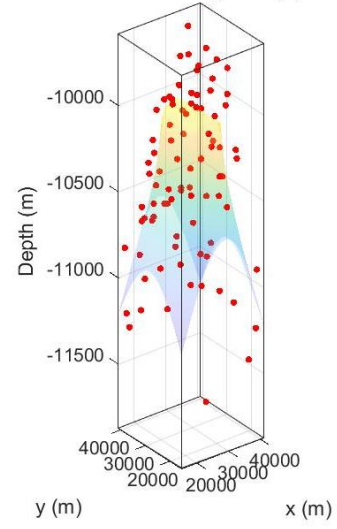
Once we compute the Delaunay triangulation, we then compute the length of all the edges. We then perform our statistical sign test to determine if our random configuration is sparse (see section 4.1.2). Figure 6.2 shows only the first five sparse configurations generated and sparsity details are shown in Table 6.4. CumRAE results are shown in Table 6.5 (see table captions or Chapter VI introductory section for table description).

6.2.1 Data

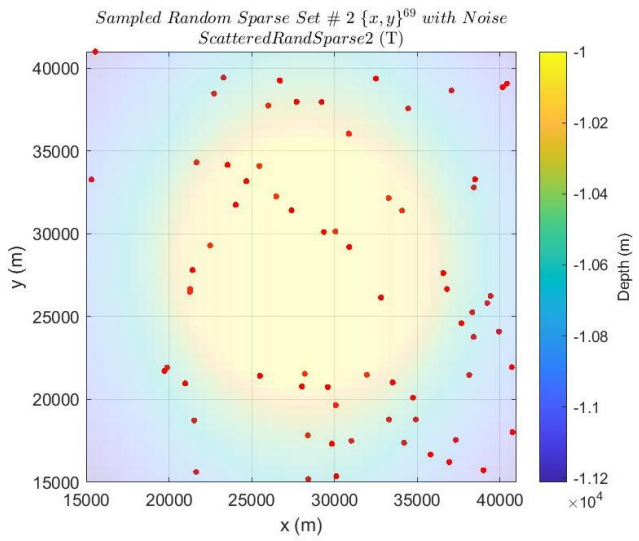


(a)

Sampled Random Sparse Set # 1 $\{x, y\}^{86}$ with Noise
ScatteredRandSparse1 (T)

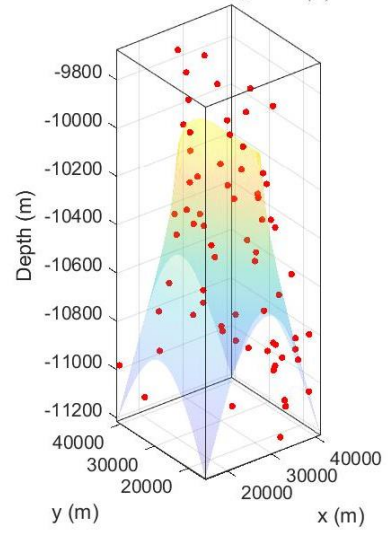


(b)

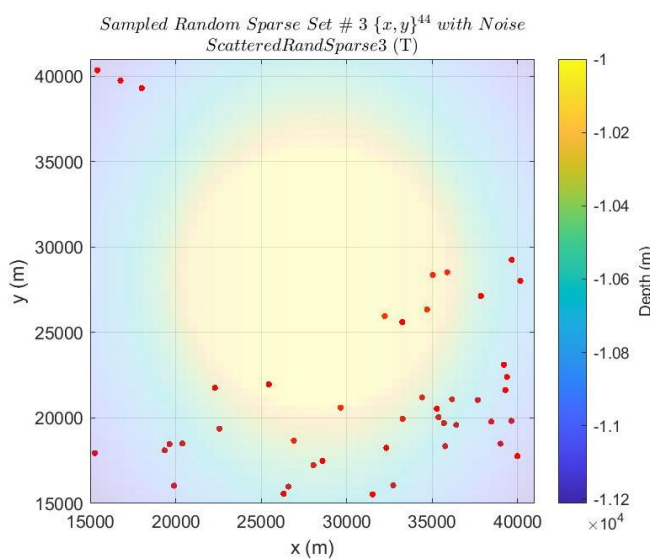


(c)

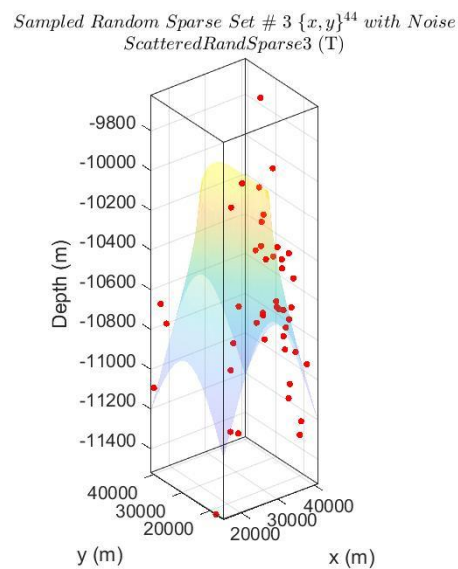
Sampled Random Sparse Set # 2 $\{x, y\}^{69}$ with Noise
ScatteredRandSparse2 (T)



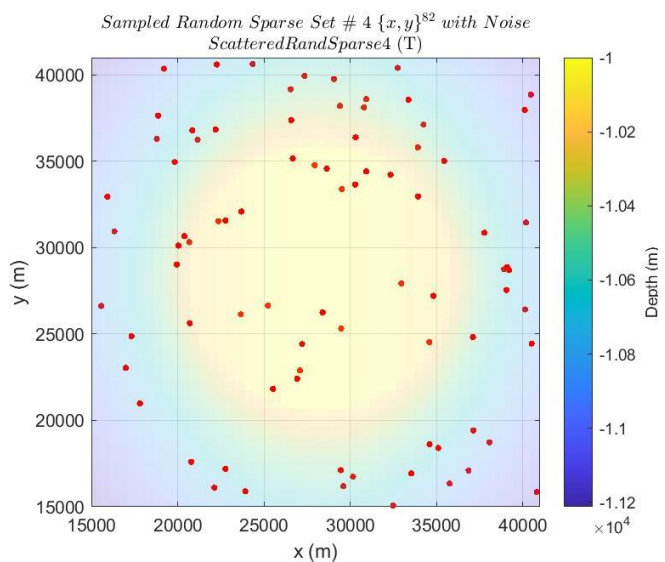
(d)



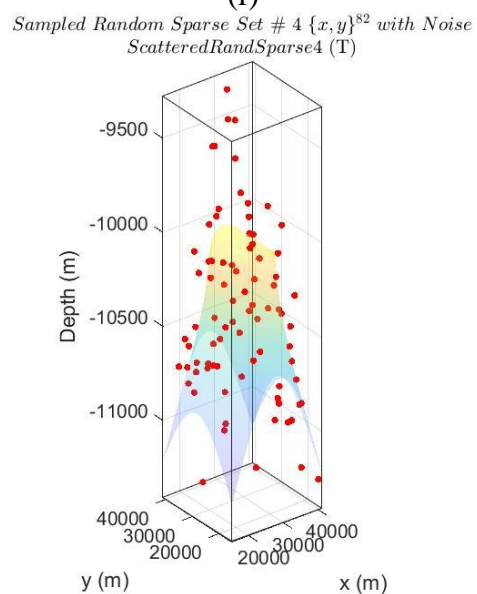
(e)



(f)



(g)



(h)

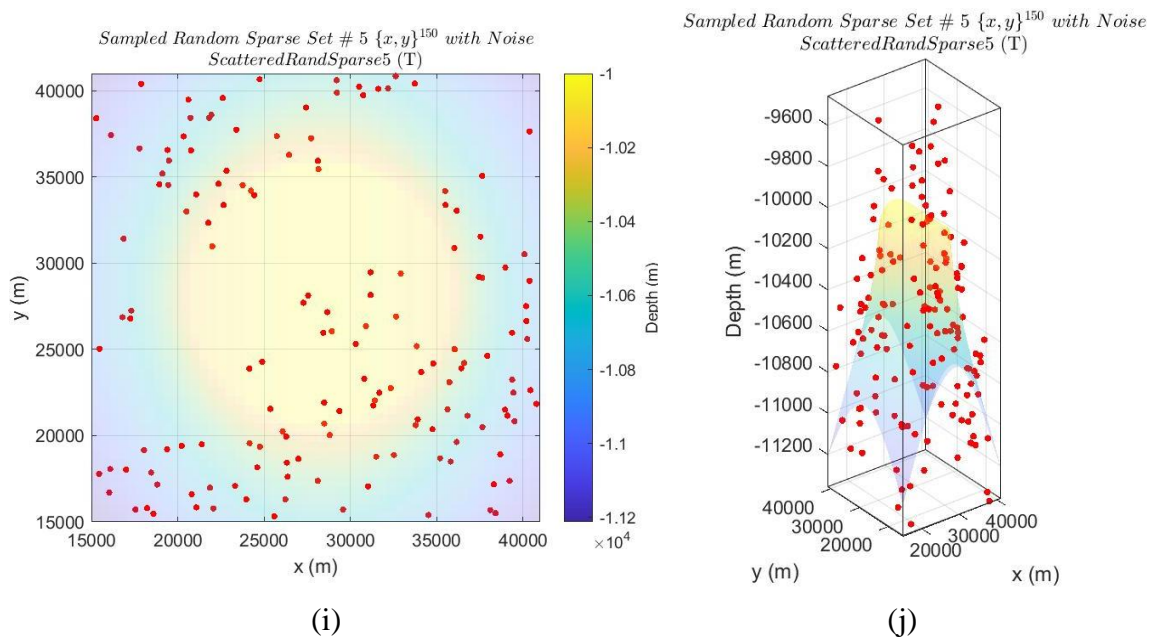


Figure 6.2 Study 2 (RE) Test 3b: Sparse configurations.

The first 5 sparse sampling configurations generated in the second study (RE) Test 3b with random censoring and random noise.

Table 6.4

Study 2 (RE) Test3b: Sparse Configuration Details

Id	Swath Width (m)	Num Pts Before	Num Pts After	Mean Sparsity (m)	Median Sparsity (m)	Max Sparsity (m)	Min Sparsity (m)	Noise Standard Deviation (m)	Noise Range (m)
1	2,338.66	92.00	86.00	3,529.61	2,995.06	22,392.03	95.68	7,294.21	[-931.584 - 820.697]
2	23,995.81	82.00	69.00	3,811.59	3,050.82	24,945.86	168.68	7,744.08	[-765.348 - 701.272]
3	21,102.62	120.00	44.00	3,105.14	2,671.97	21,555.80	125.01	8,396.68	[-585.984 - 897.459]
4	6,549.42	89.00	82.00	3,452.41	2,969.20	23,011.28	210.84	7,144.24	[-790.772 - 657.362]
5	5,112.20	197.00	150.00	2,295.35	1,993.19	20,613.15	197.39	7,340.25	[-563.258 - 804.029]
6	3,824.19	140.00	130.00	2,897.66	2,534.73	21,484.65	79.99	7,349.11	[-792.265 - 616.659]
7	6,703.17	30.00	22.00	5,764.03	5,745.81	18,685.84	893.92	7,360.95	[-757.323 - 559.214]
8	3,745.20	218.00	198.00	2,359.59	2,071.77	21,835.40	93.89	7,848.65	[-747.689 - 787.51]
9	4,846.76	12.00	7.00	8,325.99	7,704.66	18,389.12	1,349.09	7,917.96	[-210.454 - 540.699]
10	5,777.51	197.00	161.00	2,394.50	2,024.10	19,007.61	70.60	7,469.47	[-834.184 - 924.077]
11	30,661.52	129.00	74.00	2,873.80	2,489.56	19,333.53	199.94	7,246.86	[-971.309 - 629.037]
12	16,878.08	155.00	80.00	2,558.33	2,322.97	14,608.48	70.93	7,092.77	[-698.503 - 720.021]
13	23,206.68	40.00	18.00	6,023.98	4,957.43	24,321.59	697.85	7,674.59	[-439.417 - 556.546]
14	2,261.59	111.00	100.00	3,139.44	2,873.17	14,129.97	151.58	7,741.72	[-647.152 - 795.864]
15	16,607.83	211.00	176.00	2,293.52	1,958.74	24,124.53	43.01	7,587.33	[-1264.74 - 808.073]
16	3,387.50	76.00	67.00	3,603.71	3,222.90	19,410.93	263.94	7,586.63	[-597.347 - 635.548]
17	21,795.17	98.00	59.00	3,238.18	2,827.22	19,549.77	269.29	7,170.66	[-823.454 - 711.579]
18	25,778.84	79.00	66.00	3,784.06	3,306.81	21,138.16	252.65	7,142.08	[-566.996 - 706.952]
19	3,539.33	74.00	66.00	3,829.33	3,366.82	22,007.58	200.10	7,590.68	[-659.007 - 652.564]
20	7,765.63	155.00	102.00	2,616.40	2,279.77	14,920.55	109.18	7,693.31	[-854.446 - 1133.6]
21	10,102.30	110.00	74.00	3,264.42	2,606.63	23,264.73	155.12	7,969.09	[-909.872 - 727.629]
22	75,887.11	185.00	106.00	2,419.41	2,087.78	18,173.14	27.84	7,906.86	[-947.668 - 775.197]
23	6,485.60	157.00	120.00	2,606.41	2,249.62	19,301.67	205.00	7,562.34	[-766.104 - 862.156]
24	4,287.94	40.00	35.00	5,992.27	5,184.20	25,404.22	205.42	7,823.64	[-702.728 - 592.757]
25	11,261.77	137.00	76.00	2,785.79	2,410.10	19,365.40	254.95	7,053.32	[-775.907 - 771.983]
26	13,459.77	84.00	64.00	3,695.31	3,368.90	19,166.75	204.20	7,823.34	[-921.582 - 850.132]
27	8,265.24	58.00	49.00	4,016.06	3,543.90	19,041.08	415.19	7,115.34	[-625.499 - 833.35]
28	22,571.55	87.00	46.00	3,461.55	3,185.30	15,001.20	250.27	7,232.92	[-852.159 - 611.776]
29	8,284.01	179.00	171.00	2,421.05	2,241.23	14,796.55	52.14	7,554.79	[-773.479 - 863.52]
30	166.93	176.00	175.00	2,541.86	2,173.82	22,992.28	115.05	7,429.01	[-777.56 - 888.001]
31	21,901.10	17.00	15.00	6,867.22	6,745.78	15,742.70	1,647.62	6,533.22	[-497.271 - 517.329]

Table 6.4 (continued)

32	13,021.08	93.00	46.00	3,695.03	3,073.90	22,751.53	354.24	7,454.10	[-829.118 - 804.845]
33	8,922.70	165.00	150.00	2,533.83	2,166.25	20,502.39	153.62	7,526.97	[-745.232 - 752.816]
34	12,471.80	115.00	62.00	3,066.87	2,693.61	18,141.55	195.05	7,220.37	[-693.248 - 620.822]
35	100.68	50.00	49.00	4,595.78	3,734.26	21,823.05	38.80	6,925.25	[-465.84 - 493.877]
36	19,089.92	143.00	100.00	2,678.12	2,399.54	14,328.78	138.74	7,241.75	[-809.258 - 921.822]
37	49,013.78	217.00	80.00	2,245.20	2,024.20	12,795.66	132.19	7,748.60	[-907.288 - 683.221]
38	187,539.13	44.00	19.00	4,917.86	4,306.38	17,821.92	302.50	7,489.31	[-558.847 - 628.934]
39	7,619.68	83.00	50.00	3,562.47	2,858.51	15,904.80	157.04	7,263.74	[-683.381 - 778.174]
40	14,163.19	128.00	80.00	2,962.52	2,602.55	20,144.77	240.62	7,509.20	[-806.686 - 918.242]
41	10,899.39	110.00	50.00	3,022.07	2,612.37	17,083.09	138.98	6,821.39	[-1182.73 - 641.885]
42	21,290.73	213.00	117.00	2,227.13	1,980.29	17,850.84	47.28	6,963.21	[-714.623 - 703.82]
43	163,009.01	135.00	50.00	2,775.27	2,430.97	13,744.53	80.49	6,840.87	[-617.561 - 925.113]
44	12,446.26	164.00	83.00	2,663.25	2,251.88	17,659.46	100.76	7,713.50	[-857.489 - 963.615]
45	4,100.10	80.00	71.00	3,686.66	3,382.07	15,109.22	394.77	7,798.23	[-668.841 - 619.531]
46	19,720.26	65.00	30.00	4,360.03	3,649.14	22,389.27	213.09	8,060.06	[-664.859 - 664.46]
47	15,617.28	141.00	82.00	2,685.72	2,379.32	13,004.78	226.06	7,786.72	[-672.049 - 645.535]
48	9,037.84	147.00	120.00	2,712.87	2,412.01	15,913.19	111.16	7,772.93	[-810.707 - 1043.82]
49	2,254.93	185.00	168.00	2,407.66	2,098.75	20,357.68	72.38	7,384.91	[-711.355 - 999.886]
50	1,876.17	139.00	127.00	2,699.64	2,309.19	14,802.73	129.09	7,842.27	[-780.441 - 796.551]
51	1,624.55	34.00	34.00	5,438.10	4,561.97	15,860.35	647.82	7,398.91	[-802.72 - 438.851]
52	12,125.72	161.00	88.00	2,564.24	2,388.01	21,072.49	22.61	7,494.48	[-819.685 - 831.858]
53	24,355.80	120.00	45.00	2,868.91	2,793.14	12,686.96	121.24	7,599.95	[-975.561 - 1096.65]
54	20,558.12	210.00	83.00	2,311.65	2,016.71	19,945.18	90.09	7,726.65	[-1129.04 - 803.239]
55	2,307.61	26.00	25.00	6,986.21	6,540.60	17,249.93	1,842.24	8,615.97	[-798.529 - 707.175]
56	11,933.46	126.00	121.00	3,092.83	2,618.11	21,428.39	62.93	7,392.02	[-820.345 - 866.294]
57	2,734.72	160.00	143.00	2,539.07	2,284.95	16,560.93	118.31	7,573.78	[-759.437 - 641.214]
58	611.83	133.00	128.00	2,716.69	2,503.60	14,917.90	71.28	7,146.14	[-835.133 - 843.104]
59	23,496.85	189.00	73.00	2,435.08	2,089.70	20,092.46	30.99	7,716.42	[-698.554 - 723.268]
60	80,737.87	96.00	32.00	3,430.55	2,972.58	21,159.85	169.29	7,454.00	[-687.387 - 834.29]
61	15,697.57	154.00	98.00	2,618.51	2,337.19	20,955.24	106.06	7,771.83	[-874.626 - 716.431]
62	26,861.05	20.00	19.00	5,842.84	5,725.77	13,569.27	1,051.28	7,171.01	[-672.06 - 631.431]
63	32,083.03	201.00	148.00	2,317.67	2,071.07	16,814.28	78.73	7,640.72	[-685.995 - 811.994]
64	9,867.53	192.00	106.00	2,385.17	2,128.78	16,196.12	71.38	7,100.05	[-708.75 - 654.354]
65	30,763.47	63.00	36.00	4,011.68	3,545.05	15,566.52	259.79	6,761.71	[-921.067 - 755.829]
66	3,658.81	95.00	75.00	3,346.32	2,929.67	20,219.24	245.47	7,248.79	[-579.868 - 775.682]
67	6,178.02	53.00	31.00	4,204.11	4,049.18	14,909.17	632.67	6,903.78	[-614.314 - 840.009]
68	24,472.89	167.00	50.00	2,486.19	2,133.53	16,568.88	106.18	7,760.74	[-688.465 - 758.107]
69	1,638.09	156.00	151.00	2,576.87	2,248.33	18,582.26	91.98	7,764.40	[-836.12 - 1106.95]
70	14,329.60	65.00	37.00	4,017.79	3,675.16	17,852.74	104.71	7,700.51	[-648.811 - 597.211]
71	33,925.86	117.00	86.00	3,030.12	2,549.46	15,209.49	199.88	7,581.66	[-696.842 - 729.27]
72	33,617.85	56.00	39.00	4,382.59	3,759.87	21,196.03	359.85	7,802.14	[-726.484 - 844.494]
73	11,952.21	78.00	55.00	3,501.18	2,959.84	19,682.94	353.34	7,761.18	[-512.94 - 470.693]
74	10,406.54	226.00	183.00	2,214.79	1,984.39	18,798.28	123.64	7,509.33	[-694.141 - 929.727]

Table 6.4 (continued)

75	14,299.58	174.00	82.00	2,662.69	2,226.54	24,612.19	59.07	7,021.66	[-686.217 - 890.279]
76	3,858.32	47.00	41.00	4,578.28	4,124.98	14,401.57	234.93	7,601.95	[-613.245 - 575.964]
77	9,671.00	108.00	89.00	3,168.48	2,734.60	16,856.57	36.89	7,001.69	[-919.455 - 1019.56]
78	4,053.61	214.00	188.00	2,299.43	1,965.22	17,528.09	103.89	7,618.38	[-941.211 - 824.97]
79	24,632.01	25.00	18.00	5,774.26	4,499.28	16,370.39	514.22	8,458.69	[-471.604 - 435.647]
80	143,911.37	111.00	40.00	3,073.73	2,757.13	14,583.55	194.92	7,719.33	[-694.316 - 856.349]
81	10,957.40	114.00	74.00	3,022.16	2,642.46	13,461.91	340.96	7,205.59	[-748.918 - 872.746]
82	1,048.34	142.00	136.00	2,884.42	2,506.81	21,554.39	96.29	7,594.23	[-788.842 - 750.429]
83	5,549.59	83.00	74.00	3,841.47	3,342.17	23,902.79	225.70	8,015.34	[-795.794 - 892.238]
84	5,007.47	123.00	99.00	2,964.86	2,428.49	18,630.29	101.12	7,772.37	[-946.095 - 623.924]
85	120,392.21	110.00	55.00	2,975.54	2,569.96	12,073.14	134.75	7,570.58	[-816.978 - 1141.26]
86	42,126.55	50.00	19.00	4,259.47	4,020.43	14,754.66	479.68	6,837.89	[-706.284 - 647.478]
87	2,093,059.60	218.00	23.00	2,167.62	1,988.89	14,242.68	101.60	6,991.39	[-847.248 - 1035.17]
88	12,575.87	123.00	85.00	2,965.18	2,656.70	16,180.27	139.07	7,841.59	[-749.341 - 675.976]
89	31,341.25	142.00	56.00	2,758.37	2,357.15	20,904.24	145.81	7,270.38	[-674.174 - 761.666]
90	206.02	120.00	119.00	3,010.37	2,743.14	16,802.59	298.19	7,223.91	[-683.163 - 632.347]
91	5,475.54	183.00	167.00	2,407.05	2,178.35	17,484.77	115.66	7,280.94	[-952.612 - 706.426]
92	10,916.11	56.00	46.00	4,721.48	4,086.41	23,958.90	141.02	7,085.05	[-771.608 - 587.635]
93	8,821.32	67.00	36.00	4,081.94	3,446.87	23,793.11	249.16	7,540.01	[-583.983 - 706.72]
94	35,926.28	187.00	68.00	2,456.79	2,239.74	16,884.28	53.50	7,739.23	[-989.986 - 691.131]
95	23,800.38	48.00	39.00	4,824.40	4,719.36	19,060.76	472.33	7,246.67	[-910.209 - 605.738]
96	7,572.40	157.00	124.00	2,573.50	2,165.36	22,170.02	145.65	7,767.40	[-918.386 - 685.5]
97	26,211.53	219.00	50.00	2,283.48	1,961.40	23,574.75	98.13	7,619.08	[-736.03 - 863.27]
98	8,956.47	30.00	18.00	5,762.91	5,386.50	21,361.67	335.79	7,535.03	[-720.466 - 372.911]
99	2,768.20	184.00	163.00	2,354.71	2,020.36	22,860.73	26.01	6,947.81	[-888.612 - 668.582]
100	3,926.00	168.00	143.00	2,584.72	2,302.78	19,185.55	61.26	7,573.18	[-943.533 - 788.917]

Details for the 100 randomly generated sparse configurations for the second study (RE) Test 3b. For each configuration, we list the random width of the swath removed in meters; the number of points randomly sampled before and after swath removal; the mean, median, minimum, and maximum gap between points in meters; and the standard deviation and range of the random white noise sampled from a Gaussian Distribution with mean 0 and standard deviation 300 m.

6.2.2 Results

Table 6.5

Study 2 (RE) Test 3b: Sparse Configuration CumRAE Results (Results rounded to 2 decimals, but color coding is accurate.)

Id	Krig_GMTquadloess (SM01)	GMTboxcar (SM02)	GMT SIT (SM03)	Mean (SM04)	w-ELS (Planar) (SM05)	w-ELS (Custom) (SM06)	ELS (Planar) (SM07)	ELS (Custom) (SM08)	OLS (Planar) (SM09)	OLS (Custom) (SM10)	OLS (DBM(S) ~ Seamount) (SM11)	OLS (DBM(R) ~ Ridge) (SM12)	OLS (DBM(S) ~ Custom) (SM13)	OLS (DBM(R) ~ Custom) (SM14)	ELS (DBM(S) + DBM(R) ~ Seamount) (SM15)	ELS (DBM(S) + DBM(R) ~ Ridge) (SM16)	OLS (GMT SIT ~ Custom) (SM17)	mean3 (SM18)	OLS (mean ~ Custom) (SM19)	OLS (mean3 ~ Custom) (SM20)	AllIndivMean (SM21)	AllMean (SM22)
1	0.99	0.96	1.00	0.97	0.90	0.90	1.38	0.50	1.36	0.44	0.58	0.92	0.54	0.53	0.54	0.90	0.54	0.98	0.54	0.54	0.98	0.63
2	0.99	0.95	1.00	0.97	0.90	0.90	1.75	0.50	1.85	0.87	0.48	1.07	0.48	0.49	0.47	1.09	0.48	0.98	0.48	0.48	0.98	0.54
3	1.00	0.99	1.00	0.99	0.98	0.98	1.30	0.62	1.46	1.23	0.59	0.90	0.63	0.63	0.58	0.90	0.63	0.99	0.62	0.62	0.99	0.76
4	0.99	0.95	1.00	0.97	0.88	0.88	1.32	0.71	1.30	0.75	0.61	0.86	0.59	0.74	0.50	0.85	0.61	0.98	0.74	0.74	0.98	0.72
5	0.97	0.93	1.00	0.95	0.90	0.90	1.45	0.62	1.53	0.91	0.73	0.83	0.64	0.64	0.65	0.84	0.63	0.96	0.64	0.64	0.96	0.61
6	0.98	0.95	1.00	0.97	0.90	0.91	1.54	0.39	1.52	0.51	0.50	0.84	0.41	0.41	0.43	0.84	0.41	0.98	0.41	0.41	0.98	0.47
7	1.00	0.99	1.00	0.99	0.98	0.97	1.16	0.48	1.21	0.81	0.51	0.70	0.56	0.57	0.51	0.71	0.56	0.99	0.56	0.56	0.99	0.62
8	0.95	0.89	1.00	0.92	0.82	0.82	1.47	0.38	1.58	0.97	0.37	0.89	0.42	0.42	0.37	0.90	0.42	0.94	0.42	0.42	0.94	0.46
9	1.00	1.00	1.00	1.00	1.00	1.00	0.94	0.73	1.13	1.06	0.74	0.82	0.73	0.73	0.74	0.82	0.73	1.00	0.73	0.73	1.00	0.81
10	0.97	0.91	1.00	0.94	0.84	0.84	1.57	0.38	1.60	0.81	0.41	0.96	0.38	0.38	0.42	0.97	0.36	0.96	0.36	0.37	0.96	0.55
11	0.99	0.97	1.00	0.98	0.97	0.96	1.24	0.66	1.36	0.93	0.67	0.96	0.67	0.66	0.66	0.96	0.66	0.98	0.67	0.67	0.98	0.75
12	0.98	0.95	1.00	0.97	0.92	0.92	1.49	0.57	1.50	0.85	0.64	0.99	0.56	0.65	0.60	1.00	0.66	0.98	0.59	0.59	0.98	0.72
13	1.00	1.00	1.00	1.00	1.00	1.01	1.19	0.89	1.48	1.28	0.88	0.89	0.88	0.88	0.89	0.91	0.88	1.00	0.87	0.88	1.00	0.93
14	0.99	0.95	1.00	0.97	0.88	0.88	1.38	0.42	1.55	0.95	0.45	0.88	0.42	0.41	0.48	0.89	0.42	0.98	0.40	0.42	0.98	0.60
15	0.96	0.92	1.00	0.94	0.88	0.88	1.41	0.37	1.49	0.41	0.34	0.85	0.36	0.37	0.34	0.86	0.36	0.95	0.37	0.36	0.95	0.50
16	0.99	0.96	1.00	0.98	0.92	0.92	1.52	0.56	1.60	0.85	0.50	1.00	0.51	0.51	0.54	1.01	0.51	0.98	0.51	0.51	0.98	0.60
17	0.99	0.97	1.00	0.98	0.94	0.94	1.42	0.42	1.66	1.27	0.51	0.86	0.46	0.45	0.49	0.86	0.47	0.98	0.45	0.46	0.98	0.64
18	0.99	0.96	1.00	0.98	0.92	0.91	1.40	0.56	1.37	0.65	0.55	0.91	0.58	0.58	0.54	0.90	0.59	0.98	0.58	0.58	0.98	0.66
19	0.99	0.96	1.00	0.98	0.91	0.91	1.53	0.46	1.63	0.53	0.48	0.96	0.47	0.47	0.48	0.96	0.47	0.99	0.47	0.47	0.99	0.67
20	0.98	0.96	1.00	0.97	0.92	0.92	1.33	0.54	1.47	0.84	0.50	0.89	0.50	0.55	0.49	0.89	0.55	0.98	0.50	0.50	0.98	0.63
21	0.99	0.97	1.00	0.98	0.91	0.92	1.17	0.57	1.16	0.61	0.61	0.69	0.54	0.55	0.59	0.70	0.54	0.98	0.54	0.54	0.98	0.59
22	0.99	0.96	1.00	0.97	0.91	0.91	1.20	0.68	1.26	1.25	0.63	0.83	0.68	0.68	0.67	0.84	0.67	0.98	0.68	0.67	0.98	0.75
23	0.97	0.93	1.00	0.95	0.88	0.88	1.61	0.37	1.68	0.92	0.45	0.94	0.38	0.37	0.46	0.95	0.39	0.96	0.37	0.38	0.96	0.53
24	1.00	0.97	1.00	0.98	0.92	0.91	1.54	0.62	1.53	0.68	0.67	0.95	0.67	0.66	0.62	0.93	0.67	0.99	0.67	0.67	0.99	0.74
25	0.99	0.97	1.00	0.98	0.94	0.94	1.25	0.68	1.35	0.80	0.69	0.91	0.68	0.68	0.71	0.91	0.68	0.99	0.68	0.68	0.99	0.77
26	0.99	0.97	1.00	0.98	0.95	0.95	1.33	0.63	1.57	1.09	0.56	0.88	0.62	0.61	0.59	0.89	0.60	0.99	0.61	0.61	0.99	0.68
27	0.99	0.98	1.00	0.99	0.96	0.96	1.16	0.69	1.29	0.99	0.67	0.78	0.64	0.65	0.67	0.79	0.65	0.99	0.66	0.65	0.99	0.74
28	1.00	0.98	1.00	0.99	0.96	0.96	1.29	0.87	1.28	0.80	0.91	0.85	0.86	0.87	0.92	0.86	0.82	0.99	0.86	0.87	0.99	0.81
29	0.97	0.93	1.00	0.95	0.88	0.89	1.31	0.56	1.35	0.71	0.49	0.83	0.56	0.55	0.51	0.84	0.57	0.97	0.56	0.58	0.97	0.61
30	0.94	0.88	1.00	0.91	0.81	0.81	1.51	0.41	1.50	0.56	0.44	0.90	0.42	0.42	0.44	0.91	0.42	0.94	0.42	0.42	0.94	0.57
31	1.00	1.00	1.00	1.00	1.00	1.00	1.46	0.96	1.51	1.23	0.93	1.21	0.95	0.96	0.94	1.21	0.95	1.00	0.96	0.96	1.00	0.94
32	0.99	0.97	1.00	0.98	0.93	0.93	1.49	0.58	1.70	1.20	0.64	1.01	0.55	0.56	0.66	1.02	0.55	0.99	0.55	0.55	0.99	0.73
33	0.97	0.92	1.00	0.94	0.84	0.84	1.27	0.29	1.29	0.69	0.31	0.73	0.33	0.31	0.30	0.74	0.30	0.96	0.31	0.31	0.96	0.45
34	0.99	0.96	1.00	0.98	0.89	0.88	1.41	0.54	1.52	1.02	0.53	0.87	0.60	0.58	0.50	0.87	0.60	0.98	0.59	0.59	0.98	0.65
35	0.99	0.97	1.00	0.98	0.94	0.92	1.73	0.56	1.71	0.74	0.62	0.99	0.55	0.55	0.65	0.99	0.55	0.99	0.55	0.55	0.99	0.66
36	0.99	0.96	1.00	0.97	0.92	0.92	1.07	0.63	1.13	0.86	0.65	0.80	0.63	0.62	0.62	0.80	0.64	0.98	0.62	0.63	0.98	0.72
37	0.99	0.99	1.00	0.99	0.99	0.99	1.02	0.90	1.19	0.85	0.91	0.93	0.90	0.90	0.91	0.93	0.90	0.99	0.90	0.90	0.99	0.93
38	1.00	0.99	1.00	1.00	0.99	0.98	1.19	0.63	1.74	0.43	0.61	0.82	0.62	0.62	0.61	0.82	0.62	1.00	0.62	0.62	1.00	0.71
39	1.00	0.98	1.00	0.99	0.95	0.95	1.56	0.66	1.67	1.02	0.63	0.99	0.61	0.65	0.64	1.00	0.61	0.99	0.64	0.64	0.99	0.66
40	0.99	0.98	1.00	0.99	0.95	0.95	1.21	0.61	1.32	0.75	0.59	0.80	0.59	0.59	0.64	0.81	0.60	0.99	0.59	0.59	0.99	0.70
41	1.00	0.99	1.00	0.99	0.98	0.98	1.18	0.64	1.06	0.92	0.66	0.68	0.63	0.63	0.66	0.68	0.63	0.99	0.63	0.63	0.99	0.71
42	0.97	0.94	1.00	0.95	0.89	0.89	1.29	0.48	1.43	0.85	0.48	0.83	0.49	0.49	0.51	0.83	0.49	0.97	0.49	0.49	0.97	0.59
43	0.99	0.98	1.00	0.98	0.97	0.97	1.69	0.74	2.32	1.76	0.71	1.21	0.73	0.74	0.72	1.21	0.73	0.99	0.74	0.73	0.99	0.84
44	0.99	0.96	1.00	0.97	0.92	0.92	1.55	0.37	1.71	1.54	0.44	0.91	0.37	0.37	0.43	0.92	0.37	0.98	0.37	0.37	0.98	0.52
45	0.99	0.96	1.00	0.98	0.91	0.92	1.47	0.68	1.49	0.76	0.90	0.96	0.69	0.68	0.87	0.97	0.69	0.98	0.68	0.68	0.98	0.71

Table 6.5 (continued)

46	1.00	0.99	1.00	0.99	0.98	0.97	1.19	0.69	1.55	0.70	0.71	0.74	0.69	0.69	0.71	0.74	0.69	0.99	0.69	0.69	0.99	0.76
47	0.98	0.96	1.00	0.97	0.95	0.95	1.30	0.46	1.22	1.06	0.44	0.80	0.45	0.45	0.44	0.81	0.46	0.98	0.45	0.44	0.98	0.59
48	0.98	0.95	1.00	0.97	0.91	0.91	1.33	0.37	1.36	0.68	0.39	0.78	0.38	0.37	0.38	0.78	0.38	0.98	0.38	0.38	0.98	0.54
49	0.96	0.91	1.00	0.94	0.84	0.84	1.35	0.35	1.36	0.48	0.40	0.82	0.35	0.34	0.43	0.82	0.34	0.96	0.36	0.36	0.96	0.51
50	0.98	0.95	1.00	0.96	0.88	0.87	1.25	0.40	1.33	0.75	0.45	0.82	0.37	0.38	0.44	0.82	0.37	0.97	0.38	0.37	0.97	0.55
51	1.00	0.99	1.00	0.99	0.96	0.97	1.22	0.57	1.24	0.61	0.62	0.84	0.59	0.58	0.61	0.83	0.58	1.00	0.59	0.59	1.00	0.67
52	0.99	0.97	1.00	0.98	0.94	0.94	1.42	0.59	1.72	1.42	0.56	0.90	0.65	0.58	0.58	0.91	0.65	0.98	0.58	0.65	0.98	0.69
53	0.99	0.98	1.00	0.99	0.99	0.98	1.36	0.59	1.52	1.20	0.62	0.91	0.58	0.58	0.63	0.91	0.58	0.99	0.58	0.58	0.99	0.78
54	0.99	0.98	1.00	0.98	0.97	0.96	1.02	0.50	1.11	0.80	0.50	0.75	0.50	0.50	0.49	0.74	0.50	0.99	0.50	0.50	0.99	0.60
55	1.00	0.99	1.00	0.99	0.99	0.98	1.33	0.51	1.34	1.00	0.56	0.90	0.53	0.52	0.55	0.90	0.53	1.00	0.52	0.52	1.00	0.67
56	0.98	0.93	1.00	0.95	0.88	0.88	1.41	0.42	1.49	0.89	0.48	0.90	0.43	0.42	0.45	0.90	0.43	0.97	0.43	0.43	0.97	0.54
57	0.96	0.92	1.00	0.94	0.87	0.86	1.73	0.37	1.77	0.69	0.43	1.04	0.36	0.37	0.45	1.05	0.39	0.96	0.37	0.37	0.96	0.54
58	0.97	0.92	1.00	0.95	0.82	0.83	1.58	0.37	1.65	0.85	0.43	0.95	0.41	0.40	0.39	0.96	0.41	0.96	0.41	0.41	0.96	0.54
59	0.99	0.97	1.00	0.98	0.96	0.96	1.13	0.62	1.23	0.79	0.61	0.83	0.62	0.62	0.62	0.83	0.62	0.99	0.62	0.62	0.99	0.71
60	1.00	0.99	1.00	0.99	0.99	0.99	1.20	0.56	1.26	0.83	0.53	0.65	0.52	0.53	0.56	0.66	0.54	1.00	0.53	0.53	1.00	0.72
61	0.99	0.96	1.00	0.97	0.91	0.91	1.20	0.35	1.28	0.88	0.42	0.68	0.40	0.38	0.40	0.67	0.40	0.98	0.39	0.39	0.98	0.50
62	1.00	0.99	1.00	0.99	0.98	0.98	1.39	0.77	1.35	0.79	0.79	0.99	0.78	0.78	0.78	0.76	1.00	0.78	1.00	0.78	1.00	0.82
63	0.97	0.94	1.00	0.95	0.91	0.91	1.62	0.67	1.71	0.99	0.57	1.08	0.64	0.66	0.59	1.08	0.64	0.97	0.66	0.64	0.97	0.69
64	0.98	0.95	1.00	0.96	0.90	0.90	1.32	0.70	1.46	0.84	0.75	0.84	0.67	0.69	0.72	0.85	0.68	0.97	0.69	0.67	0.97	0.71
65	1.00	0.98	1.00	0.99	0.98	0.97	1.66	0.59	1.94	1.16	0.54	1.08	0.60	0.58	0.57	1.10	0.57	0.99	0.55	0.57	0.99	0.73
66	0.99	0.96	1.00	0.97	0.89	0.89	1.36	0.40	1.40	0.77	0.64	0.86	0.56	0.56	0.62	0.87	0.57	0.98	0.56	0.56	0.98	0.56
67	1.00	0.98	1.00	0.99	0.96	0.96	1.46	0.61	1.49	0.76	0.65	0.91	0.63	0.62	0.58	0.91	0.63	0.99	0.62	0.62	0.99	0.63
68	1.00	0.99	1.00	0.99	0.98	0.98	1.20	0.91	1.48	0.77	0.89	0.98	0.89	0.89	0.90	0.98	0.90	0.99	0.89	0.88	0.99	0.93
69	0.97	0.93	1.00	0.95	0.88	0.87	1.32	0.56	1.47	0.93	0.41	0.82	0.55	0.56	0.40	0.83	0.56	0.97	0.56	0.56	0.97	0.56
70	1.00	0.99	1.00	0.99	0.97	0.97	1.25	0.69	1.38	0.90	0.63	0.84	0.64	0.66	0.65	0.85	0.66	0.99	0.66	0.66	0.99	0.73
71	0.99	0.96	1.00	0.97	0.92	0.92	1.32	0.54	1.34	0.99	0.51	0.86	0.51	0.51	0.55	0.87	0.51	0.98	0.52	0.51	0.98	0.59
72	1.00	0.99	1.00	0.99	0.97	0.97	1.20	0.72	1.53	0.98	0.71	0.80	0.71	0.70	0.71	0.82	0.71	0.99	0.71	0.71	0.99	0.77
73	0.99	0.97	1.00	0.98	0.95	0.95	1.26	0.77	1.17	0.73	0.75	0.86	0.75	0.75	0.78	0.88	0.75	0.99	0.75	0.75	0.99	0.80
74	0.95	0.92	1.00	0.93	0.88	0.88	1.55	0.48	1.66	1.04	0.55	0.91	0.51	0.51	0.55	0.91	0.51	0.95	0.51	0.51	0.95	0.53
75	0.99	0.98	1.00	0.98	0.97	0.97	1.19	0.56	1.02	0.73	0.58	0.66	0.56	0.56	0.59	0.67	0.55	0.99	0.56	0.56	0.99	0.60
76	1.00	0.98	1.00	0.99	0.93	0.95	1.47	0.56	1.60	0.93	0.59	0.88	0.56	0.56	0.58	0.88	0.56	0.99	0.55	0.56	0.99	0.69
77	0.99	0.96	1.00	0.98	0.90	0.90	1.26	0.36	1.31	0.84	0.41	0.80	0.35	0.35	0.42	0.80	0.35	0.98	0.35	0.35	0.98	0.59
78	0.95	0.90	1.00	0.93	0.83	0.83	1.32	0.36	1.36	0.59	0.41	0.83	0.36	0.36	0.42	0.83	0.36	0.95	0.36	0.36	0.95	0.51
79	1.00	1.00	1.00	1.00	0.99	0.99	1.58	0.64	1.82	1.29	0.71	1.03	0.63	0.63	0.71	1.03	0.63	1.00	0.63	0.63	1.00	0.80
80	0.99	0.97	1.00	0.98	0.94	0.94	1.29	0.57	1.27	1.07	0.71	0.85	0.59	0.58	0.62	0.85	0.59	0.99	0.59	0.59	0.99	0.64
81	0.99	0.97	1.00	0.98	0.91	0.92	1.47	0.39	1.50	0.94	0.42	0.85	0.41	0.40	0.44	0.85	0.41	0.99	0.40	0.40	0.99	0.61
82	0.97	0.93	1.00	0.95	0.89	0.89	1.53	0.35	1.53	0.64	0.39	0.90	0.37	0.36	0.38	0.90	0.37	0.96	0.37	0.37	0.96	0.53
83	0.99	0.94	1.00	0.96	0.87	0.88	1.39	0.41	1.47	1.04	0.42	0.83	0.43	0.43	0.42	0.84	0.43	0.97	0.43	0.43	0.97	0.47
84	0.99	0.96	1.00	0.97	0.92	0.92	1.55	0.36	1.61	0.65	0.41	0.95	0.38	0.38	0.40	0.95	0.38	0.98	0.38	0.38	0.98	0.52
85	1.00	0.98	1.00	0.99	0.97	0.96	1.06	0.87	1.39	1.18	0.92	0.95	0.88	0.88	0.90	0.95	0.88	0.99	0.88	0.88	0.99	0.92
86	1.00	1.00	1.00	1.00	1.00	1.00	1.15	0.85	1.20	0.76	0.84	0.85	0.81	0.84	0.85	0.87	0.84	1.00	0.84	0.84	1.00	0.87
87	1.00	1.00	1.00	1.00	1.01	1.00	1.12	0.57	0.99	1.07	0.59	0.60	0.59	0.58	0.59	0.60	0.58	1.00	0.58	0.58	1.00	0.65
88	0.98	0.95	1.00	0.97	0.92	0.92	1.56	0.70	1.63	1.23	1.00	0.96	0.74	0.71	0.91	0.95	0.74	0.98	0.72	0.72	0.98	0.76
89	1.00	0.99	1.00	0.99	0.98	0.98	1.06	0.84	0.67	0.43	0.85	0.85	0.85	0.85	0.84	0.84	0.85	1.00	0.85	0.85	1.00	0.80
90	0.97	0.91	1.00	0.94	0.84	0.83	1.58	0.55	1.63	0.75	0.43	0.90	0.55	0.55	0.42	0.90	0.60	0.96	0.55	0.55	0.96	0.52
91	0.98	0.93	1.00	0.95	0.86	0.86	1.49	0.38	1.53	0.79	0.39	0.92	0.43	0.42	0.41	0.93	0.43	0.96	0.43	0.43	0.96	0.50
92	1.00	0.97	1.00	0.98	0.92	0.91	1.58	0.48	1.58	0.78	0.55	1.05	0.48	0.48	0.55	1.05	0.48	0.99	0.48	0.48	0.99	0.65
93	1.00	0.99	1.00	1.00	0.99	0.99	1.47	0.70	1.82	1.49	0.89	0.98	0.85	0.80	0.86	0.99	0.85	1.00	0.82	0.85	1.00	0.89
94	0.99	0.99	1.00	0.99	0.98	0.98	1.13	0.83	1.24	1.15	0.86	0.89	0.83	0.83	0.85	0.88	0.84	0.99	0.83	0.83	0.99	0.88
95	1.00	0.98	1.00	0.99	0.96	0.96	1.33	0.45	1.32	0.64	0.47	0.85	0.46	0.46	0.47	0.85	0.46	0.99	0.46	0.47	0.99	0.65
96	0.98	0.93	1.00	0.95	0.85	0.86	1.55	0.38	1.58	0.88	0.41	0.95	0.40	0.39	0.40	0.96	0.40	0.97	0.40	0.40	0.97	0.50
97	1.00	0.99	1.00	0.99	0.99	0.99	1.17	0.56	1.96	2.15	0.54	0.75	0.56	0.56	0.54	0.75	0.56	1.00	0.57	0.56	1.00	0.72
98	1.00	0.99	1.00	0.99	0.97	0.97	1.61	0.55	1.56	0.89	0.60	1.06	0.61	0.58	0.60	1.05	0.58	1.00	0.65	0.61	1.00	0.71
99	0.96	0.89	1.00	0.92	0.81	0.81	1.46	0.33	1.47	0.46	0.39	0.86	0.32	0.32	0.36	0.86	0.33	0.95	0.32	0.32	0.95	0.52
100	0.97	0.91	1.00	0.94	0.81	0.81	1.31	0.39	1.32	0.75	0.47	0.82	0.40	0.39	0.47	0.82	0.40	0.96	0.40	0.40	0.96	0.48

CumRAE for all interpolators at 100 randomly generated sparse configuration of random censoring and noise for the second study

(RE) Test 3b on the hybrid morphology. The columns are our selected methods identified by SM<Id> in Table 3.1 on page 100.

Selected from our first study (UEs), Krig_GMTquadloess (SM01) is our seamount interpolator and GMTboxcar (SM02) is our ridge interpolator. GMT SIT (EM31) is our benchmark. A value of 1.00 (middle green) indicates equal performance to the benchmark, values greater than 1.00 (dark green) performed worse than the benchmark, and values less than 1.00 (light green), performed better than the benchmark. For each level, the minimum CumRAE is annotated in red. CumRAE allows for direct comparison between methods.

6.3 Friedman’s Test

In this section, we utilize the Friedman’s test to examine when and why different DBM algorithms succeed or fail. The Friedman’s test allowed us to compare the variations in the different test cases by removing the effects of the different input configurations from the analysis so that the effects of the interpolation scheme **which is of main interest** may be investigated. This section is divided into a suite of subsections, with each subsection highlighting a specific investigative finding.

We used Friedman’s test rankings to compare our selected set of interpolation schemes rather than cross-validation because of computational constraints. We utilize Tukey’s HSD correction (Milton & Arnold, 2003; Montgomery, 2017) to remedy increased experiment-wise error from multiple comparisons – too many comparisons in a single test increases the experiment-wise error rate.

The six subsections each have a figure showing their results through a set of lettered panels. Panels

- (a) and (b) are Friedman’s ANOVAs,
- (c) and (d) are post-hoc analyses of multiple comparisons with Tukey’s HSD correction, and
- (e) and (f) are RMS boxplots.

Furthermore, the panels are grouped by the second study tests, where panels

- (a), (c), and (e) are Test 3a random configurations (left-hand side) and
- (b), (d), and (f) are Test 3b sparse configurations (right-hand side).

In each figure, we list the interpolation schemes utilized and summarize which had significantly lower median CumRAE. The significance level was $\alpha = 0.05$ for all

tests. All inferences were made with 95% confidence. Table 6.6 summarizes the Friedman’s tests performed in the following sections.

Table 6.6

Friedman’s Tests Performed to Evaluate Nominal-Informed Modeling and Ensembles in our Second Study (REs).

Id	Abbreviation		Title	Description
1	NI		Importance of Nominal-Informed Modeling	Compares feature-favoring DBMs and their ensembles to the current GMT SIT standard.
2	PR		Importance of Post-Regression with Nominal-Informed Models	Compare estimating a final DBM from an ELS or OLS fit on a DBM to see if post-regressing DBMs is beneficial.
3	Importance of Regressing on Accurate Data with Nominal-Informed Models:			Compares estimating a final DBM from an ELS or OLS fit on data of different accuracy to see if selection of regressed data matters.
	1	ADall	Compare Five (5) Interpolators	Compare OLS fit of a nominal-informed model on inputs to DBMs.
	2	ADsubset	Compare Four (4) Interpolators	Compare only post-regressed DBMs from Test 3.2 to reduce experiment-wise error to see if nominal-informed feature-favoring DBMs or their ensembles are more beneficial.
4	AII		Importance of Utilizing All Influential Information	Compare utilizing information from both disagreeing classifiers to that of either to see if beneficial.
5	AIP		Importance of Utilizing All Influential Primitives in the ELS Regression Model when Estimating from Fit	Compare different nominal-informed models in estimating a final DBM from an ELS fit (post-regressing) on an ensemble DBM to see if a fully nominal-informed model is more beneficial.
6	wE		Importance of w-ESL over ELS	Compares w-ELS to ELS to see why w-ELS is preferred.

Friedman’s tests presented in sections 6.3.1 through 6.3.6, corresponding to Id and title. Findings are discussed in section 6.4.

A brief review of terminology (as regarded to generating a DBM):

- Un-informed (interpolator/DBM or model): does not use nominal information in modeling (uses de facto standard GMT SIT [EM31])
- Nominal-informed (interpolator/DBM or model): uses nominal information to guide DBM construction.
 - Partially informed: uses only part of available nominal data (e.g., use information from 1 classifier)
 - Fully informed: utilizes all nominal information provided by all classifiers.
- Feature-favoring: interpolator shows aptitude for a given geomorphology.

- Disagreeing/conflicting classifiers/DBMs/nominal data: multiple classifiers produce different classification (nominal) values for the same data. DBMs generated for different nominal values disagree/conflict.

Table 6.7

Cheat Sheet: Friedman's Tests for our Second Study (REs) Test 3a and 3b.

Subsection 1 (NI) Importance of Nominal-Informed Modeling		
SM01		DBM _(S)
SM02		DBM _(R)
SM03		DBM _(B)
SM04	Mean	DBM _(E)
SM06	w-ELS	DBM _(E) ~ Custom Model; extracts w
SM08	ELS	DBM _(E) ~ Custom Model; uses fit
SM10	OLS	Input ~ Custom Model
Subsection 2 (PR) Importance of Post-Regressing with a Nominal-Informed Model		
SM01		DBM _(S)
SM02		DBM _(R)
SM03		DBM _(B)
SM06	w-ELS	DBM _(E) ~ Custom Model; extracts w
SM08	ELS	DBM _(E) ~ Custom Model; uses fit
SM10	OLS	Input ~ Custom Model
SM13	OLS	DBM _(S) ~ Custom Model
SM14	OLS	DBM _(R) ~ Custom Model
SM17	OLS	DBM _(B) ~ Custom Model
Subsection 3.1 (ADall) Importance of Regressing on Accurate Data with a Nominal-Informed Model: Compare Five Interpolators		
SM08	ELS	DBM _(E) ~ Custom Model; uses fit
SM10	OLS	Input ~ Custom Model
SM13	OLS	DBM _(S) ~ Custom Model
SM14	OLS	DBM _(R) ~ Custom Model
SM17	OLS	DBM _(B) ~ Custom Model
Subsection 3.2 (ADsubset) Importance of Regressing on Accurate Data with a Nominal-Informed Model: Compare Four Interpolators		
SM08	ELS	DBM _(E) ~ Custom Model; uses fit
SM13	OLS	DBM _(S) ~ Custom Model
SM14	OLS	DBM _(R) ~ Custom Model
SM17	OLS	DBM _(B) ~ Custom Model
Subsection 4 (All) Importance of Utilizing All Influential Information (Feature-favoring DBMs and Primitives in Model)		
SM08	ELS	DBM _(E) ~ Custom Model; uses fit
SM11	OLS	DBM _(S) ~ Seamount Model
SM12	OLS	DBM _(R) ~ Ridge Model
Subsection 5 (AIP) Importance of Utilizing All Influential Primitives when Estimating from ELS Fit		
SM04	Mean	DBM _(E)
SM07	ELS	DBM _(E) ~ Planar Model; uses fit
SM08	ELS	DBM _(E) ~ Custom Model; uses fit
SM15	ELS	DBM _(E) ~ Seamount Model; uses fit
SM16	ELS	DBM _(E) ~ Ridge Model; uses fit
Subsection 6 (wE) Importance of w-ELS over ELS		
SM03		DBM _(B)
SM04	Mean	DBM _(E)
SM05	w-ELS	DBM _(E) ~ Custom Model; extracts w
SM06	w-ELS	DBM _(E) ~ Custom Model; extracts w
SM07	ELS	DBM _(E) ~ Planar Model; uses fit
SM08	ELS	DBM _(E) ~ Custom Model; uses fit

Quick reference guide of investigated interpolators. Shorthand identifies DBMs and model (~ denotes regression).

6.3.1 Study 2 Subsection 1: Importance of Nominal-Informed Modeling (NI)

In this first Friedman’s investigative section (NI), we compare interpolators to investigate the importance of **nominal-informed** modeling. Nominal-informed modeling includes the use of nominal data to select feature-favoring interpolators for feature-favoring DBMs and design regression model. The seven interpolators chosen to investigate the efficacy of nominal-informed modeling are:

1. seamount interpolator Krig_GMTquadloess (SM01),
2. ridge interpolator GMTboxcar (SM02),
3. benchmark interpolator GMT SIT (SM03),
4. un-informed equally weighted ensemble (SM04),
5. w -ELS custom model extracting w (SM06),
6. ELS custom model using fitted regression (SM08), and
7. OLS custom model on input soundings (SM10).

The first three interpolators are single interpolators. The first two were selected from the first study (UEs) according to nominal data as the feature-favoring seamount (SM01) and ridge (SM02) interpolators to produce nominal-informed feature-favoring $\text{DBM}_{(S)}$ and $\text{DBM}_{(R)}$. The third is our chosen un-informed benchmark interpolator GMT SIT (SM03) producing an un-informed $\text{DBM}_{(B)}$ and is the only interpolator that is completely un-informed by the nominal data.

The fourth is our un-informed equally weighted ensemble (SM04) where the ensemble weights are un-informed, but the ensemble members are the nominal-informed feature-favoring DBMs. The remaining three (SM06, SM08, and SM10) utilize a fully

nominal-informed custom regression model whereby its composition was informed by the nominal data. Of the last three methods, the custom model is fit on the ensemble DBM ($\text{DBM}_{(E)}$) for both w -ELS (SM06) and ELS (SM08) method, and on the scattered input soundings for the OLS (SM10) method.

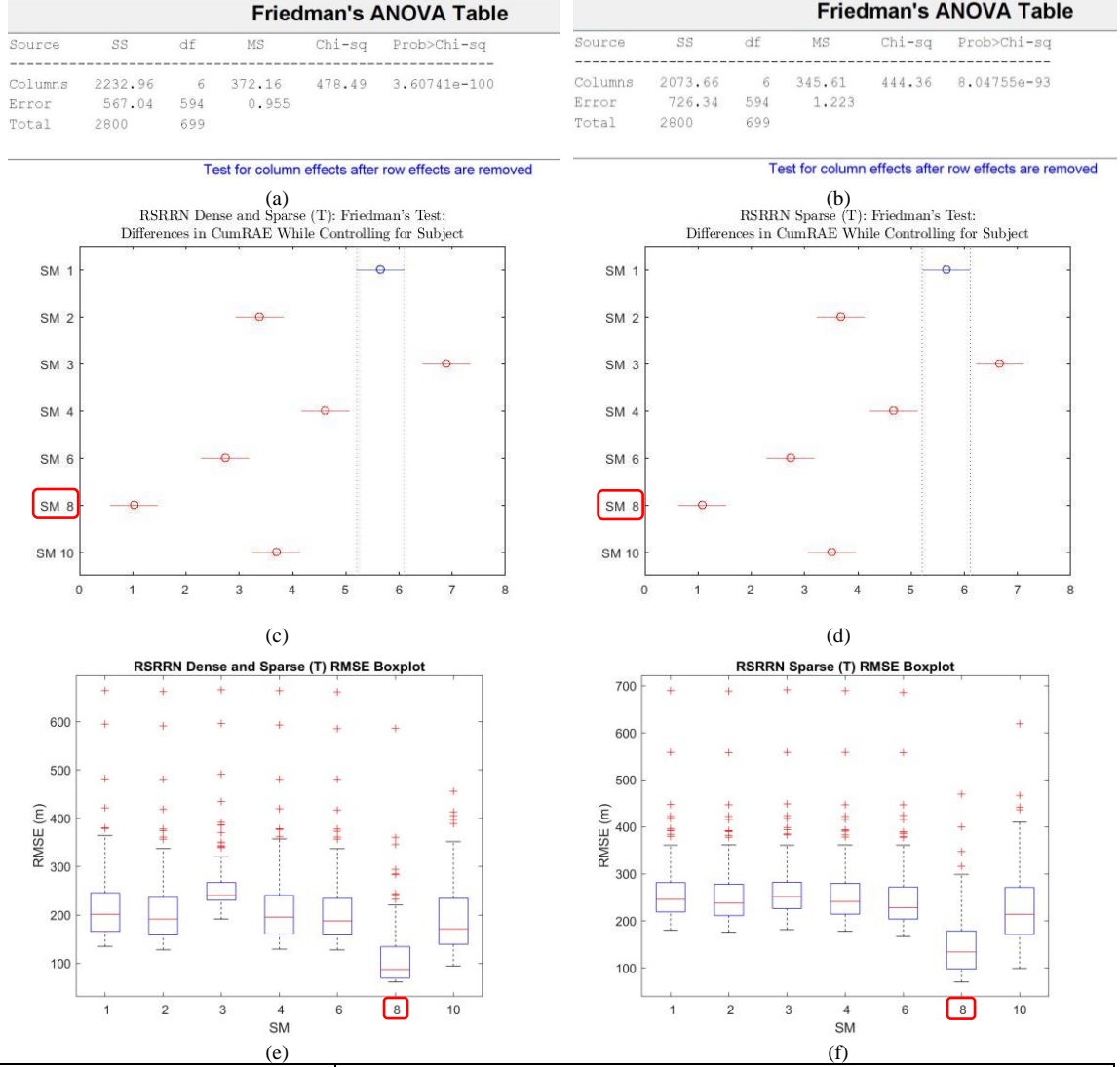
All the ensemble methods (SM04, SM06, and SM08) combine the nominal-informed feature-favoring DBMs ($\text{DBM}_{(S)}$ and $\text{DBM}_{(R)}$) in some manner to produce a final ensemble DBM (DBM_E). The w -ELS (SM06) method computes weight w and weights $\text{DBM}_{(S)}$ and $\text{DBM}_{(R)}$ in an informed differentially weighted ensemble for the final ensemble DBM ($\text{DBM}_{(E)}$). The ELS (SM08) method estimates a final DBM_E from a regressed fit on an unascertained $\text{DBM}_{(E)}$, having an unknown weighting of $\text{DBM}_{(S)}$ and $\text{DBM}_{(R)}$, instead of extracting a weight w as in w -ELS. Since w -ELS is intrinsically ELS, it also models on an unascertained $\text{DBM}_{(E)}$ before constructing a final $\text{DBM}_{(E)}$.

These seven interpolators were chosen to investigate the following questions (comparisons to investigate):

- Can we improve performance over the benchmark by using nominal data to select feature-favoring interpolators?
 - Does either SM01 or SM02 outperform SM03?
- Can ensembles outperform the single interpolators?
 - Does either SM04, SM06, or SM08 outperform SM03?
 - Does either SM04, SM06, or SM08 outperform SM01 or SM02?
- Can ensembles benefit from a nominal-informed differential weighting?
 - Does either SM06 or SM08 outperform SM04?

- How beneficial is utilizing a nominal-informed custom model?
 - How does SM10 compare to the rest?
 - How does SM06 compare to SM08?

Figure 6.3 shows the results of our first Friedman’s investigative subsection 6.3.1 (NI). Red boxes indicate the interpolator that was most accurate for each configuration set (both Test 3a and 3b). In both (a-b) Friedman’s ANOVAs, there is a statistical difference between interpolators, and both multiple comparisons (c-d) are nearly the same. Boxplots (e-f) show larger values for Test 3b sparse configurations (f), giving larger medians for all interpolators except our benchmark GMT SIT (SM03) and resulted in more stable medians and IQRs (dispersions) between the interpolators. Estimating a final ensemble DBM ($\text{DBM}_{(E)}$) from an ELS custom model fit (SM08) was the most accurate (c-d) and had the lowest median RMS (e-f), on average.



SM01	Krig_GMTquadloess (seamount interpolator) $DBM_{(S)}$
SM02	GMTboxcar (ridge interpolator) $DBM_{(R)}$
SM03	GMT SIT (benchmark interpolator) $DBM_{(B)}$
SM04	Mean (un-informed equally weighted ensemble) $DBM_{(E)} \sim (0.5)DBM_{(S)} + (0.5)DBM_{(R)}$
SM06	w-ELS (Custom Model) (nominal-informed differentially weighted ensemble) $DBM_{(E)} \sim$ Custom Model; extracts w
SM08	ELS (Custom Model) (nominal-informed regression on ensemble DBM) $DBM_{(E)} \sim$ Custom Model; uses fit
SM10	OLS on input soundings (Custom Model) (nominal-informed regression on input soundings) Input \sim Custom Model

Figure 6.3 Study 2 subsection 6.3.1 (NI) results on the truncated hybrid.

(a-b) Friedman's ANOVAs, (c-d) post-hoc analyses of multiple comparisons with Tukey's HSD correction, and (e-f) RMS boxplots. (a), (c), and (e) are Test 3a random configurations. (b), (d), and (f) are Test 3b sparse configurations. We list interpolation schemes utilized. Red boxes indicate the interpolator with the best accuracy for each configuration set.

Figure 6.4 takes a closer look at Figure 6.3d, of which findings will apply to both sets of configurations (Test 3a and 3b).

At the top, we have our two selected nominal-informed feature-favoring seamount (SM01) and ridge (SM02) interpolators, annotated in red in Figure 6.4, followed by the un-informed benchmark GMT SIT (SM03). The nominal-informed feature-favoring truncated seamount interpolator (SM01) had worse accuracy than the other nominal-informed feature-favoring ridge interpolator (SM02), but both nominal-informed interpolators (SM01 and SM02) performed better than the un-informed benchmark GMT SIT (SM03), which was the least accurate of the seven interpolators. This result is both important and worrisome; GMT SIT is one of the most utilized methods.

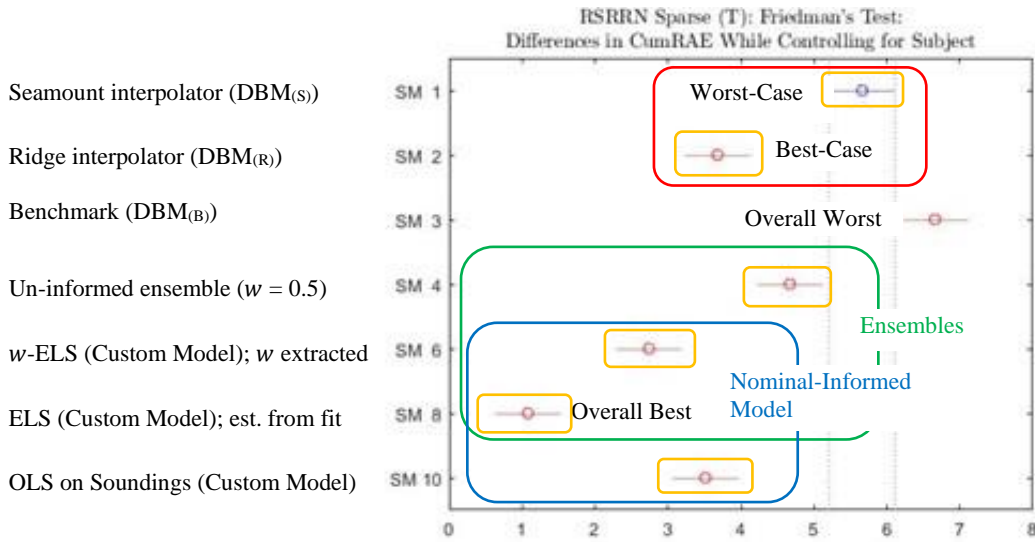


Figure 6.4 Analysis of subsection 6.3.1 (NI).

Analysis of Figure 6.3d. Inferences apply to both second study (RE) Test 3a and 3b configurations. These interpolators investigate the importance of nominal-informed models. Feature-favoring interpolators (red), ensembles (green), and nominally informed interpolators (blue) are indicated, along with the overall worst and best performing interpolators, according to CumRAE.

The ridge interpolator (SM02) had better accuracy than the seamount interpolator (SM01) which is contrary to our hybrid composition of 75% seamount. Since feature-favoring interpolators are not necessarily mutually exclusive to identified primitives, we constrained the selection of feature-favoring interpolators for the given nominal data to be different but not necessarily uniquely best. We know that ensembles are beneficial, in general, and from the first study (UEs), there exists scenarios where our seamount interpolator is preferred. The use of distinct, heterogenous interpolators in an ensemble encourages capturing more of the underlying geomorphology correctly. For these reasons, we posit the ridge interpolator (SM02) was able to model most of our hybrid with higher accuracy than the seamount interpolator (SM01), however, because both interpolators were feature-favoring, we know there are regions where the seamount interpolator (SM01) may have accuracies better than the ridge interpolator (SM02). Even though the seamount interpolator (SM01) did not have better accuracy than the ridge interpolator (SM02) for most of the hybrid, those areas where accuracy was better may be crucial to obtaining better accuracy than the ridge interpolator alone by mitigating its failures. Further work is needed to clarify our results in this case.

The next three interpolators are our ensembles, annotated in green in Figure 6.4, un-informed equally weighted (SM04), followed by *w*-ELS (SM06), and ELS (estimated from the fit) (SM08). The un-informed ensemble (SM04) had better accuracy than the least accurate ensemble member, the seamount interpolator (SM01), but not as well as the most accurate ensemble member, the ridge interpolator (SM02), allowing us to avoid the failures of the worse-case DBM (SM01) by averaging in an ensemble. The un-informed

ensemble (SM04) exemplified what we would typically expect of an un-informed equally weighted ensemble: accuracy that is an average of its two members. The un-informed ensemble (SM04) was statistically different from both ensemble members (SM01 and SM02), on average.

Both w -ELS (SM06) and ELS (SM08) methods are nominally-informed differential ensembles (ensembles that utilize a nominal-informed model in determining ensemble member weights), annotated in blue in Figure 6.4, with the ELS (SM08) method being the most accurate overall followed by the w -ELS (SM06) method.⁵⁷ This suggests that estimating a final DBM from an ELS fit, rather than extracting weight w to use in a w -weighted ensemble, more strongly incorporates nominal information by optimizing its utilization when estimating from a nominal-model fit. However, as we will see later in subsection 6.3.6 (wE), this strong utilization is beneficial only when the primitive functional forms utilized in the model closely approximate the geomorphology, else the more robust w -ELS is preferential.

The last compared interpolator is the OLS custom model fit on the input soundings (SM10). This is another interpolator that estimates from a nominal-informed model. The three interpolators utilizing a nominal-informed model (SM06, SM08, and SM10), annotated in blue in Figure 6.4, all performed better than the un-informed equally

⁵⁷ Recall that ELS differs from w -ELS by using the ELS algorithm to estimate the ensemble DBM from the regression fit of the nominally informed custom model on the ensemble member DBMs whereas w -ELS only uses ELS to estimate weight w of which one then extracts and utilizes to weight the ensemble DBMs externally from ELS.

weighted ensemble (SM04), suggesting utilizing a nominal-informed model (either in an ensemble or on the input soundings) is beneficial to reducing inaccuracies and improving DBMs.

The ensembles (SM04, SM06, and SM08) and the OLS nominal-informed interpolators (SM10) performed better than the benchmark GMT SIT (SM03) de facto standard in constructing DBMs. In fact, this Friedman’s investigative subsection (NI) finds that interpolators utilizing any nominal information via either the feature-favoring interpolators, a nominal-informed model, or both were more accurate than the benchmark GMT SIT (SM03) de facto standard for DBMs.

Figure 6.4 shows the importance of modeling smarter by utilizing all available information, such as the shape of the seafloor given as nominal data from classifiers in disagreement. First, we note that accuracy improved if local regression using a quadloess window with kriging or local regression using a boxcar window without kriging followed GMT SIT. This supports our findings from the first study (UEs) (see section 5.2), and we posit that this is due to GMT SIT acting as a pre-processing step whereby it up-samples the sparse and unequally distributed soundings into a grid from which further processing with more sophisticated methods such as local regression and kriging may occur.

Secondly, the equal-weight ensemble (SM04) demonstrated how ensembles do no worse than the average of their members (SM01 and SM02), helping us to avoid the worst-case scenario of utilizing a DBM with higher inaccuracies (SM01), on average. Interestingly, our w -weighted ensemble (SM06) was not significantly different from the best-performing ensemble member (SM02), on average. We posit that this is due to

restricting our ensembles to two members. Ensembles shine when there are many diverse members from which bias and variance may be averaged out.

Even more interestingly, OLS with input soundings (SM10) was not significantly different from the best performing ensemble member (SM02) or the equal-weighted ensemble (SM04), on average. This shows the power of nominal-informed modeling. The regression model, inferred from the nominal values discovered by the classifiers as a weighted combination of primitives, was accurate enough to allow the modeling of the scattered soundings in a parametric OLS regression to rival the single non-parametric regression techniques being compared where it had better accuracy than two of those interpolators (SM01 and SM03) and was comparable to the other (SM02). If we, instead, estimate a DBM from the fit of the custom weighted-primitive model to a weighted ensemble of DBMs (SM08), we significantly increased the accuracy over that of regressing on the scatter soundings (SM10), making ELS (SM08) the most accurate, outperforming all other methods, on average.

We further investigate the effects of nominal-informed modeling with six additional Friedman’s investigative subsections. The first takes a closer look at fitting the custom weighted-primitive model to DBMs (what we call post-regressing), the next two tests look at the accuracy of the data on which we regress when fitting the model, the fourth looks at utilizing all information from disagreeing classifiers instead of selecting one, the fifth looks at the importance capturing all influential primitives in the model, and the sixth looks at when w -ELS is preferential over ELS.

6.3.2 Study 2 Subsection 2: Importance of Post-Regressing with a Nominal-Informed Model (PR)

In this second Friedman’s investigative subsection (PR), we compare interpolators to investigate the importance of **p**ost-**r**egressing DBMs with a nominal-informed model.

These nine interpolators are:

1. seamount interpolator Krig_GMTquadloess (SM01),
2. ridge interpolator GMTboxcar (SM02),
3. benchmark interpolator GMT SIT (SM03),
4. w -ELS custom model extracting w (SM06),
5. ELS custom model using fitted regression (SM08),
6. OLS custom model on input soundings (SM10),
7. OLS custom model on seamount DBM (SM13),
8. OLS custom model on ridge DBM (SM14), and
9. OLS custom model on benchmark DBM (SM17).

Again, the first three interpolators are the single interpolators; the first two were selected from the first study (UEs) as the feature-favoring seamount (SM01) and ridge (SM02) interpolators producing $\text{DBM}_{(S)}$ and $\text{DBM}_{(R)}$, and the third is the chosen benchmark interpolator (SM03) producing $\text{DBM}_{(B)}$. The next two are our informed ensemble w -ELS (SM06) and ELS (SM08) both utilizing a custom model fit to the ensemble $\text{DBM}_{(E)}$ of unascertained ensemble weights. The remaining four are nominal-informed OLS methods each utilizing the custom model. The first of these four fits to the

input soundings (SM10), while the last three methods fit to the DBMs produced by the seamount (SM13), ridge (SM14), and benchmark GMT SIT (SM17) interpolators.

These nine interpolators were chosen to investigate the following questions (comparisons to investigate):

- Can post-regressing DBMs improve performance?
 - Does SM13, SM14, and SM17 have better accuracy than SM01, SM02, and SM03, respectively?
- Do post-regressing benefits depend on the DBM?
 - How does SM08 compare to SM13, SM14, and SM17?
- How does simply regressing the nominal-informed model on the sampling inputs compare to post-regressing on DBMs?
 - How does SM10 compare to SM13, SM14, and SM17?
- How does post-regressing DBMs compare to our *w*-ELS (SM06)?
 - How does SM06 compare to the rest?

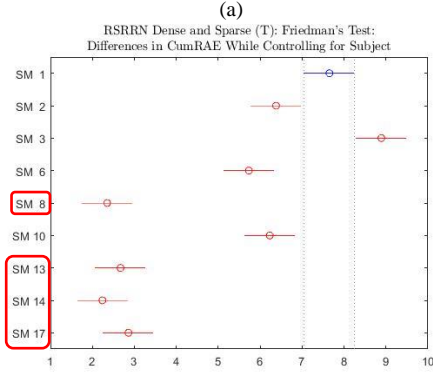
Figure 6.5 shows the results of this second Friedman’s investigative subsection (PR) and demonstrates the importance of post-regressing DBMs with a nominal-informed model, to estimate a final DBM from the fit. Red boxes indicate comparable interpolators that were most accurate for each configuration set (Test 3a and 3b). In both (a-b) Friedman’s ANOVAs, there is a statistical difference between interpolators. There are differences between the relative performance of the first three interpolators in the multiple comparisons (c-d) between configurations (Test 3a and 3b), but these differences do not affect inferences made and are due to experiment-wise error. The relative

performance of the first three interpolators was determined in the first Friedman's investigative section 6.3.1 (NI).

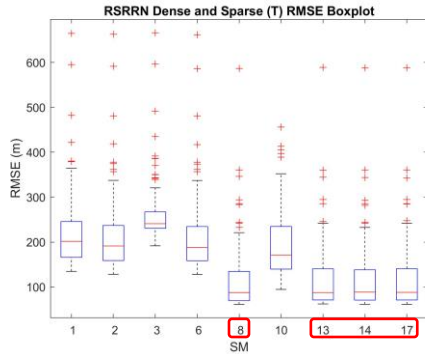
Boxplots (e-f) show larger values for Test 3b sparse configurations (f) giving larger medians for all interpolators except our benchmark GMT SIT (SM03) and resulted in more stable medians and IQRs (dispersions) between the interpolators. Our post-regressed DBMs (SM08, SM13, SM14, and SM17) were the best performing (c-d) and had the lowest median RMS (e-f), on average.

Friedman's ANOVA Table					
Source	SS	df	MS	Chi-sq	Prob>Chi-sq
Columns	5075.34	8	634.418	676.71	7.37366e-141
Error	924.66	792	1.167		
Total	6000	899			

Test for column effects after row effects are removed



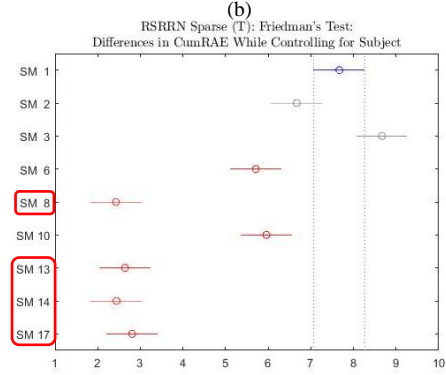
(c)



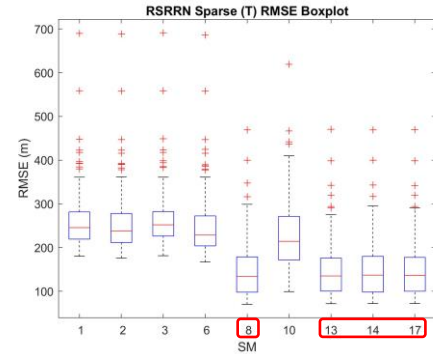
(e)

Friedman's ANOVA Table					
Source	SS	df	MS	Chi-sq	Prob>Chi-sq
Columns	4833.66	8	604.207	644.49	6.33376e-134
Error	1166.34	792	1.473		
Total	6000	899			

Test for column effects after row effects are removed



(d)



(f)

SM01	Krig_GMTquadloess (seamount interpolator) DBM _(S)
SM02	GMTboxcar (ridge interpolator) DBM _(R)
SM03	GMT SIT (benchmark interpolator) DBM _(B)
SM06	w-ELS (Custom Model) (nominal-informed differentially weighted ensemble) DBM _(E) ~ Custom Model; extracts w
SM08	ELS (Custom Model) (nominal-informed regression on ensemble DBM) DBM _(E) ~ Custom Model; uses fit
SM10	OLS on input soundings (Custom Model) (nominal-informed regression on input soundings) Input ~ Custom Model
SM13	OLS (Custom Model) on seamount DBM (seamount interpolator) DBM _(S) ~ Custom Model
SM14	OLS (Custom Model) on ridge DBM (ridge interpolator) DBM _(R) ~ Custom Model
SM17	OLS (Custom Model) on benchmark DBM (benchmark interpolator) DBM _(B) ~ Custom Model

Figure 6.5 Study 2 subsection 6.3.2 (PR) results on the truncated hybrid.

(a-b) Friedman's ANOVAs, (c-d) post-hoc analyses of multiple comparisons with Tukey's HSD correction, and (e-f) RMS boxplots.

(a), (c), and (e) are Test 3a random configurations. (b), (d), and (f) are Test 3b sparse configurations. We list the interpolation schemes utilized. Red boxes indicate comparable interpolators with the best accuracy for each configuration set.

We take a closer look at Figure 6.5d in Figure 6.6, of which our findings will apply to both sets of configurations (Test 3a and 3b). Although there are differences between Figure 6.5 (c) and (d), the inferences made herein are unaffected.

At the top Figure 6.6, we have our DBMs from the two selected feature-favoring seamount (SM01) and ridge (SM02) interpolators followed by the DBM from the benchmark GMT SIT interpolator (SM03), and our *w*-ELS ensemble (SM06), annotated in solid red. These methods (SM01, SM02, SM03, and SM06) produce DBMs that are not post-regressed with our custom model. Their post-regressed DBM counterparts (SM08, SM13, SM14, and SM17) are annotated dashed red. OLS regression of the custom model on input soundings (SM10) is annotated in purple.

The post-regressed methods (SM08, SM13, SM14, and SM17) (dashed red) had the lowest inaccuracies and were comparable to each other. Each post-regressed DBM (SM08, SM13, SM14, and SM17) (dashed red) was not only significantly more accurate than its non-regressed DBM counterpart (SM01, SM02, SM03, and SM06) (solid red) but significantly more accurate than all the non-post-regressed DBMs (solid red) and regressing on scattered soundings (SM10) (purple), on average.

Utilizing the nominal-informed model on the input soundings (SM10) was again comparable to *w*-ELS (SM06), suggesting the simpler computations of OLS utilizing the nominal-informed model on input soundings (SM10) nets similar accuracy to that of differentially weighting DBMs via our *w*-ELS (SM06). However, both incurred worse accuracy than any of the post-regressed DBM methods (SM08, SM13, SM14, and SM17), further supporting the importance of post-regressing the nominal-informed model

on DBMs for accuracy gains and not just the utilization of the nominal-informed model either inherently in ELS to estimate the extracted weight w or in OLS on input soundings.

The comparability of the post-regressed DBMs suggests similar accuracy regardless of DBM selection (whether either feature-favoring, benchmark, or an ensemble DBM). These findings are examined further in the next two Friedman’s investigative subsections where we investigate accuracy when regressing the custom model on the different data (DBMs and input soundings).

The results from this Friedman’s investigative subsection (PR) suggest post-regressing on non-parametric DBMs with a nominal-informed model is beneficial, on average. As noted previously, post-regressing a DBM will more strongly incorporate nominal information by optimizing its utilization, but as we will see later when comparing ELS with w -ELS in subsection 6.3.6 (wE), this strong utilization is beneficial only when the primitive functional forms closely approximate the geomorphology, else we may incur worse performance.

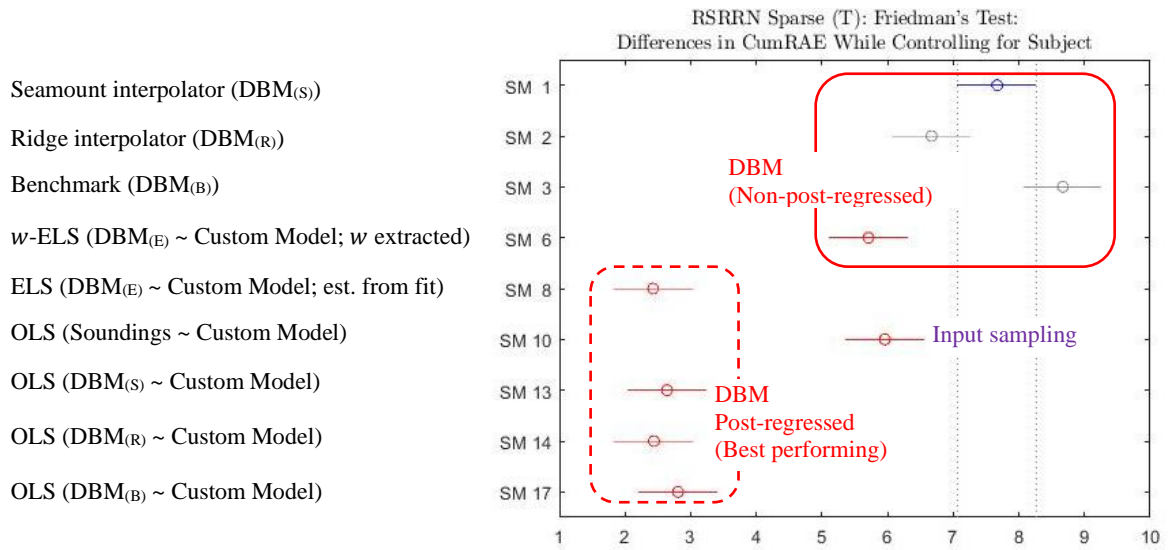


Figure 6.6 Analysis of subsection 6.3.2 (PR).

Analysis of Figure 6.5d. Inferences apply to both second study (RE) Test 3a and 3b configurations. These interpolators investigate the importance of post-regressing on a DBM. Post-regressed DBMs (dashed red) were the best performing and were comparable to each other. Non-post-regressed DBMs (solid red) performed worse than their post-regressed counterparts (dashed red).

6.3.3 Study 2 Subsection 3: Importance of Regressing on Accurate Data with a Nominal-Informed Model when Estimating from Fit

In this section, we further investigate the findings subsection 6.3.2 (PR), where accuracy in post-regressing DBMs did not depend on the DBM selected, by investigating the general question of whether data accuracy upon which we regress a completely nominal-informed model to estimate a final DBM from is important.

Two Friedman's tests are performed in this section, and the interpolators utilized are a subset of those from the Friedman's investigative subsection 6.3.2 (PR). Friedman's investigative subsection 6.3.3.1 compares five interpolators (ADall) of which Friedman's investigative subsection 6.3.3.2 compares four of the interpolators (ADsubset).

Comparing the set of minimal interpolators needed for each investigation ensures experiment-wise error is kept minimal to not obscure statistical differences.

6.3.3.1 Study 2 Subsection 3.1: Comparing Five Interpolators (ADall)

In this Friedman’s investigative subsection (ADall), we compare five interpolators to investigate the importance of regressing on **accurate data** with a nominal-informed model when estimating a final DBM from the fit. These interpolators were also a subset of subsection 6.3.2 (PR) which investigated post-regressing on DBMs where those regressing on DBMs (SM08, SM13, SM14, and SM17) were found comparable, having the lowest inaccuracies. Here, we investigate a different and more general question: is the nominal-informed model sensitive to accuracy of the regressed data when estimating a final DBM from the fit? The five interpolators are:

1. ELS custom model using fitted regression (SM08),
2. OLS custom model on input soundings (SM10),
3. OLS custom model on seamount DBM (SM13),
4. OLS custom model on ridge DBM (SM14), and
5. OLS custom model on benchmark DBM (SM17).

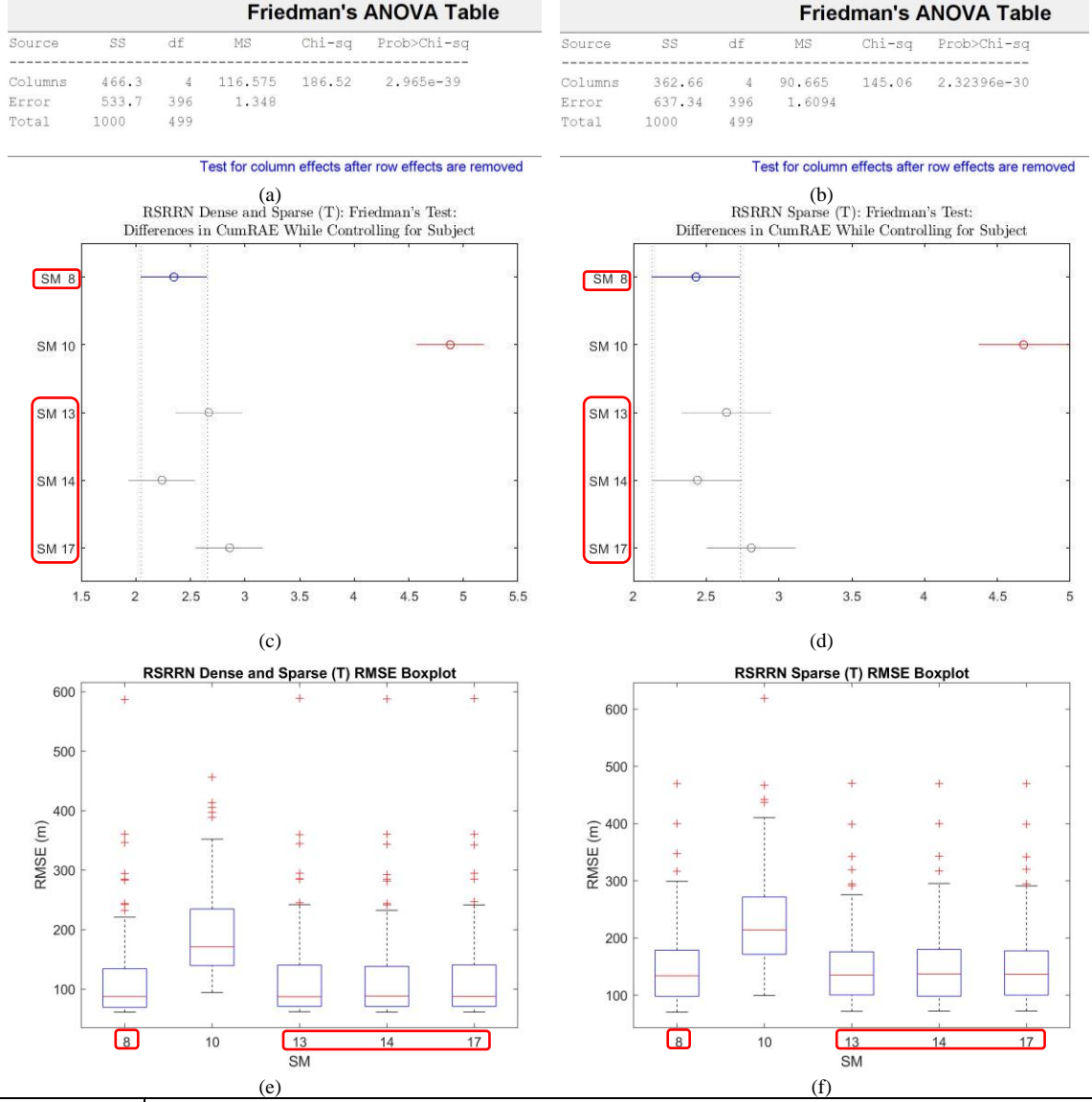
All interpolators utilize the fully nominal-informed custom model, each fit on different data to estimate a final DBM. The first interpolator ELS (SM08) fits on the unascertained weighted ensemble of the seamount and ridge DBMs and the second interpolator OLS (SM10) fits on the input soundings. The remaining three interpolators fit on the DBMs produced from the seamount (SM13), ridge (SM14), and benchmark GMT SIT (SM17) interpolators.

These five interpolators were chosen to investigate the following questions (comparisons to investigate):

- Does regressing with a nominal-informed model depend on the accuracy of the data upon which is regresses when estimating a final DBM?
 - How does SM10 compare to the rest?
 - How does SM08, SM13, SM14, and SM17 compare?

We expect to see results regarding the relative performance of OLS on the soundings (SM10) having worse accuracy than post-regressing DBMs (SM08, SM13, SM14, and SM17), as seen in subsection 6.3.2 (PR). However, this subsection (ADall) will take a closer look at whether those post-regressed DBMs are still comparably the most accurate or if experiment-wise error was obstructing statistical differences in accuracy.

Figure 6.7 shows the results for this Friedman's investigative subsection (ADall). Red boxes indicate comparable interpolators that were most accurate for each configuration set (Test 3a and 3b). In both (a-b) Friedman's ANOVAs, there is a statistical difference between interpolators and both the multiple comparisons (c-d) are nearly the same. Boxplots (e-f) show larger values for Test 3b sparse configurations (f) giving larger medians for all interpolators and resulted in more stable medians and IQRs (dispersions) between the interpolators. Our post-regressed DBMs (SM08, SM13, SM14, and SM17) were comparable, having the lowest inaccuracies (c-d) and the lowest median RMS (e-f), on average. These findings match those found in subsection 6.3.2 (PR).



SM08	ELS (Custom Model) (nominal-informed regression on ensemble DBM) DBM _(E) ~ Custom Model; uses fit
SM10	OLS on input soundings (Custom Model) (nominal-informed regression on input soundings) Input ~ Custom Model
SM13	OLS (Custom Model) on seamount DBM (seamount interpolator) DBM _(S) ~ Custom Model
SM14	OLS (Custom Model) on ridge DBM (ridge interpolator) DBM _(R) ~ Custom Model
SM17	OLS (Custom Model) on benchmark DBM (benchmark interpolator) DBM _(B) ~ Custom Model

Figure 6.7 Study 2 subsection 6.3.3.1 (ADall) results on the truncated hybrid.

(a-b) Friedman's ANOVAs, (c-d) post-hoc analyses of multiple comparisons with Tukey's HSD correction, and (e-f) RMS boxplots.

(a), (c), and (e) are Test 3a random configurations. (b), (d), and (f) are Test 3b sparse configurations. We list the interpolation schemes utilized. Red boxes indicate comparable interpolators with the best accuracy for each configuration set.

Clearly, regressing the nominal-model on input soundings (SM10) is the most inaccurate, as expected from subsection 6.3.2 (PR). Intuitively, this makes sense as the DBMs (post-regressed upon in SM08, SM13, SM14, and SM17), have already been pre-processed to remove noise and impute density, allowing for errors in post-regressed DBMs (and their estimated final DBMs) to be minimized. Non-parametric methods (either nominal-informed feature-favoring seamount or ridge interpolator, or the uninformed benchmark GMT SIT interpolator) first handle these sparse and noisy input soundings to produce DBMs, before utilizing OLS/ELS in a post-regression to estimate the final DBM. These findings are foundational to regression. In general, when regressing on data that has unequal density distributions, OLS has increased bias and variance. This is especially the case when soundings are sparse and noisy. These inaccuracies can be reduced by first utilizing better suited non-parametric methods.

This investigative subsection (ADall) was not able to differentiate between post-regressing on different DBMs, again aligning with the findings from subsection 6.3.2 (PR) where post-regressed DBMs with a nominal-informed custom model were comparable, having the least inaccurate, on average.

In summary, fitting to the soundings (SM10) was significantly less accurate than fitting to a DBM (SM08, SM13, SM14, and SM17), on average, and exemplified a fundamental tenet of regression: the more accurate the data (DBM or soundings) prior to fitting the regression model of weighted primitives, the more accurate the final DBM estimated from the fit, on average. This finding is consistent with the results in (Ladner et

al., 2017) where they iteratively remove data outliers before constructing their final DBMs.

6.3.3.2 Study 2 Subsection 3.2: Comparing Four Interpolators (ADsubset)

We continue investigating the sensitivity of estimating a final DBM from a nominal-informed model fit regarding accuracy of regressed data by specifically looking at how post-regressing on different DBMs affect accuracy when estimating the final DBM from the fully nominal-informed custom model fit.

In this Friedman’s investigative subsection (ADsubset), we compare interpolators which are a subset of both subsection 6.3.2 (PR) and subsection 6.3.3.1 (ADall) to minimize experiment-wise error (failures to identify significant differences) for a better look into whether benefits from estimating a final DBM from post-regressing a DBM with a fully nominal-informed custom model depends on DBM choice. These interpolators were found to be comparably the most accurate in our initial investigation into the benefits of post-regressing DBMs in subsection 6.3.2 (PR) and in our more general investigation into the benefits of regressing on accurate data in subsection 6.3.3.1 (ADall).

This investigative subsection (ADsubset) compares four interpolators (those which were comparable, having the best accuracy in subsection 6.3.3.1 [ADall] as well as subsection 6.3.2 [PR]):

1. ELS custom model using fitted regression (SM08),
2. OLS custom model on seamount DBM (SM13),
3. OLS custom model on ridge DBM (SM14), and

4. OLS custom model on benchmark DBM (SM17).

In subsection 6.3.3.1 (ADall), we found no difference between fitting the custom model on any DBM (ensembled [SM08], seamount [SM13], ridge [SM14], or benchmark [SM17]), only between fitting on either a DBM (SM08, SM13, SM14, and SM17) or the input soundings (SM10), where not fitting on a DBM was least accurate, on average, when estimating a final DBM from the fit.

Now, we would like to see if there were any differences in accuracy between fitting on either of the DBMs (SM08, SM13, SM14, and SM17) that were not revealed due to increased experiment-wise error from too many comparisons.

Figure 6.8 shows the results of this Friedman’s investigative subsection (ADsubset). Red boxes indicate comparable interpolators that were more accurate for each configuration set (Test 3a and 3b).

- In (a) Friedman’s ANOVA for the Test 3a random configurations, there is a statistical difference between interpolators, shown in (c).
 - For Test 3a random configurations (c), post-regressing the nominal-informed model on the ensemble DBM (SM08) and the ridge DBM (SM14) had better accuracy than post-regressing on the GMT SIT benchmark DBM (SM17), when estimating a final DBM from the fit.
- In (b) Friedman’s ANOVA for the Test 3b sparse configurations, there is no statistical difference between interpolators, resulting in all interpolators having comparable accuracy (d).

- For Test 3b sparse configurations (d), larger uncertainty caused there to be no differences between the interpolators; all interpolators performed comparable, on average. Post-regressing DBMs with a nominal-informed model to estimate a final DBM had the same accuracy regardless of the DBM regressed (whether nominal-informed or un-informed) when configurations are sparse (Test 3b), suggesting there was not enough difference in the DBMs to warrant using one over the other.

This contrasts with the findings of comparable accuracy from subsection 6.3.2 (PR) and subsection 6.3.3.1 (ADall), exemplifying the negative effects of too many comparisons increasing the experiment-wise error.

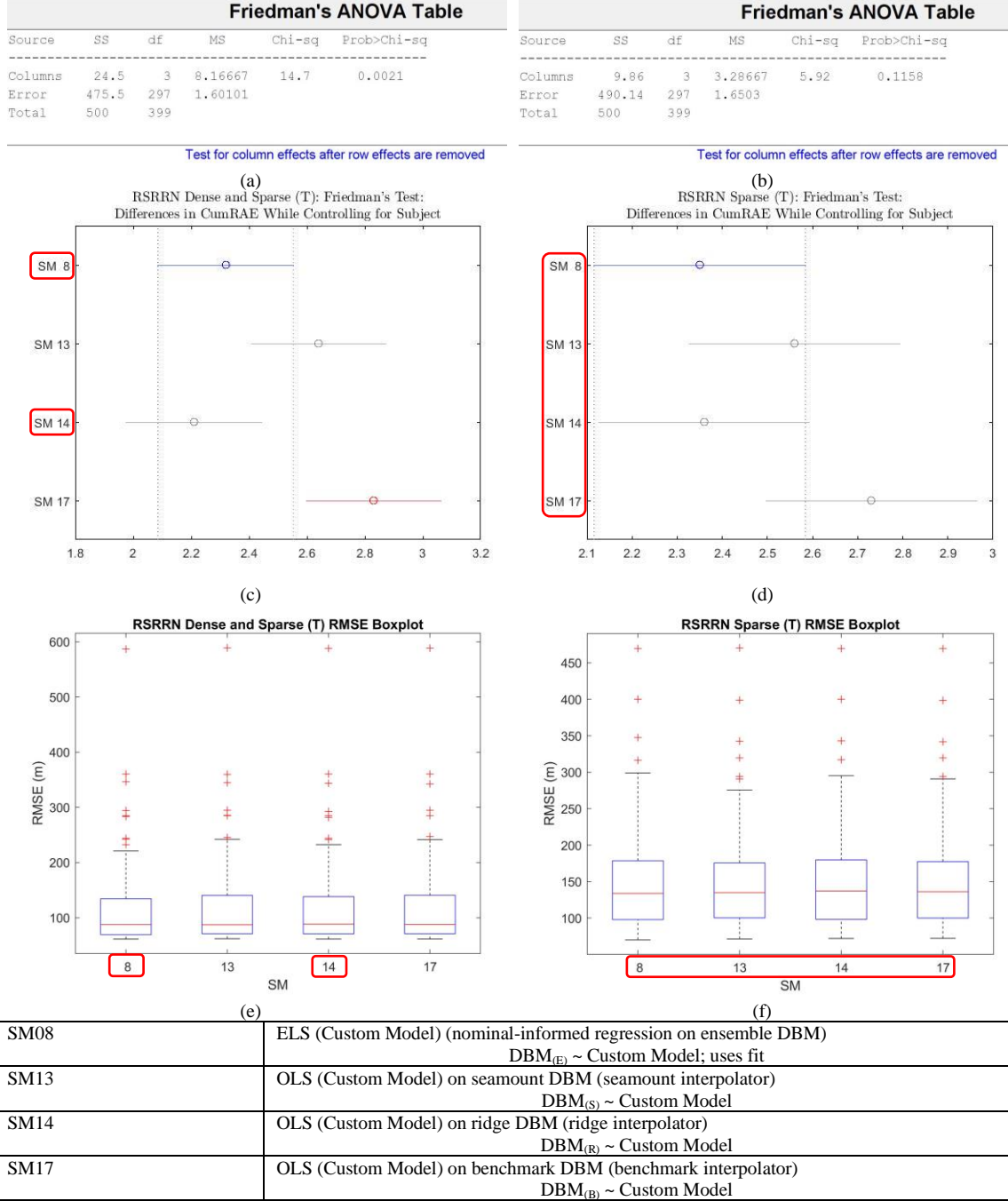


Figure 6.8 Study 2 subsection 6.3.3.2 (ADsubset) results on the truncated hybrid.

(a-b) Friedman's ANOVAs, (c-d) post-hoc analyses of multiple comparisons with Tukey's HSD correction, and (e-f) RMS boxplots.

(a), (c), and (e) are Test 3a random configurations. (b), (d), and (f) are Test 3b sparse configurations. We list the interpolation schemes utilized. Red boxes indicate comparable interpolators (c) having better accuracy than the least accurate for the Test 3a random configuration set and (d) with none having better accuracy for the Test 3b sparse configuration set.

So even though

- the accuracy of the single DBMs were statistically different, on average, depending on the nominal-information used (nominal-informed feature-favoring or un-informed) as illustrated in subsection 6.3.1 (NI), under sparsity (Test 3b),

the final DBMs estimated from post-regressing on these DBMs of different accuracy with the nominal-informed model was not. This suggests that

- the DBMs regressed provided near redundant information to the regression to where neither were able to better constrain the regression model, ergo the comparably larger uncertainties for estimated final DBMs that were not different enough in accuracy.

Under sparsity (Test 3b),

- post-regressing DBMs of different accuracy (as when utilizing different nominal-information or none) with a nominal-informed model converged to comparable accuracy for estimated final DBMs. Whereas, in the case of Test 3a random configurations (c), post-regressing the partially nominal-informed feature-favoring ridge DBM (SM14) or the fully nominal-informed ensemble (SM08) is more accurate, on average, than post-regressing the un-informed GMT SIT benchmark DBM (SM17), when estimating a final DBM.

Now, under the Test 3a random configurations (by having dense and sparse sampling configurations) (c), the nominal-informed ridge (SM14) and ensemble (SM08)

DBM provide additional information to the regression to better constrain the regression model than the un-informed GMT SIT DBM (SM17).

- Including dense configurations along with sparse in the Test 3a random configurations was enough to improve the average accuracy of these methods (SM08 and SM14), suggesting that a set of dense only configurations may be even more accurate.

While we did not see any significant differences between regressing on the ensemble DBM (SM08) or its ensemble members (SM13 and SM14), on average, under either configuration set (Test 3a or 3b) (c-d),

- we do see similar behavior of an ensemble to its members as seen in subsection 6.3.1 (NI) where regressing on the ensemble DBM (SM08) lies between its ensemble members (SM13 and SM14).

It would be interesting to see where and when this ensemble behavior holds, and accuracy is not comparable (to study the robustness of comparability of the post-regressed ensemble DBM and post-regressed feature-favoring ensemble members). To do this, we may need more diverse hybrid morphologies and primitives.

Boxplots (e-f) show larger values and dispersion for the Test 3b sparse configurations (f) giving larger medians for all interpolators and resulted in slightly more stable medians and IQRs (dispersions) between the interpolators.

- Under sparsity (Test 3b), post-regressing a nominal-informed model on any DBM (whether either partially nominal-informed feature-favoring,

fully nominal-informed ensemble, or un-informed) when estimating a final DBM from the fit, had comparable accuracy, on average.

- Under random configurations (Test 3a), post-regressing on the fully nominal-informed ensemble DBM (SM08) or partially nominal-informed feature-favoring ridge DBM (SM14) was more accurate and had a lower median RMS (e) than post-regressing on the un-informed benchmark GMT SIT DBM (SM17), when estimating a final DBM from the fit, on average.

In summary,

- from subsection 6.3.2 (PR), we found that estimating a final DBM from a nominal-informed custom model fit (DBM or sounding) is more accurate than the de facto GMT SIT, and overall, the most accurate when on a DBM (post-regressed).
- Subsection 6.3.3.1 (ADall) confirmed post-regressing on DBMs is more accurate than regressing on less accurate original input soundings, when estimating a final DBM from the fit.
- This subsection (ADsubset),
 - confirms the findings of no difference in final DBMs estimated from post-regressing on DBMs of different accuracy (as when utilizing different nominal-information or none), under sparsity (Test 3b),

- while under random configurations (Test 3a), shows that regressing on the partially nominal-informed feature-favoring ridge or fully nominal-informed ensemble DBM is more accurate than regressing on the un-informed DBM.

6.3.4 Study 2 Subsection 4: Importance of Utilizing All Influential Information (AII)

Interpolators in subsection 6.3.3.2 (ADsubset) post-regressed the fully nominal-informed custom model on either a fully (ensemble of all feature-favoring), partially (a single feature-favoring), or un-informed (non-feature-favoring GMT SIT) DBM. The interpolators in this subsection (AII) only post-regress either a fully or partially nominal-informed model on their nominal-informed DBM counterparts to investigate the benefits of partial nominal-informed modeling, when estimating a final DBM from the fit. Essentially, this subsection (AII) compares interpolators which utilize information from either disagreeing classifier (partially informed) or both (fully informed)

In this Friedman’s investigative subsection (AII), we compare interpolators to investigate the importance of utilizing **all influential information** (different feature-favoring DBMs, and functional forms for the model) provided by nominal data from disagreeing classifiers. The three interpolators compared are:

1. ELS custom model using fitted regression (SM08),
2. OLS seamount model on seamount DBM (SM11), and
3. OLS ridge model on ridge DBM (SM12).

With these interpolators, this subsection (AII) compares estimating a final DBM from an ELS fit of a custom model on an ensemble DBM (SM08) to that of OLS

modeling each constitute nominal-informed part separately. Each ensemble member feature-favoring DBM is regressed by its corresponding nominal-informed primitive model: the seamount primitive is modeled on the DBM produced by seamount interpolator (SM11), and the ridge primitive is modeled on the DBM produced by the ridge interpolator (SM12). All three interpolators, thus, post-regress DBMs, each utilizing different nominal information.

The first interpolator estimates a final DBM from an ELS fit of a fully nominal-informed custom model on a fully nominal-informed ensemble of partially nominal-informed feature-favoring DBMs (SM08). The second interpolator regresses a partially nominal-informed seamount model on the partially nominal-informed feature-favoring seamount DBM (SM11), and the third interpolator regresses the other partially nominal-informed ridge model on the other partially nominal-informed feature-favoring ridge DBM (SM12), both estimating a final DBM from their fits.

Each interpolator utilizes the nominal information differently. The first interpolator (SM08) uses information provided from both disagreeing classifiers (utilizing different feature-favoring interpolators to capture more of the underlying geomorphology correctly, where interpolators may not be mutually exclusive to the identified primitives) while the other interpolators (SM11 and SM12) use information provided from only one of the classifiers.

These interpolators investigate how utilizing all conflicting information in estimating a DBM from fitting both primitive functional forms provided by each classifier on an ensemble of feature-favoring DBMs determined by each classifier via

ELS compares to selecting one classifier to provide one primitive functional form and the one feature-favoring DBM it regresses upon via OLS.

These three interpolators were chosen to investigate the following questions (comparisons to investigate):

- Does utilizing all nominal information (different feature-favoring DBMs and functional forms for the model) provided by disagreeing classifiers improve accuracy?
 - How does SM08 compare to the rest?

Figure 6.9 shows the results of this Friedman's investigative subsection (AII) and demonstrates the importance of utilizing all nominal information from disagreeing classifiers. Red boxes indicate comparable interpolators that were more accurate for each configuration set (Test 3a and 3b). In both (a-b) Friedman's ANOVAs, there is a statistical difference between interpolators. However, only for Test 3a configurations (c) were all interpolators statistically different from each other. There is a difference between the relative performance of the first two interpolators (SM08 and SM11) in the multiple comparisons (c-d) between configurations (Test 3a and 3b).

Under Test 3a random configurations (c),

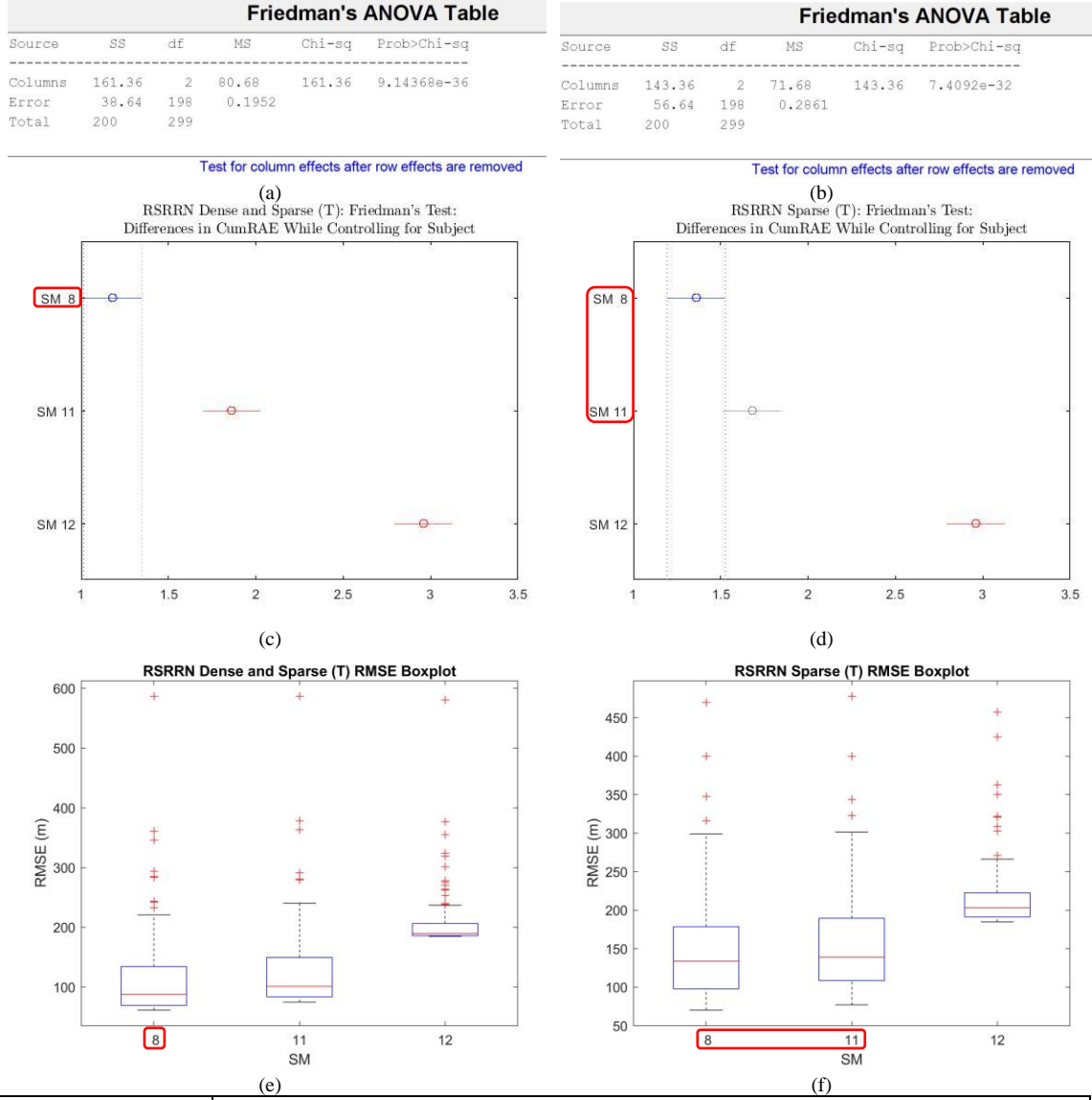
- estimating a final DBM from an ELS fit of the fully informed custom model on an ensemble of DBMs (SM08) was the most accurate,
- followed by estimating from an OLS fit of the partially informed seamount model on the seamount DBM (SM11), and

- lastly, with the worst accuracy, estimating from an OLS fit of the partially informed ridge model on the ridge DBM (SM12).

Under Test 3b sparse configurations (d), however,

- estimating from an ELS fit of the fully informed custom model on an ensemble of DBMs (SM08) was comparable to estimating from an OLS fit of the partially informed seamount model on the seamount DBM (SM11),
- with estimating from the OLS fit of the other partially informed ridge model on the ridge DBM (SM12) still the least accurate, on average.

Boxplots (e-f) show larger values for the Test 3b sparse configurations (f). The Test 3b sparse configurations (f) had larger medians for all interpolators and resulted in more stable medians and IQRs (dispersions) between the interpolators.



SM08	ELS (Custom Model) (nominal-informed regression on ensemble DBM) DBM _(E) ~ Custom Model; uses fit
SM11	OLS (Seamount Model) on seamount DBM (nominal-informed DBM from seamount interpolator) DBM _(S) ~ Seamount Model
SM12	OLS (Ridge Model) on ridge DBM (nominal-informed DBM from ridge interpolator) DBM _(R) ~ Ridge Model

Figure 6.9 Study 2 subsection 6.3.4 (AII) results on the truncated hybrid.

(a-b) Friedman's ANOVAs, (c-d) post-hoc analyses of multiple comparisons with Tukey's HSD correction, and (e-f) RMS boxplots.

(a), (c), and (e) are Test 3a random configurations. (b), (d), and (f) are Test 3b sparse configurations. We list the interpolation schemes utilized. Red boxes indicate comparable interpolators with the best accuracy for each configuration set.

The increase in RMS for estimating from the ELS fit of a custom model on the ensemble DBM (SM08) is larger than that of estimating from the OLS fit of a seamount model on the seamount DBM (SM11), placing the already close RMS medians for the Test 3a random configurations (e) closer (d) for the Test 3b sparse configurations. This explains the change in relative performance between Test 3a and 3b configurations (c-d) where ELS utilizing the custom model on the ensemble DBM (SM08) was the most accurate (c) for Test 3a random configurations, but under sparsity (Test 3b) (d), became comparable to OLS with the seamount model on the seamount DBM (SM11).

The main objective of this Friedman's investigative subsection (AII) is to determine if utilizing all information provided from disagreeing classifiers is beneficial to improve accuracy of a final DBM estimated from a post-regression fit over that of selecting only the information from one classifier to use.

Both disagreeing classifiers are only utilized when the ensemble DBM is fit with the custom model (SM08). Both DBM and model are fully informed by both classifiers and includes both seamount and ridge information: the ensemble DBM is an unascertained weighting of the seamount DBM and the ridge DBM, and the custom model is a weighting of both the seamount and ridge primitives. Utilizing one classifier selects either the seamount DBM with the seamount primitive model (SM11) or the ridge DBM with the ridge primitive model (SM12). The DBM and model are partially informed by one of the classifiers.

Clearly, for both Test 3a and 3b configurations,

- we see evidence that utilizing different nominal information affects the accuracy of the final DBM estimated from the post-regressed fit.
 - Evidence is most clear for Test 3a random configurations where utilizing all nominal information was the most accurate (SM08)
 - followed by the second most informative seamount nominal information (SM11), and
 - lastly, by the least informative ridge nominal information (SM12).
- Evidence is not as clear for Test 3b sparse configurations, where utilizing both the seamount and ridge nominal information (SM08) was comparable to utilizing only the seamount nominal information (SM11).

This subsection (AII) finds that

- utilizing information from both disagreeing classifiers was beneficial to improving accuracy, on average.
- However, under sparsity (Test 3b), the ridge DBM was unable to provide enough additional information to the ensemble to constrain the regression of the true custom model (SM08) any better than if we had used information from only one of the disagreeing classifiers identifying the seamount primitive to fit in a poorer model on the seamount DBM (SM11).
 - Adding the ridge DBM in an ensemble DBM did not improve the accuracy of the seamount DBM prior to post-regressing with the better custom model (SM08) substantial enough for better accuracy

than utilizing the seamount DBM with the poorer seamount model (SM11) alone, under sparsity (Test 3b).

We posit the failings of the custom model under sparsity (Test 3b) is due to model complexity – more complex models require more (informative) data to estimate their parameters accurately. The high complexity of the custom model requires more (informative) data to accurately estimate the weighting of the seamount and ridge primitives than the simpler seamount model requires to accurately estimate its parameters. Under sparse configurations (Test 3b), there was not enough information available for the custom model to be more accurate than the seamount model.

Our hybrid morphology is 75% seamount primitive. With sparse data configurations (Test 3b) producing less accurate DBMs, there is more chance for ELS to incorrectly weight the ridge primitive of the custom model more than the seamount primitive, whereas when utilizing the seamount model, we eliminate the possibility of weighting the ridge primitive more than the seamount primitive by forcing the use of the seamount primitive only. With that said,

- unless the underlying weighting of the primitives is known beforehand, estimating from an OLS fit of a partially informed model is ill-advised.
- ELS serves to estimate this weighting of primitives, and as such, it is better to estimate from the fully nominal-informed custom model fit on an ensemble DBM (SM08) than from either partially nominal-informed model fit on only one feature-favoring DBM because weight w is unknown.

Additionally, as we will further see in subsection 6.3.5 (AIP), this demonstrates how estimating from an ELS fit utilizing a poor model can decrease accuracy, a known phenomenon of regression, and how a fully informed custom model can become a poor model under sparse configurations (Test 3b).

In general,

- estimating from an ELS fit
 - utilizing a model of all nominal-information from disagreeing classifiers
 - on an ensemble of feature-favoring DBMs of all nominal-information from disagreeing classifiers (SM08)
- showed propensity to be
 - the most accurate and
 - have the lowest median RMS, and
- was of the most accurate (c-d) and of the lowest median RMS (e-f), on average.

The findings from subsection 6.3.3.2 (ADsubset) coupled with those from this subsection (AII), lead to our next Friedman’s investigative subsection 6.3.5 (AIP) where we investigate the efficacy of utilizing different nominal-informed models on an ensemble DBM to estimate a final DBM from the post-regression fit.

Broadly contrasting between the sets of interpolators from these subsections for easy dissemblance, the interpolators in subsection 6.3.3.2 (ADsubset) post-regressed the same custom model on different DBMs, this subsection (AII) post-regressed different

models on different DBMs, and subsection 6.3.5 (AIP) will post-regress different models on the same DBM.

6.3.5 Study 2 Subsection 5: Importance of Utilizing All Influential Primitives in the ELS Regression Model, when Estimating from Fit (AIP)

Interpolators in subsection 6.3.3.2 (ADsubset) post-regressed a fully nominal-informed model on either a fully, partially, or un-informed DBM and the interpolators in subsection 6.3.4 (AII) post-regressed different nominal-informed models on their nominal-informed DBMs. In this subsection (AIP), interpolators post-regress different nominal-informed models on the fully nominal-informed ensemble DBM to investigate the efficacy of utilizing a model that contains all influential information when estimating a final DBM from the post-regressed fit.

In this fifth Friedman’s investigative subsection (AIP), we compare interpolators for investigating the importance of utilizing **all influential primitives** in the ELS regression model when estimating a final DBM from the ELS fit. The five interpolators investigated are:

1. un-informed equally weighted ensemble (SM04),
2. ELS planar model using fitted regression (SM07),
3. ELS custom model using fitted regression (SM08),
4. ELS seamount model using fitted regression (SM15), and
5. ELS ridge model using fitted regression (SM16).

All interpolators are an ensemble of the seamount and ridge DBM. All but the first (SM04) estimate a final DBM from an ELS fit, and for brevity we limit the use of

this repetitive statement regarding ELS. The first interpolator is the un-informed equally weighted ensemble (SM04), and the remaining interpolators are differentially weighted ensembles estimated from ELS fits utilizing either an un-informed planar model (SM07), a fully nominal-informed custom model (SM08), or a partially nominal-informed seamount (SM15) or ridge (SM16) model.

All interpolators are ensemble methods utilizing feature-favoring ensemble members selected from the first study (UEs). All ELS interpolators (SM07, SM08, SM15, and SM16) post-regress on an unascertained-weighted ensemble of feature-favoring DBMs with different nominal-informed models. The custom model capitalizes on the nominal information provided by incorporating all the functional forms of the primitives identified by the classifiers. In contrast, the planar model utilizes none of the functional forms identified, while both seamount and ridge models utilize only one. In other words, these interpolators are ensembles with different amounts of nominal information. The more complex custom model (SM08) uses the most nominal information provided by both disagreeing classifiers, while the un-informed equal-weights ensemble (SM04) may only include nominal information indirectly when the ensemble member DBMs were constructed through their feature-favoring interpolators.

These interpolators were chosen to investigate the importance of utilizing all the functional forms identified by the classifiers in ELS when estimating from the fit and were chosen to investigate the following questions (comparisons to investigate):

- Does accuracy when estimating from an ELS fit depend on how informed the model is?

- How do the partially nominal-informed models (SM15 and SM16) compare to the fully nominal-informed model (SM08)?
- How does the un-informed planar model (SM07) compare to the rest?

Figure 6.10 shows the results of our fifth Friedman’s investigative subsection (AIP) and demonstrates the importance of utilizing all influential primitives when estimating a final DBM from an ELS fit. Red boxes indicate comparable interpolators that were most accurate for each configuration set (Test 3a and 3b). In both (a-b) Friedman’s ANOVAs, there is a statistical difference between interpolators.

Under Test 3a random configurations (c),

- ELS with the fully informed custom model (SM08) was the most accurate,
- followed by ELS with the seamount model (SM15), on average.
- Next, follows the comparable ELS with the ridge model (SM16) and un-informed equal-weight ensemble (SM04), on average.
- Finally, ELS with planar model (SM07) was the least accurate, on average.

Under Test 3b sparse configurations (d),

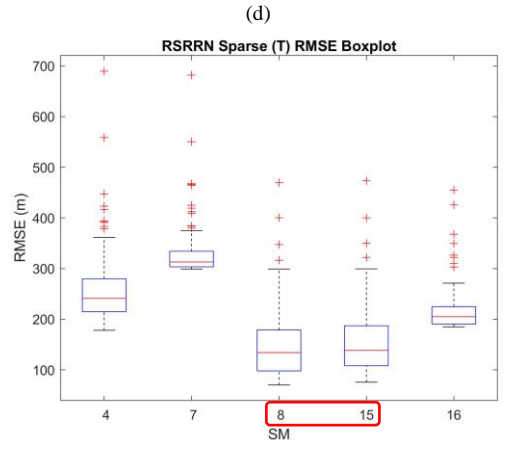
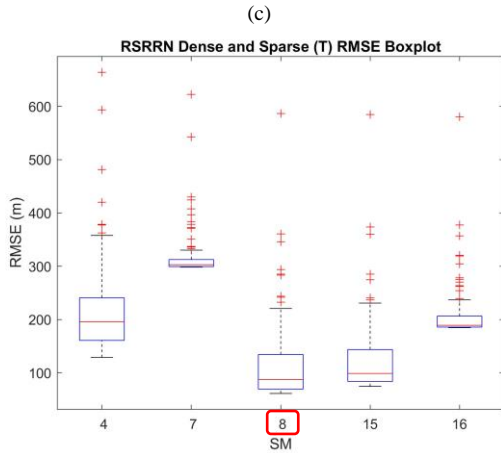
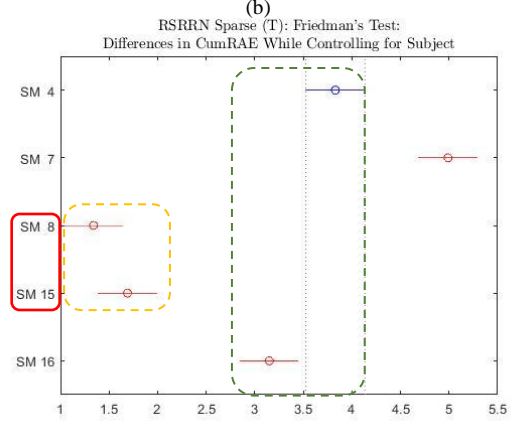
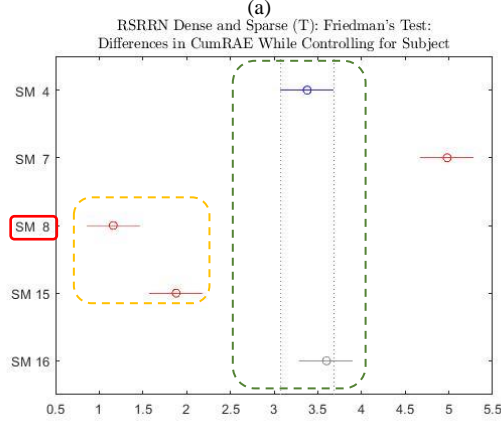
- ELS with the fully informed custom model (SM08) and the seamount model (SM15) were comparably the most accurate,
- followed by ELS with the ridge model (SM16),
- then the un-informed equal-weight ensemble (SM04), and
- finally, the least accurate ELS with the planar model (SM07), on average.

Friedman's ANOVA Table					
Source	SS	df	MS	Chi-sq	Prob>Chi-sq
Columns	906.48	4	226.62	362.59	3.34907e-77
Error	93.52	396	0.236		
Total	1000	499			

Test for column effects after row effects are removed

Friedman's ANOVA Table					
Source	SS	df	MS	Chi-sq	Prob>Chi-sq
Columns	914.32	4	228.58	365.73	7.04159e-78
Error	85.68	396	0.216		
Total	1000	499			

Test for column effects after row effects are removed



SM04	Mean (un-informed equally weighted ensemble) $DBM_{(E)} \sim (0.5)DBM_{(S)} + (0.5)DBM_{(R)}$
SM07	ELS (Planar Model) (nominal-informed regression on ensemble DBM) $DBM_{(E)} \sim \text{Planar Model}$; uses fit
SM08	ELS (Custom Model) (nominal-informed regression on ensemble DBM) $DBM_{(E)} \sim \text{Custom Model}$; uses fit
SM15	ELS (Seamount Model) (nominal-informed regression on ensemble DBM) $DBM_{(E)} \sim \text{Seamount Model}$; uses fit
SM16	ELS (Ridge Model) (nominal-informed regression on ensemble DBM) $DBM_{(E)} \sim \text{Ridge Model}$; uses fit

Figure 6.10 Study 2 subsection 6.3.5 (AIP) results on the truncated hybrid.

(a-b) Friedman's ANOVAs, (c-d) post-hoc analyses of multiple comparisons with Tukey's HSD correction, and (e-f) RMS boxplots.

(a), (c), and (e) are Test 3a random configurations. (b), (d), and (f) are Test 3b sparse configurations. We list the interpolation schemes utilized. Red boxes indicate comparable interpolators with the best accuracy for each configuration set.

There are two differences in the relative performance of the interpolators in the multiple comparisons (c-d) between configurations (Test 3a and 3b). sparsity (Test 3b),

Firstly (yellow dashed box),

- under sparsity (Test 3b) (d), ELS with the custom model (SM08) is now comparable to ELS with the seamount model (SM15).
 - Under Test 3a random configurations (c), ELS with the custom model (SM08) was the most accurate.
- This comparability of the custom and seamount models under sparsity (Test 3b) was similarly seen in subsection 6.3.4 (AII) where the models were post-regressed on their nominal-informed DBM counterparts instead of an ensemble DBM.
- The high complexity of the custom model (SM06) suffers in estimating its model parameters accurately (most notably, weight w) such that accuracy is worse than utilizing the simpler model with only the seamount primitive which was responsible for 75% of our hybrid.
- Additionally, the completely informed custom model (SM08) may be even more beneficial on a set of dense sampling configurations only.

Secondly (green dashed box),

- under sparsity (Test 3b) (d), ELS with the ridge model (SM16) was more accurate than the un-informed equal-weight ensemble (SM04).
 - under Test 3a random configurations (c), they were comparable.

- The ridge primitive is responsible for 25% of our hybrid and thus, is a poor model. However, the ridge model is still a nominal-informed model, utilizing more nominal information than the un-informed equal-weight ensemble (SM04) which only intrinsically utilizes nominal information through its feature-favoring DBMs.
 - This difference in the amount of nominal information employed between the two interpolators is irrelevant for Test 3a random configurations (c), but important when under sparsity (Test 3b) (d), where utilizing that nominal-informed, albeit poor, ridge model to estimate a final DBM from the ELS fit (SM16) was beneficial for improving accuracy over the un-informed methods (SM04 and SM07). The additional nominal information incorporated guides the final DBM estimates.

Both differences in relative performance

- are due to sparsity (Test3b) affecting accuracy and
- support the use of nominal information as beneficial under sparsity.

Boxplots (e-f) show larger values for the Test 3b sparse configurations (f). The Test 3b sparse configurations (f) had larger medians for all interpolators and resulted in more stable medians and IQRs (dispersions) between the interpolators.

The increase in RMS for estimating from the ELS fit of a custom model (SM08) was larger than that of the seamount model (SM16), which remained relatively constant, placing the already close RMS for Test 3a random configurations (e) closer (f) for Test

3b sparse configurations. This explains the first difference in relative performance where ELS utilizing the custom model (SM08) was the most accurate (c) for Test 3a random configurations but as data became sparse (Test 3b) (d), ELS utilizing the custom model (SM08) was comparable to that of the seamount model (SM15).

Similarly, the increase in RMS for estimating from the un-informed ensemble (SM04) is larger than that of estimating from ELS utilizing a ridge model (SM16), which remained relatively constant, placing the already close RMS median for the un-informed ensemble (SM04) for the Test 3a random configurations (e) larger (d) than ELS with the ridge model (SM16) for the Test 3b sparse configurations. This explains the second difference in relative performance between Test 3a and 3b configurations (c-d) where these two interpolators were comparable for Test 3a random configurations (c) but as data became sparse (Test 3b), the un-informed ensemble (SM04) became less accurate (d).

In general,

- we see a progression where accuracy improved as our model better represented our hybrid (from another view when we captured all geomorphological features in the seabed).
 - Since only 25% of our hybrid is a ridge, fitting the ridge model (SM16) was less accurate than when fitting with the seamount model (SM15), with the custom model (SM08) being the most accurate, under Test 3a random configurations (c), and comparably the most accurate to fitting the seamount model (SM15), under

sparsity (Test 3b) (d), as the custom model best represented the hybrid morphology.

- Moreover, all methods which fitted a model informed by the nominal data (SM08, SM15, and SM16) had better accuracy than the un-informed planar model (SM07), and the informed models which captured most of the surface (SM08 and SM15) had better accuracy than the un-informed equal-weighted ensemble (SM04).
 - Under sparsity (Test 3b), the nominal-informed models (SM08, SM15, and SM16) had better accuracy than both un-informed interpolators (SM04 and SM07).
- We conclude that utilizing all influential primitive forms identified by nominal information in a post-regression model utilized by ELS improves accuracy, when estimating a final DBM from the fit. This follows OLS theory and supports subsection 6.3.4 (AII).
 - The performance of the interpolators reflected how well the models fit the geomorphology; accuracy decreased as bias increased.
 - The more complex and correct fully informed custom model (SM08) was more accurate,
 - followed by (or comparable to, under sparsity [Test 3b]) the partially informed seamount primitive model (SM15),
 - then the partially informed ridge primitive model (SM16)

- which matches the contributions of each primitive in the hybrid surface.
- The least accurate was the un-informed planar model (SM07)
- followed by the un-informed ensemble (SM04).

As later supported in subsection 6.3.6 (wE),

- if primitive functional forms provided by the classifiers are incorrect or not available, it is better to use an un-informed equally weighted ensemble (SM04) than estimating from an ELS fit of a poor model, as demonstrated by (c-d) in this subsection (AIP).
 - The importance of utilizing nominal-informed models over the un-informed ensemble (SM04) depends on how much information (the model) is correctly inferred by the classifiers.
 - The un-informed ensemble (SM04) is an equally weighting of DBMs whereas our ELS (SM07, SM08, SM15, and SM16) methods estimate from the model fits.
 - Equally weighting DBMs avoids inappropriately estimating a final DBM from the fit of an incorrect models.
 - More generally, the importance of externally weighting DBMs in an ensemble instead of estimating a final DBM from ELS post-regressing fit, depends on the correctness of the inferred model, discussed in subsection 6.3.6 (wE) (instead, subsection 6.3.6 [wE]

recommends the more robust differential weighting of DBMs in an ensemble external to ELS).

The accuracy of an equal-weighted ensemble depends on the accuracy of its ensemble members. The accuracy of the equal-weighted ensemble will degrade with sparsity due to accuracy degradation of its ensemble members. Under sparsity, we expect ensemble member DBMs to provide similar information, reducing ensemble benefits in improving accuracy. In contrast, estimating a final DBM from the ELS fit utilizing a nominal-informed, even if poor, model maintains accuracy, under sparsity, by utilizing the model to guide DBM estimation. The more informed the model, the better the final DBM estimates are guided for improved accuracy from utilizing a more appropriate model. In accordance with regression theory, a well approximated model reduces bias and variance (i.e., improved accuracy).

In general,

- utilizing all influential primitives in the nominal-model when estimating from the ELS fit was
 - among the most accurate (c-d) and
 - among the lowest median RMS (e-f), on average.
- Utilizing all nominal information in an ELS model when estimating a final DBM from the fit was
 - beneficial to improving accuracy,
 - especially for sparse data, on average.

6.3.6 Study 2 Subsection 6: Importance of w -ELS over ELS (wE)

In this sixth Friedman’s investigative subsection (wE), we compare interpolators for investigating the importance w -ELS over ELS. These six interpolators investigate w -ELS versus ELS:

1. benchmark interpolator GMT SIT (SM03),
2. un-informed equally weighted ensemble (SM04),
3. w -ELS planar model extracting w (SM05),
4. w -ELS custom model extracting w (SM06),
5. ELS planar model using fitted regression (SM07), and
6. ELS custom model using fitted regression (SM08).

The first interpolator is our benchmark GMT SIT (SM03), followed by un-informed equally weighted ensemble (SM04), w -ELS with a planar (SM05) and custom (SM06) model, and ELS with a planar (SM07) and custom (SM08) model. All but the first interpolator are ensemble methods. All w -ELS and ELS methods are differentially weighted ensembles utilizing feature-favoring ensemble members selected from the UEs. While all w -ELS and ELS methods are nominally informed, they utilize the nominal information to different extents. Those utilizing the custom model (SM05 and SM08), further extend their utilization of the nominal information via the fully nominal-informed custom model, whereas those utilizing the planar model (SM05 and SM07), do not capitalize on additional exploits of the nominal information and fit with an un-informed simpler, generic model.

These six interpolators were chosen to investigate the following questions (comparisons to investigate):

- How does the planar model compare to the custom model?
 - How does SM05 compare to SM06? SM07 to SM08?
 - How does SM05 and SM07 compare to SM06 and SM08?
- How does the planar models compare to the un-informed ensemble?
 - How does SM05 and SM07 compare to SM04?
- How does the planar models compare to the benchmark GMT SIT?
 - How does SM05 and SM07 compare to SM03?

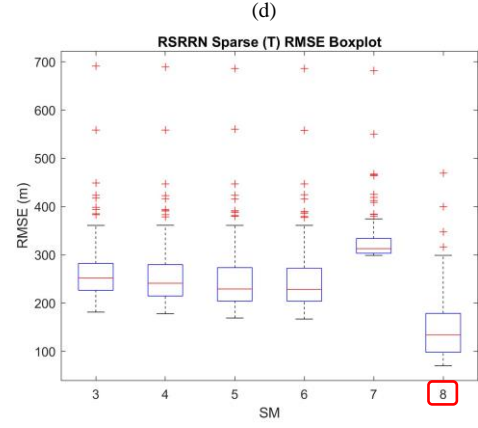
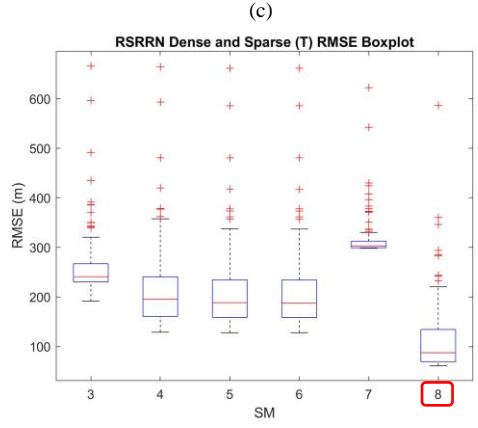
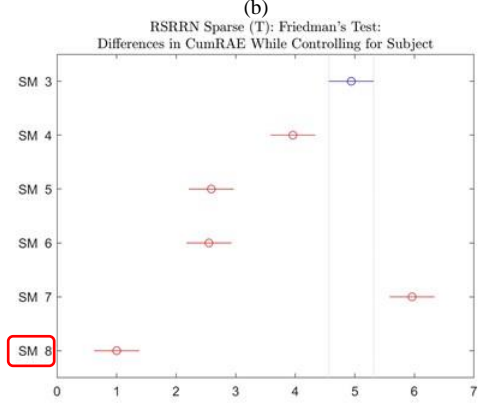
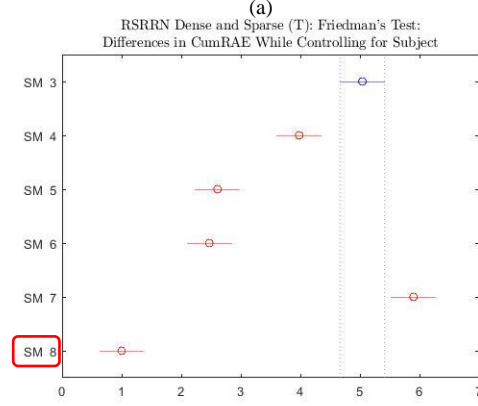
Figure 6.11 shows the results of our sixth Friedman’s investigative subsection (wE) and demonstrates the importance of w-ELS over ELS. Red boxes indicate the interpolator that was most accurate for each configuration set (Test 3a and Test 3b). In both (a-b) Friedman’s ANOVAs, there is a statistical difference between interpolators and both the multiple comparisons (c-d) are nearly the same. The boxplots (e-f) show larger values for the Test 3b sparse configurations (f) giving larger medians for all interpolators and resulted in more stable medians and IQRs (dispersions) between the interpolators. Our ELS ensemble method with the custom model (SM08) was the most accurate (c-d) and had the lowest median RMS (e-f), on average.

Friedman's ANOVA Table					
Source	SS	df	MS	Chi-sq	Prob>Chi-sq
Columns	1646.5	5	329.3	470.43	1.92336e-99
Error	103.5	495	0.209		
Total	1750	599			

Test for column effects after row effects are removed

Friedman's ANOVA Table					
Source	SS	df	MS	Chi-sq	Prob>Chi-sq
Columns	1631.74	5	326.348	466.21	1.563e-98
Error	118.26	495	0.239		
Total	1750	599			

Test for column effects after row effects are removed



SM03	GMT SIT (benchmark interpolator) $DBM_{(B)}$
SM04	Mean (un-informed equally weighted ensemble) $DBM_{(E)} \sim (0.5)DBM_{(S)} + (0.5)DBM_{(R)}$
SM05	w-ELS (Planar Model) (nominal-informed differentially weighted ensemble) $DBM_{(E)} \sim \text{Planar Model}$; extracts w
SM06	w-ELS (Custom Model) (nominal-informed differentially weighted ensemble) $DBM_{(E)} \sim \text{Custom Model}$; extracts w
SM07	ELS (Planar Model) (nominal-informed regression on ensemble DBM) $DBM_{(E)} \sim \text{Planar Model}$; uses fit
SM08	ELS (Custom Model) (nominal-informed regression on ensemble DBM) $DBM_{(E)} \sim \text{Custom Model}$; uses fit

Figure 6.11 Study 2 subsection 6.3.6 (wE) results on the truncated hybrid.

(a-b) Friedman's ANOVAs, (c-d) post-hoc analyses of multiple comparisons with Tukey's HSD correction, and (e-f) RMS boxplots.

(a), (c), and (e) are Test 3a random configurations. (b), (d), and (f) are Test 3b sparse configurations. We list the interpolation schemes utilized. Red boxes indicate interpolator with the best accuracy for each configuration set.

Figure 6.11 shows how the strong influence of the primitive shapes provided by the classifiers can impact accuracy and why it might be better to be conservative and use w -ELS (w extracted) instead of ELS (fitted), as it is robust to deviations of the primitive forms from the true geomorphological shape.

Figure 6.12 takes a closer look at Figure 6.11d but inferences found are for both sets of configurations. These interpolators investigate the importance of w -ELS (middle blue box) over ELS (bottom green box). The first interpolator in each box utilizes the planar model followed by that which uses the custom model.

- ELS utilizing the planar model (SM07) is the least accurate while ELS with the custom model (SM08) is the most accurate, on average.
 - This strong dependency of accuracy on the model demonstrates the vulnerability of ELS to how well the geomorphological primitives utilized in the custom nominal-informed model approximate the true geomorphology.
- In contrast, w -ELS is robust to this vulnerability demonstrated by the planar (SM05) and custom (SM06) having comparable accuracy.
 - While being less accurate than ELS utilizing the custom model (SM08), it is more accurate than ELS when utilizing the un-informed simpler planar model (SM07), as well as the un-informed equally weighted ensemble (SM04) and the benchmark GMT SIT (SM03).

In general,

- using ELS to estimate a DBM instead of extracting the weights to apply to the ensemble DBM members in a w -ELS informed ensemble approach, can lead to a significant drop in accuracy.
 - Estimating from an ELS fit is highly sensitive to the primitive functional forms used, having accuracy highly dependent on how well the primitive functional forms approximate the true geomorphology.
 - Informed w -ELS ensembles avoid this strong dependency by only utilizing the primitive functional forms to estimate the weights to use in differentially averaging DBMs, leaving the DBMs as the primary source of influence in the ensembled DBM. Robustness to poorly chosen primitive functional forms is a desirable property of w -ELS.

In subsection 6.3.2 (PR), we found that post-regressing with the nominal-informed custom model leads to better accuracy regardless of the DBM. However, this finding of primitive sensitivity, suggests one should strongly consider whether the gains of utilizing a custom model in methods other than w -ELS are worth the risk.

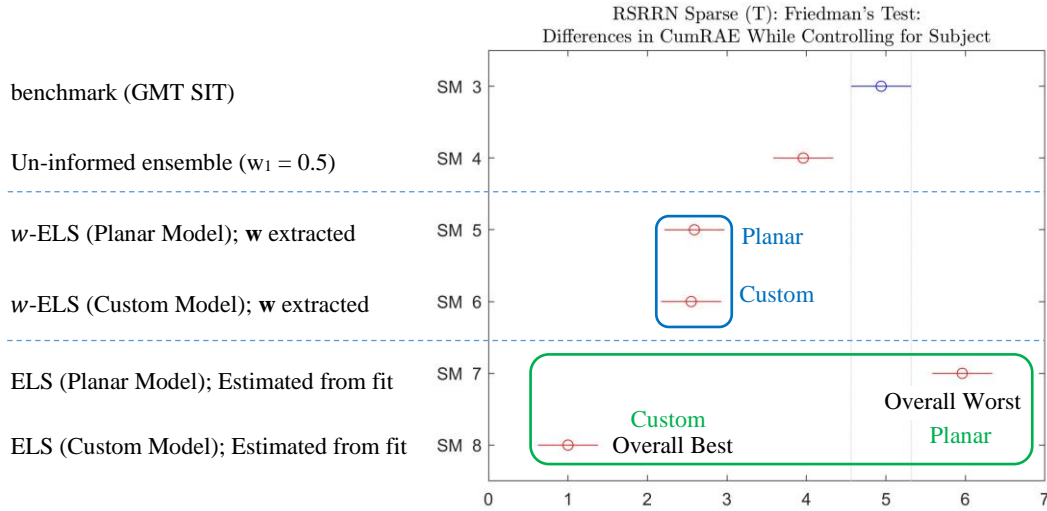


Figure 6.12 Analysis of subsection 6.3.6 (wE)

Analysis of Figure 6.11d. Inferences apply to both second study (RE) Test 3a and 3b configurations. These interpolators (separated by dashed horizontal lines) investigate the importance of w -ELS (middle blue box) over ELS (bottom green box). The first interpolator in each box utilizes the planar model followed by the custom model. ELS utilizing the planar model (SM07) is the least accurate while ELS with the custom model (SM08) is the most accurate, according to CumRAE. This demonstrates the vulnerability of ELS to how well the geomorphological primitives approximate the morphology. w -ELS is robust to this vulnerability demonstrated by the planar (SM05) and custom (SM06) having comparable accuracy.

6.4 Discussion

The statistical inferences made from the seven Friedman's investigative subsections for the second study (RE) are summarized here and the reader should refer to the previous sections for specifications and exceptions.

Post-regressing on the DBMs (SM13, SM14, and SM17) or the ensemble of DBMs (SM08) improved accuracy. On average, post-regressing with a nominal-informed model had better accuracy than both ensembles and individual feature-favoring interpolators.

We have nine main observations.

- Some interpolators may not perform statistically different from others.
- All five ensemble techniques (SM04-08) outperformed the benchmark GMT SIT (SM03), with the fitted ELS using a custom model (EM08) and the w -weighted ensembles w -ELS (SM05-06) showing better results, on average.
- Machine learners inform ensembles of a priori domain-knowledge (seafloor shape).
- Learned weights from a geomorphological primitive space are robust (generalizable).
- Without a priori, equally weighted ensemble averages (SM04) performed well, outperforming our benchmark GMT SIT (SM03), and avoiding worst-case interpolator selection.
- With a priori domain knowledge, differently weighted ensemble averages may do better.
- An informed, topologically aware ensemble, given a priori topological domain knowledge, improved accuracy significantly (w -ELS/ELS).
- The feature-favoring DBMs along with w -ELS and the identified primitive basis shape functions, computed more accurate ensemble weights.
- Differentially weighting feature-favoring DBMs according to the ELS estimated ensemble weight w , were robust to poorly identified primitive basis shape functions.

When we are not given the functional form of the primitives, an ensemble DBM improved numerical properties. Ensembles may avoid a worst-case scenario and may even improve accuracy when averaged with the near best-case scenario. When nominal data informed us of which interpolators were feature-favoring, those feature-favoring DBMs and their ensembles had significantly better accuracy than the benchmark GMT SIT (SM03) and equal-weighted ensemble (SM04).

The truncated seamount feature-favoring interpolator was less accurate than the feature-favoring interpolator selected for the smoother ridge, on average, for our hybrid, but both were more accurate than our benchmark GMT SIT which is the most widely used interpolator. The differentially weighted informed ensemble (w -ELS) produced accuracies that were an average of the two feature-favoring interpolators and avoided the worst-case scenario accuracies. Post-regressing either a feature-favoring DBM or their ensemble with a fully informed custom model produced the best accuracies. In theory, post-regressing an ensemble DBM applies the benefits of ensembles towards an accurate DBM for post-regression, which improves accuracy. Utilizing all nominal information (feature-favoring DBMs and functional forms) provided by disagreeing classifiers provided the best accuracies.

Both post-regression and ensembles utilize nominal information and care should be taken when optimizing the extent to which nominal information is used. Estimating from ELS (optimizing the use of the nominal-informed model) is more beneficial than extracting a weight w to weight DBMs in a differentially weighted ensemble because the former maximizes the benefits of knowing the seafloor shape. In fact, we found that post-

regressing any DBM to be beneficial, but post-regressing on an informed DBM produced by an interpolator selected by nominal information may be even more beneficial.

When modeling a feature that has been sparsely surveyed, we run the risk of missing key characteristics that define the feature's shape, for example, not sampling the apex of a seamount. By inferring the regression model to utilize in a post-regression from the nominal data identifying the seafloor shape, we can better impute values because we have been given additional information regarding how to model. The regression model serves as a correction to the DBMs, allowing us to rectify, for example, the apex of a seamount that may have not been represented. Although our hybrid surface was constructed from the primitives used in the regression model, we posit that this will remain factual as classifiers will identify and provide these nominal values based on some informed criteria found in the data.

While ensembles improve overfitting and reduce outliers by alleviating adverse effects of a single interpolator, post-regressing any DBM (feature-favoring or benchmark GMT SIT) with the selected primitive shapes chosen based on nominal data significantly increased accuracy more than extracting weight w from ELS for a differentially weighted ensemble or for an equally weighted ensemble, regardless of if it was an ensemble DBM that was post-regressed. However, post-regressing is highly dependent on how well the functional forms of the selected primitive shapes from the nominal data utilized in the post-regressed model approximate the true morphology. A poorly approximated model will result in accuracy worse than either our differentially weighted informed ensemble or

an equally weighted un-informed ensemble. It is this robustness provided by the ensembles that make them desirable for bathymetric modeling.

Several subsections exhibited differences in accuracy for methods between Test 3a and 3b. It would be interesting to see how a set of only dense configurations, say Test 3c, would compare to Test 3a and 3b.

Test 3a allowed us to make inferences about the general population of dense and sparse sampling configurations (as experimentally designed by the RE second study). Test 3b allowed us to make inferences about the general subpopulation of sparse configurations. Including a Test 3 would allow inferences about the general subpopulation of dense configurations. Populations are for our synthetic hybrid morphology.

Contrasting Test 3a random configurations with Test 3b sparse configurations allowed us to see how robust the methods were to sparsity. In the same vein, it would be interesting to see how the two subpopulations compare to each other, as well as to the general population. This would inform us of which methods may be better when density is unknown (i.e., a general method to use when un-informed or an in-formed method to use for improved accuracy when nominal information is available about density). Extending our current use of nominal information to inform us of seafloor shape with nominal information to inform us of density may further improve accuracy when modeling bathymetry as well as further the advancement of DBM automation and guidance.

CHAPTER VII – SUMMARY

In this dissertation, we demonstrated that the addition of nominal data with ensemble averaging adds knowledge about a region for improved accuracy of DBMs in areas with sparse data. Benefits of this capability to add knowledge to (or in other words, be informed about) a region for an improved gridding are applicable to all environmental sciences, including terrestrial, seafloor, and planetary. In this dissertation, we investigated the efficacy of utilizing nominal data and ensembles when modeling bathymetric surfaces.

In the introduction section 1.1, we enumerated some of the benefits of ensemble methods such as boosting, which are considered state-of-the-art in AI. Feeding the results of such classifiers (nominal data) back into our ensemble *w*-ELS interpolator produced, on average, significantly improved results. From our experimentations, I have learned that ensemble methods, on average, improve accuracy in DBM models, and that the nominal data garnered from AI classifiers has the potential to improve DBM accuracy significantly more. I have shown that the usefulness of AI classifiers lies not only in their resulting classification (ex. a seamount is present) but through their extended lifetime of supported benefits by utilizing that classifier to build a better interpolator for the specific seabed under investigation.

We began this study by developing and modifying extensions to the MergeBathy software suite for processing bathymetric data, and coding and applying the CURVE algorithm for uncertainty estimation for methods lacking inherent estimation, typical of efficient methods for sparse bathymetry. These software tools allowed us to design and implement a large set of complex experiments in an efficient and organized manner.

I also constructed a new interpolation methodology, which we refer to as *w*-ELS, that provides a pathway to feedback nominal data provided by AI classifiers into the interpolators supporting DBM construction. This allowed us to compare most existing interpolators which are built into MergeBathy with this new AI-informed interpolation approach. The method lends itself to the follow scenarios: we utilize AI classifiers and discover that region A has a ridge, region B has a seamount, and region C has both. With this information we construct three different interpolators for the three different regions, each of which utilize the respective geological primitives corresponding to the now known features in those regions.

In the first of our two studies, we identified interpolators that showed aptitude (favoritism) for a geomorphology (feature). We note that under additive noise we found that the popular interpolators GMT and MBZ SIT were not feature-favoring (this surprising negative result needs further investigation). We selected from this first study two interpolators of different underlying assumptions to serve as feature-favoring primitive interpolators in our second study.

Our second study investigated the efficacy of ensemble DBMs informed by nominal data by comparing this method with non-informed methods. Our *w*-ELS approach to modeling bathymetry utilized all available nominal data (regardless of whether in harmony) to construct a nominal-informed DBM. Our two-fold aim was to identify situations where a DBM may or may not benefit from an ensemble approach; and second, to demonstrate that a priori domain-specific AI classifications may be used to impute data to produce a more realistic seabed in regions of sparse data coverage. Using Friedman's tests and the CumRAE metric, I showed that the *w*-ELS method was superior

and produced statistically significant improvements over not only the individual interpolation methods but also ensembles of these methods.

More specifically, for our experiments we found:

- Un-informed modeling with the industry standard interpolator for gridding bathymetry, GMT SIT DBM, was the least accurate.
- Nominal-informed modeling improved accuracy.
 - Ensembles of nominal-informed DBMs improved accuracy.
 - Nominal information to select feature-favoring interpolators improved accuracy.
 - Nominal information to select ensemble weights improved accuracy (*w*-ELS/ELS).
 - Utilizing nominal-information was beneficial even when the nominal classifications were inconsistent.
- The *w*-ELS was significantly more accurate and preferential.
 - Post-regressing on non-parametric DBMs (ELS) was the most accurate but was dependent upon the accuracy of the AI classifiers.

In Figure 7.1, we present an example of our new nominal-informed ensemble *w*-ELS compared to the industry standard GMT SIT. This is the second configuration example study 2 Test 3a presented in section 6.1. The (a) truth data is randomly sampled with random noise and random swath removed shown as red points overlaid in (b). From the (b) random input configuration, we generated DBMs using (c) the industry standard GMT SIT and (d) our new nominal-informed ensemble *w*-ELS. Notice, our new method

w -ELS (d) avoids large spikes in the GMT SIT DBM (c); (d) is more physically realistic and more conservative than (c).

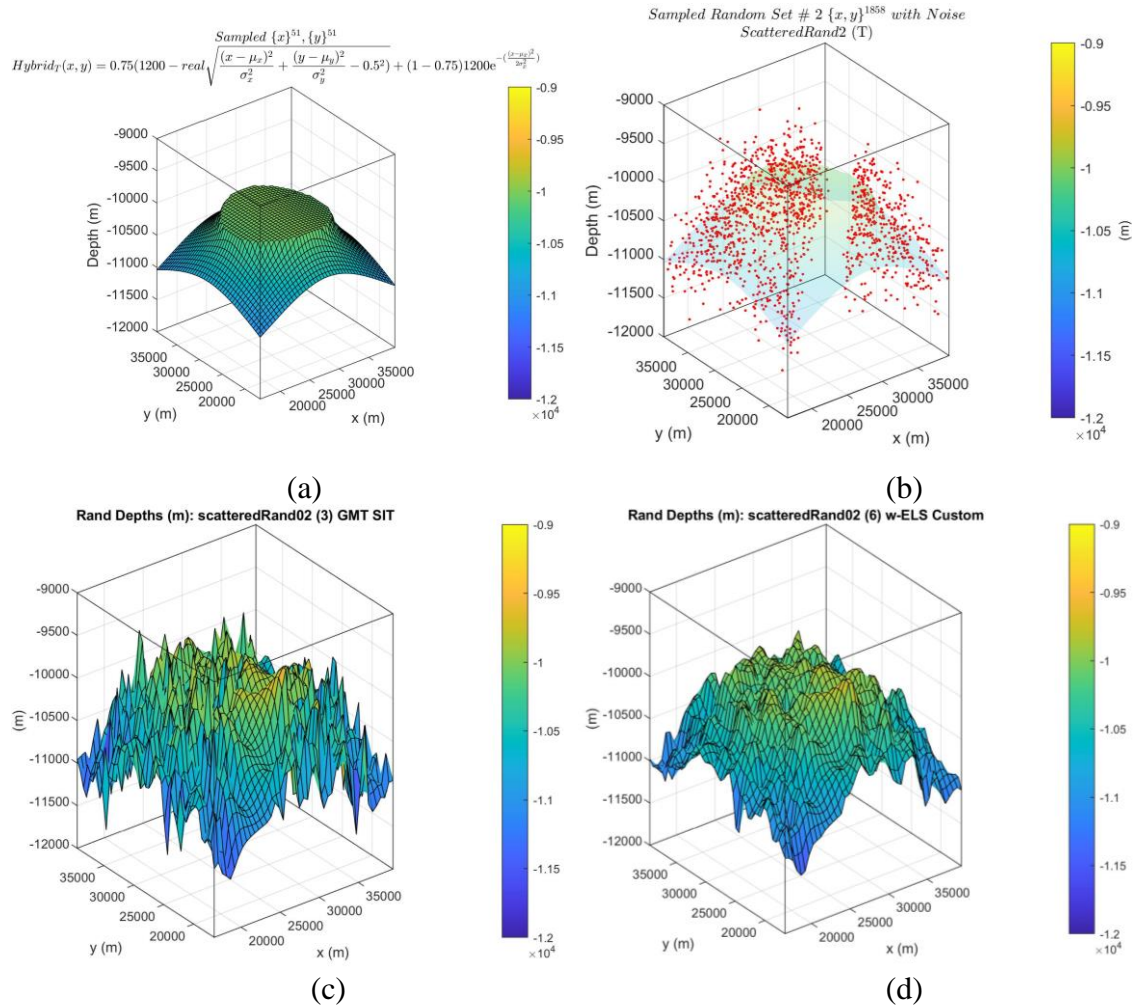


Figure 7.1 Example of our new nominal-informed ensemble w -ELS compared to the industry standard GMT SIT.

This is the second configuration example from study 2 Test 3a presented in section 6.1. The (a) truth data is randomly sampled with random noise and random swath removed shown as red points overlaid in (b). From the (b) random input configuration, we generated DBMs using (c) the industry standard GMT SIT and (d) our new nominal-informed ensemble w -ELS. Notice, our new method w -ELS (d) avoids large spikes in the GMT SIT DBM (c); (d) is more physically realistic and more conservative than (c).

As a proof of concept, this work has many veins for investigation in future work.

We may obtain a better representation of seamount and ridge populations by creating unbiased databases of known (measured) seamounts and ridges. Further, studying the

differences between bathymetry and topography, explored in (V. Lucieer et al., 2019), (Lecours et al., 2016), and (Franklin, 2020) will allow this field to take advantage of the rapidly growing primitive-form nominal based work currently being pursued by the GIS community.

We would like to see mixture model theory used to investigate compositional components of morphological surfaces from DBM of dense, well surveyed areas. We may use mixture models in an unsupervised ML technique, a supervised ML technique, or both. For example, in unsupervised ML, we may use mixture models to infer the set of sub-classifications underpinning a data set via clustering (Hastie et al., 2009), or in supervised learning, we may inject and test specific morphology-shape primitive functions. Through a combination of unsupervised and supervised learners, we may begin forming the set of morphology-shape primitive functions available to serve as bathymetric primitives. Uncovering these primitive classifications would be subsequently beneficial to others (V. Lucieer et al., 2019) outside the field of bathymetric modeling as well.

Additional interpolation scheme testing on more primitives, focusing on smooth versus discontinuous primitive shapes, is also needed. Lastly, and most interesting, nominal data may tell us more about the uncertainty. Statistically based uncertainty is not always appropriate for sparse data, but the nominal data a priori knowledge provides has the potential to inform and hence improve our uncertainty calculations.

APPENDIX A – MergeBathy (2015) Metadata

Software metadata

Nr	(executable) Software metadata description	
S1	Current software version	5.0.3
S2	Permanent link to executables of this version	https://github.com/Sammie-Jo/MergeBathy_Repos-mergeBathy_CPP
S3	Legal Software License	None
S4	Computing platform / Operating System	Windows x86, x64, Linux x86, and Linux x64
S5	Installation requirements & dependencies	None.
S6	If available Link to user manual - if formally published include a reference to the publication in the reference list	https://github.com/Sammie-Jo/MergeBathy_Repos-mergeBathy_DOCS/mergeBathy_UserGuide.docx
S6	Support email for questions	Samantha.zambo@gmail.com

Code metadata

Nr	Code metadata description	Please fill in this column
C1	Current Code version	5.0.3
C2	Permanent link to code / repository used of this code version	https://github.com/Sammie-Jo/MergeBathy_Repos-mergeBathy_CPP
C3	Legal Code License	None
C4	Code Versioning system used	GitHub
C5	Software Code Language used	C, C++
C6	Compilation requirements, Operating environments & dependencies	Windows x86, x64, Linux x86, and Linux x64
C7	If available Link to developer documentation / manual	https://github.com/Sammie-Jo/MergeBathy_Repos-mergeBathy_CPP/mergeBathy_UserGuide.docx
C8	Support email for questions	Samantha.zambo@gmail.com

APPENDIX B – Contributions

We acknowledge contributions made for each chapter.

- ABSTRACT
 - Group work and co-authored with Paul Elmore, A. Louise Perkins, and Brian Bourgeois.
- CHAPTER I– INTRODUCTION
 - Group work and co-authored with Paul Elmore, A. Louise Perkins, and Brian Bourgeois.
- CHAPTER II– BACKGROUND
 - 2.1 Bathymetry
 - Group work and co-authored with Paul Elmore, A. Louise Perkins, and Brian Bourgeois.
 - 2.2 Bathymetry Modeling
 - Group work and co-authored with Paul Elmore, A. Louise Perkins, and Brian Bourgeois.
 - 2.3 Regression
 - I implemented in a script various statistical and diagnostic tools to validate and inspect DBMs and regressions.
 - I implement in a script frequentist and Bayesian linear mixed model, along with statistical and diagnostic tools to validate and perform inferences.
 - 2.4 MergeBathy (2015)

- Co-authors from the adapted paper and poster, and developers include Todd Holland, Nathaniel Plant, Kevin Duvieih, Paul Elmore, Will Avera, Brian Bourgeois, A. Louise Perkins, and David Lalejini (S. J. Zambo et al., 2016, 2017a; S. Zambo et al., 2018).
- The following text highlights my involvement in MergeBathy and applies to both C++ and MATLAB versions.
 - I modified, extended, and validated MergeBathy versions, originally developed by Todd Holland and Nathaniel Plant, and extended by Paul Elmore.
 - I extensively debugged MergeBathy for correct computations and DBM generation, and significantly improved performance and stability.
 - I rectified multi-threading and cross-platform compilation.
 - I aligned output from C++ and MATLAB versions.
 - I developed a suite of test cases to validate MergeBathy.
 - I updated MergeBathy documentation and test cases originally developed by Todd Holland and Nathaniel Plant.
 - I updated and implemented test cases developed by Paul Elmore.
 - I implemented and validated many computational procedures including Brian Bourgeois' Kalman filter

algorithm, handling of uncertainty, and Paul Elmore's CURVE discussed in section 2.6.

- I implemented and validated the CURVE algorithm into the opensource GMT software code base for their inclusion.
- I compiled and updated third-party libraries.
- I implemented additional user-specified input parameters for better user control and flexibility, for example, uncertainty handling.
- I implemented the bathymetric attributed grid (BAG) files output format (Brian R. Calder et al., 2005; Open Navigation Surface Working Group, 2006).^{58, 59}
- I setup Mercurial, “a free, distributed source control management tool” (Mercurial, n.d.).
- I setup MergeBathy (pre-compiled, source code, examples, data, documentation) for open-source development and freeware availability for bathymetric processing on GitHub.
- MergeBathy was a project deliverable to the Naval Oceanographic Office. The Naval Oceanographic Office is responsible for worldwide ocean mapping and MergeBathy is one of their key tools to produce hydrographic products.

⁵⁸ BAG is a non-proprietary file format developed by the Open Navigation Surface Working Group; version 1.0.0 (Brian R. Calder et al., 2005; Open Navigation Surface Working Group, 2006).

⁵⁹ BAG utilizes additional third-party libraries not listed.

- 2.5 MergeBathy Interpolation Schemes
 - MergeBathy interpolators were originally implemented by Todd Holland and Nathaniel Plant and extended by the author.
- 2.6 Uncertainty Estimation for Sparse Data Gridding Algorithms
 - Group work with Paul Elmore, A. Louise Perkins, and Brian Bourgeois.
 - Co-authors from the adapted paper and poster include Paul Elmore, A. Louise Perkins, and Brian Bourgeois (S. J. Zambo et al., 2015a, 2015b).
 - The CUBE propagated uncertainty equation was originally developed by Brian Calder. The additive bottom-slope term was suggested by Brian Calder in communication with Paul Elmore. Paul Elmore added this bottom-slope term and developed the CURVE algorithm.
 - I implemented and validated the CURVE algorithm into the MergeBathy C++ and MATLAB versions.
 - I implemented and validated the CURVE algorithm into the opensource GMT software code base for their inclusion.
- CHAPTER III– A NEW INFORMED ENSEMBLE APPROACH TO BATHYMETRY UTILIZING MACHINE LEARNERS
 - 3.1 Geomorphological Seafloor Primitive Nominal Data
 - Group work and co-authored with Paul Elmore and A. Louise Perkins.

- I developed a model composed of nominal primitives.
 - I implemented a 2D Gaussian seamount and a 1D Gaussian ridge primitive, and hybrid mixtures thereof proposed by A. Louise Perkins in a script.
 - I devised and implemented an additional more diverse 2D truncated cone seamount primitive and hybrid mixtures thereof with the 1D Gaussian ridge in a script.
- 3.2 ELS for an Informed Differentially Weighted Ensemble of DBMs
 - Group work and co-authored with Paul Elmore and A. Louise Perkins.
 - I implemented ELS and w -ELS computations.
 - I implemented a planar regression model.
 - I devised and implemented nominal-informed custom regression models.
 - Evaluation and diagnostic tools for ELS and w -ELS.
 - Original discussions for using classifications in an interpolator were done with A. Louise Perkins.
- 3.3 Additional Methods to Assess
 - I devised and implemented additional methods in a script to evaluate against w -ELS/ELS.
- CHAPTER IV– RESEARCH APPROACH
 - Group work with Paul Elmore and A. Louise Perkins.

- I implemented in a script RMS, and signal-to-noise and entropy information metrics attribution for DBMs proposed by Paul Elmore for their evaluation.
- I implemented additional standard error metrics including CumRAE, and image evaluation metric attributions for DBMs in a script for DBM evaluation.
- I implemented various visualization and regression diagnostic plots, and statistical tests in a script.
- I implemented experiments proposed by Paul Elmore according to experimental designs (Montgomery, 2017).
- I devised and implemented a randomized experiment according to experimental designs (Montgomery, 2017).
- I setup and utilized cloud computing environments for additional computation resources.
- I implemented frequentist and Bayesian analyses of experiments.
- CHAPTER V– FIRST STUDY: FEATURE-FAVORING INTERPOLATION
 - I implemented un-replicated controlled experiments proposed by Paul Elmore.
 - I added replication and performed frequentist and Bayesian analyses.
- CHAPTER VI– SECOND STUDY: EVALUATING ENSEMBLES
 - I devised and implemented a replicated randomized study with randomized swath removal, density, and noise. Originally, Paul Elmore

suggested an un-replicated controlled experiment with determined swath removal, density, and noise levels.

- I developed and implemented a right-tail sign test with Delaunay triangulation to obtain a set of sparse configurations.
- I utilized Friedman's test and performed multiple comparisons with Tukey's HSD test, correcting experiment-wise error with $\alpha = 0.05$, to make inferences on the general population of experimental configurations with 95% confidence.
- CHAPTER VII– SUMMARY
 - Group work with Paul Elmore and A. Louise Perkins.

REFERENCES

- Abeel, T., Peer, Y. V. de, & Saeys, Y. (2009). Java-ML: A machine learning library. *Journal of Machine Learning Research*, 10(Apr), 931–934.
<https://www.jmlr.org/papers/volume10/abeel09a/abeel09a.pdf>
- Amazon Web Services. (n.d.). *Amazon Elastic Compute Cloud Documentation*. Retrieved February 22, 2021, from <https://docs.aws.amazon.com/ec2/index.html>
- AML Oceanographic. (2016). *What is a Multi-beam System?*
<http://www.amloceanographic.com/CTD-Sound-Velocity-Environmental-Instrumentation-Home/Multibeam-Overview>
- Anderson, B. D. O. & Moore, J. B. (1979). *Optimal filtering* (Thomas Kailath, Ed.). Prentice-Hall, Inc.
- Aracri, S., Giorgio-Serchi, F., Suaria, G., Sayed, M. E., Nemitz, M. P., Mahon, S. & Stokes, A. A. (2021). Soft robots for ocean exploration and offshore operations: A perspective. *Soft Robotics*. <https://doi.org/10.1089/soro.2020.0011>
- Armstrong, J. S. (2001). Evaluating forecasting methods. In *Principles of Forecasting* (pp. 443–472). Springer. https://doi.org/10.1007/978-0-306-47630-3_20
- Armstrong, J. S. (2001). *Principles of forecasting: a handbook for researchers and practitioners* (Vol. 30). Springer Science & Business Media.
- Armstrong, J. S. & Collopy, F. (1992). Error measures for generalizing about forecasting methods: Empirical comparisons. *International Journal of Forecasting*, 8(1), 69–80.
- Armstrong, J. S., Green, K. C. & Graefe, A. (2015). Golden rule of forecasting: Be conservative. *Journal of Business Research*, 68(8), 1717–1731.
- Aslett, L. (2020). *RStudio Server Amazon Machine Image (AMI)* .
https://www.louisaslett.com/RStudio_AMI/

- Becker, J., Sandwell, D., Smith, W., Braud, J., Binder, B., Depner, J., Fabre, D., Factor, J., Ingalls, S., Kim, S. & others. (2009). Global bathymetry and elevation data at 30 arc seconds resolution: SRTM30_PLUS. *Marine Geodesy*, 32(4), 355–371.
- Bestwick, J., Huttly, W. & Wald, N. (2010). Evaluation of a proposed mixture model to specify the distributions of nuchal translucency measurements in antenatal screening for Down’s syndrome. *Journal of Medical Screening*, 17(1), 13–18.
- Bezanson, J., Edelman, A., Karpinski, S. & Shah, V. B. (2017). Julia: A fresh approach to numerical computing. *SIAM Review*, 59(1), 65–98. <https://doi.org/10.1137/141000671>
- Bourgeois, B. S., Elmore, P. A., Avera, W. E. & Zambo, S. J. (2016). Achieving comparable uncertainty estimates with Kalman filters or linear smoothers for bathymetry data. *Geochemistry, Geophysics, Geosystems*, 17(7), 2576–2590. <https://doi.org/10.1002/2015GC006239>
- Breiman, L. (1996). Bagging predictors. *Machine Learning*, 24(2), 123–140.
- Breiman, L. (2001). Random forests. *Machine Learning*, 45(1), 5–32.
- Breiman, L., Friedman, J., Stone, C. J. & Olshen, R. (1984). Classification and Regression Trees . In *Wadsworth Statistics/Probability*. Chapman and Hall/CRC.
- Bürkner, P.-C. (2017). brms: An R package for Bayesian multilevel models using Stan. *Journal of Statistical Software*, 80(1), 1–28. <https://doi.org/10.18637/jss.v080.i01>
- Bürkner, P.-C. (2018). Advanced Bayesian multilevel modeling with the R package brms. *The R Journal*, 10(1), 395–411. <https://doi.org/10.32614/RJ-2018-017>
- Calder, B. (2006). On the uncertainty of archive hydrographic data sets. *IEEE Journal of Oceanic Engineering*, 31(2), 249–265.
- Calder, B. & Elmore, P. (2017). Development of an Uncertainty Propagation Equation for Scalar Fields. *Marine Geodesy*, 40(5), 341–360.

- Calder, B. R. (2019a). Parallel variable-resolution bathymetric estimation with static load balancing. *Computers & Geosciences*, 123, 73–82.
- Calder, B. R. (2019b). Resolution determination through Level of aggregation analysis. *U.S. Hydrographic Conference (US HYDRO)*.
- Calder, B. R., Byrne, S., Lamey, B., Brennan, R. T., Case, J. D., Fabre, D., Gallagher, B., Ladner, R. W., Moggert, F. & Paton, M. (2005). The Open Navigation Surface Project. *Center for Coastal and Ocean Mapping*. <http://scholars.unh.edu/ccom/1011>
- Calder, B. R., Dijkstra, S. J., Hoy, S., Himschoot, K. & Schofield, A. (2018). *A design for a trusted community bathymetry system*.
- Calder, B. R., Dijkstra, S. J., Hoy, S., Himschoot, K. & Schofield, A. (2020). A design for a trusted community bathymetry system. *Marine Geodesy*, 43(4), 327–358.
- Calder, B. R. & Mayer, L. A. (2003). Automatic processing of high-rate, high-density multibeam echosounder data. *Geochemistry, Geophysics, Geosystems*, 4(6). <https://doi.org/10.1029/2002GC000486>
- Calmant, S., Berge-Nguyen, M. & Cazenave, A. (2002). Global seafloor topography from a least-squares inversion of altimetry-based high-resolution mean sea surface and shipboard soundings. *Geophysical Journal International*, 151(3), 795–808.
- Caress, D. W. & Chayes, D. N. (2021). *MB-System: Mapping the Seafloor*. <https://www.mbari.org/products/research-software/mb-system/>
- Carpine-Lancre, J., Fisher, R., Harper, B., Hunter, P., Jones, M., Kerr, A., Laughton, A., Ritchie, S., Scott, D. & Whitmarsh, M. (2003). *The History of GEBCO 1903-2003: The 100-year story of the General Bathymetric Chart of the Oceans* (p. 140). GIOC bv. https://www.gebco.net/data_and_products/history_of_gebco/documents/history_of_gebco.pdf

- Cleveland, W. S. (1979). Robust locally weighted regression and smoothing scatterplots. *Journal of the American Statistical Association*, 74(368), 829–836.
- Cleveland, W. S. & Devlin, S. J. (1988). Locally weighted regression: An approach to regression analysis by local fitting. *Journal of the American Statistical Association*, 83(403), 596–610.
- Cleveland, W. S., Devlin, S. J. & Grosse, E. (1988). Regression by local fitting: Methods, properties, and computational algorithms. *Journal of Econometrics*, 37(1), 87–114.
- Cleveland, W. S. & Loader, C. (1996). Smoothing by local regression: Principles and methods. In *Statistical theory and computational aspects of smoothing* (pp. 10–49). Springer.
- Cortes, C. & Vapnik, V. (1995). Support-vector networks. *Machine Learning*, 20(3), 273–297.
- Cressie, N. A. (1990). The origins of kriging. *Mathematical Geology*, 22(3), 239–252.
- Cressie, N. A. C. (1993). Statistics for spatial data. *Probability and Mathematical Statistics*.
- Criminisi, A., Shotton, J. & Konukoglu, E. (2011). Decision forests for classification, regression, density estimation, manifold learning and semi-supervised learning. *Microsoft Research Cambridge, Tech. Rep. MSRTR-2011-114*, 5(6), 12.
- Curtin, R. R., Cline, J. R., Slagle, N. P., March, W. B., Ram, P., Mehta, N. A. & Gray, A. G. (2013). MLPACK: A scalable C++ machine learning library. *Journal of Machine Learning Research*, 14, 801–805. <https://mlpack.org/>
- Davis, J. C. (2002). *Statistics and data analysis in geology* (p. 387). John Wiley & Sons.
- De Boor, C. (1962). Bicubic spline interpolation. *Journal of Mathematics and Physics*, 41(1), 212–218.

- Diez, D. M., Barr, C. D. & Cetinkaya-Rundel, M. (2013). *OpenIntro statistics* (2nd ed.). CreateSpace.
- Draper, N. R. & Smith, H. (2014). *Applied regression analysis* (3rd ed.). John Wiley & Sons.
- Elmore, P. A., Calder, B., Masetti, G., Yager, R. R. & Petry, F. E. (2018). *Development of consistent and recordable fusion methods using bathymetry sources of differing subjective reliabilities for navigation or seafloor mapping [Presentation]*.
- Elmore, P. A., Petry, F. E. & Yager, R. R. (2017). Geospatial Modeling Using Dempster-Shafer Theory. *IEEE Transactions on Cybernetics*, 47(6), 1551–1561.
- Elmore, P. A. & Steed, C. A. (2008). *Algorithm design study for bathymetry fusion - review of current state-of-the-art and recommended design approach*.
- Elmore, P. A. & Zambo, S. J. (2013). *System and method for estimating uncertainty for geophysical gridding routines lacking inherent uncertainty estimation (Patent Application No. 13/961,597. Patent Publication No. 20140257700) [Patent]*.
- Elmore, P. A. & Zambo, S. J. (2014). *System and method for estimating uncertainty for geophysical gridding routines lacking inherent uncertainty estimation (Patent Application No. 14/200,153. Patent Publication No. 20140257750) [Patent]*.
- Epstein, E. S. (1969). Stochastic dynamic prediction. *Tellus*, 21(6), 739–759.
- Esri. (n.d.-a). *The ArcGIS Pro Geoprocessing Tool Reference v2.7: How OLS Regression Works*. Retrieved February 2021, from <https://pro.arcgis.com/en/pro-app/latest/tool-reference/spatial-statistics/how-ols-regression-works.htm>
- Esri. (n.d.-b). *The ArcGIS Pro Geoprocessing Tool Reference v2.7: Regression Analysis Basics*. Retrieved February 2021, from <https://pro.arcgis.com/en/pro-app/latest/tool-reference/spatial-statistics/regression-analysis-basics.htm>

- Fisher, R. A. (1936). The use of multiple measurements in taxonomic problems. *Annals of Eugenics*, 7(2), 179–188.
- Frank E. Harrell, J. (2001). *Regression modeling strategies: With applications to linear models, logistic regression, and survival analysis* (2nd ed.). Springer.
<https://doi.org/10.1007/978-3-319-19425-7>
- Franklin, S. E. (2020). Interpretation and use of geomorphometry in remote sensing: a guide and review of integrated applications. *International Journal of Remote Sensing*, 41(19), 7700–7733.
- Freund, Y. & Schapire, R. E. (1997). A decision-theoretic generalization of on-line learning and an application to boosting. *Journal of Computer and System Sciences*, 55(1), 119–139. <https://doi.org/10.1006/jcss.1997.1504>
- Gabry, J. & Mahr, T. (2021). *bayesplot: Plotting for Bayesian models (R package version 1.8.0) [Computer software]*. <https://mc-stan.org/bayesplot/>
- Gabry, J., Simpson, D., Vehtari, A., Betancourt, M. & Gelman, A. (2019). Visualization in Bayesian workflow. *Journal of the Royal Statistical Society Series A (Statistics in Society)*, 182(2), 389–402. <https://doi.org/10.1111/rssa.12378>
- Gavin, H. (2011). The Levenberg-Marquardt method for nonlinear least squares curve-fitting problems. *Department of Civil and Environmental Engineering, Duke University*.
- GEBCO Compilation Group. (2020). *GEBCO 2020 Grid*.
<https://doi.org/10.5285/a29c5465-b138-234d-e053-6c86abc040b9>
- Gelman, A., Carlin, J. B., Stern, H. S., Dunson, D. B., Vehtari, A. & Rubin, D. B. (2014). *Bayesian Data Analysis* (3rd ed.). Taylor & Francis.
- Gelman, A. & Hill, J. (2006). *Data analysis using regression and multilevel/hierarchical models*. Cambridge University Press. <https://doi.org/10.1017/CBO9780511790942>

- Geman, S., Bienenstock, E. & Doursat, R. (1992). Neural networks and the bias/variance dilemma. *Neural Computations*, 4, 58. <https://doi.org/10.1162/neco.1992.4.1.1>
- General Bathymetric Chart of the Oceans. (2020). *General Bathymetric Chart of the Oceans (GEBCO)*. www.gebco.net
- Geurts, P., Ernst, D. & Wehenkel, L. (2006). Extremely randomized trees. *Machine Learning*, 63(1), 3–42.
- Geyer, C. J. (2006). 5601 Notes: Smoothing. *Statistics*, 5601.
- Goldberger, A. S. (1962). Best linear unbiased prediction in the generalized linear regression model. *Journal of the American Statistical Association*, 57(298), 369–375.
- GRID-Arendal. (n.d.). *Blue Habitats: Seamounts*. Retrieved February 2021, from https://www.bluehabitats.org/?page_id=1678
- Hartig, F. & Lohse, L. (2020). *DHARMA: Residual diagnostics for hierarchical (multi-level / mixed) regression models (R package version 0.3.3.0) [Computer software]*. <http://florianhartig.github.io/DHARMA/>
- Hastie, T., Tibshirani, R. & Friedman, J. (2009). *The elements of statistical learning: Data mining, inference, and prediction* (2nd ed.). Springer-Verlag New York.
- Henderson, C. (1949). Estimation of changes in herd environment. *Journal of Dairy Science*, 32(1), 706–715.
- Henderson, C. R. (1963). Selection index and expected genetic advance. *Statistical Genetics and Plant Breeding*, 982, 141–163.
- Hengl, T. (2009). *A practical guide to geostatistical mapping* (2nd ed.). Office for Official Publications of the European Communities. http://spatial-analyst.net/book/system/files/Hengl_2009_GEOSTATe2c1w.pdf

- Hengl, T. & Reuter, H. I. (Eds.). (2008). *Geomorphometry: Concepts, software, applications* (Vol. 33, p. 772). Elsevier.
- Hoffman, M. D. & Gelman, A. (2011). *The no-u-turn sampler: Adaptively setting path lengths in Hamiltonian Monte Carlo*.
- Holland, T. (2005). *NRL MergeBathy User's Guide*.
- Holman, R., Plant, N. & Holland, T. (2013). cBathy: A robust algorithm for estimating nearshore bathymetry. *Journal of Geophysical Research: Oceans*, 118(5), 2595–2609.
- Hu, M. Z., Li, J. C., Li, H., Shen, C. Y., Jin, T. Y. & Xing, L. L. (2015). Predicting global seafloor topography using multi-source data. *Marine Geodesy*, 38(2), 176–189.
<https://doi.org/10.1080/01490419.2014.934415>
- International Hydrographic Organization. (n.d.-a). *Crowdsourced Bathymetry (CSB) Viewer v2.4.1*. Retrieved March 30, 2018, from
<https://maps.ngdc.noaa.gov/viewers/csb/>
- International Hydrographic Organization. (n.d.-b). *IHO Data Centre for Digital Bathymetry (DCDB)*. Retrieved February 12, 2021, from
<https://www.ngdc.noaa.gov/iho/>
- International Hydrographic Organization. (2008). *IHO standards for hydrographic surveys (Special Publication No. 44)* (5th ed.). International Hydrographic Bureau.
http://www.iho.int/iho_pubs/standard/S-44_5E.pdf
- International Hydrographic Organization. (2018). *The IHO Crowdsourced Bathymetry Cookbook: Guidance on Crowdsourced Bathymetry* (1st ed.).
- International Hydrographic Organization - Intergovernmental Oceanographic Commission. (2019). *The IHO-IOC GEBCO Cook Book* (p. 493).
https://www.star.nesdis.noaa.gov/socd/lisa/GEBCO_Cookbook/documents/CookBook_20191031.pdf

- Jakobsson, M., Calder, B. & Mayer, L. (2002). On the effect of random errors in gridded bathymetric compilations. *Journal of Geophysical Research-Solid Earth*, 107(B12), Article 2358.
- Kalman, R. E. (1960). A new approach to linear filtering and prediction problems. *Journal of Basic Engineering*, 82(1), 35–45.
- Kastrisios, C., Ware, C., Calder, B., Butkiewicz, T., Alexander, L. & Hauser, O. (2020). Nautical chart data uncertainty visualization as the means for integrating bathymetric, meteorological, and oceanographic information in support of coastal navigation. *100th American Meteorological Society Annual Meeting*.
- Kennedy, P. (2008). *A guide to Econometrics* (6th ed.). Blackwell Publishing.
- Kruschke, J. (2015). *Doing Bayesian data analysis: A tutorial with R, JAGS, and Stan* (2nd ed.). Academic Press.
- Ladner, R. W., Elmore, P., Perkins, A. L., Bourgeois, B. & Avera, W. (2017). Automated cleaning and uncertainty attribution of archival bathymetry based on a priori knowledge. *Marine Geophysical Research*, 38(3), 291–301.
<https://doi.org/10.1007/s11001-017-9304-9>
- Lawson, E., Smith, D., Sofge, D., Elmore, P. & Petry, F. (2017). Decision forests for machine learning classification of large, noisy seafloor feature sets. *Computers & Geosciences*, 99, 116–124.
- Lecours, V., Dolan, M. F., Micallef, A. & Lucieer, V. L. (2016). A review of marine geomorphometry, the quantitative study of the seafloor. *Hydrology and Earth System Sciences*, 20(8), 3207–3244.
- LeDell, E. (2016). *Winning Kaggle 101: Introduction to Stacking*. Berkeley Institute for Data Science. <http://www.slideshare.net/TedXiao/winning-kaggle-101-introduction-to-stacking>

- Li, J. & Heap, A. D. (2008). *A review of spatial interpolation methods for environmental scientists*.
- Lucieer, V., Dolan, M. & Lecours, V. (Eds.). (2019). *Marine geomorphometry* (Printed Edition of the Special Issue Published in *Geosciences*, p. 400). MDPI AG.
<https://doi.org/10.3390/books978-3-03897-955-5>
- Lucieer, V., Lecours, V. & Dolan, M. F. J. (2018). Charting the course for future developments in marine geomorphometry: An introduction to the special issue. *Geosciences*, 8(12). <https://doi.org/10.3390/geosciences8120477>
- Masetti, G., Faulkes, T. & Calder, B. (2019). Opening the black boxes in ocean mapping: design and implementation of the hydrooffice framework. In *Proceeding of the Australian Marine Sciences Association (Freemantle, AMSA), Perth, Australia* (pp. 7–11).
- Masetti, G., Mayer, L. A. & Ward, L. G. (2018). A bathymetry-and reflectivity-based approach for seafloor segmentation. *Geosciences*, 8(1), 14.
- Matheron, G. (1963). Principles of geostatistics. *Economic Geology*, 58(8), 1246–1266.
- MathWorks. (2015a). *Computer Vision System Toolbox (Release 2015b) [Computer software]*.
- MathWorks. (2015b). *Fuzzy Logic Toolbox (Release 2015b) [Computer software]*.
- MathWorks. (2015c). *MATLAB (Release 2015b) [Computer software]*.
- MathWorks. (2015d). *Neural Network Toolbox (Release 2015b) [Computer software]*.
- MathWorks. (2015e). *Statistics and Machine Learning Toolbox (Release 2015b) [Computer software]*.

- MathWorks. (2019). *MATLAB (Release 2019b) [Computer software]*.
- Mayer, L. A. (2006a). Frontiers in seafloor mapping and visualization. *Marine Geophysical Researches*, 27(1), 7–17.
- Mayer, L. A. (2006b). Frontiers in seafloor mapping and visualization. *Marine Geophysical Researches*, 27(1), 7–17.
- Mayer, L., Jakobsson, M., Allen, G., Dorschel, B., Falconer, R., Ferrini, V., Lamarche, G., Snaith, H. & Weatherall, P. (2018). The Nippon Foundation—GEBCO Seabed 2030 Project: The Quest to See the World’s Oceans Completely Mapped by 2030. *Geosciences*, 8(2), 63.
- McElreath, R. (2020). *Statistical rethinking: A Bayesian course with examples in R and STAN*. CRC Press.
- McLachlan, G. (2004). *Discriminant analysis and statistical pattern recognition* (Vol. 544). John Wiley & Sons.
- Meinhold, R. J. & Singpurwalla, N. D. (1983). Understanding the Kalman filter. *The American Statistician*, 37(2), 123–127.
<https://doi.org/10.1080/00031305.1983.10482723>
- Mercurial*. (n.d.). <https://www.mercurial-scm.org/>
- Micallef, A., Krastel, S. & Savini, A. (Eds.). (2017). *Submarine geomorphology*. Springer International Publishing.
- Microsoft. (2016). *Microsoft Azure Machine Learning [Computer software]*.
<https://azure.microsoft.com/en-us/services/machine-learning/>
- Microsoft, & R Core Team. (2019). *Microsoft R Open & MKL [Computer software]*.
<https://mran.microsoft.com/>

Milton, J. S. & Arnold, J. C. (2003). *Introduction to probability and statistics* (4th ed.). McGraw-Hill Higher Education.

Mitchell, N. C. (2001). Transition from circular to stellate forms of submarine volcanoes. *Journal of Geophysical Research: Solid Earth*, 106(B2), 1987–2003.
<https://doi.org/10.1029/2000JB900263>

Montgomery, D. C. (2017). *Design and analysis of experiments* (9th ed.). John Wiley & Sons, Inc.

O'Rourke, J. (1998). *Computational Geometry in C* (2nd ed.). Cambridge University Press.

Oguntimilehin, A., Adetunmbi, A. & Abiola, O. (2013). A machine learning approach to clinical diagnosis of Typhoid Fever. *International Journal of Computer and Information Technology*, 2(4), 671–676.

Open Navigation Surface Working Group. (2006). *Format specification document: Description of Bathymetric Attributed Grid Object (BAG) version 1.0.0 (Version release 1.0)*.

Paciorek, C. (2008). Technical Vignette 3: Kriging, interpolation, and uncertainty: Department of Biostatistics. *Harvard School of Public Health, Version, 1*.

Paciorek, C. J. (2010). The importance of scale for spatial-confounding bias and precision of spatial regression estimators. *Statistical Science: A Review Journal of the Institute of Mathematical Statistics*, 25(1), 107.

Pedregosa, F., Varoquaux, G., Gramfort, A., Michel, V., Thirion, B., Grisel, O., Blondel, M., Prettenhofer, P., Weiss, R., Dubourg, V., Vanderplas, J., Passos, A., Cournapeau, D., Brucher, M., Perrot, M., Duchesnay, E. & Duchesnay, É. (2011). Scikit-learn: Machine learning in Python. *Journal of Machine Learning Research*, 12, 2825–2830.

Perkins, A. L. (1995). Regional Gulf Stream initial conditions for the SPEM primitive equation model. *Marine Technology Society Journal*, 29(2), 15–23.

- Perkins, A. L. (2016). *Ensemble data fitting [Poster presentation]*.
<https://doi.org/10.13140/RG.2.1.3690.4726>
- Petry, F., Elmore, P. & Yager, R. (2015). Combining uncertain information of differing modalities. *Information Sciences*, 322, 237–256.
<https://doi.org/10.1016/j.ins.2015.06.009>
- Pierce, J. E. & Rust, B. W. (1985). Constrained least squares interval estimation. *SIAM Journal on Scientific and Statistical Computing*, 6(3), 670–683.
- Pike, R. J., Evans, I. S. & Hengl, T. (2009). Geomorphometry: A brief guide. In Hengl, T. and Reuter, H. I. (Ed.), *Geomorphometry: Concepts, software, applications* (Vol. 33, pp. 3–30). Elsevier.
- Pinheiro, J. & Bates, D. (2006). *Mixed-effects models in S and S-PLUS*. Springer Science & Business Media.
- Pitcher, T. J., Morato, T., Hart, P. J., Clark, M. R., Haggan, N. & Santos, R. S. (2008). *Seamounts: Ecology, fisheries & conservation*. John Wiley & Sons.
- Plant, N. G., Holland, K. T. & Puleo, J. A. (2002). Analysis of the scale of errors in nearshore bathymetric data. *Marine Geology*, 191(1-2), 71–86.
- Polikar, R. (2006). Ensemble based systems in decision making. *Circuits and Systems Magazine, IEEE*, 6(3), 21–45.
- Press, W. H., Teukolsky, S. A., Vetterling, W. T. & Flannery, B. P. (2007). *Numerical Recipes: The art of scientific computing* (3rd ed.). Cambridge University Press.
- Rokach, L. (2010). Ensemble-based classifiers. *Artificial Intelligence Review*, 33(1-2), 1–39.

- Sammut, C. & Webb, G. I. (Eds.). (2011). Bias variance decomposition. In *Encyclopedia of machine learning* (pp. 100–101). Springer Science & Business Media.
<https://doi.org/10.1007/978-0-387-30164-8>
- Sandwell, D. T., Müller, R. D., Smith, W. H., Garcia, E. & Francis, R. (2014). New global marine gravity model from CryoSat-2 and Jason-1 reveals buried tectonic structure. *Science*, 346(6205), 65–67. <https://doi.org/10.1126/science.1258213>
- Sandwell, D. T. & Smith, W. H. F. (2009). Global marine gravity from retracked Geosat and ERS-1 altimetry: Ridge segmentation versus spreading rate. *Journal of Geophysical Research: Solid Earth*, 114(B1).
- Sapp, S., van der Laan, M. J. & Canny, J. (2014). Subsemble: An ensemble method for combining subset-specific algorithm fits. *Journal of Applied Statistics*, 41(6), 1247–1259. <https://doi.org/10.1080/02664763.2013.864263>
- Schapire, R. E. (1989). The strength of weak learnability. *30th Annual Symposium on Foundations of Computer Science*, 28–33. <https://doi.org/10.1109/SFCS.1989.63451>
- Schmidt, V., Chayes, D., Caress, D. & Aquarium, M. B. (2003). The MB-System™ 5.0 Cookbook. 2003, 9(08).
- Searle, S. R., Casella, G. & McCulloch, C. E. (2006). *Variance components* (2nd ed., pp. 1–501). John Wiley & Sons, Inc.
- Shalizi, C. R. (2019). *Advanced data analysis from an elementary point of view*. Cambridge University Press.
<https://www.stat.cmu.edu/~cshalizi/ADAfaEPoV/ADAfaEPoV.pdf>
- Shogun Toolbox Foundation. (2016). *The Shogun Machine Learning Toolbox (Version 4.1.0) [Computer software]*.
- Sinclair, D. A. (2010). *S-hull: A fast sweep-hull routine for Delaunay triangulation*.
<http://www.s-hull.org>

- Smith, D., Lawson, E., Sofge, D., Elmore, P. & Petry, F. (2016). *Recognition of Seafloor Features by Decision Tree Algorithms in Scenes of Gridded Sonar Data [Poster presentation]*. <https://doi.org/10.13140/RG.2.1.1672.4881>
- Smith, W. H. F. & Sandwell, D. T. (1994). Bathymetric prediction from dense satellite altimetry and sparse shipboard bathymetry. *Journal of Geophysical Research: Solid Earth*, 99(B11), 21803–21824. <https://doi.org/10.1029/94JB00988>
- Smith, W. H. & Sandwell, D. T. (1997). Global sea floor topography from satellite altimetry and ship depth soundings. *Science*, 277(5334), 1956–1962.
- Smith, W. & Wessel, P. (1990). Gridding with continuous curvature splines in tension. *Geophysics*, 55(3), 293–305.
- Srinivasan, B. V., Duraiswami, R. & Murtugudde, R. (2010). Efficient kriging for real-time spatio-temporal interpolation. *Proceedings of the 20th Conference on Probability and Statistics in the Atmospheric Sciences*, 228–235.
- Stan Development Team. (2020). *RStan: The R interface to Stan (R package version 2.21.2) [Computer software]*. <http://mc-stan.org/>
- Stan Development Team. (2021). *Stan modeling language users guide and reference manual (Version 2.25)*. <https://mc-stan.org>
- Steed, C. A. & Rankin, W. E. (2003). *OAML Feathering Algorithm overview*.
- Submarine Geomorphology Working Group*. (2021). <http://www.geomorph.org/submarine-geomorphology-working-group/>
- Tavana, M., Liu, W., Elmore, P., Petry, F. E. & Bourgeois, B. S. (2016). A practical taxonomy of methods and literature for managing uncertain spatial data in geographic information systems. *Measurement*, 81, 123–162. <https://doi.org/10.1016/j.measurement.2015.12.007>

- The Apache Software Foundation. (2016). *Apache Spark MLlib [Computer software]*. <http://spark.apache.org/mllib/>
- The GMT Developers. (2021). *The Generic Mapping Tools (GMT)*. <https://www.generic-mapping-tools.org/>
- The GMT Team. (2020a). *triangulate*. GMT 6.1.1. <https://docs.generic-mapping-tools.org/latest/triangulate.html>
- The GMT Team. (2020b). *triangulate*. GMT 5.4.6_c5d65a4_2019.11.05 Documentation. <https://docs.generic-mapping-tools.org/latest/triangulate.html>
- The Julia Project. (2021). *The Julia Language (version 1.6)*. <https://docs.julialang.org/en/v1/>
- Tobler, W. R. (1970). A computer movie simulating urban growth in the Detroit region. *Economic Geography*, 46(sup1), 234–240.
- Tozer, B., Sandwell, D. T., Smith, W. H. F., Olson, C., Beale, J. R. & Wessel, and P. (2019). Global bathymetry and topography at 15 arc seconds: SRTM15+. *Earth and Space Science*, .
- Trivedi, D., Rahn, C. D., Kier, W. M. & Walker, I. D. (2008). Soft robotics: Biological inspiration, state of the art, and future research. *Applied Bionics and Biomechanics*, 5(3), 99–117. <https://doi.org/10.1080/11762320802557865>
- U.S. Naval Oceanographic Office (NAVO). (2003). *Digital Bathymetric Data Base Variable Resolution (DBDB-V)*. https://www7320.nrlssc.navy.mil/DBDB2_WWW/dbdb5/NRLCOM_dbdb2.html
- Vapnik, V. N. (1998). *Statistically learning theory* (Simon Haykin, Ed.). John Wiley & Sons, Inc.
- Verron, J., Bonnefond, P., Andersen, O., Ardhuin, F., Bergé-Nguyen, M., Bhowmick, S., Blumstein, D., Boy, F., Brodeau, L., Crétaux, J.-F., Dabat, M. L., Dibarboure, G.,

- Fleury, S., Garnier, F., Gourdeau, L., Marks, K., Queruel, N., Sandwell, D., Smith, W. H. F. & Zaron, E. D. (2020). The SARAL/AltiKa mission: A step forward to the future of altimetry. *Advances in Space Research*. <https://doi.org/10.1016/j.asr.2020.01.030>
- Wang, A., Tao, C., Zhang, G., Shen, C. & Liu, Y. (2021). Seafloor classification based on deep-sea multibeam data—Application to the Southwest Indian Ridge at 50.47°E. *Journal of Applied Geophysics*, 104259. <https://doi.org/10.1016/j.jappgeo.2021.104259>
- Wang, Z. & Bovik, A. C. (2009). Mean squared error: Love it or leave it? A new look at signal fidelity measures. *IEEE Signal Processing Magazine*, 26(1), 98–117. <https://doi.org/10.1109/MSP.2008.930649>
- Wang, Z., Bovik, A. C., Sheikh, H. R. & Simoncelli, E. P. (2004). Image quality assessment: From error visibility to structural similarity. *IEEE Transactions on Image Processing*, 13(4), 600–612. <https://doi.org/10.1109/tip.2003.819861>
- Wang, Z. & Li, Q. (2007). Video quality assessment using a statistical model of human visual speed perception. *JOSA A*, 24(12), B61–B69.
- Weatherall, P., Marks, K., Jakobsson, M., Schmitt, T., Tani, S., Arndt, J. E., Rovere, M., Chayes, D., Ferrini, V. & Wigley, R. (2015). A new digital bathymetric model of the world's oceans. *Earth and Space Science*, 2(8), 331–345. <https://doi.org/10.1002/2015EA000107>
- Werbos, P. J. (1982). Applications of advances in nonlinear sensitivity analysis. In *System modeling and optimization* (pp. 762–770). Springer.
- Wessel, P., Luis, J. F., Uieda, L., Scharroo, R., Wobbe, F., Smith, W. H. F. & Tian, D. (2019). The Generic Mapping Tools version 6. *Geochemistry, Geophysics, Geosystems*, 20. <https://doi.org/10.1029/2019GC008515>
- Wessel, P., Smith, W. H. F., Scharroo, R., Luis, J. & Wobbe, F. (2013). Generic mapping tools: improved version released. *Eos, Transactions American Geophysical Union*, 94(45), 409–410.

- West, B. T., Welch, K. B. & Galecki, A. T. (2014). *Linear mixed models: a practical guide using statistical software*. CRC Press.
- Wolpert, D. H. (1992). Stacked generalization. *Neural Networks*, 5(2), 241–259.
- Wolpert, D. H. & Macready, W. G. (1997). No free lunch theorems for optimization. *Evolutionary Computation, IEEE Transactions on*, 1(1), 67–82.
<https://doi.org/10.1109/4235.585893>
- Wooldridge, J. M. (2015). *Introductory econometrics: A modern approach* (6th ed.). Nelson Education.
- Wölfl, A.-C., Snaith, H., Amirebrahimi, S., Devey, C. W., Dorschel, B., Ferrini, V., Huvenne, V. A., Jakobsson, M., Jencks, J., Johnston, G. & others. (2019). Seafloor mapping-the challenge of a truly global ocean bathymetry. *Frontiers in Marine Science*, 6, 283.
- Zambo, S., Holland, T., Plant, N., Duvieilh, K., Elmore, P., Avera, W., Bourgeois, B., Perkins, A. L. & Lalejini, D. (2018). MergeBathy (2015). *SoftwareX*, 7, 180–183.
<https://doi.org/10.1016/j.softx.2018.05.005>
- Zambo, S. J. (2017). *CURVE for GMT [Computer software and source code]*.
https://github.com/Sammie-Jo/GMT_CURVE
- Zambo, S. J., Elmore, P. A., Avera, W., Holland, T. & Perkins, A. L. (2016). *Introducing MergeBathy [Poster presentation]*. <https://doi.org/10.13140/RG.2.1.2242.5363>
- Zambo, S. J., Elmore, P. A., Perkins, A. L. & Bourgeois, B. S. (2015a). *Uncertainty estimation for sparse data gridding algorithms*.
- Zambo, S. J., Elmore, P. A., Perkins, A. L. & Bourgeois, B. S. (2015b). *Uncertainty estimation for sparse data gridding algorithms [Poster presentation]*.
https://www.gebco.net/about_us/gebco_symposium/documents/gebco_sd_2015_zambo.pdf

- Zambo, S. J., Holland, T., Plant, N., Duvieih, K., Elmore, P., Avera, W., Bourgeois, B. S. & Perkins, A. L. (2017a). *MergeBathy [Computer software and source code]*. https://github.com/Sammie-Jo/MergeBathy_Repos-mergeBathy_CPP
- Zambo, S. J., Holland, T., Plant, N., Duvieih, K., Elmore, P., Avera, W., Bourgeois, B. S. & Perkins, A. L. (2017b). *MergeBathy [Data for published examples]*. https://github.com/Sammie-Jo/MergeBathy_Repos-mergeBathy_DATA_CENTER
- Zambo, S. J., Holland, T., Plant, N., Duvieih, K., Elmore, P., Avera, W., Bourgeois, B. S. & Perkins, A. L. (2017c). *MergeBathy [Documentation]*. https://github.com/Sammie-Jo/MergeBathy_Repos-mergeBathy_DOCS
- Zambo, S. J., Holland, T., Plant, N., Duvieih, K., Elmore, P., Avera, W., Bourgeois, B. S. & Perkins, A. L. (2017d). *MergeBathy [Source code for published examples]*. https://github.com/Sammie-Jo/MergeBathy_Repos-TEST_CENTER
- Zhou, Q. M. & Liu, X. J. (2004). Error analysis on grid-based slope and aspect algorithms. *Photogrammetric Engineering and Remote Sensing*, 70, 957–962.
- Zimmerman, D. & Cressie, N. (1992). Mean squared prediction error in the spatial linear model with estimated covariance parameters. *Annals of the Institute of Statistical Mathematics*, 44(1), 27–43.
- Ziyin, W., Fanlin, Y., Yong, T., Xiaowen, L., Dineng, Z., Guanying, H., Kai, Z., Jieqiong, Z., Shaohua, J., Dianpeng, S., Xiaohu, L., Huaiming, L., Shengping, W., Zhenyi, C., Jianyun, Y., Jihong, S., Weifeng, D., Xuefeng, X., Zhu Xinke, Z. W., ... He, L. (2021). *High-resolution seafloor survey and applications*. Springer Singapore. <https://doi.org/10.1007/978-981-15-9750-3>